ФОТО ЭЛЕКТРОНИКА

PHOTOELECTRONICS

INTER-UNIVERSITIES SCIENTIFIC ARTICLES

Founded in 1986

Number 19

The results of theoretical and experimental studies in problems of optoelectronics, solar power and semiconductor material science for photoconductive materials are adduced in this collection. The prospective directions for photoelectronics are observed.

The collection is introduction into the List of special editions of Ukrainian Higher Certification Comission in physics-mathematics and tehnical sciences.

For lecturers, scientists, post-graduates and students.

У збірнику наведено результати теоретичних і експериментальних досліджень з питань оптоелектроніки, сонячної енергетики і напівпровідникового матеріалознавства фотопровідних матеріалів. Розглянуто перспективні напрямки розвитку фотоелектроніки.

Збірник включено до Переліку спеціальних видань ВАК України з фізико-математичних та технічних наук.

Для викладачів, наукових працівників, аспірантів, студентів.

В сборнике приведены результаты теоретических и экспериментальных исследований по вопросам оптоэлектроники, солнечной энергетики и полупроводникового материаловедения фотопроводящих материалов. Рассмотрены перспективные направления развития фотоэлектроники.

Сборник включен в Список специальных изданий ВАК Украины по физико-математическим и техническим наукам.

Для преподавателей, научных работников, аспирантов, студентов.

TABLE OF CONTENT

V. P. VELESCHUK, O. I. VLASENKO, M. P. KISSELYUK, O. V. LYASHENKO, S. G. NEDIL'KO,
V. P. SHCHERBATSKY

e-mail: lyashenk@univ.kiev.ua
Institute of Semiconductor Physics of NASU, 03028, 45 Prospect Nauki, Kyiv, Ukraine
Kyiv National University of Taras Shevchenko, 03680, 2 Prospect Glushkova, Kyiv, Ukraine

ELECTROLUMINESCENCE OF NATURALLY AGED LIGHT-EMITTING DIODE STRUCTURES BASED ON GALLIUM PHOSPHIDE.

It was shown that naturally aged structures based on gallium phosphide with green and red colours of radiation can withstand direct currents, which are tens times higher than any maximum values of currents for just produced structures. Considerable displacement (by 0.28−0.3 eV) of a green band of electroluminescence of structures at a self-heating by passing current and full quenching of a red band at degradation of structures were fixed. Physical mechanisms of these phenomena are discussed.

INTRODUCTION

With growing process of gallium phosphide based light-emitting diode structures completed, and after technological stages of light-emitting diodes fabrication these structures are in a complex metastable condition with high level of internal mechanical strains (IMS), non-uniform throughout the volume of a crystal [1−5], thus the most part of dislocations still remains to be nonequilibrium defects [3−5], fixed on stoppers.

Earlier it has been established [6] that in GaAsP/GaP light-emitting diode structures reduction of number of defects with small energy of activation takes place due to processes of natural ageing. These defects actively participate in processes of defects formation and microfractures. These processes take place in active area of structures and area of contacts, are accompanied by acoustic emission (AE), and result in degradations of both intensity of electroluminescence (EL) and other parameters of light-emitting diode structures [7−9]. Process of natural ageing occurs mainly at the expense of binding of dot defects and dislocations in clusters, *i.e.* at formation of new complexes of defects with higher energy of activation E that leads to increase of their degradation resistance [6, 7]. It is essential, as a prime condition for stable work without degradation of light-emitting diodes is prevention of occurrence and multiplication of defects of different dimensionality in their active area [1, 4, 6−15] and in the area of their ohmic contacts [2, 13, 16].

On the other hand, now processes of ageing without external influence, *i.e.*, processes of natural ageing are scantily known. It, in particular, is connected with necessity of measurements during reasonably long time, which should be comparable to characteristic time of these relaxation processes.

The shifts received by us earlier ($\Delta\lambda$ ~20−50 nm) in red and green bands in naturally aged $GaAs_{0,15}P_{0,85}$/GaP structures (with formation of an infra-red band), which are accompanied by intensive AE [9], considerably exceed typical known shifts — $\Delta\lambda$ ~5−7 nm [11], whereby AE is often absent. For $GaAs_{0,15}P_{0,85}$/GaP light-emitting diodes in this case cardinal change of colour of radiation from green to red takes place. Estimation of temperature of overheating for shifts $\Delta\lambda$ ~20−50 nm within the limits of known modifications of Varshni relationship made by us (using different data [9]) gives too high values — from 250 to 400 K.

Research of influence of natural ageing of low-dimensional GaP/GaP and GaAsP/GaP heterostructures on change of their electrical and optical characteristics, and also determination of mechanisms of cardinal transformation of electroluminescence spectra at superthreshold current density was the work purpose.

EXPERIMENT

Industrial light-emitting diodes on the basis of GaP:N/GaP structures with green luminescence, GaP:N, Zn-O/GaP structures with red luminescence in a metal-glass package with the sizes of structure 450x450 μm, and also GaAsP:N, Zn-O/GaP structures of yellow luminescence in the polymeric package were investigated. These structures have been made in the early eighties, and as we had been fixed substantial growth of AE threshold and destruction currents in similar structures, it gives promise to expect that in them the processes of natural ageing occurred.

In addition to standard linear increase of the current at spectra measurement (Figs. 1, 2), in this work algorithm of step-by-step increase of J with the optimised mode of step-by-step J change was used for achievement of critically high currents J in light-emitting A^3B^5 structures. This algorithm corresponds to confident actuation of potentially active (for the specified J) sources of AE according to the Kaiser law.

Approximate calculations of empirical dependences between current intensity and number of the step of its increase established earlier were performed. In Figure 3 dependence of direct current I of light emitting structures on the step number n of its increases is presented. I_n=10 mA, time between steps varied from 3 to 10 minutes.
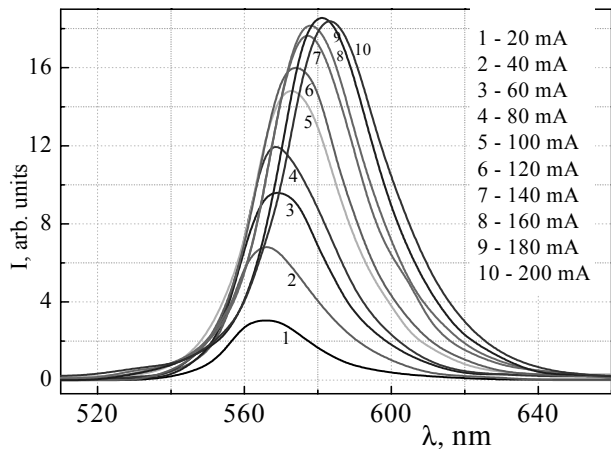
Fig.1. Electroluminescence spectra of the GaP: N, Zn-O/ GaP structures and the plan of the radiative jumps.
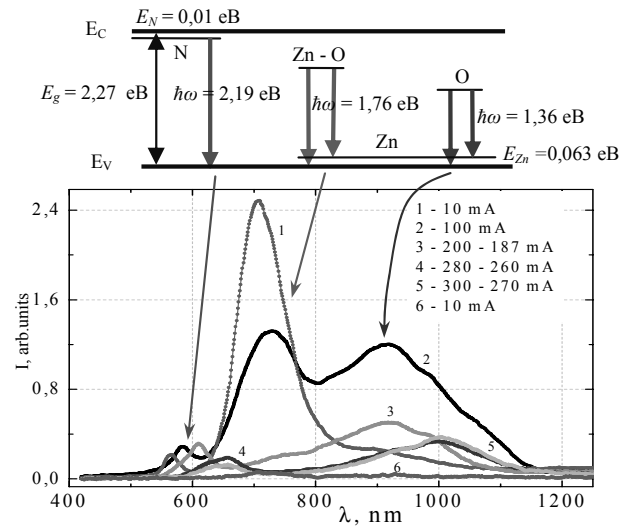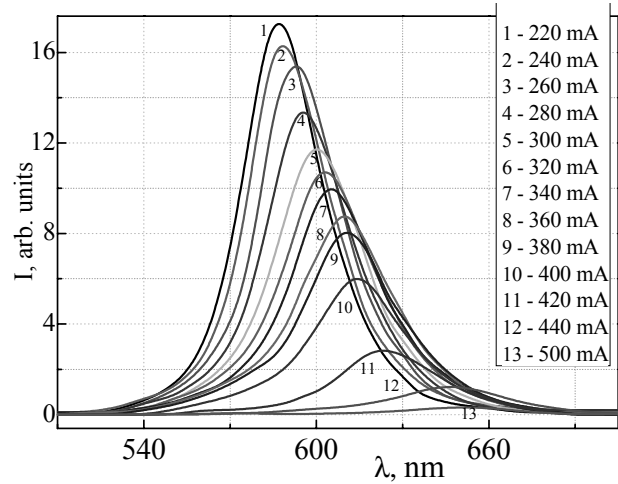
Fig.2. Electroluminescence spectra of the GaP:N/GaP structures at increase of the current.
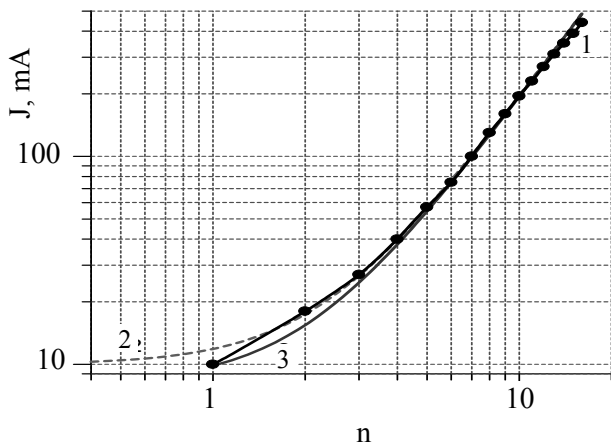
Fig.3. Dependence $J(n)$ for structures direct-current on step of increase of the current: 1 - experimental curve, 2 - $J(n) = 1,86n^2+10$, 3 - $J(n) = 1,86n^2+8$

The specified dependence (curve 1) was determined empirically on the basis of measurements of more than 300 samples. Curves 2 and 3 in Fig. 3 are function $J(n) = an^2+b$ type, where n is the number of the step, constants $a=1,86$ and $b=10$ for curve 2; $a=1,86$, $b=8$ for curve 3.

RESULTS

Spectra of GaP: N and Zn-O/GaP structures are presented in Fig. 1 at different currents, tens times exceeding their possible admissible values specified by manufacturer. Reversible and irreversible degradations of bands were observed, namely, decrease of their intensities and displacement with temperature partially restored at current decrease. At current increase along with irreversible degradation of EL bands reversible decrease in intensity (I) of the red band at $\lambda = 700$ nm (1.76 eV) and intensity increase of IR band at $\lambda = 910$ nm (1.36 eV), were revealed *i.e.*, redistribution of their intensities took place. The spectrum at 10 mA before and after current increase to 100 mA did not change. In the case if current exceeded 200 mA irreversible decrease in EL intensity of the red band I_R and increase in intensity of the IR-band I_{IR} took place (Fig. 1). At the maximum current (before structure destruction) complete irreversible disappearance of the red band was observed, but IR band was retained.

Spectra of GaP: N/GaP structures at currents lower than 500 mA are shown in Fig. 2. Initially they have only the green band at $\lambda = 565$ nm. For these structures reversible and irreversible degradations of intensity were observed too. It was revealed therewith that a part of aged GaP: N/GaP structures at currents $250-300$ mA and temperature $500-600°C$ degrade slowly and do not fail, unlike just manufactured ones (≈ 1 year) structures of such type for which these currents exceeded destruction currents. Such values of currents earlier ($25-30$ years ago) have been also unattainable for these aged structures.

The maximum displacement of the green band registered by us, which was caused by recombination on the isoelectronic centres of nitrogen N_p, makes 90 nm (0.3 eV) for GaP: N, Zn-O/GaP structures and 84 nm (0.28 eV) for GaP: N/GaP structures (Figs. 1, 2), that essentially exceeds known displacement $\Delta\lambda \sim 5-7$ nm [1, 11] and even displacement $\Delta\lambda \sim 20-50$ nm registered by us earlier [9].

Band displacement occurs both at considerable self-heating of structure by passing current with intensity of $450-500$ mA (thus the structure temperature increases to more than $600°C$), and external heating

(to 600°C). Colour of radiation of aged GaP:N/GaP structures monotonously varies therewith from green to red. Considerable displacement of the maximum of the green band by 0.28−0.3 eV is caused be narrowing of the forbidden bandwidth with growth of the active area temperature. Dependence of green band peak position in GaP:N/GaP structures on current and dependence of E_g on temperature for GaP are shown in Fig. 4. From this figure we notice that by and large these dependences are similar.
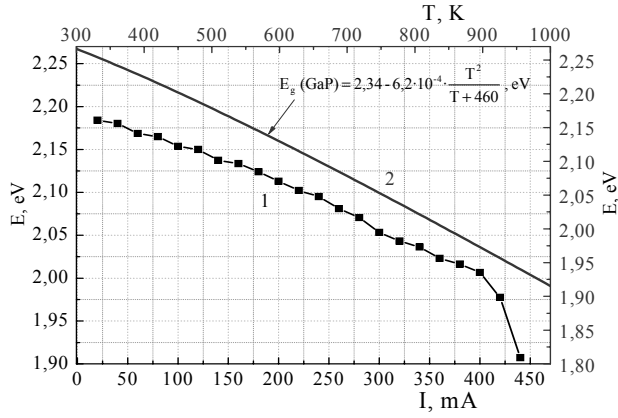
Fig.4. Dependence of the maximum of EL green band of the GaP:N/GaP structure on current (1) and dependence E_g GaP on temperature (2)

It was revealed that GaP:N, Zn-O structures under study degraded faster than GaP:N/GaP structures. This fact is in line with results presented in [12]. It is supported also by the fact that after natural ageing maximal achievable current in our experiment for the first structures was 400 mA, and for the second ones it was 500 mA.

It should be noted that at the increase of heterojunction current not only displacement of EL bands, but also redistribution of EL intensity on the structure surface take place (Fig. 5). As follows from Fig. 5, at reasonably small currents rather uniform distribution of intensity is observed at moderate displacement of the band $\Delta\lambda$. If currents are close to currents of destruction and extreme shifts of the band are observed, then EL intensity in the area of the cross-like electrode substantially (by a factor of ten) exceeds the intensity on periphery of the radiating surface of the structure. The temperature of this surface can be judged by the appearance of EL intensity maxima in the area of partially fused electrode.

DISCUSSION

By and large irreversible degradation of EL structures is connected with both defects formation in the area of contacts, which results in growth of their resistance, and defects formation in active area (*p-n* heterojunction), which results in the increase of nonradiative recombination as well as in reduction of injection ratio [1, 2, 4, 6−15].

Let us discuss both reversible and irreversible degradations and redistribution of relative intensities I of the red and IR bands. The red band at 1.76 eV (700 nm) of GaP: N, Zn-O/GaP structures corresponds to radiating recombination of free holes with electrons, bound on the Zn−O centres and represents two closely spaced lines caused by recombination on donor-acceptor pairs (DAP) $(Zn_{Ga}−O_P)−Zn_{Ga}$ or recombination of bound excitons on close DAP $Zn_{Ga}−O_P$ (insert in Fig. 1 represents radiative jumps). Zinc is a small acceptor with ionisation energy E_{Zn} = 0.061 eV, and position of the line 1.76 eV means that electron-binding energy on the complex is of about 0.4 eV [11].
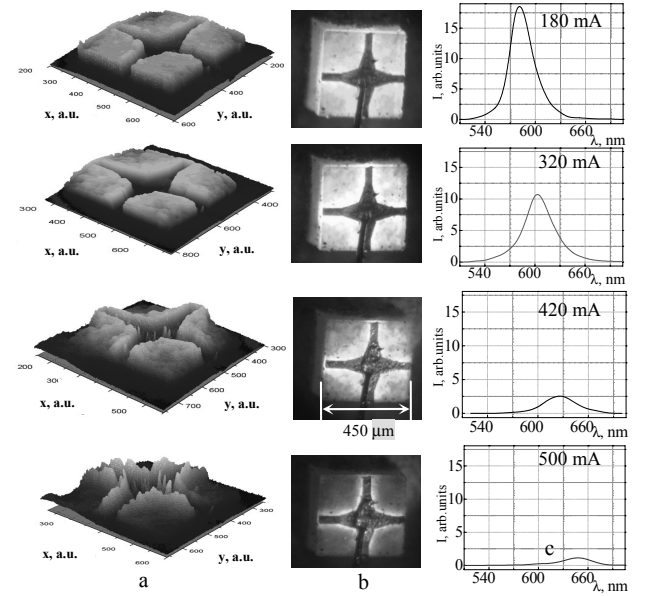
Fig. 5. Distribution of EL integral intensity of the GaP: N /GaP surface I(S) (a), photo of structure (b) and I(λ) for green band of EL at different currents (c).

Emission line in infra-red band is located at 1.36 eV (910 nm). It corresponds to radiation recombination on distant DAP with participation of the deep donor O_P and shallow acceptor Zn_{Ga} (insert in Fig. 1) or recombination of the free electron defects with bound electron on O_P.

For DAP in GaP with shallow impurities at distance between impurity atoms $r>115E$ the radiative jump energies are described well by expression [11]:

$$Ph\nu = E_g − (E_A + E_D) + e^2 / \varepsilon r − e^2 b^5 / \varepsilon r^6 \qquad (1)$$

where E_A and E_D are energy positions in the forbidden zone of the acceptor and donor, which form DAP, respectively, r is the distance between donor and acceptor centres, $\varepsilon−$ is dielectric constant, b is a constant of dipole-dipole polarised interaction between neutral impurity centres in the initial exited state. Last summond takes into account interaction of electrons with the acceptor, a hole with the donor and electrons and holes. Interaction between the ionised impurities (with interaction energy $e^2/\varepsilon r$) prevents the bounding of electrons and holes on very close pairs, except for cases when at least one of values E_A or E_D is very high [11].

It should be noted that the band 1.36 eV with participation of O_P donor is not shifted with growth of current density and temperature, unlike the band 1.76 eV (see Fig. 1). Absence of shift of the radiation band maximum 1.36 eV can be explained by strong linear electro-phonon interaction, when relative depth of a

trap is not changed with temperature [11]. Let us note that Zn−O trap can be in the empty state occupied by electron or exciton.

Reversible degradation of the red band can be explained by the fact that with temperature raise recombination on DAP is quenched due to the channel of radiative recombination of free holes on neutral donors O_P. This effect is not connected with EL intensity reduction due to increase of phonon absorption with temperature increase. The red band (1.76 eV) passes in the band 1.36 eV, caused by O_P donor. It is the reason for reversible redistribution of relative intensities I of the red and IR bands.

Irreversible degradation of the band 1.76 eV and growth of the band 1.36 eV occurs at the expense of disintegration of Zn_{Ga}-O_P DAP, appearance of dot defects, and diffusion of Zn and O in non-uniform electric, thermal and thermoelastic fields, thus diffusion of p-n — heterojunction takes place [10].

Zinc as an element of the first and transitive group diffuses by dissociation mechanism of diffusion: in the form of a negative ion (Zn_{Ga}^-) by vacancies of gallium sublattice and in the form of positive ion (Zn_i^{2+}) by interstitial sites. The local electric field therewith has accelerating action on diffusion of ions of replacement and decelerating action on diffusion of ions by interstitial sites.

Before degradation oxygen in p-layer of such structures is uniformly distributed with thickness. In [4] heterogeneity of distribution and oxygen concentration increase in vicinity of p-n — heterojunction after structure degradation was fixed at current density 20 A/cm^2 during 500 hours, which was connected with partial disintegration of Zn-O complexes [4].

High values of diffusion constant and solubility of oxygen atoms caused by the big difference of their tetrahedral radii with those of GaP basic elements lead to high mobility of O in gallium phosphide lattice.

Transition (diffusion) of mobile positive ions, in particular Zn, from p-area into n-area owing to decrease of a barrier height at direct displacement at high currents [10], and also from p$^+$-area into p-area also takes place [13].

By and large features and degradation mechanisms of just produced light-emitting structures of such a type are described in detail, e. g., in [2, 4, 6−15]. In our case substantial growth of maximal possible admissible parameters, namely, current, voltage, temperatures of these structures was fixed after long (25−30 years) ageing processes. In addition, this made it possible to reach considerable displacements of the EL green band maximum without structure destruction.

Let us note that considerable lowering of duration of the degradation first stage was revealed for the light-emitting diodes, which were put into operation after two years of their storage under natural conditions. It was caused by diffusion of Zn_i interstitial atoms to p-n-heterojunction [13].

Naturally, at currents ~500 mA the degradation caused by appearance of dislocations in active area of these structures is also possible. If the average distance between dislocations l becomes comparable to diffu-

sion length of minority carriers L, EL intensity drastically falls as a result of nonradiative recombination of carriers on dislocations, as $l = \rho_D^{-1/2}$ where ρ_D is the dislocation density [14].

It is known that the increase of dislocation density in epitaxial layers of gallium phosphide to $\rho_D = (2\div5)\cdot10^5$ cm^{-2}, which corresponds to average distance between dislocations $l = (2\div4)$ L, results in reduction of quantum efficiency of the green luminescence approximately by a factor of two [14]. For green band L = 5÷7 µm, for the red band L ≤ 2 µm. At $\rho_D = 10^7$ cm^{-2} (l = 3.2 µm) quantum efficiency of GaP structures with green radiation is equal to zero [14]. Thus, in these aged structures ρ_D does not reach the value of 10^7 cm^{-2} at degradation by the current lower than 400−500 mA.

At the same time at full quenching of the red band in GaP: N, Zn-O and in GaAsP: N, Zn-O structures at currents 300−400 mA the green band remained. In GaP: N/GaP structures it did not disappear even at 500 mA. Dislocations have considerably lower influence on intensity of the red band at the specified dislocation density, as for this band L ≤ 2 µm, and disappearance of the red band should occur at $\rho_D = 2.5\cdot10^7$ sm^{-2}. As discussed above, full disappearance of the red band takes place due to disintegration of the Zn−O DAP.

Thus, at the increase of current density and EL degradation at the expense of appearance of dislocations in active area, the green band is shifted to the red area, and red band disappears completely. At the same time from positions of EL dislocation quenching concept the green band should disappear first.

In our case it points, on the one hand, to such dominating mechanism of degradation of EL green and red bands as formation of dot defects, in particular, exit of Zn in interstitial site and formation of V_{Ga} [10−13]. From the other hand, substantial increase of activation energy of dislocations formation in naturally aged structures and reduction of number of structure defects with small activation energy E obtain an indirect evidence.

CONCLUSIONS

It was shown that in naturally aged GaP/GaP and GaAsP/GaP structures at superthreshold increase of heterojunction current the catastrophic−shift of EL spectrum into the red area takes place simultaneously with appearance of acoustic emission. As this takes place, light-emitting diodes based on these structures keep working capacity at currents, which exceed maximal known currents by the factor of tens.

Mechanisms of transformation of EL spectra were analyzed at superthreshold currents, which result in reversible and irreversible degradations of EL intensity, in particular, to disappearance of the red EL band.

It was shown that the dominating mechanism of degradation in naturally aged GaP/GaP and GaAsP/GaP structures at superthreshold currents is formation and diffusion of dot defects instead of formation of dislocations.

References

1. Ф. Е. Шуберт *Светодиоды.* — М.: Физматлит, пер. с англ. А. Э. Юновича. — 2008.С. 496 .
2. Е. Ф. Венгер, Р. В. Конакова, Г. С. Коротченков, В.В. Миленин, Э.В. Руссу, И.В. Прокопенко *Межфазные взаимодействия и механизмы деградации в структурах металл-InP и металл-GaAs.* — Киев: "КТНК", –1999.С. 260
3. М. А. Путято, Ю. Б. Болховитянов, А. П. Василенко, А. К. Гутаковский Кристаллическое совершенство пленок GaP, выращенных методом молекулярной эпитаксии на подложках Si с использованием атомарного водорода // ФТП. — 2009.Т.43, № 9. — С. 1275–1279 .
4. С. В. Булярский *Глубокие центры безизлучательной рекомбинации в светоизлучающих приборах.* — Кишинев, Изд. "Штиинца". — 1997. С. 103
5. С. В. Булярский, В. В. Светухин *Физические основы управления дефектообразованием в полупроводниках.* — Ульяновск: УлГУ. — 2002 С. 386
6. В. П. Велещук, О. В. Ляшенко Акустична емісія світловипромінювальних структур на основі сполук A^{3}B^5 обумовлена постійним прямим струмом // *УФЖ.* — 2003. Т. 48, № 9. — С. 941–945
7. В. П. Велещук, О. І. Власенко, О. В. Ляшенко, Ю. О. Мягченко, А. Байдулаєва, Р. Г. Чуприна, М.В. Кравцов, О. Д. Будов Акустична емісія при релаксації локальних термомеханічних напруг в процесі деградації світловипромінюючих гетероструктур на основі InGaN та GaAsP // *УФЖ.* — Т.53, №3. — 2008.С. 240–246 .
8. О. В. Ляшенко, З.К. Власенко, В.П. Велещук, Ю. О. Мягченко Зсув спектрів електролюмінесценції та акустична емісія в світловипромінюючих GaP$_{0,85}$As$_{0,15}$/GaP структурах // "Оптоэлектроника и полупроводниковая техника". — 2008. Т.43. — С. 107–110
9. V. P. Veleshchuk, O. V. Lyashenko, Yu.A. Myagchenko, R. G. Chuprina Evolution of the Electro-luminescence Spectra and the Acoustic Emission of the Epitaxial Structures of GaAsP // J.Appl.Spectroscopy. — 2004. Vol.71, N4 — P. 553−557 .
10. А. А. Птащенко Деградация светоизлучающих диодов. Обзор // Журнал Прикладной Спектроскопии. — 1990.Т. 33, № 5. — С. 781–803
11. А. А. Берг, П. Д. Дин. *Светодиоды* — М.: Мир, — 1999.С.686 .
12. Т. В. Торчинская, А. А. Шматов, В. И. Строчков, М. К. Шейнкман. Преобразование глубоких центров в процессе деградации GaP <N, Zn-O> светоизлучающих диодов // ФТП, 1996, Т. 20, вып. 4. — С. 701−707 .
13. Т. В. Торчинская, М. К. Шейнкман. Связь кинетики деградации GaP:N, Zn-O светодиодов с интенсивностью красной полосы свечения // Письма ЖТФ. 1997. — Т.13, №20. — С.1221.
14. W. A. Brantley, O. G. Lorimor, P. D. Dapkus S. E. Haszhko, R. H. Saul. Effect of dislocations on green electroluminescence efficiency in GaP grown by liquid phase epitaxy // J.Appl. Phys., 1999, vol. 46, N6. — P. 2629−2637.
15. I. A. Bocharova, S. A. Malyshev. Deep levels of defects in diode structures based on gallium phosphide // J.Appl. Spectroscopy. — 2006. Vol.73, N1. — P.85−89
16. Т. В. Бланк, Ю. А. Гольдберг, Е. А. Поссе Протекание тока по металлическим шунтам в омических контактах к широкозонным полупроводникам A^{III}B^V // ФТП. — 2009.Т.43, №9. — С. 1204−1209 .

Veleschuk V. P., Vlasenko O. I., Kisselyuk M. P., Lyashenko O. V., Nedil'ko S. G., Shcherbatsky V. P.

ELECTROLUMINESCENCE OF NATURALLY AGED LIGHT-EMITTING DIODE STRUCTURES BASED ON GALLIUM PHOSPHIDE.

Abstract

It was shown that naturally aged structures based on gallium phosphide with green and red colours of radiation can withstand direct currents, which are tens times higher than any maximum values of currents for just produced structures. Considerable displacement (by 0.28−0.3 eV) of a green band of electroluminescence of structures at a self-heating by passing current and full quenching of a red band at degradation of structures were fixed. Physical mechanisms of these phenomena are discussed.

Key words: heterostructure, electroluminescence, defect, acoustic emission

Велещук В. П., Власенко О. І., Киселюк М. П., Ляшенко О. В., Неділько С. Г., Щербацький В. П.

ЕЛЕКТРОЛЮМІНЕСЦЕНЦІЯ ПРИРОДНО ЗІСТАРЕНИХ СВІТЛОДІОДНИХ СТРУКТУР НА ОСНОВІ ФОСФІДУ ГАЛІЮ.

Резюме

Показано, що природньо-зістарені структури на основі фосфіду галію зеленого і червоного кольорів випромінювання можуть витримувати прямі струми, які в десятки разів перевищують будь-які максимальні значення струмів для свіжовиготовлених структур. Зафіксований значний зсув (на 0,28..0,3 еВ) зеленої смуги електролюмінесценції структур при саморазігріві протікаючим струмом і повне гасіння червоної смуги при деградації структур. Обговорені фізичні механізми даних явищ.

Ключові слова: гетероструктура, електролюмінесценція, дефект, акустична емісія

Велещук В. П., Власенко А. И., Киселюк М. П., Ляшенко О. В., Неделько С. Г., Щербацкий В. П.

ЭЛЕКТРОЛЮМИНЕСЦЕНЦИЯ ЕСТЕСТВЕННО СОСТАРЕННЫХ СВЕТОДИОДНЫХ СТРУКТУР НА ОСНОВЕ ФОСФИДА ГАЛЛИЯ.

Резюме

Показано, что естественно-состаренные структуры на основе фосфида галлия зеленого и красного цветов излучения могут выдерживать прямые токи, в десятки раз превышающие любые максимальные значения токов для свежеизготовленных структур. Зафиксировано значительное смещение (на 0,28..0,3 еВ) зеленой полосы электролюминесценции структур при саморазогреве протекающим током и полное гашение красной полосы при деградации структур. Обсуждены физические механизмы данных явлений.

Ключевые слова: гетероструктура, электролюминесценция, дефект, акустическая эмиссия

R. VITER, V. SMYNTYNA, I. KONUP, I. LYDINA, J. PUUSTINEN, J. LAPPALAINEN, V. IVANITSA.

Experimental physics department, Odessa I. I. Mechnikov University, Odessa, Ukraine,
+38067 66 39 327, viter_r@mail.ru
Microbiology department, Odessa I. I. Mechnikov University, Odessa, Ukraine
Department of Electrical and Information Engineering,
University of Oulu, Oulu, Finland

INVESTIGATION OF OPTICAL AND STRUCTURAL PROPERTIES OF TIN OXIDE-PORPHYRIN STRUCTURES FOR OPTICAL SENSORS APPLICATION.

Tin oxide-porhyrin structures deposited on glass substrates have been investigated for 2-Mercaptoethanol detection. Tin oxide layer was deposited by electro-spray pirolysis. Porphyrin layers were grown by dipping the substrates into porphyrin solution in water and toluene. Structural properties were characterized by XRD and AFM methods. Optical transmittance in range of 200−1100 nm of the structures was performed before and after adsorption of 2-Mercaptoethanol on their surfaces. Optical response of the structures to 2-Mercaptoethanol at room temperature is reported. The influence of 2-Mercaptoethanol adsorption to optical transmittance was discussed.

INTRODUCTION.

Tin oxide is well known material for sensor application. Tin dioxide sensitive properties were studied by many authors. In spite of good sensitivity to different compounds it has low selectivity, which was compensated by varying of operation temperature or using metal dopants.

Porphyrins are often used for optical sensor applications [1,2]. It was reported that adsorption of molecules on porphyrin structures changed absorption spectra in visible light [2]. Absorption maximum position shift was observed under gas molecules adsorption [2].

2-Mercaptoethanol is organic liquid used in some biological applications. 2-Mercaptoethanol is considered a toxin, causing irritation to the nasal passageways and respiratory tract upon inhalation and irritation to the skin.

The combination of tin oxide and porphyrins deposited by sol gel method was already successfully used for gas detection [3]. It is expected that layered SnO_2-porphyrin structure are suitable for 2-Mercaptoethanol detection.

In the previous works tin oxide-porphyrine sensors were based on resistivity measurements. In this case additional power was consumed to heat them up to operating temperatures of 200−350 ^{0}C. On the other hand, optical sensors based on absorbance and transmittance measurements operate at room temperatures.

In the present work, optical, structural characterization of tin oxide-porphyrine structures and sensitivity tests to 2-mercaptoethanol are reported.

EXPERIMENTAL.

Tin oxide layers were deposited by electro-spray pirolysis technique. Tin chloride ethanol solution with 0.01 mol/l concentration was used. Deposition of the layers was performed on glass substrates at 330 ^{0}C with 17 kV of applied voltage.

5, 10, 15, 20-tetrakis-(N-methyl-4-pyridyl)-porphynato-Cu-tetra iodide (Cu-Porph) and 5, 15-di −(N-methyl-4-pyridyl)-10,20-di (n-nonyl)-porphynato-tin dichloride (Sn-Porph) were deposited on top of tin oxide layer by dip coating into water and toluene solutions, correspondently.

Structural properties of the deposited films were investigated with X-ray diffraction (XRD) and Atomic Force microscopy (AFM) methods.

Phase identification of as deposited and annealed films has been studied by means of XRD (Philips MW 1380) instrumentation with CuKα radiation (λ=0,154 nm). The incident angle of X-rays was 2°. The measurements were performed with a constant speed 1/8 °/min in the 2θ range 20−60°.

Atomic force microscopy (Veeco Dimensions 3100) was used to investigate the surface morphology of obtained samples in tapping mode. The bearing area curves (BAC) and rms roughness R_q values have been calculated from AFM images to show surface morphology of the samples.

For optical characterization of the samples UV-1700 UV-VIS spectrophotometer has been used. Transmittance spectra have been measured at the range of wavelengths 200−1100 nm with 1 nm step.

RESULTS AND DISCUSSION.

XRD spectra of tin oxide films are plotted in fig.1. The one can see peaks at 26.5, 34.4 and 51.6, corresponding to tetragonal phase of tin oxide. By means of numerical methods average grain size d and lattice strain ε were estimated from XRD data. The obtained values for d and ε were 7 nm and 0.0027, correspondently.

The surface images of SnO_2 and SnO_2-porphyrin films are presented in fig.2. Tin oxide surface consisted of surface agglomerates with average dimension 100 nm (fig.2a). The roughness value Rq for tin oxide film was 26 nm.
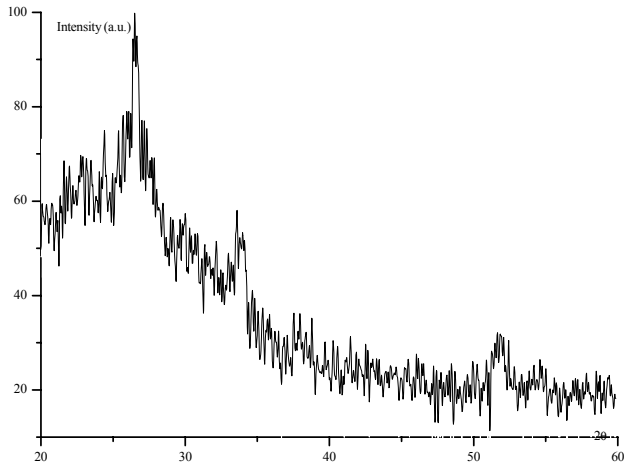
Fig.1. XRD spectrum of tin oxide layer.
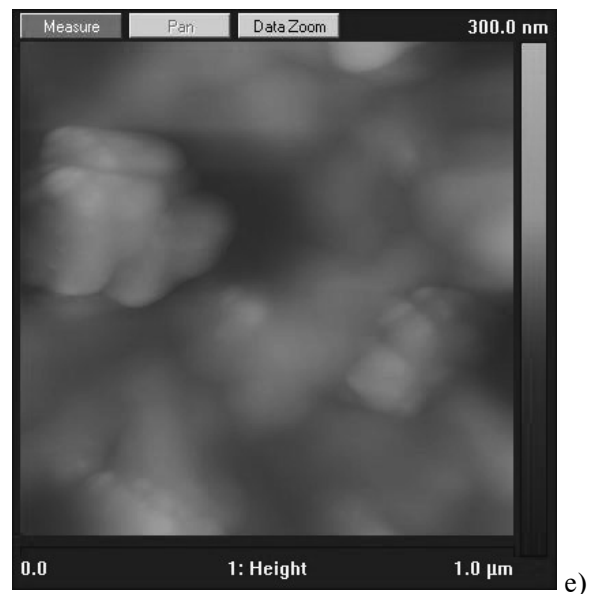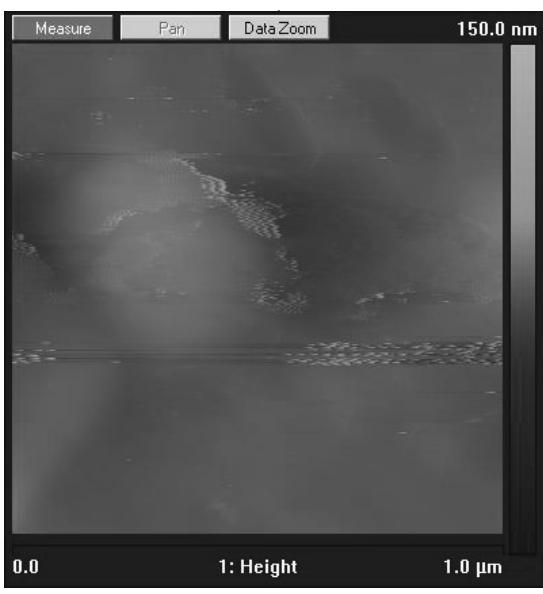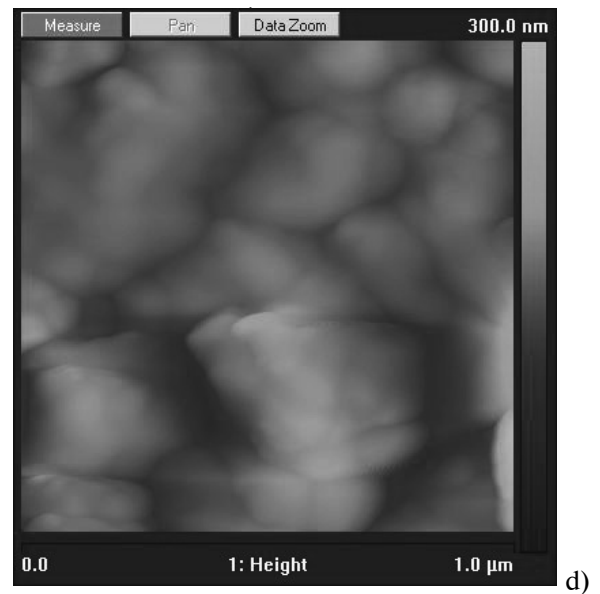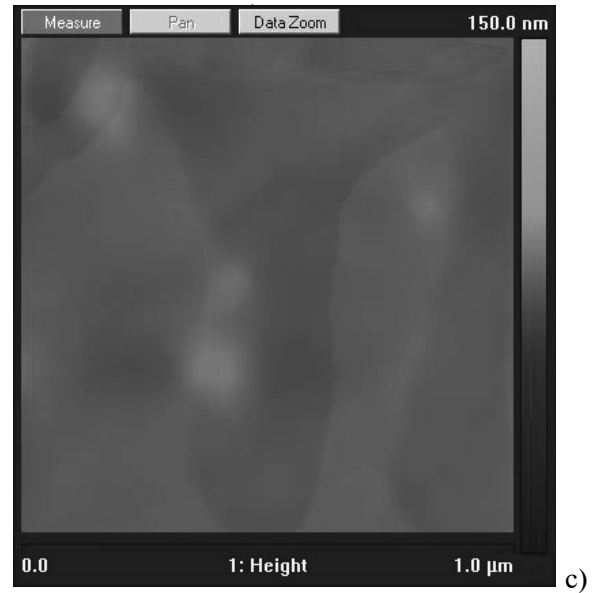
Fig. 2: AFM image: a) SnO_2, b) Cu-Porph, c) Sn-Porph, d) SnO_2-Cu-Porph, e) SnO_2-Sn-Porph.

Surface structure of porphyrins was really smooth (Rq=1.2ч1.4 nm) (fig.2b, 2c). After deposition of porphyrin layers on top of tin oxide the surface was still rough (fig.2d, 2e). The surface roughness (Rq) was about 21 and 18,5 nm for SnO_2-Cu-Porph and SnO_2-Sn-Porph, correspondently. It can be concluded that porphyrin layer 'smoothes' tin oxide surface.

Optical transmittance data of the samples are plotted in fig.3, 4. Both Cu-Porph and Sn-Porph transmittance spectra have minimums at 418 nm (fig.3b) and 440 (fig.4b) corresponding to the Soret band. The Q-band is absent for Cu-Porph but appears for Sn-Porph as transmittance minimums at 570 and 610 nm (fig.4b). After deposition of porphyrins on top of tin oxide film, blue shift of minimums was observed for Sn-Porph and red shift was Cu-Porph (fig3c, fig.4c). In case of Cu-Porph, minimum transformed to plateau (fig3c). This phenomenon is similar to the one observed in [4] where red shift of minimums was observed. The shift of the transmittance minimums indicates the occurrence of a strong interaction between tin oxide and porphyrin [4]. It was shown that porphyrins mostly exist as monomers on metal oxides. The heteroaggregates formation is possible between them what leads to optical properties changes [4].

Transmittance spectra of the sample were measured after 2-Mercaptoethanol adsorption on the their surface. The response of the samples to 2-Mercaptoethanol was different: the transmittance value dropped for SnO_2-Sn-Porph and enhanced for SnO_2-Cu-Porph structures in the range of 410−430 nm (fig. 3d, fig.4d).
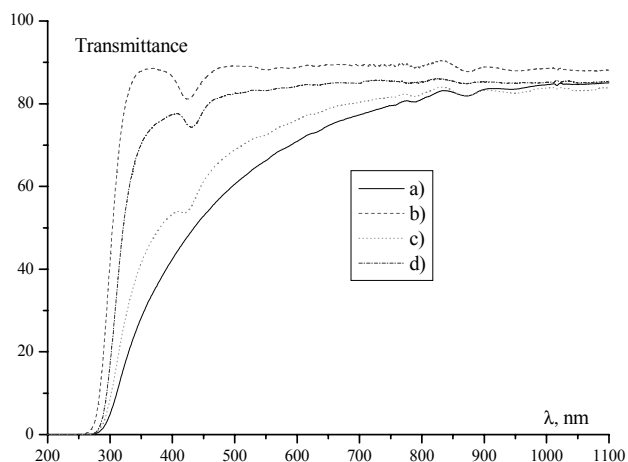
Fig. 3. Transmittance spectra: a) SnO_2, b) Cu-Porph, c) SnO_2-Cu-Porph, d) SnO_2- Cu-Porph-2-Mercaptoethanol.

It is known that tin oxide is poorly sensitive to organic compounds at room temperatures [3]. Therefore, porphyrine is key point in interaction between the structures with 2-Mercaptoethanol. As Soret bands correspond to ϖ-electrons transitions [5] the possible mechanism of 2-Mercaptoethanol adsorption comes through interaction adsorbed molecules with unsatu-

rated bonds of porphyrins. It results to changes in heteroaggregates bonding and brings to optical changes.

However, it is necessary to perform additional measurements of electrical properties to reveal or contradict this interaction mechanism. Next works will be devoted to resolution of this problem.
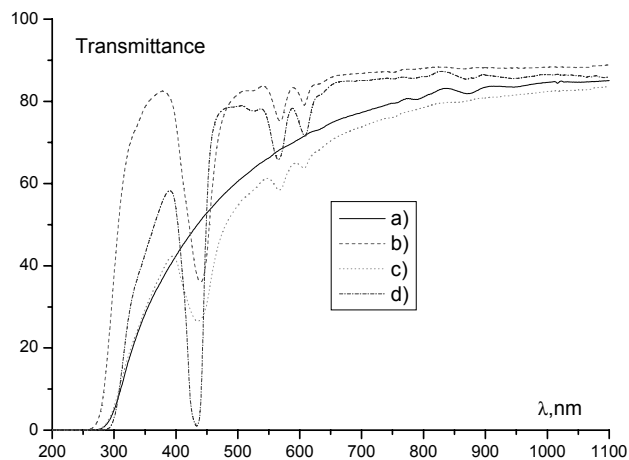
Fig. 4. Transmittance spectra: a) SnO_2, b) Sn-Porph, c) SnO_2-Sn-Porph, d) SnO_2- Sn-Porph-2-Mercaptoethanol.

CONCLUSION.

Porphyrins form heteroaggregates with tin oxide after their deposition on top of metal oxide surface what was proofed by Soret band shift and AFM data. 2-Mercaptoethanol adsorption on top of the surface led to transmittance changes what can be used in optical sensors. Adsorption mechanism can be explained by interaction of 2-Mercaptoethanol with unsaturated bonds of porphyrins.

References

1. A. Dunbar, T. H. Richardson, A. J. McNaughton, W. Barford, J. Hutchinson, C. A. Hunter, Understanding the interactions of porphyrin LB films with NO_2// Colloids and Surfaces A: Physicochem. Eng. Aspects. — 2006. — Vol. 284−285. — P. 339−344
2. Isabelle Leray, Marie-Claude Vernie`res, Claude Bied-Charreton, Porphyrins as probe molecules in the detection of gaseous pollutants: detection of benzene using cationic porphyrins in polymer films // Sensors and Actuators B. — 1999. — Vol. 54. — P. 243−251
3. E. A. Makeeva, M. N. Rumyantseva, A. M. Gaskova, B. A. Ismailov, V. A. Vasnev, Sensor properties of hybrid SnO_2-polysilazane materials // Proceedings of the Eurosensors XXIII conference, Procedia Chemistry. — 2009. — Vol. 1. — P. 172−175
4. Huihua Deng, Zuhong Lu, Haifang Mao and Yaochun Shen, Cosensitization and photoelectric conversion of a nanostructured electrode with tetrasulfonated porphyrins TiO_2 // J. Chem. Soc., Faraday Trans. — 1998. — Vol. 94. — N 5. — P. 659−663
5. Akrajas Ali Umar, Muhamad Mat Salleh, Muhammad Yahaya, Self-assembled monolayer of copper (II) meso-tetra(4-sulfanatophenyl) porphyrin as an optical gas sensor, Sensors and Actuators B. — 2004. — Vol. 101. — P. 231−235

R. Viter, V. Smyntyna, I. Konup , I. Lydina, J. Puustinen, J. Lappalainen, V. Ivanitsa.

INVESTIGATION OF OPTICAL AND STRUCTURAL PROPERTIES OF TIN OXIDE-PORPHYRIN STRUCTURES FOR OPTICAL SENSORS APPLICATION.

Summary.

Tin oxide-porhyrin structures deposited on glass substrates have been investigated for 2-Mercaptoethanol detection. Tin oxide layer was deposited by electro-spray pirolysis. Porphyrin layers were grown by dipping the substrates into porphyrin solution in water and toluene. Structural properties were characterized by XRD and AFM methods. Optical transmittance in range of 200−1100 nm of the structures was performed before and after adsorption of 2-Mercaptoethanol on their surfaces. Optical response of the structures to 2-Mercaptoethanol at room temperature is reported. The influence of 2-Mercaptoethanol adsorption to optical transmittance was discussed.

Key words: tin oxide, porphyrin, optical sensors, 2-Mercaptoethanol detection.

Р. В. Вітер, В. А. Сминитна, І. П. Конуп, І. Лидіна, Я. Пуустінен, Ю. Лаппалайнен, В. О. Іваниця.

ДОСЛІДЖЕННЯ ОПТИЧНИХ ТА СТРУКТУРНИХ ВЛАСТИВОСТЕЙ СТРУКТУР ОКСИД ОЛОВА-ПОРФІРИН ДЛЯ ОПТИЧНИХ СЕНСОРІВ.

Резюме

У роботі досліджено властивості структур оксид олова-порфірин для визначення молекул меркаптоетанолу. Оксид олова було нанесено методом електро-спрей піролізу на скляні підкладинки. Порфірини наносилися із розчинів органічних сполук. Структурні властивості зразків було досліджено за допомогою методів дифракції рентгенівського випромінювання та атомно-силової мікроскопії. Оптичні властивості було досліджено в діапазоні хвиль 200−1100 нм. Визначено вплив адсорбції меркаптоетанолу на оптичні властивості структур та обговорено механізм взаємодії молекул з поверхнею зразків.

Ключові слова: оскид олова, порфірин, оптичні сенсори, детектування меркапотетанолу.

Р. В. Витер, В. А. Смынтына, И. П. Конуп, И. Лыдина, Я. Пуустиннен, Ю. Лаппалайнен, В. А. Иваница.

ИССЛЕДОВАНИЕ ОПТИЧЕСКИХ И СТРУКТУРНЫХ СВОЙСТВ СТРУКТУР ОКСИД ОЛОВА- ПОРФИРИН ДЛЯ ОПТИЧЕСКИХ СЕНСОРОВ.

Резюме

В работе исследованы свойства стурктур оксид олова- порфирин для определения молекул меркаптоэтанола. Оксид олова наносился на стеклянные подложки при помощи метода электро-спрэй пиролиза. Порфирины наносились из растворов органических растворителей. Структурные свойства образцов изучались при помощи методов дифракции рентгеновского излучения и атомно-силовой микроскопии. Оптические свойства были исследованы в интервале длин волн 200−1100 нм. Установлено влияние адсорбции меркаптоэтанола на оптические свойства структур и предложен механизм взаимодействия молекул с поверхностью образцов.

Ключевые слова: оксид олова, порфирин, оптические сенсоры, определение меркаптоэтанола.

O. YU. KHETSELIUS

I. I. Mechnikov Odessa National University, str. Pastera, 27, Odessa, 65016, Ukraine
e-mail: nuclei08@mail.ru

NUCLEAR-QED THEORY OF HYPERFINE, ELECTROWEAK, PARITY NON-CONSERVATIVE EFFECTS IN HEAVY ATOMS, NUCLEI AND NEW STARK PUMPING PNC EXPERIMENTS

The combined QED perturbation theory formalism and relativistic nuclear mean-field theory are applied to studying the fundamental parameters of the hyperfine, electroweak, parity non-conservation (PNC) interactions in heavy atoms, nuclei. There are firstly predicted the nuclear weak charged for some atoms and new objects for the PNC Stark pumping experiments with cold-atom fountain are noted.

The fundamental purposes of the high-precision atomic PNC studies are to search for new physics beyond the standard model of the electroweak interaction by precise evaluation of the weak charge Q_W and to probe parity violation in the nucleus by evaluation of the nuclear anapole moment. The recent LEP experiments are fulfilled [1,2], that yield extremely accurate values for Z-boson properties. Although the spectacular experimental achievements of particle physics in the last decade have strengthened the Standard Model (SM) as an adequate description of nature, they have also revealed that the SM matter represents a mere 5% or so of the energy density of the Universe, which clearly points to some physics beyond the SM despite the desperate lack of direct experimental evidence. The sector responsible for the spontaneous breaking of the SM electroweak symmetry is likely to be the first to provide experimental hints for this new physics. The detailed review of these topics can be found in refs. [1–6], in particular, speech is about brief introducing the SM physics and the conventional Higgs mechanism and a survey of recent ideas on how breaking electroweak symmetry dynamics can be explained. Atomic optical and Stark pumping PNC measurements have been completed in Cs (0.35 % accuracy [1]), Tl (1.7 %), Bi (2 %), Pb (1.2 %). A few atomic PNC experiments (in heavy systems such as Fr, Ba$^+$, Ra$^+$, Yb) are currently in progress. Atomic-optics tests of the standard model provide important constraints on possible extensions of the standard model. A recent analysis [2] of parity-violating electron-nucleus scattering measurements combined with atomic PNC measurements placed tight constraints on the weak neutral-current lepton-quark interactions at low energy, improving the lower bound on the scale of relevant new physics to ~ TeV. The precise measurement of the PNC amplitudes in Cs [1] led to an experimental value of the small contribution from the nuclear-spin dependent PNC accurate to 14%. So, form the one side there is very actual necessity of the further development and increasing of the theoretical approaches accuracy and carrying out new atomic optical and Stark pumping PNC experiments. The multi-configuration relativistic Hartree-Fock (RHF) and Dirac-Fock (MCDF) approximation (c.f.[3,4,17,26] is the most reliable version of calculation for multi-electron systems with a large nuclear charge; in these calculations one- and two-particle relativistic effects and radiative QED corrections are taken into account, however an accuracy of theses methods is out of the necessary test one. This fact has stimulated a development of different versions of the many-body perturbation theory (PT), namely, the PT with RHF and DF zeroth approximations, QED-PT and nuclear QED PT (N-QED PT) [1–43]. In present paper the N-QED PT approach is used for studying the fundamental parameters of the hyperfine, electroweak, PNC interactions in heavy atoms (nuclei) and new objects for the Stark pumping experiments are proposed. We firstly predict the values of the weak charge Q_W for some heavy atoms.

The basises of the N-QED PT, which is the combination of the ab initio QED PT formalism and nuclear relativistic middle-field (RMF) approach that allows to make a prйcised account of the relativistic, correlation, nuclear, radiative effects, are in details described in serried of papers [10,38–44]. So, we are limited only by the key aspects. The wave electron functions zeroth basis is found from the Dirac equation solution with potential, which includes the core ab initio potential, electric, polarization potentials of nucleus. All correlation corrections of the second and high orders of PT (electrons screening, particle-hole interaction etc.) are accounted for [10]. The concrete nuclear model is based on the relativistic mean-field (RMF) model of a nucleus. More concretely, we used so called NL3-NLC and generalized Ivanov et al approach (see details in refs. [4,12]), which are among the most successful parameterizations available. Further one can write the Dirac-Fock -like equations for a multi-electron system {core-nlj}. Radial parts F and G of two components of the Dirac function for electron, which moves in the potential $V(r,R)$ are defined by solution of the Dirac equations (PT zeroth order). The general potential includes the electrical and polarization potentials of a nucleus. The radiative QED (the self-energy part of the Lamb shift and the vacuum polarization contribution) are accounted for within the QED formalism [4,10]. The hyperfine structure constants are defined as follows. The interaction Hamiltonian is the standard:

$$H_I = e\bar{j}_e^\mu \bar{A}_\mu + e\bar{J}_N^\mu \bar{A}_\mu \qquad (1)$$

where j_e^μ, j_N^μ are Lorentz covariant current operators for the electron and the nucleus respectively:

$$\bar{j}_e^\mu = \bar{\widehat{\psi}}_e \gamma^\mu \widehat{\psi}_e \qquad (2)$$

$$\bar{J}_N^\mu = \frac{1+\tau_3}{2}\bar{\widehat{\psi}}_N \gamma^\mu \overline{\psi}_N + \frac{\lambda}{2M}\partial_\nu(\bar{\widehat{\psi}}_N \sigma^{\mu\nu}\overline{\psi}_N) \qquad (3)$$

Here $\sigma^{\mu\nu} = \frac{1}{2}\left[\gamma^\mu,\gamma^\nu\right]$. The rest notations are standard. Using the first-order perturbation based on the S-matrix method one can get the expression for the hyperfine structure. Usually the transverse part of the photon propagator is defined as follows:

$$\frac{1}{4\pi}\frac{\delta_{12}}{|x1-x2|} \qquad (4)$$

But more consistent scheme is proposed in refs. [10,44] and consist in using (after transition to no-time diagrams) the following expression:

$$\frac{1}{4\pi}\frac{1}{|x1-x2|}\exp(i|\omega|x_{12})(1-\alpha_1\alpha_2) \qquad (5)$$

So, it allows to take into account the Breit effect (magnetic interaction). Further, as usually, the reduced matrix element in (6) can be divided on the electron part and on the Dirac part and the anomalous part for a nucleus. In order to define all parts the corresponding relativistic wave functions of the electron and single-particle states of a nucleus are required (look above).

Further let us consider the elements of calculating the PNC transition amplitude. The dominative contribution to the PNC amplitude is provided by the spin-independent part of the operator for a weak interaction, which should be added to the atomic Hamiltonian [5]:

$$H = H_{at} + \mu\sum_j H_W(j), \quad H_W^1 = \frac{G}{2\sqrt{2}}Q_W\gamma_5\rho(r), \quad (6)$$

Where -is the Fermi constant of the weak interaction, γ_5 —is the Dirac matrice, $\rho(r)$-is a density of the charge distribution in a nucleus and Q_W is a weak charge of a nucleus, linked with number of neutrons N and protons Z and the Weinberg angle θ_W in the Standard model (c.f. [1−3]):

$$Q_W = Z(1-4\sin^2\theta_W) - N \qquad (7)$$

With account for the radiative corrections, equation (7) can be rewritten as shown in refs.[5,18]:

$$Q_W = \{Z(1-[4.012\pm0.010]\sin^2\theta_W) - N\}\times$$
$$\times(0.9857\pm0.0004)(1+0.0078T)$$
$$\sin^2\theta_W = 0.2323 + 0.00365S - 0.00261T) \qquad (8)$$

The parameters S,T parameterize the looped corrections in the terms of conservation (S) and violation (T) of an isospin. The spin-dependent contribution to the PNC amplitude has three distinct sources: the nuclear anapole moment, the Z-boson exchange interaction from nucleon axial-vector currents $(A_n V_e)$, and the combined action of the hyperfine interac-

tion and spin-independent Z-boson exchange from nucleon vector $(V_n A_e)$ currents [7,9,34]. The anapole moment contribution strongly dominates. The above-mentioned interactions can be represented by the Hamiltonian

$$H_W^i = \frac{G}{\sqrt{2}}k_i(\alpha\cdot I)\rho(r) \qquad (9)$$

where k(i=a) is an anapole contribution, k(i=2)=k_{Z0}—axial-vector contribution, k(i=kh)=k_{Q_w} is a contribution due to the combined action of the hyperfine interaction and spin-independent Z exchange . The estimate of the corresponding matrix elements is in fact reduced to the calculation of the integrals as [10]:

$$<i|H_W^1|j> = i\frac{G}{2\sqrt{2}}Q_W\delta_{k_i-k_j}\delta_{m_i m_j}\times$$
$$\times\int_0^\infty dr[F_i(r)G_j(r)-G_i(r)F_j(r)]\rho(r) \qquad (10)$$

The general expression for the corresponding PNC amplitude for a-b transition is written as:

$$<a|PNC|b> =$$
$$= -\sum_n[\frac{<b|e\alpha_\nu A^\nu|n><n|H_W^{(1)}|a>}{\varepsilon_a - \varepsilon_n} +$$
$$+\frac{<b|H_W^{(1)}|n><n|e\alpha_\nu A^\nu|a>}{\varepsilon_b - \varepsilon_n} \qquad (11)$$

The corresponding spin-dependent PNC contribution is :

$$<a|PNC|b>^{sd} = k_a <a|PNC|b>^{(a)} +$$
$$+k_2 <a|PNC|b>^{(2)} + k_{hf} <a|PNC|b>^{(hf)} \qquad (12)$$

where
$$<a|PNC|b>^{(hf)} =$$

$$\sum_{\substack{m\neq a \\ n\neq a}} \frac{<a|H_W^{(1)}|n><n|H_W^{(hf)}|m><m|e\alpha_\nu A^\nu|b>}{(\varepsilon_a-\varepsilon_m)(\varepsilon_a-\varepsilon_n)} +$$

$$+\sum_{\substack{m\neq a \\ n\neq a}} \frac{<a|H_W^{(hf)}|n><n|H_W^{(1)}|m><m|e\alpha_\nu A^\nu|b>}{(\varepsilon_a-\varepsilon_m)(\varepsilon_a-\varepsilon_n)} +$$

$$+\sum_{\substack{m\neq a \\ n\neq b}} \frac{<a|H_W^{(1)}|m><m|e\alpha_\nu A^\nu|n><n|H_W^{(hf)}|m>}{(\varepsilon_a-\varepsilon_m)(\varepsilon_b-\varepsilon_n)} +$$

$$+\sum_{\substack{m\neq a \\ n\neq b}} \frac{<a|H_W^{(hf)}|m><m|e\alpha_\nu A^\nu|n><n|H_W^{(hf)}|b>}{(\varepsilon_a-\varepsilon_m)(\varepsilon_b-\varepsilon_n)} +$$

$$+\sum_{\substack{m\neq b \\ n\neq b}} \frac{<a|e\alpha_\nu A^\nu|n><n|H_W^{(1)}|m><m|H_W^{(hf)}|b>}{(\varepsilon_b-\varepsilon_m)(\varepsilon_b-\varepsilon_n)} +$$

$$+\sum_{\substack{m\neq b \\ n\neq b}} \frac{<a|e\alpha_\nu A^\nu|n><n|H_W^{(hf)}|m><m|H_W^{(1)}|b>}{(\varepsilon_b-\varepsilon_m)(\varepsilon_b-\varepsilon_n)} +$$

$$- <a|H_W^{(hf)}|a>\sum_{m\neq a} \frac{<a|H_W^{(1)}|m><m|e\alpha_\nu A^\nu|b>}{(\varepsilon_a-\varepsilon_m)^2} -$$

$$-\sum_{n\neq b} \frac{<a|e\alpha_\nu A^\nu|n><n|H_W^{(1)}|b>}{(\varepsilon_b-\varepsilon_n)^2}<b|H_W^{(hf)}|b>. \qquad (13)$$

Here the following notations are used: $|a>=|aIF_FM_F>$, $|b>=|bIF_IM_I>$, I — spin of a nucleus, $F_{I,F}$-is a total momentum of an atom and M — its z component (I,F are the initial and final states). It should be noted the expressions for the matrix elements $<a|PNC|b>^{(a)}$, $<a|PNC|b>^{(2)}$ are similar to Eq. (13). The full description of the corresponding matrix elements and other details of the general method are presented in refs.[4,10,39–44].

In table 1 we listed the values of the hyperfine structure (hfs) energy and magnetic moment (in nuclear magnetons) of nucleus in ^{207}Tl, calculated on the basis of different theoretical models [12–14]. In table 2 there are listed the PNC amplitudes (in units of $10^{-11}iea_B(-Q_W)/N$), which are calculated by the different methods (without the Breit corrections): DF, RHF, MCDF, many-body perturbation theory (MBPT) and

our nuclear-QED PT results (other data from refs. [25–34]). In table 3 we list the nuclear spin dependent corrections to the PNC ^{133}Cs: 6s-7s amplitude E_{PNC}, calculated by different theoretical methods (in units of the $k_{a,2,hf}$ coefficient): MBPT, DF-PT, the shell model, N-QED PT (present paper) (from refs. [9,27,28,34]).

Table 1
The hfs energy and magnetic moment (in nucl. magnetons) In ^{209}Pb, ^{207}Tl

	^{207}Tl			
Magn. moment [μ_N]	HS	NLC	Tomaselli	N-QED
Theory	1.8769	1.8758	1.6472	1.8764
Exp. [14]	1.8765(5)			
HFS[eV]	HS	NLC	Tomaselli	N-QED
ΔE^1_{HFS}	3,721	3,729	3,2592	3,5209
ΔE_{QED}		-0,0201	-0,0178	-0,0207
Total	3,701	3,708	3,2592	3,5002

Table 2
PNC amplitudes (in units of $10^{-11}iea_B(-Q_W)/N$), which are calculated by different methods (without the Breit corrections): DF, RHF, MCDF, MBPT and nuclear-QED PT.

Atom Trans.	Spin of Nucl.	Nucl. moment μ_N	Weak charge Q_W	Radius (fm) of nucleus	DF	RHF	MCDF	MBPT	N-QED (our data)
^{133}Cs 6s-7s	7/2	2.5826	-73.19	4.837	-0.741	-0.926 -0.897	-0.935 -0.905	-0.897 -0.904	-0.8985
^{223}Fr 7s-8s	3/2	1.1703	-128.08	5.640	-13.72	-16.63	-15.72	-15.49	-15.515

Table 3
The nuclear spin dependent corrections (in units of the $k_{a,2,hf}$ coefficient) to the PNC ^{133}Cs: 6s-7s amplitude E_{PNC}, calculated by different theoretical methods (see text).

Correction	MBPT	Shell model	DF	N-Qed PT
K (sum)	0.1169	0.1118	0.1102 0.1082	0.1159
k_2- the Z-boson exchange interaction from nucleon axial-vector currents (A_nV_e)	0.0140	0.0140	0.0111 0.0084	0.0138
k_{hf} — the combined action of the hyperfine interaction and spin-independent Z exchange	0.0049	0.0078	0.0071 0.0078	0.0067
k_a —anapole moment	0.0980	0.090	0.0920	0.0954

In table 4 there are presented the estimated values of the weak charge Q_W for different heavy atoms, predicted in different approaches (from refs. [18,27,28,34]). Let us underline that the correct values of the weak charge are firstly predicted by us for ^{205}Tl and ^{173}Yb atoms. The analysis of results shows that in principle a majority of theoretical approaches provides physically reasonable agreement with the Standard model data, but the important question is how much exact this agreement. However, the prйcised estimates indicate on the tiny deviation from the Standard model. In our opinion, now the most interesting subject is the rare-earth element. The corresponding value Q_W for Yb is listed. The heavy atoms and multicharged ions of Tm, Eu, Dy, Sn are now in consideration.

These elements have very complicated hyperfine structure and its spectrum of highly excited states is very dense. It is easily to understand that the distance between levels decreases exponentially with the number of excited particles. Respectively, according to the PT, this can lead to enhancement of small perturbations, e.g. electroweak interactions. Obviously, one could say about the statistical dynamical and possibly

Table 4
The estimated values of the weak charge Q_W for different heavy atoms, predicted in different approaches (from refs. [18,27,28,30,34]).

Atom:	Standard model	RHF+ Breit	MCDF	MBPT	N-QED (our data)
^{133}Cs	-73.19(13)	-72.66 -71.70	-69.78 -71.09	-72.69 -72.18	-72.62
^{205}Tl	-116.81(4)	-116.20	---	---	-116.15
^{173}Yb	-95.44(5)	---	---	---	-92.31

Note: Transition for Yb Yb $5p^64f^{14}6s^2$ $^1S_0$ -$5p^64f^{14}6s5d$ $^3D_1$;

quasi-elastic mechanisms. From other side, hitherto nobody has seen an enhancement in macroscopic systems with infinitely dense spectra. There are a few tiny explanations of the 'killing" this enhancement. However, the rare-earth elements have very interesting spectra of autoionization resonances (with very unusual from physical point of view their behavior in a weak electric and laser fields; the known effect of giant broadening [4]). The elementary comments shows that the perspectives of the PNC experiments with Stark pumping of the individual states in the rare-earth atoms (and probably more effective multicharged ions

of these elements) and simultaneously polarized laser field dressing (with a cold-atom fountain or interferometer) could provide comfortable conditions for observation of the weak effects. It is possible an existence of the dc Stark shift, arisen from the electroweak nuclear anapole moment violating P , but not T. It is characterized by the pseudo scalar $\xi k \wedge \mathbf{E} \cdot \mathbf{B}$ involving the photon angular moment and static electric and magnetic fields. In any case it's self-understood that only a prŭcised, experiment may make more clear this fundamental topic.

References

1. Grojean C., New approaches to electroweak symmetry breaking// Physics −Uspekhi. — 2007. — Vol.50. — P.3- 42; Review of Particle Properties, Particle Physics Booklet (AIP). — July, 1996.
2. Shabalin E. P., What future for CP- and T-violation studies and CPT-invariance tests?//Physics- Uspekhi. — 2001. — Vol.171. — P.951−976.
3. Grant I. P., Relativistic Quantum Theory of Atoms and Molecules. — Oxford, 2008. — 650P.
4. Glushkov A. V., Relativistic Quantum Theory. Quantum, mechanics of Atomic Systems. — Odessa: Astroprint, 2008. — 900P.
5. Khriplovich I. B., Parity Nonconservation in Atomic Phenomena. — Gordon and Breach, Philadelphia, 1999. — 250P.
6. Grojean C., New approaches to electroweak symmetry breaking// Physics-Uspekhi. — 2007. — Vol. 177. — P.3–42.
7. Khriplovich I. B., Discovery of anapole moment//Physics-Uspekhi. — 1997. — Vol.167. — 1214−1216.
8. Auerbach N., Search for electric dipole moments in atoms of radioactive nuclei// J. Phys. G: Nucl. Part. Phys. — 2008. — Vol.35. — P. 014040.
9. Safronova M. S., Rupsi Pal, Jiang D., Kozlov M. G., Johnson W. R., Safronova U. I., New directions in atomic PNC// Nucl. Phys.A. — 2009. — Vol.827. — P.411−413.
10. Khetselius O.Yu., Hyperfine structure of spectral lines of the heavy atoms and multicharged ions. — Odessa: Astroprint, 2008. — 210P.
11. Gaigalas G., Gaidamauskas E., Jonsson P., Multiconfiguration Dirac-Hartree-Fock calculations for the hyperfine-structure parameters and the scalar-pseudoscalar interaction constant of ^{133}Cs// Journal of Physics CS. — 2008. — Vol.130. — P.012008.
12. Nagasawa T., Haga A., Nakano M., Hyperfine splitting of hydrogenlike atoms based on relativistic mean field theory// Phys.Rev.C. — 2004. — Vol.69. — P. 034322:1−10.
13. Bouchiat M. A., Linear Stark effect in dressed atoms as a signal to measure a nuclear anapole moment with a cold-atom fountain or interferometer// Phys.Rev.Lett. — 2007. — Vol.98. — P.043003.
14. Tomaselli M., Kuhl T., Seelig P., Holbrow C. and Kankeleit E., Hyperfine splittings of hydrogenlike ions and the dynamic-correlation model for one-hole nuclei// Phys.Rev.C. — 1998. — Vol.58, N3. — P.1524−1534.
15. Tomaselli M., Schneider S. M., Kankeleit E., Kuhl T., Ground state magnetization of ^{209}Bi in a dynamic-correlation model// Phys.Rev.C. — 1995. — Vol.51, N6. — P.2989−2997.
16. Labzowsky L. N., Johnson W. R., Soff G., Schneider S. M., Dynamic proton model for the hyperfine structure of H-like ion ^{209}Bi^{+82}// Phys.Rev.A. — 1995. — Vol.51, N6. — P.4597−4602.
17. Bieron J., Pyykko P., Degree of accuracy in determining the nuclear electric quadrupole moment of radium//Phys.Rev. A. — 2005. — Vol.71. — P.032502.
18. Porsev S. G., Rakhlina Yu.G., Kozlov M. G., Non-conservation of spatial parity in atomic ytterbium// JETP Lett. — 1999. — Vol.61. — P.449−453.
19. Dzuba V. A., Flambaum V. V., Sushkov O. P., Polarizabilities and parity nonconservation in the Cs atom and limits on the deviation from the standard electroweak model//Phys. Rev.A. — 1999-Vol.56. — P.R4357−4360.
20. Safronova M. S., Johnson W. R., Derevianko A. Relativistic many-body calculations of energy levels, hyperfine constants, electric-dipole matrix elements, and static polarizabilities for alkali-metal atoms//Phys.Rev.A. — 1999. — Vol.60. — P.044103.
21. Bennett S. C., Roberts J. L., Wieman C. E., Measurement of the dc Stark shift of the $6S$-$7S$ transition in atomic caesium// Phys.Rev.A. — 1999. — Vol.59. — P.3254−3260.
22. Dzuba V. A., Flambaum V. V., Off-diagonal hyperfine interaction and parity nonconservation in cesium// Phys.Rev.A. — 2000. — Vol.62. — P.052101.
23. Johnson W. R., Bednyakov I., Soff G., Vacuum-polarization corrections to the parity-nonconserving $6s$-$7s$ transition amplitude in ^{133}Cs//Phys.Rev.Lett. — 2001. — Vol.87. — P. 233001.
24. Dzuba V. A., Harabati C., Johnson W. R., Safronova M. S., Breit correction to the parity-nonconservation amplitude in cesium//Phys.Rev.A. — 2001. — Vol.63. — P.044103.
25. Kozlov M. G. , Porsev S. G., Tupitsyn I. I., High-Accuracy calculation of $6s$-$7s$ parity-nonconserving amplitude in Cs// Phys.Rev.Lett. — 2001. — Vol.86. — P.3260−3263.
26. Johnson W. R., Sapistein J., Blundell S. A., Atomic structure calculations associated with PNC experiments in atomic caesium // Phys. Scripta T. — 1999. — Vol.46. — P.184−192.
27. Vasilyev A. A., Savukov I. M., Safronova M. S., Berry H. G., Measurement of $6s$-$7p$ transition probabilities in atomic Cs and revised value for the weak charge Q_W// Phys.Rev.A. — 2002. — Vol. 66. — P.020101.
28. Johnson W. R., Safronova M. S., Safronova U. I., Combined effect of coherent Z exchange and hyperfine interaction in parity-nonconserving interaction//Phys.Rev.A-2003. — Vol. 67. — P.062106.
29. Shabaev V. M., Tupitsyn I. I., Pachucki K., Plunien G., Yerokhin V. A., Radiative and correlation effects and parity-nonconserving transition amplitude in heavy alkali-metal atoms// Phys.Rev.A. — 2005. — Vol.72. — P.062105.
30. Safronova M. S., Johnson W. R., Safronova U. I., Cowan T.E., Relativistic many-body theory calculation of the Stark-induced amplitude of the 6p-7p transition in thalium// Phys.Rev.A. — 2006. — Vol.74. — P.022504.
31. Dzuba V. A., Flambaum V. V., Safronova M. S., Breit interaction and parity-nonconservation in many-electron atoms// Phys.Rev.A. — 2006. — Vol.73. — P.022112.
32. Glushkov A. V., Ambrosov S. V., Khetselius O.Yu., et al, QED calculation of the super heavy elements ions: energy levels, radiative corrections and hfs for different nuclear models// Nucl. Phys.A.: Nucl.and Hadr. Phys. — 2004. — Vol.734. — Pe 21−28.
33. Kuchiev M.Yu., Flambaum V. V., Radiative corrections to parity nonconservation in atoms and test of the standard model// J. Phys. B. — 2003. — Vol.36. — P. R191−222.
34. Johnson W. R., Safronova M. S., Safronova U. I., Combined effect of coherent Z exchange and the hyperfine interaction in the atomic parity-non-conserving interaction// Phys. Rev. A. — 2003. — Vol.67. — P.062106.
35. Serot B. D., Walecka J. D. , Advances in Nuclear Physics Vol. 16: The Relativistic Nuclear Many Body Problem. Plenum Press, New York, 1996.
36. Sahoo B. K., Gopakumar G., Chaudhuri R. K. , Das B. P., Merlitz H., Mahapatra U. S., Makherjee D., Magnetic dipole hyperfine interactions in ^{137}Ba$^+$ and the accuracies of neutral weak interaction matrix elements//Phys.Rev.A-2003. — Vol.68. — P.040501.
37. Derevianko A., Porsev S. G., Dressing lines and vertices in calculations of matrix elements with the coupled-cluster method and determination of Cs atomic properties// Phys. Rev. A. — 2005. — Vol.71. — P.032509.
38. Glushkov A. V., Khetselius O.Yu., Ambrosov S. V. et al, QED calculation of heavy ions with account for the correlation, radiative and nuclear effects// Recent Advances in Theory of Phys. and Chem. Systems (Berlin, Springer). — 2006. — Vol.15. — P.285−300.
39. Glushkov A. V., Khetselius O.Yu., Lovett L., et al, Gauge-invariant QED perturbation theory approach to calculating nuclear electric quadrupole moments, hyperfine structure constants for heavy atoms and ions// Frontiers in Quantum Systems in Chemistry and Physics (Berlin, Springer). — 2008. — Vol.18. — P.505−522.
40. Khetselius O.Yu., On sensing nuclei of the lanthanide isotopes by means of laser spectroscopy of hyperfine structure ^{165}Ho, ^{169}Tm// Sensor Electr. Microsyst. Techn. — 2008. — N2. — P.5−9.

41. Khetselius O.Yu., On possibility of sensing nuclei of the rare isotopes by means of laser spectroscopy of hyperfine structure// Sensor Electr. Microsyst. Techn. — 2008. — N3. — P.28–33.
42. Khetselius O.Yu., Relativistic calculating the hyperfine structure parameters for heavy-elements and laser detecting the isotopes and nuclear reaction products//Phys. Scripta T. — 2009. — Vol.135. — P. 014023.
43. Khetselius O.Yu., On sensing nuclei of the [207]Bi &[207]Pb isotopes by means of laser spectroscopy of hyperfine// Sensor Electr. and Microsyst. Techn. — 2009. — N2. — P.26–29.
44. Khetselius O.Yu., Relativistic perturbation theory calculation of the hyperfine structure parameters for some heavy-element isotopes//Int. Journ. of Quantum Chemistry. — 2009. — Vol.109. — P. 3330–3335.

O. Yu. Khetselius

NUCLEAR-QED THEORY OF HYPERFINE, ELECTROWEAK, PARITY NON-CONSERVATIVE EFFECTS IN HEAVY ATOMS, NUCLEI AND NEW STARK PUMPING PNC EXPERIMENTS

Abstract.
The combined QED perturbation theory formalism and relativistic nuclear mean-field theory are applied to studying the fundamental parameters of the hyperfine, electroweak, parity non-conservation (PNC) interactions in heavy atoms, nuclei. There are firstly predicted the nuclear weak charged for some atoms and new objects for the PNC Stark pumping experiments with cold-atom fountain are noted.
Key words: hyperfine structure, electroweak interaction, parity non-conservation, heavy atoms and nuclei, nuclear-QED theory

О. Ю. Хецелиус

ЯДЕРНО-КЭД ТЕОРИЯ СВЕРХТОНКИХ, ЭЛЕКТРОСЛАБЫХ, НЕСОХРАНЕНИЯ ЧЕТНОСТИ ЭФФЕКТОВ В ТЯЖЕЛЫХ АТОМАХ, ЯДРАХ И НОВЫЕ PNC ЭКСПЕРИМЕНТЫ С ШТАРКОВСКОЙ НАКАЧКОЙ

Резюме.
КЭД теории возмущений и релятивистская ядерная теория среднего поля использованы для изучения параметров сверхтонкого, электрослабого, не сохраняющего четность взаимодействий в тяжелых атомах, ядрах. Впервые предсказаны значения слабого заряда ядра для ряда атомов и указаны новые возможности PNC экспериментов с штарковской накачкой (фонтан холодных атомов).
Ключевые слова: сверхтонкое, электрослабое взаимодействие, несохранение четности, тяжелые атомы и ядра, ядерно-КЭД теория, эксперименты с штарковской накачкой

О. Ю. Хецеліус

ЯДЕРНО-КЕД ТЕОРІЯ НАДТОНКИХ, ЕЛЕКТРОСЛАБКИХ, НЕЗБЕРЕЖЕННЯ ПАРНОСТІ ЕФЕКТІВ У ВАЖКИХ АТОМАХ, ЯДРАХ ТА НОВІ PNC ЕКСПЕРИМЕНТИ З ШТАРКІВСЬКОЮ НАКАЧКОЮ

Резюме.
КЕД теорія збурень і релятивістська ядерна модель середнього поля використані для визначення параметрів надтонкої, електрослабкої взаємодії та ефекту незбереження парності у важких атомах, ядрах. Вперше передбачені значення слабкого заряду ядра для ряду атомів и указані нові можливості PNC експериментів з штарківською накачкою (фонтан холодних атомів).
Ключові слова: надтонка, електрослабка взаємодія, незбереження парності, важкі атоми та ядра, ядерно-КЕД теорія, експерименти з штарківською накачкою

F. O. PTASHCHENKO

Odessa National Maritime Academy, Odessa, Didrikhsona St., 8, Odessa, 65029, Ukraine

CHARACTERISTICS OF SILICON TRANSISTORS AS GAS SENSORS

The influence of ammonia and water vapors on *I-V* characteristics of the forward and reverse emitter—collector, base—collector and emitter—base currents as well as on the kinetics of the corresponding currents in silicon transistors was studied. The gas sensitivity of the transistors is much higher than the sensitivity of silicon *p-n* junctions. This effect is due to formation of a surface conductive channel, which shorts the base—collector junction. A similar channel in the emitter—base junction decreases the amplification factor of the transistor and the gas sensitivity at low bias voltages. The sensitivity of the transistors to ammonia vapors is much higher than to water vapors. The response time of the sensors at room temperature is of 100 s.

1. INTRODUCTION

Gas sensors on *p-n* junctions [1, 2] have some advantages in comparison with these, based on oxide polycrystalline films [3] and Schottky diodes [4]. *P-n* junctions in wide-band semiconductors have high potential barriers for charge carriers, which results in low background currents, high sensitivity and selectivity to the gas components [5, 6].

The advantage of silicon *p-n* junctions as gas sensors is that they are compatible with silicon amplifying elements. Characteristics of *p-n* junctions in silicon as gas sensors were studied in previous works [7—9]. It was shown that the gas sensitivity of silicon *p-n* structures at forward biases is caused by enhancing of surface recombination, as a result of band bending in *p*-region, due to electric field of adsorbed ions. The gas sensitivity of studied *p-n* structures at reverse biases is due to forming of a surface conductive channel which shorts the *p-n* junction.

The purpose of this work is a comparative study of the influence of ammonia and water vapors on stationary *I—V* characteristics of emitter—collector, base—collector and emitter—base junctions in silicon planar transistors, as well as on the kinetics of corresponding currents.

2. EXPERIMENT

The measurements were carried out on silicon *n-p-n* and *p-n-p* transistors of the structure shown in fig 1. The *n* regions were doped with phosphorus and *p* regions with boron. The top surface was not cowered, so there was only a natural oxide layer.

The effect of vapors over water solutions of several NH$_3$ concentrations and over distilled water was studied on stationary *I-V* characteristics, as well as on the current kinetics in transistors. The sensitivity of the *n-p-n* transistors was higher than *p-n-p* ones.

I—V characteristics of the emitter-collector current of an *n-p-n* transistor in air with ammonia vapors of partial pressures 100Pa, 200Pa and 500Pa are presented in fig. 2 with curves 1, 2 and 3, respectively. Curve 4 was measured in water vapors at a pressure of 2000 Pa. The ordinates of curve 4 are multiplied

by 10. The measurements in dry air give currents $I < 10^{-9}$ A.
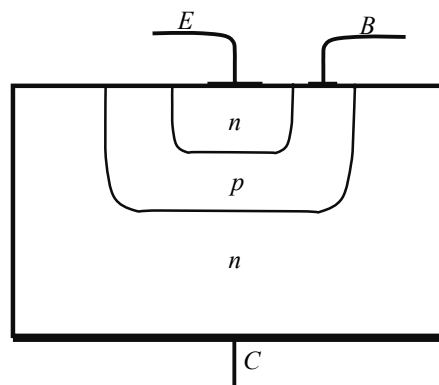
Fig. 1. Structure of the transistor.

The (absolute, current-) sensitivity of a gas sensor can be defined as

$$S_I = \Delta I / \Delta P , \qquad (1)$$

where ΔI is the change in the current (at a fixed voltage), which is due to a change ΔP in the corresponding gas partial pressure [10]. An analysis of the data, presented in fig. 2, gives for the sensitivity of the transistor to ammonia vapors at a voltage of 4V an estimation $S \simeq 1.3$ mA/kPa, while for the silicon *p-n* junctions S=20 µA/kPa [9]. The transistor works as a gas sensor with inherent amplification.

An analogous analysis of the curve 4 in fig. 2 gives for the sensitivity to water vapors an estimation of S=3 µA/kPa. Thus, the sensor is gas-selective. The sensitivity of the transistor to ammonia vapors is ~400 times higher than to water vapors.

I—V curves in fig. 2 are nonlinear. The sensitivity at low bias voltages up to 1V is much lower than at higher biases.

Fig. 3 illustrates the kinetics of the emitter—collector current in the transistor after let in- and out of ammonia vapors with a partial pressure of 500 Pa. The response time t_r for current rise was estimated as the duration of the current increase to 90% of its stationary value after letting in the vapor into the container with the sample. And the decay time t_d was obtained in a similar way, for the current decrease from the sta-

tionary value to 10% of it. An analysis of the data, presented in fig. 3, gives $t_r \approx 80$s and $t_d \approx 10$s. A comparison with the data, obtained in the previous work [9], show that the response time of the transistor as gas sensor is higher than that of the silicon diode sensor. And decay time of the both sensors is practically the same.
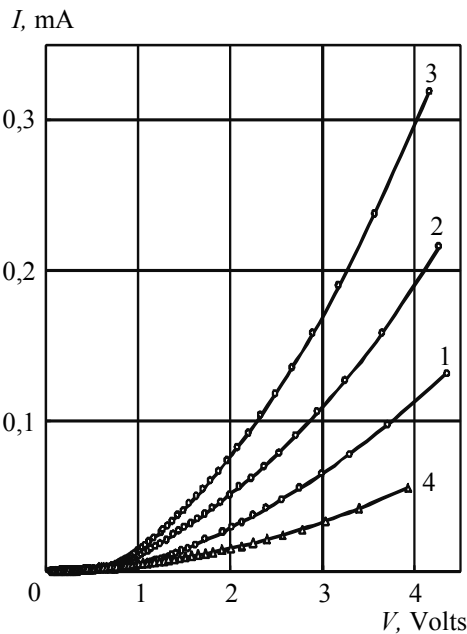
Fig. 2. I–V characteristics of the emitter-collector current of n-p-n transistor in ammonia vapors of partial pressures: 1 – 100Pa; 2 – 200Pa; 3 –500Pa, and in water vapors of pressure 2000 Pa (4). The ordinates of curve 4 are multiplied by 10.
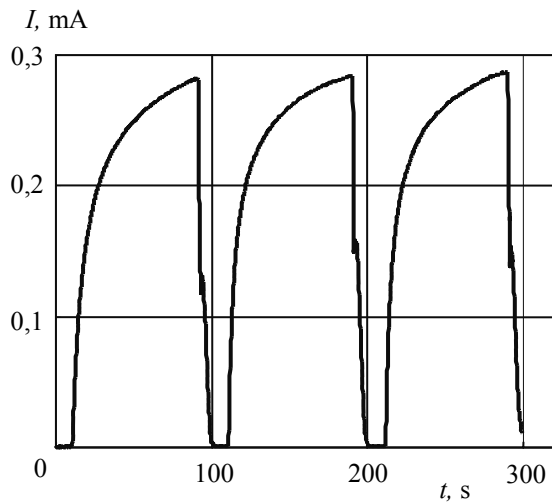
Fig. 3. Kinetics of the emitter–collector current after let in- and out of ammonia vapors with a partial pressure of 500 Pa.

3. DISCUSSION

In order to verify the mechanism of the gas sensitivity of the transistors, I–V characteristics of emitter–base forward current and of base–collector reverse current were measured. The results of these measurements are shown in fig. 4. I-V characteristic of the forward current in the emitter–base junction, placed in dry air, is presented as curve 1 in Fig. 4. I–V curve can be described with the expression

$$I(V) = I_0 \exp[qV / (nkT)] , \qquad (2)$$

where I_0 is a constant; q is the electron charge; V denotes bias voltage; k is the Boltzmann constant; T is temperature; $n \approx 1.1$ is the ideality constant. Some deviation from the value $n=1$ can be ascribed to recombination on deep levels in p-n junction and at the surface [11].

Curve 2 in Fig. 4 is the emitter–base characteristic, obtained in air with ammonia vapors of partial pressure 500Pa. A comparison between curves 1 and 2 shows that ammonia vapors change the emitter base characteristic only at low biases, where $I \leq 50$nA and $V \leq 0.5$Volts . The additional current due to ammonia molecules adsorption linearly depends on the voltage.
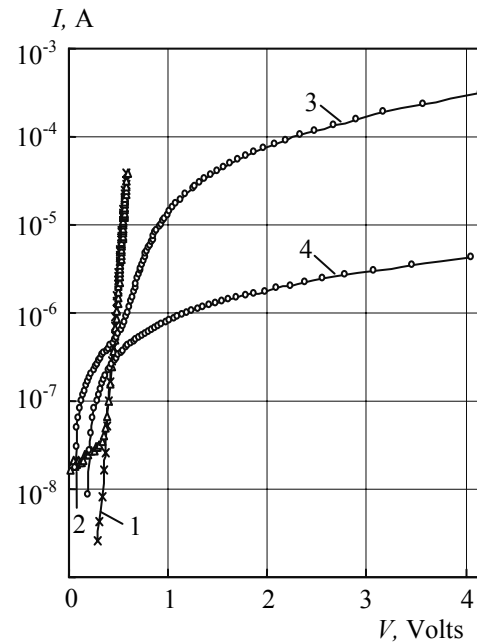
Fig. 4. I–V characteristics of the n-p-n transistor: 1, 2 – emitter–base forward currents in dry air and ammonia vapors, respectively; 3, 4 – emitter-collector and base–collector currents, accordingly. The ammonia partial pressure was of 500Pa.

Curves 3 and 4 in fig. 4 present the emitter–collector and base–collector characteristics, respectively, measured in ammonia vapors with a partial pressure of 500 Pa. The currents, obtained in dry air, were of 10^{-9}A. Curve 4 is similar to I–V characteristics of the reverse current in silicon p-n junctions in ammonia atmosphere [7–9]. A comparison between curves 3 and 4 shows, that the additional current, due to ammonia molecules adsorption, is strongly amplified in the transistor.

Fig. 5 schematically presents the influence of adsorbed donor molecules on the charge carrier distribution in the n-p-n transistor. The emitter-base and base- collector junctions cross the crystal surface, cowered by natural oxide layers 1 and 2, respectively. Adsorbed molecules are ionized and form layers of positive charge 3 and 4. The electric field of ions bends depletion regions 5 and 6 in emitter–base and base–collector junctions and forms, under a high enough ions surface density, conducting channels 7 and 8. The conductivity of the channels is enhanced with increasing surface charge.

The equivalent scheme of the transistor with adsorbed ions on the surface is shown in fig 6. The

conductive channel in the base−collector junction is presented by nonlinear resistor R_{BC}. The dependence $R_{BC}(V_{BC})$ under a fixed ammonia partial pressure is determined by curve 4 in fig. 3. The channel in the emitter−base junction is presented with resistor R_{EB}.
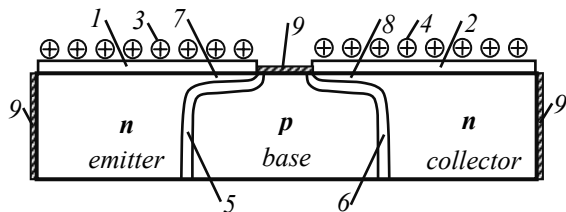
Fig. 5. Schematic of the n-p-n transistor in NH3 atmosphere: 1, 2 − oxide layers; 3, 4 − adsorbed ions; 5, 6 − depleting regions; 7, 8 − conductive n-channels; 9 − metallic contacts.
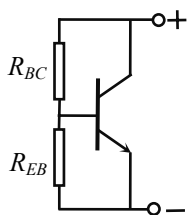
Fig, 6. The equivalent scheme of the n-p-n transistor with adsorbed positive ions.

An analysis of curve 2 in fig. 4 yields $R_{EB} = 1.4\text{MOhm}$. It is seen from fig. 6 that the conductive channel in emitter−collector junction, represented as resistor R_{EB}, decreases the amplification factor of the transistor. This explains the observed small gas sensitivity of the transistor at low bias voltages ($V<0.5\text{Volts}$). At higher voltages the injection current in the emitter−base junction is much higher than in resistor R_{EB} (in the surface channel), and the amplification factor is high.

The amplification factor of the sensor is $\beta = 74$ at a voltage of 4 Volts and $\beta = 17$ at $V=1\text{Volt}$. The observed decrease in the amplification factor at lowering voltage can be explained by the effect of the recombination at deep levels in the depletion region of the emitter−base junction.

4. CONCLUSIONS

The gas sensitivity of silicon transistors is much higher than the sensitivity of silicon p-n junctions. This effect is due to formation of a surface conductive channel, which shorts the base−collector junction. The resistance of this channel decreases with increasing vapors partial pressure. The current of this channel is amplified in the transistor. A similar channel in the emitter−base junction decreases the amplification factor of the transistor and the gas sensitivity at low bias voltages.

The sensitivity of transistors to ammonia vapors is much higher than to water vapors, which can be explained taking into account donor properties of ammonia molecules at the silicon surface.

The response time of the sensor at room temperature is of 100 s.

References

1. Ptashchenko O. O., Artemenko O. S., Ptashchenko F. O. Vliyanie gazovoi sredy na poverhnostnyi tok v p-n geterostrukturakh na osnove GaAs-AlGaAs // Fisika i khimiya tverdogo tila. — 2001. — V. 2, № 3. — P. 481 − 485.
2. Ptashchenko O. O., Artemenko O. S., Ptashchenko F. O. Vplyv pariv amiaku na poverkhnevyi strum v p-n perekhodakh na osnovi napivprovidnykiv A^3B^5 // Journal of physical studies. — 2003. — V. 7, №4. — P. 419 − 425.
3. Bugayova M. E., Koval V. M., Lazarenko B. I. et al. Gazovi sensory na osnovi oksydu tsynku (oglyad) // Sensorna electronika i mikrosystemni tehnologii. — 2005. — №3. — P. 34
4. Baluba V. I., Gritsyk V. Y., Davydova T. A. et al. Sensory ammiaka na osnove diodov Pd-n-Si // Fizika i tekhnika poluprovodnikov. — 2005. — V. 39, № 2. P. 285 − 288.
5. Ptashchenko O. O., Artemenko O. S., Dmytruk M. L. et al. Effect of ammonia vapors on the surface morphology and surface current in p-n junctions on GaP. // Photoelectronics. — 2005. — No. 14. — P. 97 − 100.
6. Ptashchenko F. O. Effect of ammonia vapors on surface currents in InGaN p-n junctions. // Photoelectronics. — 2007. — No. 17. — P. 113 − 116.
7. Ptashchenko F. O. Vplyv pariv amiaku na poverkhnevyi strum u kremniyevykh p-n perekhodakh // Ptashchenko F. O. Visnyk ONU, ser. Fizyka. — 2006. — V. 11, №. 7. — P. 116 − 119.
8. Ptashchenko O. O., Ptashchenko F. O., Yemets O. V. Effect of ammonia vapors on the surface current in silicon p-n junctions. // Photoelectronics. — 2006. — No. 16. — P. 89 − 93.
9. Ptashchenko O. O., Ptashchenko F. O., Yemets O. V. Effect of ambient atmoswphere on the surface current in silicon p-n junctions // Photoelectronics. — 2009. — No. 18. — P. 28 − 32.
10. Vashpanov Yu. A., Smyntyna V. A. Adsorbtsionnaya chuvstvitel'nost' poluprovodnikov. — Odessa: Astroprint, 2005. — 216 p.
11. Ptashchenko A. A., Ptashchenko F. A. Tunnel surface recombination in p-n junctions // Photoelectronics. — 2000. — № 10. — P. 69 − 71.

F. O. Ptashchenko

CHARACTERISTICS OF SILICON TRANSISTORS AS GAS SENSORS

Abstract
The influence of ammonia and water vapors on *I-V* characteristics of the forward and reverse emitter−collector, base−collector and emitter−base currents as well as on the kinetics of the corresponding currents in silicon transistors was studied. The gas sensitivity of the transistors is much higher than the sensitivity of silicon *p-n* junctions. This effect is due to formation of a surface conductive channel, which shorts the base−collector junction. A similar channel in the emitter−base junction decreases the amplification factor of the transistor and the gas sensitivity at low bias voltages. The sensitivity of the transistors to ammonia vapors is much higher than to water vapors. The response time of the sensors at room temperature is of 100 s.

Key words: silicon transistors, gas sensors.

Ф. О. Птащенко

ХАРАКТЕРИСТИКИ КРЕМНІЄВИХ ТРАНЗИСТОРІВ ЯК ГАЗОВИХ СЕНСОРІВ

Резюме

Досліджено вплив парів аміаку і води на ВАХ прямого і зворотного струмів емітер–колектор, база–колектор та емітер–база, а також на кінетику відповідних струмів у кремнієвих транзисторах. Газова чутливість транзисторів набагато вища, ніж чутливість кремнієвих *p-n* переходів. Даний ефект обумовлений формуванням поверхневого провідного каналу, який закорочує *p-n* перехід база–колектор. Подібний канал в переході емітер–база зменшує коефіцієнт підсилення транзистора і його газову чутливість при низьких напругах зміщення. Чутливість транзисторів до парів аміаку значно вища, ніж до парів води. Час спрацювання сенсорів при кімнатній температурі не перевищує 100 с.

Ключові слова: кремнієві транзистори, газові сенсори.

Ф. А. Птащенко

ХАРАКТЕРИСТИКИ КРЕМНИЕВЫХ ТРАНЗИСТОРОВ КАК ГАЗОВЫХ СЕНСОРОВ

Резюме

Исследовано влияние паров аммиака и воды на ВАХ прямого и обратного токов эмиттер–коллектор, база–коллектор и эмиттер–база, а также на кинетику соответствующих токов в кремниевых транзисторах. Газовая чувствительность транзисторов намного выше, чем чувствительность кремниевых *p-n* переходов. Данный эффект обусловлен формированием поверхностного проводящего канала, который закорачивает *p-n* переход база–коллектор. Подобный канал в переходе эмиттер–база уменьшает коэффициент усиления транзистора и его газовую чувствительность при низких напряжениях смещения. Чувствительность транзисторов к парам аммиака значительно выше, чем к парам воды. Время срабатывания сенсоров при комнатной температуре не превышает 100 с.

Ключевые слова: кремниевые транзисторы, газовые сенсоры.

V. A. BORSCHAK, M. I. KUTALOVA, V. A. SMYNTYNA, A. P. BALABAN, YE. V. BRYTAVSKYI, N. P. ZATOVSKAYA

Odessa I. I. Mechnikov National University,
2, Dvoryanskaya str., Odessa, 65082, Ukraine
Phone: +380(48)7266356, Fax: +380(48)7233461, e-mail: borschak_va@mail.ru

NONIDEAL HETEROJUNCTION CONDUCTIVITY

CdS-Cu$_2$S heterojunction conductivity both on continuous, and on an alternating current strongly depends on barrier parameters which can vary under illumination influence. It is established, that space charge region resistance essentially depends on its width (this dependence is close to linear) at fixed barrier height. It can testify to prevalence of tunnel multistage mechanisms of transfer over researched structure, for example, tunnel-jumping conductivity

Nonideal heterojunction basic photo-electric characteristics impossible to explain without the assumption of a determining role differing from thermoemission mechanisms current through space charge region (SCR) carry [1, 2]. Such mechanisms usually have tunnel character. In this connection, detailed studying SCR parameters influence on heterojunction conductivity is very important, as allows to specify the losses mechanism in heterophotoelements. Especially interesting seems the investigation of barrier region conductivity dependence on its width in connection with the assumption currenttransport tunnel character. We shall consider, for example rather popular in one's time typical nonideal heterojunction CdS-Cu$_2$S.

It is established, that the barrier width concentrated in more wideband CdS effectively can be changed by light from cadmium sulfide intrinsic absorption region [3, 4], where in a short circuit current mode (no voltage bias) Fermi level position in quasineutral region is a constant value, not dependent on illumination intensity. In these conditions the barrier height does not change and it is possible to determine conductivity dependence solely on SCR width.

With this purpose the heterojunction current-voltage characteristics (CVC) were received at illumination it by various intensity light with $\lambda < 620$ nm (FIG. 1). A curve measured at various illumination levels has various heterojunction photocapacity values (C$_{ph}$). It is visible, that with photocapacity growth and, hence, SCR extent reduction, at constant barrier height in point U=0 junction differential resistance decreases considerably.

Investigation conductivity active component on an alternating current (f=20kHz) were carried out by a compensation method with the use of the alternating current bridge by which the junction capacity also has been measured, at that the signal measuring amplitude did not exceed 5 mV. If for each photocapacity value to calculate the barrier width it is possible to construct its conductivity or resistance dependence on extent for alternating or a continuous current (FIG. 2). In the latter case the heterojunction resistance analysis for zero bias determined from CVC shows (fig. 1) that with SCR width increase its resistance as on continuous (curve 2), and on alternating (curve 1) currents

grows, remaining, however, on an alternating current essential smaller then stationary value, what is rather typical for tunnel-jumping transport mechanism [5].
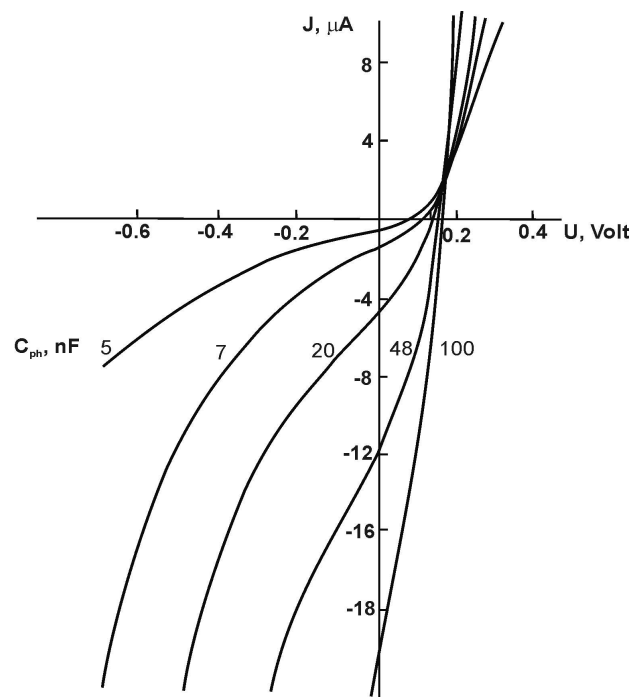
FIG. 1. CVC of CdS-Cu$_2$S heterojunction at various photocapacity values appropriate to various light levels exposure by light from CdS intrinsic absorption region.

The given curves are not exponential, and find out much weaker dependence which is coming most likely to linear, that also testifies most likely the multistage transport mechanism, but not direct tunneling.

Dependences CdS-Cu$_2$S heterojunction conductivity on continuous and alternating current on the applied bias value at various light levels exposure are given in FIG. 3. Though at illumination intensity growth conductivity always increase, however this growth for the big and small biases can be caused by the different reasons. From FIG. 3 it is visible, that at enough big biases conductivity on continuous and an alternating current differs much less, than at small biases. It can testify that with increase of an external continu-

ous voltage in the current restriction series resistance begins to play an essential role in CdS base layer which conductivity is determined by free carriers, is not connected with the transport on the located states and does not depend therefore on a measuring signal frequency. Saturation of characteristics $G=G(U)$ also testifies to it at biases close to barrier amount value.
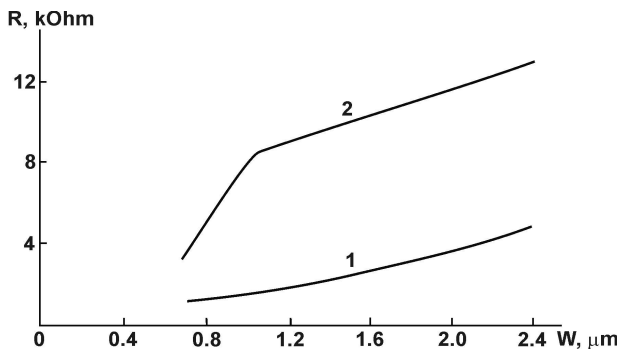
FIG. 2. Dependence of heterojunction resistance on continuous (curve 1) and alternating (f = 20 kHz, curve 2) current.
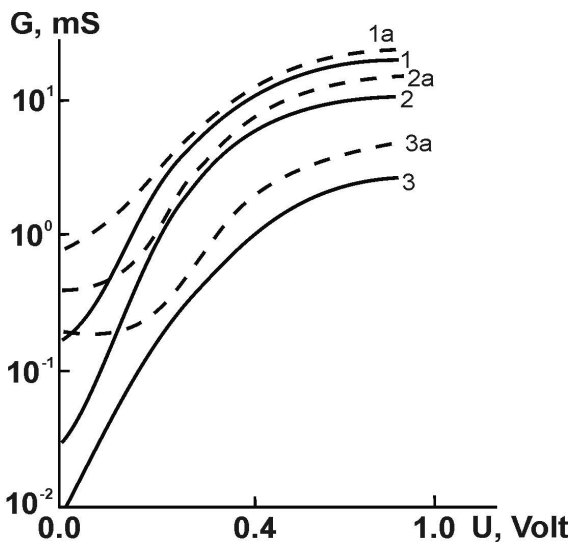
FIG. 3. Dependence of conductivity on continuous (solid curves) and alternating (dotted curves) current on positive bias value at various levels of illumination (1 and 1a- 100 rel. un.; 2 and 2a — 20 rel. un.; 3 and 3a — 2 rel. un.).

At stimulating light large intensities change to ohmic current on voltage dependence occurs at lower biases. Conductivity growth at illumination for large voltage, apparently, is caused by CdS base layer conductivity increase, and for small — barrier region conductivity growth due to SCR width reduction. As it was marked above, the measuring signal amplitude made units of millivolt, that is much less then the external bias voltage and a measuring signal did not influence on a barrier parameters. At the absence of external bias the difference between conductivity on continuous and alternating current is maximal, as in this case the running current is determined almost exclusively by a barrier height and width which conductivity can be caused by the frequency-dependent mechanism of transport on the located states [5]. Such $G=G(U)$ dependence character can results in anomalies CdS-Cu_2S volt-farad characteristics for positive biases because of measuring alternating signal voltage drop redistribution inter photo cell various layers at reduction junction resistance with the applied continuous voltage growth.

Thus, conductivity at rather small biases depends not only on height, but also on barrier width and can be determined by tunnel-recombination transport mechanism. Nonideal heterojunction conductivity both on continuous, and on an alternating current strongly depends on the barrier parameters, which can vary under illumination. Such dependence testifies to prevalence tunnel-recombination transport mechanism.

Reference

1. V. A. Borshchak, D. L. Vasilevskii. Influence of the behavior of the Fermi level on calculation of a tunnel-recombination current in a heterojunction. — Sov. Phys. Semicond., 1999, v. 23, No 11, pp. 1285–1287.
2. D. L. Vassilevski, V. A. Borschak The conductivity mechanism for thin film heterojunction. — 6th international conference on solid film and surfaces ICSFS-6, 1998, Paris, France.
3. D. L. Vassilevski, M. S. Vinogradov, V. A. Borscak, "Photon induced modulation of surface barrier: investigation and application for a new image sensor", Applied Surface Science, Dec.1996, 103(4), p.383–389.
4. D. L. Vassilevski. "Physical principles of graphic registration by non-ideal heterojunction", Sensors and Actuators, A 55, 1999 p.167–172.
5. N. F. Mott and E. A. Davis. "Electronic Processes in Non-Crystalline Materials". — "Clarendon Press". — Oxford. — 1999. — p. 437

V. A. Borschak, M. I. Kutalova, V. A. Smyntyna, A. P. Balaban, Ye. V. Brytavskyi, N. P. Zatovskaya

NONIDEAL HETEROJUNCTION CONDUCTIVITY

Abstract

CdS-Cu_2S heterojunction conductivity both on continuous, and on an alternating current strongly depends on barrier parameters which can vary under illumination influence. It is established, that space charge region resistance essentially depends on its width (this dependence is close to linear) at fixed barrier height. It can testify to prevalence of tunnel multistage mechanisms of transfer over researched structure, for example, tunnel-jumping conductivity

Key words: heterojunction, barrier, tunnel — jumping conductivity

В. А. Борщак, М. І. Куталова, В. А Сминтина, А. П. Балабан, Є. В. Бритавський, Н. П. Затовська

ПРОВІДНІСТЬ НЕІДЕАЛЬНОГО ГЕТЕРОПЕРЕХОДУ

Резюме

Провідність гетероструктури $CdS-Cu_2S$ як на постійному, так і на змінному струмі сильно залежить від параметрів бар'єра, які можуть мінятися під впливом освітлення. Встановлено, що опір області просторового заряду істотно залежить від її ширини (ця залежність близька до лінійної) при незмінній висоті бар'єра. Це може свідчити про перевагу тунельних багатоступінчатих механізмів переносу в структурі, що досліджується, наприклад, тунельно-стрибкової провідності.

Ключові слова: гетероперехід, бар·єр, тунельно — стрибкова провідність.

В. А. Борщак, М. И. Куталова, В. А Смынтына, А. П. Балабан, Е. В. Бритавский, Н. П. Затовская,

ПРОВОДИМОСТЬ НЕИДЕАЛЬНОГО ГЕТЕРОПЕРЕХОДА

Резюме

Проводимость гетероструктуры $CdS-Cu_2S$ как на постоянном, так и на переменном токе сильно зависит от параметров барьера, которые могут меняться под действием освещения. Установлено, что сопротивление области пространственного заряда существенно зависит от ее ширины (эта зависимость близка к линейной) при неизменной высоте барьера. Это может свидетельствовать о преобладании туннельных многоступенчатых механизмов переноса в исследуемой структуре, например, туннельно-прыжковой проводимости.

Ключевые слова: гетеропереход, баръер, тунельно — прыжковая проводимость.

R. M. BALABAI, P. V. MERZLIKIN

Krivoi Rog State Pedagogical University, Department of Physics, Krivoi Rog, Ukraine, Gagarina str., 54, 50086, phone:(0564)715721, e-mail: oks_pol@cabletv.dp.ua, linuxoid@i.ua.

ZnO THIN FILM AS SENSOR: AB INITIO CALCULATIONS

ZnO is a matherial for manufacturing adsorption-semiconductor sensors. Therefore an understanding of mechanisms of interactions inside such systems is important. One of valuable characteristics for this purpose is space distribution of the valence electron density. The calculations have been performed using Car-Parrinello molecular dynamic and ab initio norm-conserving pseudopotential models. CO and CH_4 adsorption on ZnO thin film was examined.

INTRODUCTION

Metal oxides (SnO_2, Fe_2O_3, ZrO_2, ZnO, In_2O_3, Ga_2O_3, WO_3 etc.) and composites are used for manufacturing semiconductor sensors. That type of sensors changes its electrical resistance under the influence of analyzed gas. Basic advantages of such sensors are low price, small size, high sensitivity and low power consumption. Pure and doped ZnO films were investigated as base for sensors of O_2[1], H_2[2], NO_x[3], ethanol [4] etc. ZnO is prospective chemically and thermally stable n-type semiconductor which is sensitive for toxic and inflammable gases. Because of the fact of its stability, ZnO is one of most widespread materials for gas sensors, cheap and convenient for production.

SETTING TASKS

It is needed the better understanding of interaction mechanism between gas molecules and semiconductor surface to apply the thin ZnO films for chemical and gas sensors. It is important to detect changes in such atomic system and their influence to electrical resistance. This problem is very difficult to solve experimentally. That is why theoretical ab initio methods are indispensable. One of them is density functional theory (DFT). Self-consistent density of electronic charge is one of the most important parameters of DFT, which totally characterizes ground state of electronic system. The method allows calculating total energy, forces and tensions. It provides a way for observation of chemical bonds. That is why ab initio calculation is required for detection of charge redistribution details in nanoscale ZnO layers during adsorption of gas molecules. For this purpose Car-Parrinello molecular dynamic [5] and ab initio norm-conserving pseudopotential [6] have been realized by means of auctorial software [7].

CALCULATION METHOD

The Car-Parrinello method (CP method) is based on density-functional theory (DFT) and the Born-Oppenheimer (OB) adiabatic approximation. For conventional DFT electronic structure calcula- tions, the Kohn-Sham (KS) equations are solved self-consistently. In the BO approximation, wave functions are considered as functions of ionic positions $\{\vec{R}_l\}$: $\{\psi_i(\vec{r}; \vec{R}_l)\}$, but in the CP method, they $\{\psi_i(\vec{r})\}$ are treated as classical dynamical variables independent of $\{\vec{R}_l\}$. They are postulated to evolve by Newton's equations of motion so that "dynamical simulated annealing" can be performed to search a global minimum of the electronic configuration.

The Lagrangian in the CP method is decribed as

$$L\left\{\psi, \dot{\psi}, \vec{R}, \dot{\vec{R}},\right\} = \mu \sum_i \int |\dot{\psi}_i(\vec{r})|^2 \, d\vec{r} + \frac{1}{2}\sum_l M_l \dot{\vec{R}}_l^2 - E[\{\psi_l(\vec{r})\}, \{\vec{R}_l\}] + \sum_i \sum_j \varepsilon_{ij}\left(\int \psi_i^*(\vec{r})\psi_j(\vec{r})dr - \delta_{ij}\right), \quad (1)$$

where $\{\psi_i\}$ are single-electron orbitals, and the electronic density $p(\vec{r})$ is assumed to be given by

$$p(\vec{r}) = \sum_i |\psi_i(\vec{r})|^2. \quad (2)$$

The first term of Eq. (1) is a fictitious classical mechanical kinetic energy of $\{\psi_i\}$. The second term is an ionic kinetic energy, and E is the total energy (the sum of the electronic energy and the ion-ion Coulomb interaction energy). Lagrangian multipliers ε_{ij} are introduced to satisfy the orthonormality constraints on $\{\psi_i\}$. The details of the electronic energy were particularly described in literature. From Eq. (2), equations of motion for ψ_i and $\vec{R}_l$ are derived as

$$\mu\ddot{\psi}_i(\vec{r}) = -\frac{\delta E}{\delta\psi_i^*(\vec{r})} + \sum_j \varepsilon_{ij}\psi_j(\vec{r}) \quad (3)$$

$$M_l \ddot{\vec{R}}_l = -\nabla_l E \quad (4)$$

If an electronic structure reaches for a state in which no force acts on ψ_i, that is, the left-hand side of Eq. (3) is equal to zero, this equation is identical with the KS equation and ψ_i becomes the eigenstate of the KS equation. To attain this, the kinetic energy of $\{\psi_i\}$ is gradually reduced until $\{\psi_i\}$ are frozen. This procedure is called "dynamical simulated annealing." If the one also relaxes the ions with Eq. (4), the minimization with respect to electronic and ionic configurations can be executed simultaneously.

It is also possible to obtain $\{R_i\}$ and $\{\psi_i\}$ without reducing the kinetic energy. If $\{\psi_i\}$ are kept close

to eigenstates during the time evolution, ionic trajectories generated by Eq. (4) are physically meaningful. When the CP method is applied to study the dynamical evolution of a system consisting of ions and electrons, it is called "ab initio molecular dynamic."

CALCULATION RESULTS AND THEIR DISCUSSION

Atomic basis of primitive tetragonal cell of superlattice represented infinite ZnO film with thickness of 5.76 E with CO or CH_4 molecules on (001) surface. It consisted of 16 zinc atoms, 16 oxygen atoms and atoms of molecule. Calculation algorithm required using of atomic basis with inverse symmetry. Therefore elementary cell contained two inversely symmetric fragments of ZnO film with gas molecules on their surfaces. So, total number of atoms in basis was 68 or 74. The chosen cell parameters allowed modeling infinite 4-layered film in X and Y directions and free surfaces in Z direction. Properties of pure ZnO film and ZnO film with molecules on O-terminated and Zn-terminated surfaces were investigated. The value of total energy of atomic systems for Γ-point of Brillion zone of superlattice, space distributions of valence electrons density and atomic coordinates were obtained. Space distribution of valence electrons density for pure films is shown on Fig. 1
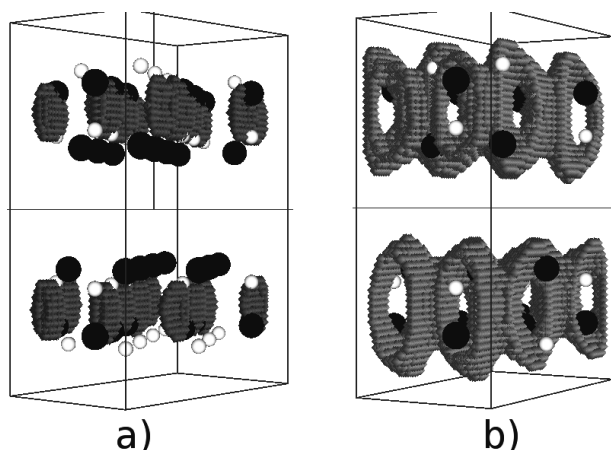
Fig. 1. Density space partial distributions of valence electrons in ZnO film (Zn — black pheres, O — white spheres) for iso-values: (a) 0.8−0.9 from maximal value, (b) 0.4−0.5 from maximal value.

It demonstrates an absence of charge cross-pieces between films. The space distribution of valence electrons density along films is shown on Fig. 2. The presence of molecules near film surfaces changes charge distribution significantly (Fig. 3 — Fig. 5).

The one can see from Fig. 3−5, that the interaction between molecule and ZnO film shows the formation of common charge regions between molecule and film. The degree of redistribution is more significant in O-terminated film. Comparison of O-terminated film (Fig. 4) and Zn-terminated film (Fig. 5) shows that O-terminated film is more active as for adsorption. In this case charge cross-piece appears between two films.
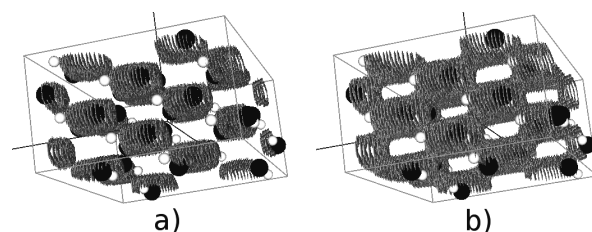
Fig. 2. Density space partial distributions of valence electrons in ZnO film (Zn — black spheres, O — white spheres) for iso-values. View to surface. (a) 0.6−0.7 from maximal value, (b) 0.5−0.6 from maximal value.
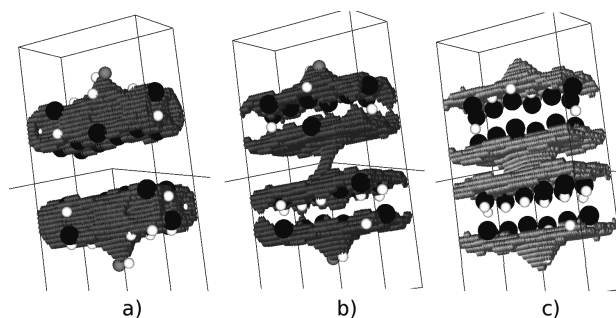
Fig. 3. Density space partial distributions of valence electrons in O-terminated ZnO film with CO molecule 2 E apart. (a) 0.8−0.9 from maximal value, (b) 0.7−0.8 from maximal value, (c) 0.6−0.7 from maximal value.
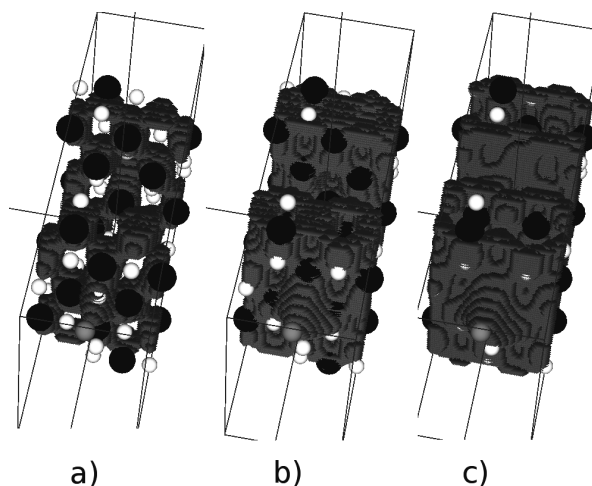
Fig. 4. Density space partial distributions of valence electrons in O-terminated ZnO film with CO molecule 2 E apart. View to surface. (a) 0.9−1.0 from maximal value, (b) 0.8−0.9 from maximal value, (c) 0.7−0.8 from maximal value.
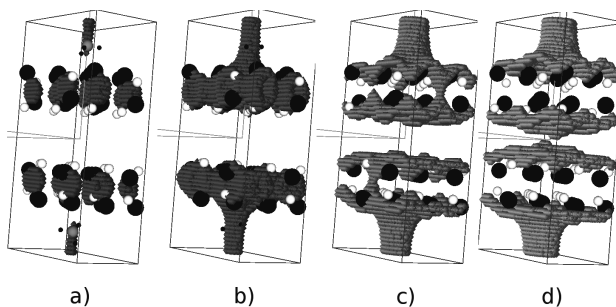
Fig. 5. Density space partial distributions of valence electrons in Zn-terminated ZnO film with CH4 molecule 2.5 E apart. (a) 0.9−1.0 from maximal value, (b) 0.8−0.9 from maximal value, (c) 0.7−0.8 from maximal value, (d) 0.5−0.6 from maximal value.
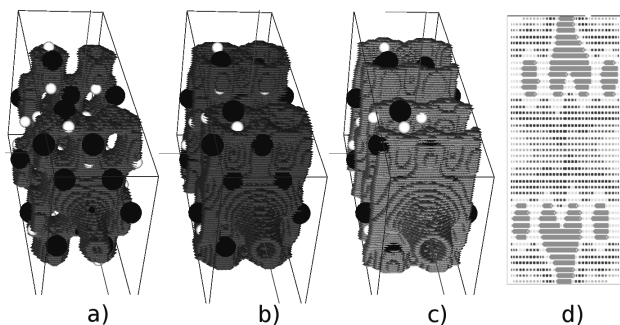
Fig. 6. Density space partial distributions of valence electrons in Zn-terminated ZnO film with CH4 molecule 2.5 E apart. View to surface. (a) 0.8−0.9 from maximal value, (b) 0.7−0.8 from maximal value, (c) 0.6−0.7 from maximal value, (d) (100) cut.

CONCLUSIONS

An analysis of valence electrons' density allows affirming that: two thin ZnO films separated by a distance of 5 E may emerge like a electrical relay which is closing after gas molecule adsorption.

O-terminated film is more sensitive for adsorption than Zn-terminated one.

References

1. Sberveglieri, G.; Groppelli, S.; Nelli, P.; Quaranta, F.; Valentini, A.; Vasanelli, L. Oxygen gassensing characteristics for ZnO(Li) sputtered thin films. *Sens. Actuators B* **199**9 7, 747−751.
2. Yamazaki, T.; Wada, S.; Noma, T.; Suzuki, T. Gas-sensing properties of ultrathin zinc oxide films. *Sens. Actuators B* **1999**, *14*, 594−595.
3. Muller, J.; Weissenrieder, S. ZnO-Thin film chemical sensors. *Fres. J. Anal. Chem.* **1999,** *349*, 380−384
4. Stambolova, I.; Konstantinov, K.; Vassilev, S.; Peshev, P.; Tsacheva, Ts. Lanthanum doped SnO2 and ZnO thin films sensitive to ethanol and humidity. *Materials Chemistry and Physics* **2000**, *63*, 104−108
5. D. Marx, J. "Hutter, Ab initio molecular dynamics: theory and implementation", published in "Modern methods and algorithms of quantum chemistry", J. Grotendorst (Ed.), John von Neuman Institute for computing, Julich, NIC Series, v. 1, ISBN 3−00−005618−1, 2000, pp. 301−449
6. C. Hartwigsen, S. Goedecker, J. Hutter. Relativistic separable dual-space Gaussian pseudopotentils from H to Rn, Phys. Rev. B, v. 58, N. 7, 1999,pp. 3641−3662
7. Балабай Р. М., Грищенко Н. В. Программное обеспечение для расчетов ab initio твердотельных структур // Матеріали Міжнародної науково-практичної конференції "Проблеми електронної промисловості у Перехідний період". — Збірник наукових праць Східноукраїнського державного .університету. — Луганськ. — 1999. — с.124−128

R. M. Balabai, P. V. Merzlikin

ZnO THIN FILM AS SENSOR: AB INITIO CALCULATIONS

ABSTRACT

ZnO is a matherial for manufacturing adsorption-semiconductor sensors. Therefore an understanding of mechanisms of interactions inside such systems is important. One of valuable characteristics for this purpose is space distribution of the valence electron density. The calculations have been performed using Car-Parrinello molecular dynamic and ab initio norm-conserving pseudopotential models. CO and CH$_4$ adsorption on ZnO thin film was examined.

Key words: Heterostructures, absorption -semiconductor sensor, pseudopotential.

Р. М. Балабай , П. В. Мерзликін.

ТОНКА ПЛІВКА ZnO ЯК СЕНСОР: РОЗРАХУНОК ІЗ ПЕРШИХ ПРИНЦИПІВ.

Резюме

Оксид цинку ZnO є матеріалом для виготовлення адсорбційно-напівпровідникових газових сенсорів. Для виготовлення таких сенсорів слід розуміти механізми взаємодії молекул газу з поверхнею ZnO. Однією з характеристик, яка дозволяє це зробити, є густина електронного заряду, яка повністю характеризує основний стан електронної системи. Для її визначення можна використовувати чисельний розрахунок з перших принципів. В рамках даного дослідження просторовий розподіл густини валентних електронів був розрахований за допомогою молекулярної динаміки Кар-Парінелло з використанням зберігаючого норму ab initio псевдопотенціала.

Ключові слова: гетероструктура, адсорбційно-напівпровідниковий газовий сенсор, псевдопотенціала.

Р. М. Балабай, П. В. Мерзликин.

ТОНКАЯ ПЛЕНКА ZnO КАК СЕНСОР: РАСЧЕТ ИЗ ПЕРВЫХ ПРИНЦИПОВ

Резюме

Оксид цинка ZnO является материалом для изготовления адсорбционно-полупроводниковых газовых сенсоров. Для изготовления таких сенсоров следует понимать механизмы взаимодействия молекул газа с поверхностью ZnO. Одной из характеристик, которая позволяет это сделать, является плотность электронного заряда, которая полностью характеризует основное состояние электронной системы. Для ее определения можно использовать численный расчет из первых принципов. В рамках данного исследования пространственное распределение плотности валентных электронов было рассчитано с помощью молекулярной динамики Кар-Паринелло с использованием нормосохраняющего ab initio псевдопотенциала.

Ключевые слова: гетероструктура, адсорбционно-полупроводниковый газовый сенсор,. псевдопотенциал.

A. V. GLUSHKOV

Odessa State Environmental University, L'vovskaya str., 15, Odessa, 65009, Ukraine
e-mail: glushkov@paco.net

LASER- ELECTRON-β-NUCLEAR SPECTROSCOPY OF ATOMIC AND MOLECULAR SYSTEMS AND CHEMICAL ENVIRONMENT EFFECT ON THE β-DECAY PARAMETERS: REVIEW

We review a new field of investigations, which lies on the boundary of the modern quantum optics and photoelectronics, laser physics and atomic and nuclear physics. We discuss the cooperative laser-electron-β-nuclear processes in atoms and molecules, including the excitation, ionization, electronic rearrangement, induced by the nuclear reactions and β-decay and a state of art of the modern calculating the β-decay parameters for a number of allowed (super allowed) transitions (^{33}P-^{33}S, ^{241}Pu-^{241}Am etc) and a chemical bond effect on β-decay parameters. A few factors are taken into account: changing the integration limits in the Fermi function integral, energy corrections for different chemical substances, and the possibility of the bound β-decay or other decay channels. We review the studies of the electronic rearrangement induced by nuclear transmutation in the β-decay $^{6}_{2}\text{He}_{4} \rightarrow (^{6}_{3}\text{Li}^{+}_{3})^{*} + e^{-} + \overline{\nu}_{e}$. The half-life period $T_{1/2}$ for β-decay of tritium atom (ion) has been estimated while taking into account the bound β-decay channel and some other accompanying effects. The estimated values of $T_{1/2}$ for the tritium β-decay and free triton decay are: $(T_{1/2})_{a}$=12.26 years (correction due to the electron-atomic effects $(\Delta T_{1/2}/T_{1/2})_{a}$=0.82%) for the tritium atom and $(T_{1/2})_{t}$=12.36 years for the triton decay. These data are in physically reasonable agreement with experimental data. We analyse the firstly [1] presented value $T_{1/2}$ in a case of the β-decay in the halogen-containing molecular tritium (^{3}HCl): $(T_{1/2})_{m}$=12.28 years (^{3}HCl); the correction due to the chemical bond effect is $(\Delta T_{1/2})_{am}$=0.024 (i.e. 0.20%).

1 INTRODUCTION

Methods for influencing the radioactive decay rate have been sought from the first years of formation of nuclear physics. Beta decay strengths influence nuclear transmutations, the pathways of stellar nucleosynthesis in stars and the resulting abundance of atomic nuclei. Nuclear transmutation (i.e. change in the nuclear charge) induced by nuclear reactions of radioactivity are often accompanied by a redistribution of the electrons around the final transmuted nucleus. Electrons originally in the ground state of the target atom (molecule) can be excited either in the bound spectrum or to the continuum of energy. Calculations of the population distribution of the atomic states of the daughter atom require a complete description of both the bound spectrum and the continuum of energy. Calculation of the β decay parameters while taking into account the cooperative electronic processes (an interaction between beta particle, generated by an atomic nucleus, and the electron shells, which surround a beta active nucleus in the atomic or molecular system) and the chemical environment contribution is now of a great theoretical and experimental interest (see, for details, Refs. [1−148]). Discrepancies in the experimental data for parameters of the β-decay in the heavy radioactive nuclei can be partly explained by contributions of the cooperative electron-nuclear processes and chemical bond effect. Naturally, the problem of detecting a neutrino mass is of a great importance. The possible source of the corresponding data about it is the β-decay spectrum shape. As it is well known, neutrinos were postulated by Pauli (1930) to properly explain the β-decay of the free neutron $\text{ń} \rightarrow \text{p} + \text{e}^{-} + \overline{}_{e}$ without violating energy-momentum conservation. In the last years new experimental feasibilities have allowed for improvements in the measurement of the β-decay parameters resulting in a more accurate definition of the neutrino mass [1−16]. These data are especially important for standardization of the beta decay parameters for a whole number of the heavy radioactive nuclei [1−16,24,29−31]. It is interesting to note that discrepancies in data on the half-life period for ^{241}Pu are not explained hitherto, though quite a reasonable comment is connected with taking into account the bound β-decay channel etc (see Refs. [3−13,15,31,41]). The population distribution of the atomic states of the daughter atom requires a complete and correct description of the cooperative electron-nuclear processes and chemical environment effect on the β-decay parameters [1−19,24,29−31]. One has to consider the following effects: i) Changing the electron wave functions because of the changing atomic electric field; changing the valence shell occupation numbers in different chemical substances; ii) The integration limits (calculating the Fermi integral function) are also changed in a case of the different chemical substances; as a rule, β-particle and neutrino take away the difference between the initial and transmuted final nuclei, provided by the nuclear and electronic rearrangement. One must also mention the additional channel, when β-electron occupies a free state in the bound atomic spectrum. Approaches implemented up to now can be characterized as force ones using, first of all, the change in energy balance of radioactive decay: creation of isomeric states, variation of energy of the chemical bond in molecules with radioactive atoms and β-decay to bound states in the ionized atoms [1−37,29−31,42−76]. The last channel was discovered for the first time in experiments on the

synchrotron and SIS/ESR (GSI, Germany), when the bound β decay $^{163}Dy^{66+} \rightarrow {}^{163}Ho^{66+}$ was studied by using the technology of the highly-or fully-ionized atomic beams (multicharged ions) [5,6,42]. In fact, the β-transition $Dy^{66+} \rightarrow Ho^{66+}$ was observed, which is accompanied by a capture of the β-particle on the K and L shell levels in the bound spectrum of the daughter atom. In fact, the complete ionization of ^{163}Dy in the storage ring of a heavy ion accelerator makes its beta decay to the K shell of ^{163}Ho possible, with a half-life of 47 days, while in the neutral atom this decay is energetically forbidden [6]. The similar effect was obtained for ^{187}Re [7]. The authors of Ref. [7] observed the bound-state β-decay of fully ionized ^{187}Re nuclei circulating in a storage ring. Let us remember also that such an effect may be responsible for creation of elements in the space and astrophysical plasma (see details in Refs. [10−16,124,143,144]). The authors of Ref. [8] reported the first measurement of a ratio $\lambda_{\beta b}/\lambda_{\beta c}$ of bound-state $(\lambda_{\beta b})$ and continuum-state $(\lambda_{\beta c})$ β−-decay rates for the case of bare $^{207}Tl^{81+}$ ions. These ions were produced at the GSI fragment separator FRS by projectile fragmentation of a ^{208}Pb beam. In Ref. [4] the half-lives of isomeric states of fully ionized ^{144}Tb, ^{149}Dy, ^{151}Er were measured. These nuclides were produced via fragmentation of about 900 MeV/u ^{209}Bi projectiles, separated in flight with the fragment separator (FRS) and stored in the cooler ring (ESR). The authors of Ref. [4] observed for the first time drastic increases of the half-lives of bare isomers by factors of up to 30 compared to their neutral counterparts. This phenomenon is due to the exclusion of the strong internal conversion and electron-capture channels in the radioactive decay of these bare nuclei. The authors of Ref. [7] reported on the study of the dominating breakup channels involving $n\alpha^6He$ or $3n2\alpha$ in the final state, with special emphasis dedicated in this contribution to the three-particle channel.

One could also mention the known change of the decay rate for ^7Be, which was measured most thoroughly. The change in the K-capture rate by $\sim 10^{-2}$ due to the influence of the energy of chemical bond and the atomic configuration of the environment (including measurements with ^7Be placed inside the fullerene C_{60}) was registered (see Refs. [10−12, 50−59,62−68]). It has been experimentally and theoretically found that the chemical environment (chemical bond, pressure etc.) effect resulted in changing ($\sim 0.1−1.0\%$) the corresponding decay constant. The helium-isotope mass-spectroscopy method for measuring the triton decay constant for various cases of the electron environment was used to determine the tritium half-life without allowance for decay to beta-electron bound states and to calculate the respective reduced half-life in Ref. [9]. More intriguing effects are considered in a case of α-decay (see Refs. [13,145−147]). Results on variation of the decay rate of Mцssbauer isomers due to interference of electromagnetic waves in the system of the emitter and a screen from the same atom in the ground state situated at a distance of $\sim 2mm$ seem quite impressive [146]. The values of the measured relative variation of the decay rate for ^{119m}Sn, ^{125m}Te reach $\sim 10\%$.

The elementary cooperative electron-β and γ-nuclear processes in atoms and molecules were considered in the pioneering papers by Migdal (1941), Levinger (1953), Schwartz (1953), Gol'dansky-Letokhov-Ivanov (1971−1976), Kaplan-Markin-Yudin (1973−1975), reviews by Batkin-Smirnov (1980), papers by Freedman (1974), Carlson et al. (1968), Intemann (1983), Isozumi et al. (1977), Law-Campbell (1975), Martin-Cohen (1975), Mukouama et al. (1978), Law-Suzuki (1982), Wauters-Vaeck (1997) et al [1−5,14,43−60,60−82,120,124]. The elementary cooperative electron α-nuclear processes were considered in the papers by Levinger (1953), Hansen (1974), Watson (1975), Anholt-Amundsen (1982), Law (1977), Mukoyama-Ito (1988) et al (see Refs. [14,43−60,60−82,120]). In this context, the known Mцssbauer, Szilard-Chalmers and other cooperative effects should be mentioned [14,60]. The consistent quantum electrodynamics (QED) theory of cooperative electron γ-nuclear processes in atoms and molecules is developed in Refs. [25−28,39−40,71−76]. In fact, it is possibly a reverse bridging between nuclear structure theory and quantum chemistry (atomic and molecular physics). Data on β-decay parameters can be used for studying the chemical bond nature, treating the spatial structure of molecular orbitals, identifying the electron states in some tritium-containing systems and diagnostics of the compounds by means of exchange of the hydrogen atoms by tritium ("tritium probe") [56,57,62−72]. In this review paper we discuss the cooperative electron-β-nuclear processes in atomic systems (laser-e-β-nuclear spectroscopy as a new trend in a modern quantum optics and spectroscopy), including the processes of excitation, ionization, and electronic rearrangement induced by nuclear reactions and β-decay. the state of art in a field of the modern calculations of the β-decay parameters for a number of allowed (superallowed) transitions (^{33}P-^{33}S, ^{241}Pu-^{241}Am etc) and a chemical bond effect on β-decay parameters. There are a few factors that have to be taken into account: changing the integration limits in the Fermi function integral, energy corrections for different chemical substances, and the possibility of the bound β-decay or other decay channels. We discuss the electronic rearrangement induced by nuclear transmutation in the β-decay $^4_2He_4 \rightarrow ({}^6_3Li^+_3)^* + e^- + \overline{\ }_e$. The half-life periods for β-decay in the tritium atom (molecule) are estimated by taking into account the bound β-decay channel correction and some other effects.

2. QUANTUM THEORY OF THE β-DECAY AND COOPERATIVE ELECTRON-β-NUCLEAR PROCESSES

2.1 Introduction: General formalism

As it is well known, the fundamental process behind β decay is weak interaction of the down (up) quarks (for example: $d \rightarrow u + e^- + \overline{\nu}_e$ etc) via the exchange of virtual bosons [81.8 ($W^{\pm}$) and 91.2 (Z^0) GeV/c^2)], opened in CERN (1983).The first theory of β-decay was proposed by E. Fermi (1934), who introduced the local (contact) 4-fermion interaction of the nucleons and leptons. Hamiltonian of the Fermi nucleon-lepton interaction is as follows:

$$H_{\hat{a}} = G_{\hat{a}}(\overline{\Psi}_p \gamma_i \Psi_n)(\overline{\Psi}_e \gamma^i \Psi_\nu). \qquad (1)$$

Here G_β is the Fermi constant, Ψ are the four-component wave functions of the particles (solutions of the Dirac equation), $\bar{\Psi}_e = \Psi^+\gamma_0$, γ^μ are the Dirac matrices, $\mu = 0,1,2,3,4$; $\gamma^0 = \gamma_0$; $\gamma^i = -\gamma_i$ (i=1,2,3). The nucleon-lepton interaction had purely vector form in the Fermi theory. The modern "V-A" theory usually uses an effective β-decay Hamiltonian which was introduced by Feynman and Gell-Mann:

$$ H_\beta = \frac{G_\beta}{\sqrt{2}} J^i(x) L_i(x) + \text{c.c.} , \qquad (2) $$

where J^μ is the nucleonic current, L_μ is the leptonic current and x is a spatial-temporal coordinate. Despite a great progress in development of the comprehensive theory for the nuclear β-decay (electroweak interactions), hitherto many practical questions are far from a satisfactory treatment. The further consistent calculations of the β-decay parameters that take into account accompanying cooperative effects are needed. The wide-spread quantum mechanical methods (such as the Hartree-Fock (HF) method, the random-phase approximation, the Coulomb approximation (CA), the Hartree-Fock-Slater (HFS) and Dirac-Fock (DF) methods, DFT etc) are usually used in the atomic calculations and calculations of the β-allowed (superallowed) transitions parameters [1,2,11−16,29−31,80−133]. The difficulties of the corresponding calculations are well known (insufficiently correct account for exchange and correlation in the wave functions of β-particle, problem of gauge invariance, generation of the non-optimized bases of the wave functions for a discrete spectrum and continuum etc). The nuclear, relativistic, radiative corrections should be accurately taken into account too. As a rule, to estimate the β-spectrum shape and decay parameters, the special tables [15,29−31] of the Fermi functions are usually used (the CA data). In some papers (see Refs. [13−16,29−31]) the HFS approach that takes into account the nuclear finite size effect was used. In Ref. [15], the finite size correction was taken into account as correction to the CA calculation result and the screening effect was calculated within the atomic model potential scheme. In some papers (see Refs. [29−31] and references therein) the DF method is used. A gauge-invariant QED PT formalism for the calculation of the spectra and wave functions for heavy atoms while taking into account the relativistic, correlation, nuclear, and QED effects has been developed in Refs. [24−28,37−41,76−82,120,122−124]. This formalism provides two optimized gauge invariant (GI) calculation schemes with the DF (GIDF) and DKS (GIDKS) zeroth approximation. Below, the DKS scheme is used in our calculation.

As it is well known, a probability of the transition from the initial state $|\xi\rangle$ with the energy E_ξ to some final state $\langle f|$ with the energy E_f per unit of time is defined as follows [15,124]:

$$ dW_{\xi,f} = (2\pi/\hbar)|<f|H|\xi> $$
$$ >|^2 (dN/dE)|_{E=E_0}, E_0 = E_f - E_\xi, \qquad (3) $$

where the value (dN/dE) defines a density of the final states of a system per unit of energy and the corresponding matrix element is:

$$ <f|H|\xi> = \int \psi_f H_\beta \psi_\xi d^3r_1 ... d^3r_A , \qquad (4) $$

where the interaction Hamiltonian H_β and wave functions of the initial ψ_ξ and final ψ_f states. The expression for a number of the β-, $\tilde{\nu}$ -particles with energy in the interval from E till $E+dE$ is as follows:

$$ dW_{\xi f} = \frac{1}{2\pi^3 \hbar^7 c^5}\left|<f|H_\beta|\xi>\right|^2 \sqrt{E_e^2 - m^2 c^4} \times $$
$$ \times E_e \left(E_0 - E_e\right)^2 dE_e, \qquad (5) $$

$$ dW_{\xi f} = \frac{1}{2\pi^3 \hbar^7 c^5}\left|<f|H_\beta|\xi>\right|^2 \sqrt{\left(E_0 - E_{\tilde{\nu}}\right)^2 - m^2 c^4} \times $$
$$ \times \left(E_0 - E_{\tilde{\nu}}\right)E_{\tilde{\nu}}^2 dE_{\tilde{\nu}}. \qquad (6) $$

Further we will study the allowed and super allowed β-transitions. The contribution of these transitions is the most significant to the resulting spectrum of the β-decay. At the same time, the forbidden transitions contribution is usually about a few percent of the total intensity. Distribution of β particles on energy in a case of the allowed transitions is as follows:

$$ dW_\beta(E)/dE = $$
$$ = \frac{1}{2\pi^3}G^2 \cdot F(E,Z)\cdot E\cdot p\cdot (E_0 - E)^2 \cdot |M|^2 . \qquad (7) $$

Here E, $p = (E^2 - 1)^{1/2}$ are a total energy and pulse of β-particle; $E_0 = 1 + (E_b/m_e c^2)$, E_b is the boundary energy of β-spectrum; $|M|$ is a matrix element, which is not dependent on an energy in a case of allowed β-transitions. The Fermi and integral Fermi functions are defined as [13,29,124]:

$$ F(E,Z) = \frac{1}{2p^2}(g_{-1}^2 + f_{+1}^2), \qquad (8) $$

$$ f(E_0,Z) = \int_1^{E_0} F(E,Z)\cdot E\cdot p\cdot (E_0 - E)^2 dE. \qquad (9) $$

Here f_{+1} and g_{-1} are the relativistic electron radial functions; the indexes $\pm 1 = \chi$, where $\chi = (l-j)/(2j+1)$. The half-life period can be defined as follows:

$$ T_{1/2} = 2\pi^3 ln2/[G_\beta^2 |M|^2 f(E_0,Z)]. \qquad (10) $$

Here two calculation schemes are usually used: i) The relativistic electron radial wave functions are calculated on the boundary of the spherical nucleus with radius R (see [13,14]); ii) The values of these functions in zero are used [24,29−31].

2.2 The DKS Basis of the Relativistic Wave Functions

As usual, a multielectron atom is described by the Dirac relativistic Hamiltonian (the atomic units are used):

$$ H = \sum_i h(r_i) + \sum_{i>j} V(r_i r_j) \qquad (11) $$

Here, $h(r)$ is one-particle Dirac Hamiltonian for electron in a field of the finite size nucleus and V is potential of the inter-electron interaction. In order to take into account the retarding effect and magnetic interaction in the lowest order on parameter α^2 (the fine structure constant) one could write [77,86]:

$$V\left(r_i r_j\right) = exp\left(i\omega_{ij} r_{ij}\right) \cdot \frac{\left(1 - \alpha_i \alpha_j\right)}{r_{ij}}, \qquad (12)$$

where ω_{ij} is the transition frequency; α_i, α_j are the Dirac matrices. The Dirac equation potential includes the electric and polarization potentials of a nucleus and exchange-correlation potentials. The standard KS exchange potential is [91]:

$$V_X^{KS}(r) = -(1/\pi)[3\pi^2 \rho(r)]^{1/3}. \qquad (13)$$

In the local density approximation the relativistic potential is [92]:

$$V_X[\rho(r), r] = \frac{\delta E_X[\rho(r)]}{\delta \rho(r)}, \qquad (14)$$

where $E_X[\rho(r)]$ is the exchange energy of the multi-electron system corresponding to the homogeneous density $\rho(r)$, which is obtained from a Hamiltonian having a transverse vector potential describing the photons. In this theory the exchange potential is [98]:

$$V_X[\rho(r), r] = V_X^{KS}(r) \cdot \{\frac{3}{2} \ln \frac{[\beta + (\beta^2 + 1)^{1/2}]}{\beta(\beta^2 + 1)^{1/2}} - \frac{1}{2}\}, \quad (15)$$

where $\beta = [3\pi^2 \rho(r)]^{1/3} / c$. The corresponding correlation functional is [91,92]:

$$V_C[\rho(r), r] = -0.0333 \cdot b \cdot \ln[1 + 18.3768 \cdot \rho(r)^{1/3}], \quad (16)$$

where b is the optimization parameter (for details see Refs. [80,124–126]). Earlier it was shown [80, 124–126] that an adequate description of the atomic characteristics requires using the optimized basis of wave functions. In Ref. [80] a new ab initio optimization procedure for construction of the optimized basis is proposed. It is reduced to minimization of the gauge dependent multielectron contribution $Im\delta E_{ninv}$ of the lowest QED PT corrections to the radiation widths of atomic levels. In the fourth order of QED PT (the second order of the atomic PT) there appear the diagrams, whose contribution to the $Im\delta E_{ninv}$ accounts for the correlation (polarization) effects. This contribution describes the collective effects and it is dependent upon the electromagnetic potentials gauge (the gauge non-invariant contribution). All the gauge non-invariant terms are multielectron by their nature (the particular case of the gauge non-invariance manifestation is a non-coincidence of the oscillator strengths values, obtained in the approximate calculations with the "length" and "velocity" transition operator forms). The above cited contribution to imaginary part of the electron energy can be defined after quite complicated calculation as [80]:

$$Im\delta E_{ninv}(\alpha - s \mid b) = -C \frac{e^2}{4\pi} \times$$

$$\times \iiint\int dr_1 dr_2 dr_3 dr_4 \sum_{n > f, m \le f} (\frac{1}{\omega_{mn} + \omega_{\alpha s}} + \frac{1}{\omega_{mn} - \omega_{\alpha s}})$$

$$\times \Psi_\alpha^+(r_1)\Psi_m^+(r_2)\Psi_s^+(r_4)\Psi_n^+(r_3) \cdot [(1 - \alpha_1 \alpha_2)/r_{12}] \times$$

$$\times \{[\alpha_3 \alpha_4 - (\alpha_3 n_{34})(\alpha_4 n_{34})]/r_{34}$$

$$\times \sin[\omega_{\alpha n}(r_{12} + r_{34})] +$$

$$+[1 + (\alpha_3 n_{34})(\alpha_4 n_{34})]\omega_{\alpha n} \cos[\omega_{\alpha n}(r_{12} + r_{34})]\}$$

$$\times \Psi_m(r_3)\Psi_\alpha(r_4)\Psi_n(r_2)\Psi_s(r_1). \qquad (17)$$

Here, C is the gauge constant, f is the boundary of the closed shells; $n \ge f$ indicating the unoccupied bound and the upper continuum electron states; $m \le f$ indicates the finite number of states in the atomic core and the states of a negative continuum (accounting for the electron vacuum polarization). The minimization of the functional $Im\delta E_{ninv}$ leads to the DKS-like equations for the electron density that are numerically solved. As a result one can get the optimal PT one-electron basis. In concrete calculations it is sufficient to use a more simplified procedure, which is reduced to the functional minimization using the variation of the correlation potential parameter b in Eq. (16) [124–126]. The differential equations for the radial functions F and G (components of the Dirac spinor) are as usually:

$$\frac{\partial F}{\partial r} + (1 + \chi)\frac{F}{r} - (\varepsilon + m - V)G = 0,$$

$$\frac{\partial G}{\partial r} + (1 - \chi)\frac{G}{r} + (\varepsilon - m - V)F = 0, \qquad (18)$$

where F, G are the large and small components respectively; χ is the quantum number. To prevent the integration step from becoming too small it is usually convenient to turn to new functions isolating the main power dependence: $f = Fr^{1-|\chi|}$, $g = Gr^{1-|\chi|}$. The Dirac equations for F and G components are transformed as follows:

$$f' = -(\chi + |\chi|)f / r - \alpha Z V g - (\alpha Z E_{n\chi} + 2/\alpha Z)g,$$

$$g' = (\chi - |\chi|)g / r - \alpha Z V f + \alpha Z E_{n\chi} f. \qquad (19)$$

Here $E_{n\chi}$ is one-electron energy without the rest energy. The boundary values are defined by the first terms of the Taylor expansion:

$$g = (V(0) - E_{n\chi})r\alpha Z/(2\chi + 1); \quad f = 1 \text{ at } \chi < 0,$$

$$f = (V(0) - E_{n\chi} - 2/\alpha^2 Z^2)\alpha Z; \quad g = 1 \text{ at } \chi > 0. \quad (20)$$

The condition $f, g \to 0$ at $r \to \infty$ determines the quantified energies of the state $E_{n\chi}$. The self-consistence condition of the continuum state functions means that the normalized functions differ by less than 10^{-6} in relation to their values at the maximum point on two neighbour iterations. The normalization of electron radial functions f and g provides the behaviour for large values r:

$$g_\chi(r) \to r^{-1}[(E + 1)/E]^{1/2} \sin(pr + \delta_\chi),$$

$$f_\chi(r) \to r^{-1}(\chi/|\chi|)[(E - 1)/E]^{1/2} \cos(pr + \delta_\chi). \quad (21)$$

2.3 Nuclear Finite Size and Radiation Effects

Usually in order to account for the nuclear finite size effect the charge distribution in the nucleus $\rho(r)$ is described by the following Gaussian function:

$$\rho(r|R) = (4\gamma^{3/2}/\sqrt{\pi})\exp(-\gamma r^2),$$

$$\int_0^\infty dr r^2 \rho(r|R) = 1; \quad \int_0^\infty dr r^3 \rho(r|R) = R, \qquad (22)$$

where $\gamma = 4/\pi R^2$, and R is the effective nuclear radius. The following R-dependence is usually assumed: $R = 1.606 \cdot 10^{-13} \cdot Z^{1/3}$ (cm). Such a definition of R is rather conventional. One could assume it as some zeroth approximation. The Coulomb potential for the spherically symmetric density $\rho(r|R)$ is:

$$V_{nucl}(r|R) = -\left((1/r)\int_0^r dr' r'^2 \rho(r'|R) + \int_r^\infty dr' r' \rho(r'|R)\right). \quad (23)$$

It is determined by the following system of differential equations:

$$V'_{nucl}(r,R) = \left(1/r^2\right)\int_0^r dr' r'^2 \rho(r',R) \equiv \left(1/r^2\right)y(r,R),$$

$$y'(r,R) = r^2 \rho(r,R),$$

$$\rho'(r,R) = -8\gamma^{5/2} \, r/\sqrt{\pi}\exp\left(-\gamma r^2\right) =$$

$$= -2\gamma r \rho(r,R) = -\frac{8r}{\pi r^2}\rho(r,R), \quad (24)$$

with the boundary conditions:

$$V_{nucl}(0,R) = -4/(\pi r) \, , \ y(0,R) = 0 \, ,$$

$$\rho(0,R) = 4\gamma^{3/2}/\sqrt{\pi} = 32/R^3 \, . \quad (25)$$

The presented nuclear model was earlier used in many calculations of the atomic and nuclear systems [91−142]. It can be improved where necessary. Moreover, any relativistic mean field model, nuclear DFT, the HF theory with density dependent forces etc may be used [91,92,98,120−126]. The procedure for taking into account the QED corrections is given in Refs. [124−126]. Different approaches to estimating the QED corrections are developed and discussed, for example, in Refs. [93−132]. Regarding the vacuum polarization effect let us note that this effect is usually taken into account by means of the Uehling potential in the first PT order. This potential is usually written as:

$$U(r) = -\frac{2\alpha}{3\pi r}\int_1^\infty dt \exp\left(-2rt/\alpha Z\right)\times$$

$$\times\left(1 + 1/2t^2\right)\frac{\sqrt{t^2 - 1}}{t^2} \equiv -\frac{2\alpha}{3\pi r}C(g), \quad (26)$$

where $g = r/\alpha Z$. The more exact approach is proposed in Refs. [77,124−126]. The Uehling potential may be approximated by the analytical Ivanov-Ivanova function [77]. The use of the new approximation for the Uehling potential allows one to decrease the calculation error for this term down to 0.5−1% [79,126]. Besides, using a quite simple analytical functional form for approximating the potential, Eq. (26) allows its easy inclusion into the general system of differential equations. At least, this procedure was earlier approbated in the precise atomic calculations [79,124−126]. The function $C(g)$ in two limited cases has the known asymptotic as follows:

$$C(g) \to \tilde{C}_1(g) = \ln(g/2) + 1.410548 - 1.037845g,$$

$$g \to 0,$$

$$C(g) \to \tilde{C}_2(g) = -1.8800\exp(-g)/g^{3/2}, \quad (27)$$

$$g \to \infty.$$

An account of the two limiting expressions for $C(g)$ is realized as follows:

$$\tilde{C}(g) = \tilde{C}_1(g)\tilde{C}_2(g)/\left(\tilde{C}_1(g) + \tilde{C}_2(g)\right). \quad (28)$$

The final expressions are as follows:

$$\tilde{\tilde{C}}(g) = \tilde{C}_1(g)\tilde{\tilde{C}}_2(g)/\left(\tilde{C}_1(g) + \tilde{\tilde{C}}_2(g)\right),$$

$$\tilde{\tilde{C}}_2(g) = \tilde{C}_2(g)f(g),$$

$$f(g) = \left((1.1022/g - 1.3362)/g + 0.8028\right). \quad (29)$$

Other details can be found in Refs. [77,124−126,148].

3 Study of the Electronic Rearrangement Induced by Nuclear

Transmutation: the β Decay of ^{6}He

Here we consider the electronic rearrangement effect induced by the β-decay of ^{6}He. The main purpose is to treat the polyelectronic system

$$^6_2\text{He}_4 \to \left(^6_3\text{Li}^+_3\right)^* + \text{e}^- + \bar{\nu}_e . \quad (30)$$
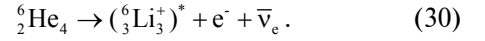
As in Ref. [51], we have calculated within the framework of the sudden approximation (since the velocity of most β- electrons is quasirelativistic) the population of the bound and continuum states of Li$^+$. If we neglect the effect of recoil of the daughter nucleus, the corresponding transition probability to a final atomic state is given by

$$|T^0_{fi}|^2 = < \Psi_f \, | \, \Psi_i >^2, \quad (31)$$

where Ψ_i corresponds to the wave function of the initial state with nuclear charge Z and Ψ_f to the wave function of the transmuted ion with nuclear charge Z' ($Z'=Z+1$ for β-decay). The sum over all the transitions involving the same initial state is 1. In Tables 1 and 2 the DKS calculation results of the energy eigenvalues (in at. units) and the excitation energies (in cm^{-1}) for $1snl$ ^1S states in the He-like ion of Li$^+$ are listed. The total energies of the lowest members of Li$^+$ ^1S Rydberg states obtained using the B-spline basis set by Wauters-Vaeck and the Hylleraas basis sets (within the complex coordinate approach) are listed in Tables 2,3 too [25,26,51].

Table 1

Eigenvalues of energy (in atomic units) for the $1snl$ ^1S states in Li$^+$

State	Hylleraas	B-spline	DKS
$1s^2$ ^1S	-7.2799135	-7.2793492	-7.2795438
$1s2s$ ^1S	-5.0408767	-5.0408201	-5.0408413
$1s3s$ ^1S	-4.7337556	-4.7337397	-4.7337488
$1s4s$ ^1S	-4.6297832	-4.6297767	-4.6297798
$1s5s$ ^1S	-4.5824274	-4.5824240	-4.5824256
$1s6s$ ^1S		-4.5569496	-4.5569529
$1s7s$ ^1S		-4.5416882	-4.5416916
$1s8s$ ^1S		-4.5318274	-4.5318322
$2s^2$ ^1S	-1.905845	-1.904924	-1.9052764
$2p^2$ ^1S	-1.630439	-1.628787	-1.6293165

The agreement between the DKS, B-spline and complex coordinate values (with using Hylleraas basis sets) is satisfactory. In Table 4 there are presented the values of calculated transition probabilities (in %; >0.05) to Li$^+$ states induced by β-decay of ^{6}He. The QED DKS results are compared in Table 3 with data of the pioneering work by Winther and B-spline data

by Wauters-Vaeck (see Refs. [48−52,120,124]). Contrary to the wave functions used in the B-spline of Wauters-Vaeck and in our scheme, the Li$^+$ wave functions used by Winther are not orthogonal. It implies that the sum over the transition probabilities to all the Li$^+$ states is not 1. In Table 4 the results of calculating the total transition probabilities for the population of different electronic states induced by the beta decay of ^{6}He are listed. It is interesting to calculate not only the transition probabilities to discrete states but also the ionization probability of one or two electrons. Using a radioactive recoil spectrometry experiment, Carlson et al. measured that single ionization probability is $(10.4\pm0.2)\%$ and B-spline and DKS values agree well with this result [24,48−52]. In the same experiment the double ionization probability was found to be $(0.042\pm0.007)\%$. The DKS value is well correlated with this result.

Table 2
Excitation energies (in cm^{-1}) for the 1snl ^1S states in Li$^+$

State	Experiment	B-spline	GIDKS
$1s^2$ ^1S	0	0	0
$1s2s$ ^1S	491335	491262	491298
$1s3s$ ^1S	558778	558653	558704
$1s4s$ ^1S	581597	581464	581502
$1s5s$ ^1S	591989	591860	591917
$1s6s$ ^1S	597581	597451	597513
$1s7s$ ^1S	600930	600800	600875
$1s8s$ ^1S	-	602964	603032

Table 3
Transition probabilities (in %) to the Li$^+$ states induced by the β-decay of ^{6}He

State	Winther	Wauters-Vaeck, B-spline	GIDKS
$1s^2$ ^1S	67.0	70.85	68.13
$1s2s$ ^1S	16.6	14.94	14.37
$1s3s$ ^1S	2.7	1.86	1.81
$1s4s$ ^1S	0.8	0.62	0.63
$1s5s$ ^1S		0.29	0.26
$1s6s$ ^1S		0.16	0.14
$1s7s$ ^1S		0.10	0.10
$2s^2$ ^1S		1.56	1.24
$2p^2$ ^1S		0.18	0.16
$2s3s$ ^1S		0.23	0.21
$2s4s$ ^1S		-	0.05

Table 4
Total transition probabilities (in %) for the population of different electronic states induced by the beta decay of ^{6}He

Final ^{6}Li$^+$ state	Experiment	Wauters-Vaeck, B-spline	DKS
Bound states	-	89.09	87.4
Autoionizing states	-	2.97	2.56
Ionization of one electron	10.4±0.2	7.47	9.85
Ionization of two electrons	0.042±0.007	0.32	0.09

Further we consider the quantity P_K, the probability per nuclear disintegration that an atomic K vacancy (a hole in the $1s^2$ shell) is created. The analysis of different calculation schemes is presented in Refs. [1,51]. In the sudden approximation this quantity is simply defined as follows [1]:

$$P_K = 1-[<\Psi_f(1s^2\,^1S)\,|\,\Psi_i(1s^2\,^1S)>]^2 . \qquad (32)$$

If electronic correlation effects are not taken into account this formula simply reduces to $1-(1s_f|1s_i)^4$, with the $1s$ radial distributions being optimized in, for example, HF approximation. This approach has been used by Carlson et al, who predicted a P_K value of 26.9% for the beta decay of ^{6}He. The introduction of electronic correlation significantly increases the probability to P_K=27.61% (Law-Campbell result), P_K=32.91% (Izozumi et al.), P_K=29.15% (Wauters-Vaeck) and P_K=31.87% (Glushkov et al). In any case one can conclude that the optimized DKS method is quite an adequate approach to the calculation of parameters for excitation, ionization, and electronic rearrangement in atoms, ions and molecules induced by the β-decay. It is obvious also that the method as applied here is not restricted to using the sudden approximation. More over the main corrections (kinematics', recoil etc.) to this approximation, for example, in a case of nuclear reactions may be further considered [51,171,72,124,149,150].

4 THEORY OF THE CHEMICAL ENVIRONMENT EFFECT ON THE β DECAY PARAMETERS

4.1 Introduction

Here we discuss the contributions of the chemical bond and electronic rearrangement effects on the numerical values of β-decay parameters following to the refs. [1,79,80]. We will consider the energy corrections due to the electronic rearrangement induced by the β-decay. The allowed (superallowed) β-transitions ^{3}H-^{3}He, ^{6}He-^{6}Li, ^{33}P-^{33}S, ^{35}S-^{35}Cl, ^{63}Ni-^{63}Cu, ^{241}Pu-^{241}Am are considered. The parameters of some allowed and super allowed β-transitions are listed in Table 5 [79,80]. Indeed, such a choice is defined by the following circumstance. The expressions (12)-(15) are exact for these transitions and the corresponding nuclear matrix elements are simplified in comparison with forbidden transitions. For example, the value $\int 1$ can be defined exactly for superallowed β$^\pm$-transitions: $\int 1=[(T\mp T_3)(T\pm T_3+1)]^{1/2}$. Here T_3 is the isospin projection, which is defined as $T_3=(Z-N)/2$. An account of the meson exchange currents (this contribution is about a few percent) for β-transition between purely isospin states does not change the result, connected with the isospin conservation. The value $\int\sigma=0$ for the superallowed $0^+\rightarrow0^+$ transition between the neighbour members of an isomultiplet and for T=1: $\int 1=\sqrt{2}$. Let us remember that the known theoretical parameter ξ for a majority of the β-transitions is [15]: $\xi=\alpha Z/2R>>1$.

The β-decay ^{241}Pu-^{241}Am is non-unique of the first forbiddance (ξ=18, i.e. $\xi>>1$). As a result, the expressions are correct for this transition too. The chemical bond effect on the β-decay parameters is studied in a number of publications (see Refs. [1−15,24−27,29−31,124−126]). An account (or non-account) of the chemical environment contribution leads to the known discrepancies in the data for half-life periods. A part of these discrepancies is due to the β-decay channel contribution (the β-particle occupies the external non-occupied atomic level). One could also take into account a few additional factors, provided by the chemical bond effect: i) Changing the electron

wave functions because of the changing atomic electric field and shell occupation numbers in different chemical substances; ii) The integration limits (Fermi integral function) are also changed in a case of the different chemical substances; as a rule, the β-particle and neutrino take away the difference between the initial and final nuclei, provided by the nuclear and electronic rearrangement. We already mentioned the bound β-decay channel. The confirmation of this de-

cay channel was found in the synchrotron and SIS/ESR experiments (GSI, Darmstadt) [3−8,42]. The mass-spectrometric St. Petersburg experiment (Russia) should also be mentioned [9]. It was the first to measure a change in the lifetime of a tritium nucleus due to changes in its electron surroundings. Despite these remarkable experimental results of previous years, accurate data on the corresponding parameters are absent for a majority of β decays.

Table 5

Parameters of the allowed (super allowed) β-transitions

Decay	Z_{mat}-Z_{daught}	$I_i^{\pi_i} \to I_f^{\pi_f}$	Type	E_0, keV	$T_{1/2}$	lg ft
^{3}H-^{3}He	$1 \to 2$	$1/2^+ \to 1/2^+$	super.	18.65	12.296 years	3.05
^{6}He-^{6}Li	$2 \to 3$	$0^+ \to 1^+$	super.	3500	0.813 sec	2.9
^{33}P-^{33}S	$15 \to 16$	$1/2^+ \to 3/2^+$	allow.	249	25.3 days	5.0
^{35}S-^{35}Cl	$16 \to 17$	$3/2^+ \to 3/2^+$	" "	167.4	87.4 days	5.0
^{42}Sc-^{42}Ca	$21 \to 20$	$0^+ \to 0^+$	super.	5409	0.683 sec	3.5
^{45}Ca-^{45}Sc	$20 \to 21$	$7/2^- \to 7/2^-$	" "	257	165 days	6.0
^{63}Ni-^{63}Cu	$28 \to 29$	$1/2^- \to 3/2^-$	" "	65.8	100 years	6.6
^{241}Pu-^{241}Am	$94 \to 95$	$5/2^+ \to 3/2^-$	1 forb.	20.8	14.4 years	5.8

4.2 Beta Decay of Tritium

In the experiment of Ref. [9] a change in the tritium nucleus lifetime due to changes in its electron surroundings was discovered. To calculate the absolute values of the difference of the decay constants $\Delta\lambda_{am}$ and half-life periods ($T_{1/2}=ln2/\lambda$) for molecular and atomic tritium $\Delta T_{1/2}=(T_{1/2})_m-(T_{1/2})_a$ we use the value: $(T_{1/2})_m = (12.296\pm0.017)$ years. The experimental values for $\Delta\lambda_{am}$ and $\Delta T_{1/2}$ are as follows [9]

$$\Delta\lambda_{am}=(4.6\pm0.8)\cdot10^{12}\,\text{sec}^{-1}, (\Delta T_{1/2})_{am}=$$

$$=(0.03152\pm0.00553)\text{ years}=11.5\pm2.0\text{ days}.$$

In the reaction $H^+ \to {}^3He^{++}+e^-+18.6$ keV the β-electrons are generated with wavelengths, which are characteristic for the atomic electron systems. In this case the interaction between the beta-electron and orbital electrons and vacancies is very effective. Further it leads to observable changes in the half-life period. It is well known [1−3,9,124] that hitherto the attempts to define nuclear constant values (which characterize the beta processes) on the basis of data for the tritium decay fail. The obtained values for the half-life period and boundary beta spectrum energy in the corresponding experiments are dependent upon the type of the studied chemical compound. As a result, there is no possibility of agreement between the experimental values of $T_{1/2}$ and E_0. It is of great interest to study an effect of the triton chemical surrounding on $T_{1/2}$. It is especially important in light of the known simplicity of such atomic structures as ^{3}H, ^{3}H$^+$, ^{3}H$^-$. Using the experimental data on the difference between the decay parameter values for atomic and molecular tritium it was experimentally found the half-life period value for the atomic tritium [9]: $(T_{1/2})_a = =(T_{1/2})_m-(\Delta T_{1/2})_{am}=(12.264\pm0.018)$ years. Further it is possible to find an absolute value of the free triton half-life period $(T_{1/2})_t$ by using the experimental value $(T_{1/2})_q$ and theoretical data on the β-decay atomic effects in ^{3}H. We have taken into account the following effects: i) the electron excitation in the bound spectrum while occupying the He level by the β-electron; ii) excita-

tion to the continuum spectrum due to the exchange of the orbital electron by β-electron; iii) the charge screening effect by the orbital electron; iv) the excited states in ^{3}He$^+$. According to Ref. [9], the corresponding correction to the value $(T_{1/2})_a$ is 0.86±0.08%, that results in the value of the free triton half-life period as follows: $(T_{1/2})_t= (12.369\pm0.020)$ years. An account of the chemical surrounding effect in a case of the T-containing compounds is an important problem not only from the point of view of the β-decay theory, but in light of using the tritium electron sensor (probe) to reveal the spatial correlations of coordinates for molecular studying object, definition of the electron density distribution, direction of the chemical bonds etc (see Refs. [1,2,9,50−52, 56−59,62−68]). The tritium electron probe possesses a complex of the known parameters, provided by specific features of the β-decay (namely, by an opposite direction of the β-electrons pulse in relation to a nucleus spin direction because of the non-conserving parity in the β-decay; definite helicity of the corresponding antineutrino; a spin of antineutrino is collinear to a pulse and the definite helicity is taken by an electron too; the exact representation of the β-electrons energy spectrum in the range from zero to the boundary energy 18.6 keV, which is not perturbed by the atomic effects). It is obvious that studying the tritium β-decay in some atomic-molecular systems allows one in principle to define a whole set of parameters for the input electron flux. Further it allows one to treat the electron structure of a system. We have estimated the numerical values of the β-decay parameters in the atom (ion) of tritium while taking into account the atomic factors. Let us note that a channel of forming β-electron in the K- shell is not significant in the case of the tritium ion β-decay [124]. Our estimate for the tritium atom half-life period is: $(T_{1/2})_a=12.26$ years; the correction to value $(T_{1/2})_a$ due to the electron-atomic effects is $0.0082\cdot12.26$ years [i.e.$(\Delta T_{1/2}/T_{1/2})_a=0.82\%$]. In result, the half-life period value $(T_{1/2})_t$ is [31,134]: $(T_{1/2})_t=12.36$ years. Obviously, there is a physically reasonable agreement between the calculated and measured values. One could

wait for more contradictory picture in the case of the β-decay in more complicated atoms because of the large complexity of taking into account the atomic effects in comparison with quite simple system ^{3}H. In Refs. [31,134] the first estimate of the T half-life period in the case of β-decay for the halogen-containing molecular T (^{3}HCl) was presented. The calculation was carried out within the non-relativistic KS approach while using the exchange-correlation potentials Eqs. (13) and (16). The obtained value for $(T_{1/2})$ is $(T_{1/2})_m$=12.28 years; the corresponding correction due to the chemical bond effect is $(\Delta T_{1/2})_{am}$=0.024, i.e. 0.20%. For comparison let us remember the experimental (molecular tritium) value: $(T_{1/2})_m$=12.296 years and the chemical bond effect correction $(\Delta T_{1/2})_{am}$= =0.03152, i.e. 0.26%. Obviously, here there is physically reasonable agreement too. From the other side, the corrections due to the chemical bond effect for the molecular tritium and halogen-containing tritium compound will be different.

4.3 The Chemical Bond Effect on the Beta Decay Parameters

Further we review the DKS calculation results for the β-decay parameters and corrections due to the chemical bond and other atomic effects [14,24–

27,30,124–126]. The energy corrections to the boundary energy of β-spectrum due to the electron shells reconstruction are presented in Table 6. The following beta decays ^{33}P$^{(0)}$-^{33}S$^{(+1)}$, ^{33}P$^{(+1)}$-^{33}S$^{(+2)}$, ^{35}S$^{(0)}$-^{35}Cl$^{(+1)}$, ^{35}S$^{(+2)}$-^{35}Cl$^{(+3)}$, ^{63}Ni$^{(0)}$-^{63}Cu$^{(+1)}$, ^{63}Ni$^{(+2)}$-^{63}Cu$^{(+3)}$, ^{241}Pu$^{(0)}$-^{241}Am$^{(+1)}$, ^{241}Pu$^{(+2)}$-^{241}Am$^{(+3)}$, ^{241}Pu$^{(+2)}$-^{241}Am$^{(+3)}$, ^{241}Pu$^{(+4)}$-^{241}Am$^{(+5)}$ are considered in ref. [1]. Calculation is carried out in the free ion approximation. The value δE corresponds to the correction to the boundary β-spectrum energy due to the electron shell reconstruction. The value $\delta^2 E$ is the difference of the corresponding corrections. Analysis shows that the DKS values are a little larger than the corresponding values that are obtained on the basis of the relativistic HFS and DF methods [14–16,24,29–31]. Obviously, the classical DF and HFS methods give a little more error in calculating the energy parameters in comparison with their optimized versions. It is worth comparing the Fermi function values for different calculation models [24, 29–31]. Two alternative definitions of the Fermi function values are usually used: i) The relativistic electron radial wave functions are calculated on the boundary of the spherical nucleus with radius R [14,15]; ii) definition of Fermi function by means of squares of expansion amplitudes of the radial wave functions $f^2_{+1}(0)+g^2_{-1}(0)$, $r{\to}0$ (see [29–31,24]).

The energy corrections to boundary energy of the β-spectrum due to the electron shells reconstruction

Decay	Configuration	The total shell energy, eV		Differences in energy, eV	
		Mat. atom	Daught. atom	δE	$\delta^2 E$
P$^{(0)}\to$S$^{(+1)}$	[Ne]$3s^23p^2_{1/2}3p_{3/2}$	9239	10782	1543	14
P$^{(+1)}\to$S$^{(+2)}$	[Ne]$3s^23p^2_{1/2}$	9230	10759	1529	
S$^{(0)}\to$Cl$^{(+1)}$	[Ne]$3s^23p^2_{1/2}3p^2_{3/2}$	10791	12471	1680	33
S$^{(+2)}\to$Cl$^{(+3)}$	[Ne]$3s^23p^2_{1/2}$	10760	12407	1647	
Ni$^{(0)}\to$Cu$^{(+1)}$	[Ar]$3d^4_{3/2}3d^4_{5/2}4s^2$	41238	44871	3633	26
Ni$^{(+2)}\to$Cu$^{(+3)}$	[Ar]$3d^4_{3/2}3d^4_{5/2}$	41214	44821	3607	
Pu$^{(0)}\to$Am$^{(+1)}$	[Rn]$5f^6_{5/2}7s^2$	806868	829365	22497	
Pu$^{(+2)}\to$Am$^{(+3)}$	[Rn]$5f^6_{5/2}$	806852	829331	22480	17
Pu$^{(+2)}\to$Am$^{(+3)}$	[Rn]$5f^4_{5/2}7s^2$	806845	829309	22464	33
Pu$^{(+4)}\to$Am$^{(+5)}$	[Rn]$5f^4_{5/2}$	806800	829245	22445	52

According to Refs. [3,24, 29–31], the difference in the Fermi function values increases with increasing Z. The same effect is characteristic for the integral Fermi function. It is found that the integral Fermi function f is changed for different β-decays {for example, ^{33}P-^{33}S (E_0=249keV), ^{35}S-^{35}Cl (E_0=167 keV) on 2–4%; ^{63}Ni-^{63}Cu (E_0=65.8 keV) on 5%, ^{241}Pu-^{241}Am (E_0=20.8 keV) — 32%} in the case of using the Fermi function definition on the basis of the wave functions values on the boundary of a nucleus and values of these functions in zero [29–31,124]. In Table 7 the quantitative chemical bond effect on the half-life period for the β-decay ^{33}P$^{(0)}$-^{33}S is listed. In column A we present the data, obtained on the basis of calculation within the optimized DF approach (GIDF). The GIDKS data are listed in column B and the standard DF calculation data in column C [24, 29–31]. We use the following notations: $\Delta f/f$ is the relative changing decay probability (Fermi integral function), which is equal to the change in the β half-life period with the opposite sign ($-\Delta T_{1/2}/T_{1/2}$). Let us give a short

comment regarding the choice of the boundary energy values. The value 249000 eV is accepted for the boundary energy of the P$^{(0)}$ decay. Analogously, the value 249014 eV is used for the decay of P$^{(+2)}$ in the first variant of calculation. The pair of the energy values 248986 and 249000 eV is chosen in the second variant of the calculation correspondingly. All presented results lead to an identical conclusion about the dependence of the change in the half-life period on the ionic degree. All versions of the calculation give very close values of $\Delta f/f$ [29–31]: $\Delta f/f$= 0.0079% (GIDF), $\Delta f/f$=0.0082% (GIDKS), $\Delta f/f$=0.0075% (DF). One concludes that the corresponding change $\Delta f/f$ is sufficiently small. The experimental data for β-decay ^{33}P$^{(0)}$-^{33}S are absent. But our data are correlated with recent theoretical and experimental data for ^{7}Be, ^{22}Na, and ^{40}K isotopes [10,11]. These data suggest that the effect of chemistry (plus pressure) is quite little and discernible. Calculation for ^{33}P-^{33}S decay shows that the integral Fermi function is less in the case of the ionized phosphor β-decay in compari-

son with the neutral phosphor. As a result, β-decay of the ionized phosphor runs more slowly. From the other side, the Fermi function value is more for neutral phosphor and its decay runs more quickly.

The chemical bond effect on the half-life period for the decay $^{33}P^{(0)} \to ^{33}S$ decay

Decay of a neutral atom				Decay of an ionized atom			$\Delta f/f$, 10^{-3} %
Atom	E_0, eV	$f(E_0,Z)$		Ion	E_0, eV	$f(E_0,Z)$	
$P^{(0)}$	249000	4.87541(-2)	A	$P^{(1+)}$	248987	4.87501(-2)	8.2
	249013	4.87617(-2)			249000	4.87580(-2)	
$P^{(0)}$	249000	4.87565(-2)	B	$P^{(1+)}$	248986	4.87524(-2)	8.39
	249014	4.87637(-2)			249000	4.87598(-2)	
$P^{(0)}$	249000	4.87529(-2)	C	$P^{(1+)}$	248988	4.87492(-2)	7.5
	249012	4.87608(-2)			249000	4.87572(-2)	

It is interesting to note that in the case of the $S^{(0)}$ decay the correction to boundary kinetic energy is more than 33 eV when compared to the case of the $S^{(+2)}$ decay. The experiment allows one to define only the sum of energies, obtained by leptons from atomic nucleus and electron shells [29–31]. In this case, the experimental value E_0 is 167400±100 eV.

There is another situation (large changes in $T_{1/2}$ value) for ^{241}Pu-^{241}Am decay. This transition is of great interest due to the different dependence of change in $T_{1/2}$ on chemical surrounding and large discrepancies in the β-decay parameters data. The typical example of Pu compounds is the pair PuO_2, PuO. In Table 8 we present the GIDKS data ($\Delta f/$ $f=-\Delta T_{1/2}/T_{1/2}$) regarding the chemical bond effect on the half-life period for the β-decay ^{241}Pu-^{241}Am. According to the DF, GIDF, GIDKS data [1,12–14], the Fermi function values in the case of the Pu double ionization are less than ~0.1−0.9% in comparison with analogous data for the neutral Pu decay. So, the neutral ^{241}Pu decay runs more slowly in comparison with ionized $Pu^{(+2)}$. The Fermi function value change is ~0.1−0.4% (the HFS data) and ~ 0.3−0.8% (GIDF data). An account of the channel of β-decay with occupying the external atomic orbitals gives a reasonable explanation of the Pu half decay period values dependent on the chemical composition [24,29−31,15,124].

The chemical bond effect on the half-life period for the decay ^{241}Pu-^{241}Am

Decay of a neutral atom			Decay of an ionized atom			
Atom	E_0, eV	$f(E_0, Z)$	Ion	E_0, eV	$f(E_0, Z)$	$\Delta f/f$, %
	20800	1.72164(-3)	$Pu^{(+2)}$	20783	1.71596(-3)	-0.33
	20817	1.72522(-3)		20800	1.71953(-3)	-0.33
$Pu^{(0)}$	20800	1.72164(-3)	$Pu^{(+2)}$	20767	1.71148(-3)	-0.59
	20833	1.72952(-3)		20800	1.71931(-3)	-0.59
	20800	1.72164(-3)	$Pu^{(+4)}$	20748	1.70615(-3)	-0.90
	20852	1.73403(-3)		20800	1.71842(-3)	-0.90

Surely, it would be desirable to compare the theoretical data with any experiment. It is known that in a compound the typical (Mulliken etc) atomic charge often is about half of the nominal oxidation state. Our results ($\Delta f/f \sim 1\%$) are correlated with other theoretical and experimental data [10,11]. From the other side, one could wait for a possible giant change in the half-lives of bare isotopes compared to their neutral counterparts [94]. The preliminary data [1] indicates such an effect. Surely, the FRS-ESR experimental studying is of a great interest in this case.

5 CONCLUDING REMARKS AND FUTURE PERSPECTIVES

We discussed a new field of investigations, which lies on the boundary of the modern quantum optics and photoelectronics, laser physics and atomic and nuclear physics [1]. It includes different interesting physical boundary processes, in particular, the cooperative electron β-nuclear processes in atomic systems (including processes of the excitation, ionization, electronic rearrangement) and chemical bond effect on the β-parameters. We reviewed the relativistic DKS treating the finite size of the nucleus, radiation and exchange-correlation corrections to the β-decay parameters for a set of the allowed (superallowed) transitions: ^{33}P-^{33}S, ^{35}S-^{35}Cl, ^{63}N-^{63}Cu, ^{241}Pu-^{241}Am etc. We discussed also the chemical bond effect on parameters of some β-transitions. The correct treatment of chemical environment effect is shown to modify the β-decay characteristics (integral Fermi function, half-life period, probability). The electronic rearrangement induced by nuclear transmutation in the β-decay $^{6}_{2}He_4 \to (^{6}_{3}Li^{+}_{3})^* + e^- + \bar{}_e$ is considered. The quantitative estimates for excitation to the final discrete states of $^6Li^+$ (including to the doubly excited autoionizing states) as well as the total probabilities for single and double ionization are listed. The half-life period for β-decay of the tritium atom (ion) has been estimated, taking into account the bound beta decay channel correction and some other accompanying effects (population of the bound states of ^3He, population of the continuum states resulting from exchanging the orbital electron by β-electron, the charge screening effect due to the orbital electron etc.). The estimated values of the half-life period $T_{1/2}$ for tritium β-decay and free triton

β-decay are as follows: $(T_{1/2})_a$=12.26 years (correction due to the electron-atomic effects $(\Delta T_{1/2}/T_{1/2})_a = 0.82\%$) for the tritium atom and $(T_{1/2})_t$=12.36 years for the free triton. These data are in physically reasonable agreement with the experimental data: $(T_{1/2})_a$= (12.264±0.018) years, $(\Delta T_{1/2}/T_{1/2})_a = 0.86\pm0.08\%$ and $(T_{1/2})_t$=(12.369± 0.020) years for atomic tritium and $(T_{1/2})_m$=(12.296±0.017) years, $(\Delta T_{1/2})_{am} = 0.03152$ (i.e. 0.26%) for the molecular tritium. The values $T_{1/2}$ in a case of β-decay for the halogen-containing molecular tritium (^{3}HCl): $(T_{1/2})_m$=12.28 years (^{3}HCl) is firstly presented and the correction due to chemical bond effect $(\Delta T_{1/2})_{am}$=0.024 (i.e. 0.20%). In conclusion let us note that the further development of the electron-β-nuclear spectroscopy of atoms, ions and molecules is of a great theoretical and practical interest. The development of new experimental methods (combination of the FRS and ESR) [3−12,147]) for the measurement of the β-decay parameters promises the further essential progress in our understanding of radioactive nuclear decays. Obviously, the storage rings are ideal tools for precise measurements of masses and beta decay lifetimes of nuclei of relevance for astrophysics. Such an approach can be useful, providing perspective for the development of new nuclear models, search of the new cooperative effects on the boundary of atomic and nuclear physics, carrying out new methods for treating the spatial structure of molecular orbitals, diagnostics of the hydrogen-containing compounds by means of exchange of the hydrogen atoms by tritium, studying the chemical bond nature and checking different theoretical models in quantum chemistry and solids physics, studying the properties of energy releasing in the tritium (DT, TT) plasmas. Finally, an availability of more exact data on the β-decay lifetimes and other (nuclear) parameters with taking into account the chemical bond and much larger bound β-decay effects is also important in astrophysics and cosmology, studying the substance transformation in the Universe, relationships for n/p, ^{3}H/^{3}He, cosmological constants etc. [1−16, 120, 124,140−150]. In any case, the electron-β (more generally, α, γ, μ)-nuclear spectroscopy of atoms and molecules opens absolutely new possibilities in the bridging of nuclear physics and traditional quantum chemistry (atomic and molecular physics) [1−16,124,140−150]. Obviously, these possibilities are strengthened by quickly developed nuclear quantum optics (see Refs. [14,20−28, 40,41,56−80,147−150]). Really, a superintense laser (more exactly, x-raser or graser) field may provide a definite measurement of the change in the dynamics of the nuclear processes, including β-(or γ- and α-) decay, as it has been underlined, for example, in Refs. [20,56−59,74,76,150].

ACKNOWLEDGMENTS

References

1. A. V. Glushkov, O.Yu.Khetselius, L.Lovett., Advances in the Theory of Atomic and Molecular Systems: Dynamics, Spectroscopy, Clusters, Nanostructures, Series: Progress in Theoretical Chem.and Phys., Eds. Piecuch P., Maruani J., Delgado-Barrio G., Wilson S. (Berlin, Springer). — 2009,Vol.20,P.125−172.

2. I. G. Kaplan, V. N. Smutny, Adv. Quantum Chem. **19**, 289 (1988); I. G. Kaplan, J. Phys. G: Nucl. Part. Phys. **23**, 683 (1997); R. Tegen, Nucl. Phys. A **706**, 193 (2002)

3. M. Madurga, M.J. G. Borge, J. C. Angelique, L. Bao, U. Bergmann, A. Butўa, J. Ceerk, J. M. Daugas, C. A. Diget, L. M. Fraile, H.O. U. Fynbo, H. B. Jeppesen, B. Jonson, E. Lienard, F. Marechal, M. Marques, V. Meot, F. Negoita, T. Nilsson, G. Nyman, F. Perrot, K. Riisager, O. Roig, O. Tengblad, E. Tengborn, M. Turrion, K. Wilhelmsen Rolander, J. Phys.CS. **111**, 012024 (2008); R.Robertson, D.Knapp, Ann.Rev.Nucl.Sci.**38**,185(1988).

4. Yu.A. Litvinov, F. Attallah, K. Beckert, F. Boscha, D. Boutina, M. Falch, B. Franzke, H. Geissel, M. Hausmann, Th. Kerscher, O. Klepper, H. — J. Kluge, C. Kozhuharov, K. E. Luьbner, G. Mьnzenberg, F. Nolden, Yu.N. Novikov, Z. Patyk, T. Radona, C. Scheidenberger, J. Stadlmann, M. Stecka, M. B. Trzhaskovskaya, H. Wollnik, Phys. Lett. B **573**, 80 (2003)

5. K. Takahashi, R. N. Boyd, G. I. Mathews, K. Yokoi, Phys. Rev. C **36**, 1522 (1987)

6. M. Jung, F. Bosch, K. Beckert, H. Eickhoff, H. Folger, B. Franzke, A. Gruber, P. Kienle, O. Klepper, W. Koenig, C. Kozhuharov, R. Mann, R. Moshammer, F. Nolden, U. Schaaf, G. Soff, P. Spдdtke, M. Steck, T. Stuьhlker, K. Sьmmerer, Phys. Rev. Lett. **69**, 2164 (1992)

7. F. Bosch, T. Faestermann, J. Friese, F. Heine, P. Kienle, E. Wefers, K. Zeitelhack, K. Beckert, B. Franzke, O. Klepper, C. Kozhuharov, G. Menzel, R. Moshammer, F. Nolden, H. Reich, B. Schlitt, M. Steck, T. Stuьhlker, T. Winkler, K. Takahashi, Phys. Rev. Lett. **77**, 5190 (1996)

8. T. Ohtsubo, F. Bosch, H. Geissel, L. Maier, C. Scheidenberger, F. Attallah, K. Beckert, P. Beller, D. Boutin, T. Faestermann, B. Franczak, B. Franzke, M. Hausmann, M. Hellstrцm, E. Kaza, P. Kienle, O. Klepper, H. J. Kluge, C. Kozhuharov, Yu. Litvinov, M. Matos, G. Mьnzenberg, F. Nolden, Yu. Novikov, M. Portillo, T. Radon, J. Stadlmann, M. Steck, T. Stuьhlker, K. Sьmmerer, K. Takahashi, H. Weick, M. Winkler, T. Yamagushi, Phys. Rev. Lett. **95**, 052501 (2005)

9. Yu.A. Akulov, B. A. Mamyrin, Phys. Lett. B **600**, 41 (2004); Phys. Atom. Nuclei **67**, 464 (2004); Physics Uspekhi **174,** 1791 (2004); Phys. Lett. B **610**, 45 (2005)

10. G. T. Emery, Ann. Rev. Nucl. Sci. **22**, 165 (1972); T. Ohtsuki, H. Yuki, M. Muto, J. Kasagi, K. Ohno, Phys. Rev. Lett. **93**, 112501 (2004); Y. Nir-El, G. Haquin, Z. Yungreiss, M. Hass, G. Goldring, S. K. Chamoli, B. S. Nara Singh, S. Lakshmi, U. Kuьster, N. Champault, A. Dorsival, G. Georgiev, V. Fedoseyev, B. A. Marsh, D. Schumann, G. Heidenreich, S. Teichmann, Phys. Rev. C **75**, 012801 (2007)

11. G. Gyьrky, J. Farkas, C. Yalзin, G. G. Kiss, Z. Elekes, Zs. Fьlцp, E. Somorjai, Europhys. Lett. **83**, 42001 (2008); K.K. M. Lee, G. Steinle-Neumann, Earth and Planet. Sci. Lett. **267**, 628 (2008); R. Blackburn, T. Yassine, Int. J. Rad. Appl. C. Rad. Phys. And Chem. **40**, 263 (1992); A.M. Nicolцs, A. Trifone, S.J. Nassiff, J. Radioanal. Nucl. Chem. **125**, 473 (1988)

12. T. Kurtukian-Nieto, J. Benlliure, K. Schmidt, Nucl. Instr. and Methods in Phys. Res. A: Acceler., Spectr., Det. and Ass. Equip. **589**, 472 (2008); V. Kozlov, N. Severijns, D. Beck, M. Beck, S. Coeck, B. Delaurй, A. Lindroth, S. Kopecky, P. Delahaye, F. Wenander, V. V. Golovko, I. S. Kraev, T. Phalet and ISOLDE, NIPNET and TRAPSPEC Collab., Int. J. Mass. Spectr. **251**, 159 (2006)

13. V. L. Mikheev, V. A. Morozov, N. V. Morozova, Phys. of Particles and Nucl. Lett. **5**, 371 (2008); V. I. Vysotskii, Phys. Rev. C **58**, 337 (1998)

14. A. Dykhne, G. Yudin, Sudden Perturbations and Quantum Evolution (UFN, Moscow, 1996)

15. B. S. Gelepov, L. Zyryanova, Yu. Suslov, Beta Processes (Nauka, Leningrad, 1978); V. Rusov, V. Tarasov, D. Litvinov, Theory of Beta Processes in Georeactor (URS, Moscow, 2008)

16. Photonic, Electronic and Atomic Collisions, ed. by F. Aumar and H. Winter (World Scientific, Singapore, 1997)

17. C. Ching, T. Ho, Phys. Rev. **112**, 1 (1984)

18. I. Kopytin, K. Karelin, A. Nekipelov, Phys. Atom. Nucl. **67**, 1429 (2004); I. Izosimov, A. Kazimov, V. Kalinnikov, Phys. Atom. Nucl. **67**, 1876 (2004)

19. L. I. Urutskov, D. V. Filippov, Physics-Uspekhi **174,** 1355 (2004); F. F. Karpeshin, M. B. Trzhaskovskaya, Yu.P. Gangrskii, JETP **99**, 286 (2004)

20. C. Mьller, A. Di Piazza, A. Shahbaz , T. J. Bьrvenich, J. Evers, H. Z. Hatsagortsyan, C. H. Keitel, Laser Physics **11**, 175 (2008); T. J. Burnevich, J. Evers, C. H. Keitel, Phys. Rev. C **74**, 044601 (2006); Phys. Rev. Lett. **96**, 142501 (2006); A. Shahbaz, C. Mьller, A. Staudt, T. J. Burnevich, C. H. Keitel, Phys. Rev. Lett. **98**, 263901 (2007)

21. M. Romanovsky, Laser Physics **1**, 17 (1998); M. R. Harston, J. J. Caroll, Laser Physics **7**, 1452 (2004); E. V. Tkalya, Phys. Rev. A **75**, 022509 (2007)

22. I. Ahmad, R. Dunfird, H. Esbensen, D. S. Gemmell, E. P. Kanter, U. Run, S. H. Siuthwirth, Phys. Rev. C **61**, 051304 (2000); S. Kishimoto, Y. Yoda, Y. Kobayashi, S. Kitao, R. Haruki, R. Masuda, M. Seto, Phys. Rev. C **74**, 031301 (2006)

23. S. Olariu, T. Sinor, C. B. Collins, Phys. Rev. B **50**, 616 (1994); A. V. Glushkov, L. N. Ivanov, Preprint ISAN RAS, N-2AS (1991); Preprint ISAN RAS, N-3AS (1991)

24. A. V. Glushkov, S. V. Ambrosov, A. V. Loboda, Yu.G. Chernyakova, O.Yu. Khetselius, A. A. Svinarenko, Nucl. Phys. A **734S**, 21 (2004)

25. A. Glushkov, S. Malinvoskaya, O. Khetselius, Eur. Phys. J. T **160**, 195 (2008)

26. A. Glushkov, S. Malinvoskaya, O. Khetselius, Mol. Phys. **106**, 1257 (2008)

27. A. V. Glushkov, O.Khetselius, S. V. Malinovskaya, Frontiers in Quantum Systems in Chemistry and Phys., Progress in Theoretical Chemistry and Physics, vol. 18, eds. S.Wilson, P.Grout, J. Maruani, G. Delgado-Barrio, P.Piecuch (Springer, Berlin,2008), p. 523

28. A. V. Glushkov, S. Malinovskaya, L. Vitabetskaya, Y. Dubrovskaya, O.Yu. Khetselius, in Recent Advances in Theoretical Physics and Chemistry Systems, Progress in Theoretical Chemistry and Physics, vol. 15, ed. by J. — P. Julien, J. Maruani, D. Mayou, S. Wilson, G. Delgado-Barrio (Springer, Berlin, 2006), p. 301

29. H.Behrens, J.Janske, Landolt-Berstein: New Series, Group 1, vol. 4 (Berlin, Springer, 1999)

30. I. Band, M. Listengarten, M. B. Trzhaskovskaya, Izv. AN USSR **51**, 1998 (1986)

31. A. Glushkov, O. Khetselius, T. Florko, Y. Dubrovskaya, Sensor Electr. and Microsyst. Techn. **3**, 21 (2006); **4,** 11 (2007); **5**, 41 (2008)

32. N. Nica, J. C. Hardy, V. E. Iacob, W. E. Rockwell, M. B. Trzhaskovskaya, Phys. Rev. C **75**, 024308 (2007)

33. N. Nica, J. C. Hardy, V. E. Iacob, S. Raman, C. W. Nestor M. B. Trzhaskovskaya, Phys. Rev. C **70**, 054305 (2004)

34. S.Raman, M.Ertugrul, C.Nestor, M.Trzhaskovskaya, At. Data Nuc.Data Tabl. **92**, 207 (2006)

35. S. Raman, C. Nestor, A. Ichihara, M. Trzhaskovskaya, Phys. Rev. C **66**, 044312 (2004)

36. L. N. Ivanov, E. P. Ivanova, L. Knight, Phys. Rev. A **48,** 4365 (1993)

37. A. V. Glushkov, L. N. Ivanov, E.P Ivanova, Autoionization Phenomena in Atoms, (Moscow University Press, Moscow, 1986)

38. A. V. Glushkov, S. V. Malinovskaya, A. V. Loboda, E. P. Gurnitskaya, D. A. Korchevsky, J. Phys.C. **11**, 188 (2005)

39. A. V. Glushkov, S. V. Ambrosov, A. V. Loboda, E. P. Gurnitskaya, G. P. Prepelitsa, Int. J. Quantum Chem. **104**, 562 (2005)

40. A. Glushkov, S. Malinovskaya, G. Prepelitsa, V. Ignatenko, J. Phys.C. **11**, 199 (2004)

41. A. Glushkov, Atom in Electromagnetic Field. Numerical Models, (KNT, Kiev, 2005)

42. P. Kienle, Phys. Scripta **46**, 81 (1993)

43. A. B. Migdal, J. Phys. USSR **4**, 449 (1941)

44. J. S. Levinger, Phys. Rev. **90**, 11 (1953); J. Phys. Radium **16**, 556 (1955)

45. P. A. Amudsen, P. H. Barker, Phys. Rev. C **50**, 2466 (1994)

46. R. Anholt, P. A. Amundsen, Phys. Rev. A **25**, 169 (1982)

47. O. Bohr, B. Motelsson, Structure of Atomic Nucleus, (Plenum, New York, 1971)

48. Th. Carlson, C. W. Nestor, T. C. Tucker, F. B. Malik, Phys. Rev. **169**, 27 (1968)

49. G. Ciochetti, A. Molinari, Nuovo Cim. **40**, 69 (1965)

50. T. Mukoyama, Sh. Ito, Phys. Lett. A **131**, 182 (1988); T. Mukoyama, S. Shimizu, J. Phys. G: Nucl. Phys. **4**, 1509 (1978)

51. L. Wauters, N. Vaeck, Phys. Rev. C **53**, 497 (1996)

52. L. Wauters, N. Vaeck, M. Godefroid, H. van der Hart, M.Demeur, J.Phys. B **30**, 4569 (1997)

53. A. V. Glushkov, I. T. Makarov, E. Nikiforova, M. I. Pravdin, Astropart.Physics **4**, 15 (1995)

54. A. V. Glushkov, L. G. Dedenko, M. I. Pravdin, I. E. Sleptsov, JETP **99**, 123 (2004) ; A. V. Glushkov, M. I. Pravdin et al, JETP :Lett. **87**, 345 (2008); JETP Lett. **87**, 190 (2008);

55. P. Piecuch, M. Wloch, J. R. Gour, D. J. Dean, M. Hjorth-Jensen, T. Papenbrock, in Nuclei and Mesoscopic Physics, vol. 995, ed. by V. Zelevinsky (AIP, Melville, NY, 2005), p. 28

56. V. I. Gol'danskii, Sov. Phys. — Uspekhi **19**, 180 (1976); G. G. Baldwin, J. C. Salem, V. I. Gol'dansky, Rev. Mod. Phys. **53,** 687 (1981)

57. V. S. Letokhov, in Application of Lasers in Atomic, Molecular and Nuclear Physics, ed. by A. M. Prokhorov, V. S. Letokhov (Nauka, Moscow, 1979), p. 412

58. V. S. Letokhov, V. I. Gol'dansky, JETP. **67**, 513 (1974); L. N. Ivanov, V. S. Letokhov, Com. Mod. Phys. D **4**, 169 (1985); A. V. Glushkov, L. N. Ivanov, S. V. Malinovskaya, Preprint ISAN RAS, N-1AS (1991); A. V. Glushkov, L. N. Ivanov, V. S. Letokhov, Preprint ISAN RAS, N-3AS (1991);

59. I. G. Kaplan, A. P. Markin, Reports of the USSR Acad. Sci. **223**, 1172 (1973); **232**, 319 (1977); JETP **64**, 424 (1973); JETP **69**, 9 (1975)

60. R. M Mussbauer, Z. Phys. A: Hadrons and Nuclei **151**, 124 (1958); L. Szilard, T. Chalmers, Nature (London) **134**, 462 (1934)

61. D. J. Dean, M. Hjorth-Jensen, K. Kowalski, P. Piecuch, M. Wloch, in Condensed Matter Theories, ed. by J. W. Clark, R. M. Panoff, H. Li (Nova Sci. Publishers, 2006)

62. J. S. Hansen, Phys. Rev. A **9**, 40 (1974)

63. J. Law, Nucl. Phys. A **286**, 339 (1977); Can. J. Phys. **58**, 504 (1980)

64. E. G. Drukarev, M. I. Strikman, JETP **64**, 1160 (1986)

65. J. Law, J. L. Campbell, Phys. Rev. C **25**, 514 (1982)

66. R. L. Wolfgang, R. Anderson, R. W. Dodson, J. Chem. Phys. **24**, 16 (1956); R. L. Martin, J. S. Cohen, Phys. Lett. A **110**, 95 (1985)

67. A. Glushkov, S. Malinovskaya, Rus. J. Phys. Chem. **62**, 100 (1988); **65**, 2970 (1988)

68. A. Glushkov, S. Malinovskaya, in New Projects and New Lines of Research in Nuclear Physics, ed. by G. Fazio, F. Hanappe (World Scientific, Singapore, 2003), p.242

69. V. Z. Maidikov, in New Projects and New Lines of Research in Nuclear Physics, ed. by G. Fazio, F. Hanappe (World Scientific, Singapore, 2003), p.227

70. A. Glushkov, S. Malinovskaya, A. Loboda, G. Prepelitsa, J. Phys.Cs. **35**, 420 (2006)

71. A. V. Glushkov, S. V. Malinovskaya, Yu.G. Chernyakova, A. A. Svinarenko, Int. J. Quantum Chem. **99**, 889 (2004)

72. A. V. Glushkov, S. V. Malinovskaya, Int. J. Quantum Chem. **104**, 496 (2005)

73. L. Bandurina, I. Krivsky, A. Lendel, S. Medvedev, Nucl. Phys. **39**, 296 (1984)

74. V. S. Letokhov, Phys. Lett. A **46**, 257 (1974)

75. V. S. Letokhov, Laser Specktroskopie (Akad. — Verlag, Berlin, 1977)

76. L. N. Ivanov, V. S. Letokhov, JETP **68**, 748 (1975); JETP **71**, 19 (1976)

77. E. P. Ivanova, L. N. Ivanov, E. V. Aglitsky, Phys. Rep. **166**, 315 (1988)

78. V. S. Letokhov, V. G. Minogin, JETP **69**, 1568 (1985)

79. E. P. Ivanova, L. N. Ivanov, JETP **83**, 258 (1996)

80. A. V. Glushkov, L. N. Ivanov, Phys. Lett. A **170**, 33 (1992); J. Phys. B: At. Mol. Opt. Phys. **26**, L379 (1993)

81. A. V. Glushkov, JETP Lett. **55**, 97 (1992); Preprint ISAN N 5AS, Moscow-Troitsk (1990).
82. A. V. Glushkov, Low Energy Antiproton Physics, **796**, 206 (2005); A. V. Glushkov, Phys. of Atom. Nuclei. **72**, 85 (2009).
83. M. Hehenberger, H. McIntosh, E. Brдndas, Phys. Rev. A **10**, 1494 (1974); A. V. Glushkov, S. V. Ambrosov, A. V. Ignatenko, D. A. Korchevsky, Int. J. Quantum Chem. **99**, 936 (2004)
84. A. V. Glushkov, O.Khetselius, A.Loboda, A.Svinarenko, Frontiers in Quantum Systems in Chemistry and Physics, Progress in Theoretical Chemistry and Phys., vol. 18, eds.S.Wilson, P.Grout., J.Maruani, G. Delgado-Barrio, P.Piecuch (Springer, Berlin, 2008), p. 501−558
85. A. V. Glushkov, E. P. Ivanova, J. Quant. Spectr. Rad. Transfer. **36**, 127 (1986)
86. E. P. Ivanova, L. N. Ivanov, A. V. Glushkov, A. Kramida, Phys. Scripta **32**, 512 (1985)
87. J. C. Slater, The Consistent Field Method for Molecules and Solids: Quantum Theory of Molecules and Solids, vol. 4 (McGraw-Hill, New York, 1974)
88. E. G. Gross, W. Kohn, Exchange-Correlation Functionals in Density Functional Theory (Plenum, New York, 2005)
89. S. Wilson, in Recent Advances in Theoretical Physics and Chemistry Systems, Progress in Theoretical Chemistry and Physics, vol. 16, ed. by J. Maruani, S. Lahmar, S. Wilson, G. Delgado-Barrio (Springer, Berlin, 2007), p. 11−80.
90. S.Wilson,Handbook on Molecular Physics &Quantum Chemistry (Wiley, N-Y.,2003), 680P.
91. W. Kohn, L.Sham, Phys. Rev. A **140**, 1133 (1964); P. Hohenberg, W. Kohn, Phys. Rev. B **136**, 864 (1964)
92. R. M. Dreizler, Phys. Scripta T **46**, 167 (1993)
93. P. Indelicato, J. P. Desclaux, Phys. Scripta T **46**, 110 (1993)
94. A.Glushkov, O.Khetselius, in Nuclear Physics in Astrophysics NPA-III (Dresden, Germany, 2007), p. 95; J. Phys. G., to be published
95. K. N. Koshelev, L. N. Labzowsky, I. I. Tupitsyn, J. Phys. B **37**, 843 (2004)
96. J. Bieron, P. Pyykkц, P. Jonsson, Phys. Rev. A **71**, 012502 (2005); J. Bieron, P. Pyykkő, Phys. Rev. A **71**, 032502 (2005)
97. P. Mohr, Atom. Data Nucl. Data Tabl. **24**, 453 (1993); Phys. Scripta T **46**, 44 (1993)
98. M. P. Das, M. V. Ramana, A. K. Rajagopal, Phys. Rev. **22**, 9 (1980)
99. K. Cheng, Y. Kim, J. Desclaux, Atom. Data Nucl. Data Tabl. **24**, 11 (1979)
100. G. Drake, Phys. Scripta T **46**, 116 (1993)
101. H. M. Quiney, I. P. Grant, Phys. Scripta T **46**, 132 (1993)
102. I. Klaft, S. Borneis, T. Engel, B. Fricke, R. Grieser, G. Huber, T. Kuhl, D. Marx, R. Neumann, S. Schroder, P. Seelig, L. Volker, Phys. Rev. Lett. **73**, 2425 (1994)
103. G. Gould, Phys. Scripta T**46**, 61 (1993); S. Blundell, Phys. Scripta T **46**, 144 (1993)
104. V. Dzuba, V. Flambaum, P. Silvestrov, O. Sushkov, Phys. Rev. A **44**, 2828 (1991)
105. H. Persson, I. Lindgren, S. Salomonson, Phys. Rev. Lett. **76**, 204 (1996)
106. W. Johnson, J. Sapirstein, S. Blundell, Phys. Scripta **46**, 184 (1993)
107. S. N. Tiwary, Rivista del Nuovo Cimento **18,** 1 (1995)
108. K. N. Koshelev, L. N. Ivanov, Phys. Rev. A **42**, 5784 (1990)
109. L. N. Ivanov, E. P. Ivanova, JETP. **110**, 483 (1996)
110. J.Bieron, C. F. Fisher, S.Fritzsche, K.Pachucki, J.Phys.B: At.Mol.Phys. **37**, L305 (2004)
111. U. Safranova, T. Cowan, M. Safranova, J. Phys. B: At. Mol. Phys. **38**, 2741 (2005)
112. V. Dzuba, V. Flambaum, M. S. Safranova, Phys. Rev. A **73**, 022112 (2006)
113. U. I. Safranova, M. S. Safranova, W. R. Johnson, Phys. Rev. A **71**, 052506 (2005)
114. V. Yerokhin, A. N. Artemyev, V. M. Shabaev, Phys. Rev. A **75**, 062501 (2007)
115. B. Sahoo, G. Gopakumar, R. Chaudhuri, B. Das, H. Merlitz, U. Mahapatra, D. Mukherjee, Phys. Rev. A **68**, 040501 (2003)
116. J. Santos, F.Parenre, S.Boucard, P.Indelicato, J.Desclaux, Phys.Rev.A**71**,032501 (2005)
117. A. Derevianko, S. G. Porsev, Phys. Rev. A **71**, 032509 (2005)
118. V. Zagrebaev, Yu. Oganessian, M. Itkis, W. Greiner, Phys. Rev. C **73**, 031602 (2006)
119. I. Theophilou, S. Thanos, A. Theophilou, J. Chem. Phys. **127**, 234103 (2007)
120. A. V. Glushkov, Relativistic and Correlation Effects in Spectra of Atomic Systems (Nauka, Moscow-Odessa, 2006)
121. I. P. Grant, Relativistic Quantum Theory of Atoms and Molecules, Theory and Computation, vol. 40 (Springer, Berlin, 2007), p. 587
122. E. P. Ivanova, I. P. Grant, J. Phys. B **31**, 2871 (1998); E. P. Ivanova, N. A. Zinoviev, Quant. Electronics **29**, 484 (1999); Phys. Lett. A **274**, 239 (2000)
123. K. G. Dyall, K. Faegri, Jr. Introduction to Relativistic Quantum Theory (Oxford University Press, Oxford, 2007), 650P.
124. A. V. Glushkov, Relativistic Quantum Theory. Quantum Mechanics of Atomic Systems (Astroprint, Odessa, 2008), 900P.
125. A. V. Glushkov, O.Yu. Khetselius, E. P. Gurnitskaya, A. V. Loboda, T. A. Florko, D. E. Sukharev, L. Lovett, in Frontiers in Quantum Systems in Chemistry and Physics, Progress in Theoretical Chemistry and Physics, vol. 18, ed. by S. Wilson, P. J. Grout., J. Maruani, G. Delgado-Barrio, P. Piecuch (Springer, Berlin, 2008), p.505
126. A. V. Glushkov, S. V. Ambrosov, A. V. Loboda, E. P. Gurnitskaya, O.Yu. Khetselius, in Recent Advances in Theoretical Physics and Chemistry Systems, Progress in Theoretical Chemistry and Physics, vol. 15, ed. by J. — P. Julien, J. Maruani, D. Mayou, S. Wilson, G. Delgado-Barrio (Springer, Berlin, 2006), p. 285
127. A. V. Glushkov, S. V. Malinovskaya, G.Prepelitsa, A.Ignatenko, J.Phys.Cs. **11**, 199 (2005)
128. The Fundamentals of Electron Density, Density Matrix and Density Functional Theory in Atoms, Molecules and the Solid State, Progress in Theoretical Chemistry and Physics, vol. 14, ed. by N. Gidopoulos and S. Wilson (Springer, Berlin, 2004), p.1
129. I. P. Grant, H. M. Quiney, Int. J. Quantum Chem. **80**, 283 (2000)
130. Supercomputing, Collision Processes, and Applications, Physics of Atoms and Molecules, ed. K.Bell, K.Berrington, D.Crothers, A. Hibbert, K. Taylor (Kluwer, N. — Y., 1999)
131. Advanced Topics in Theoretical Chemical Physics, Progress in Theoretical Chemistry and Physics, vol. 12, ed. by J. Maruani, R. Lefebvre, E. Brдndas (Springer, Berlin, 2004)
132. S. Wilson, J. Mol. Struct.: Theochem. **547**, 279 (2001)
133. A. Glushkov, S. Malinovskaya, E. Gurnitskaya, O. Khetselius, J.Phys.CS **35**, 426 (2006)
134. A. V. Glushkov, Rus. J. Struct. Chem. **29**, 3 (1988)**; 30**, 159 (1989); **31**, 9 (1990); **32**, 11 (1992); **34**, 3 (1993); Rus. J. Phys. Chem. **66**, 589 (1992); **66**, 1259 (1992).
135. A. V. Glushkov, Opt.Spectr.**62**, 966, 1212 (1988); **66**, 31 (1989); **66**,446 (1989); **66**,1180 (1989); **66**,1298 (1989); **70**, 952 (1991); **71**, 395 (1991); **72**, 542 (1992); **76**, 5, 885 (1994).
136. A. V. Glushkov, S. V. Malinovskaya, et al, Int. J. Quantum Chem. **104**, 512 (2005); **104**, 496 (2005); **104**, 562 (2005); **109**, 1717 (2009); **109**, 3331 (2005);
137. A. V. Glushkov,A.Loboda,E. P. Gurnitskaya,A. Svinarenko,Phys.Scr.T**135**, 014022 (2009)
138. A. V. Glushkov, S. V. Malinovskaya, Yu.V. Dubrovskaya, L. A. Vitavetskaya, in Recent Advances in Theoretical Physics and Chemistry Systems, Progress in Theoretical Chemistry and Physics, vol. 15, ed. by J. — P. Julien, J. Maruani, D. Mayou, S. Wilson, G. Delgado-Barrio (Springer, Berlin, 2006), p. 301−348.
139. V. N. Gedasimov, A. G. Zelenkov, V.Kulakov, V. A. Pchelin, M. V. Sokolovskaya, A. Soldatov, L. V. Chistyakov, JETP **94**, 1169 (1984)
140. K. Kar, S. Sarkar, A. Ray, Phys. Lett. B **261**, 217 (1991)
141. A. V. Glushkov, V. D. Rusov, S. V. Ambrosov, A. V. Loboda, in New Projects and New Lines of Research in Nuclear Physics, ed. by G. Fazio, F. Hanappe (World Scientific, Singapore, 2003), p. 126−142.
142. V. D. Rusov, V. N. Pavlovich, V. Vaschenko, V. Tarasov, T. Zelentsova, V. Bolshakov, D. Litvinov, S. Kosenko, O. Byegunova, J. Geophys. Res. B **112**, 09203 (2007); Rusov V. D., Glushkov A. V., Loboda A., Khetselius O.Yu., Svinarenko A. A., Khokhlov V., Prepelitsa G. P., Advances in Space Research. **42**, 1614 (2008).
143. Q. Sun, Z. — G. Huang, H. — G. Piao, Z. — Q. Luo, Chinese Astr. Astrophys. **31**, 229 (2008)
144. J. A. Behr, G. Gwinner, J. Phys. G: Nucl. Part. Phys. **36**, 033101 (2009)

145. K.Kettner, H.Becker, F. Strieder, C. Rolfs, J. Phys. G: Nucl. Part. Phys. **32**, 489 (2006)
146. S.Godovikov, Izv.RAN,Ser.Phys. **65**,1063 (2001); N.Zinner, Nucl.Phys.A**781**,81 (2007)
147. C. Bertulani, Nucl. Phys. A **626**, 187 (1997)
148. A. V. Glushkov, O.Khetselius, A.Loboda, E. P. Gurnitskaya, Meson-Nucleon Physics and Structure of the Nucleon, ed. by S. Krewald, H. Machner (IKP, Juelich, Germany), SLAC Trans. C070910 (Menlo Park, CA, USA) **2**, 186 (2007); A. V. Glushkov, ibid. **2**, 111 (2007)
149. S.Aseev, B.Mironov, S.Chekalin, V. S. Letokhov, JETP Lett. **87**, 361 (2008);
150. A. V. Glushkov, P. A. Kondratenko, Ya.I. Lepikh, A. P. Fedchuk, A. A. Svinarenko, L.Lovett, Int. Journ. Quant.Chem. **109,** 3473 (2009); A. V. Glushkov, Nuclear Quantum Optics. — Wiley, 2010.

A. V. Glushkov

LASER- ELECTRON-β-NUCLEAR SPECTROSCOPY OF ATOMIC AND MOLECULAR SYSTEMS AND CHEMICAL ENVIRONMENT EFFECT ON THE β-DECAY PARAMETERS: REVIEW

Abstract

We review a new field of investigations, which lies on the boundary of the modern quantum optics and photoelectronics, laser physics and atomic and nuclear physics. We discuss the cooperative laser-electron-β-nuclear processes in atoms and molecules [1], including the excitation, ionization, electronic rearrangement, induced by the nuclear reactions and β-decay and a state of art of the modern calculating the β-decay parameters for a number of allowed (super allowed) transitions (^{33}P-^{33}S, ^{241}Pu-^{241}Am etc) and a chemical bond effect on β-decay parameters. A few factors are taken into account: changing the integration limits in the Fermi function integral, energy corrections for different chemical substances, and the possibility of the bound β-decay or other decay channels. We review the studies of the electronic rearrangement induced by nuclear transmutation in the β-decay $^{6}_{2}\text{He}_4 \rightarrow \left(^{6}_{3}\text{Li}^{+}_{3} \right)^{*} + e^{-} + \overline{\nu}_e$. The half-life period $T_{1/2}$ for β-decay of tritium atom (ion) has been estimated while taking into account the bound β-decay channel and some other accompanying effects. The estimated values of $T_{1/2}$ for the tritium β-decay and free triton decay are: $(T_{1/2})_a$=12.26 years (correction due to the electron-atomic effects $(\Delta T_{1/2}/T_{1/2})_a$=0.82%) for the tritium atom and $(T_{1/2})_t$=12.36 years for the triton decay. These data are in physically reasonable agreement with experimental data by Akulov-Mamyrin [9]. We analyse the firstly presented [1] value $T_{1/2}$ in a case of the β-decay in the halogen-containing molecular tritium (^{3}HCl): $(T_{1/2})_m$=12.28 years (^{3}HCl); the correction due to the chemical bond effect is $(\Delta T_{1/2})_{am}$=0.024 (i.e. 0.20%).

Key words: laser-electron-β-nuclear spectroscopy, cooperative effects, beta-decay

А. В. Глушков

ЛАЗЕРНАЯ ЭЛЕКТРОН-β-ЯДЕРНАЯ СПЕКТРОСКОПИЯ АТОМНЫХ И МОЛЕКУЛЯРНЫХ СИСТЕМ И ЭФФЕКТ ВЛИЯНИЯ ХИМИЧЕСКОГО ОКРУЖЕНИЯ НА ПАРАМЕТРЫ БЕТА РАСПАДА: ОБЗОР

Резюме

Представлен обзор исследований в новой области, лежащей на стыке современной квантовой оптики и фотоэлектроники, лазерной, атомной и ядерной физики. Обсуждаются особенности кооперативных лазерно-электрон-β-ядерных процессов в атомах и молекулах, а также твердых телах [1], включающие возбуждение, ионизацию, электронное перераспределение, индуцированные ядерными реакциями, β-γ-распадом. Дан обзор проблематики вычисления параметров β- распада для ряда разрешенных (сверх разрешенных) переходов (^{241}Pu-^{241}Am и др), а также эффекта влияния химической связи на параметры β-распада, включая такие факторы как изменение пределов интегрирования функции Ферми, вклад канала связанного β-распада и других каналов. Количественно оценено электронное перераспределение, индуцированное ядерной трансмутацией в β-переходе: $^{6}_{2}\text{He}_4 \rightarrow \left(^{6}_{3}\text{Li}^{+}_{3} \right)^{*} + e^{-} + \overline{\nu}_e$. Период полураспада $T_{1/2}$ для β-распада атома трития (иона) оценен с учетом вклада канала связанного β-распада и ряда др. физических эффектов. Оценены значения $T_{1/2}$ для β-распада трития и распада свободного тритона: $(T_{1/2})_a$=12.26 лет (поправка за счет электрон-атомных кооперативных эффектов $(\Delta T_{1/2}/T_{1/2})_a$=0.82%) для атома трития и $(T_{1/2})_t$=12.36 лет для распада тритона. Приведенные теоретические данные находятся в приемлемом согласии с недавними экспериментальными данными Акулова-Мамырина [9]. Проанализированы впервые представленные в [1] оценки $T_{1/2}$ в случае β-распада для галоген- содержащего молекулярного трития (^{3}HCl): $(T_{1/2})_m$=12.28 лет (^{3}HCl); поправка на эффект химического окружения $(\Delta T_{1/2})_{am}$=0.024 (i.e. 0.20%).

Ключевые слова: лазерная электрон-β-ядерная спектроскопия, кооперативные эффекты, бета-распад

УДК 539.184

А. В. Глушков

ЛАЗЕРНА ЕЛЕКТРОН-β-ЯДЕРНА СПЕКТРОСКОПІЯ АТОМНИХ І МОЛЕКУЛЯРНИХ СИСТЕМ ТА ЕФЕКТ ВПЛИВУ ХІМІЧНОГО ОТОЧЕННЯ НА ПАРАМЕТРИ БЕТА РОЗПАДУ: ОГЛЯД

Резюме

Представлено огляд досліджень у новій галузі на стику сучасної квантової оптики і фотоелектроніки, лазерної, атомної, ядерної фізики. Обговорюються особливості кооперативних лазерно-електрон-β- ядерних процесів в атомах і молекулах, а також твердих тілах [1], включаючи збудження, іонізацію, електронний перерозподіл, який індукований ядерними реакціями, β-γ-розпадом. Наданий огляд проблематики визначення параметрів β-розпаду для ряду дозволених (над дозволених) переходів (^{241}Pu-^{241}Am інш.), а також ефекту впливу хімічного зв'язку на параметри β-розпаду з урахуванням таких факторів як змінення меж інтегрування при знаходженні функції Фермі, внесок каналу зв'язанного β- розпаду та інших каналів. Оцінений електронний перерозподіл, індукований ядерною трансмутацією у β-розпаді: $^{6}_{2}\text{He}_4 \rightarrow \left(^{6}_{3}\text{Li}^{+}_3\right)^{*} + e^{-} + \overline{\nu}_e$. Період полу-розпаду $T_{1/2}$ для β- розпаду атома тритія (іона) оцінено з урахуванням внеску каналу зв'язанного β- розпаду і інших фізичних ефектів. Оцінені значення $T_{1/2}$ для β- розпаду тритія і розпаду вільного тритону: $(T_{1/2})_a$=12.26 років (поправка на урахування електрон-атомних кооперативних ефектів $(\Delta T_{1/2}/T_{1/2})_a$=0.82%) для тритію і $(T_{1/2})_t$=12.36 років для розпаду тритону. Наведені теоретичні дані знаходяться у прийнятній згоді із недавніми експериментальними даними Акулова-Мамиріна [9]. Проаналізовані вперше наведені в [1] оцінки $T_{1/2}$ у випадку β- розпаду для молекулярного тритія, що містить галоген (^{3}HCl): $(T_{1/2})_m$=12.28 років (^{3}HCl); поправка на ефект хімічного оточення $(\Delta T_{1/2})_{am}$=0.024 (i.e. 0.20%).

Ключові слова: лазерна електрон — β- ядерна спектроскопія, кооперативні ефекти, бета-розпад

YU. F. VAKSMAN, YU. A. NITSUK, V. V. YATSUN, YU. N. PURTOV

I. I. Mechnikov National University, 65026 Odessa, Ukraine

DIFFUSION OF TRANSITION-METAL IONS (Fe, Ni) IN ZINC CHALKOGENIDES

The ZnS, ZnSe, ZnTe single crystals doped with iron and nickel are investigated. The diffusion doping is carried out from metallic nickel and powderlike iron in helium and argon atmosphere. The optical density spectra are investigated in the wavelength range of 2−3.8 eV. From the value of the absorption edge shift, the nickel and iron concentrations in crystals under investigation is determined. It is shown that nickel and iron doping results in appearance of absorption lines in the visible spectral region.

The nickel and iron impurity diffusion profile is determined by measuring the relative optical density of crystals in the visible spectral region. The diffusivities of nickel and iron in ZnS, ZnSe, ZnTe crystals are calculated at temperatures of 1020−1320 K.

The last years wide interest was paid to zinc-chalcogenides (ZnS, ZnSe, ZnTe) due to their new application fields. The ZnS and ZnSe crystals doped with transitional metals have been used as active media and gates in lasers of medium infrared (IR) radiation range [1,2]. The ZnTe crystals doped with iron and nickel are perspective materials for a photorefraction [3]. Therefore the fabrication of zinc chalcogenides crystals doped with transition-metal ions is actual problem.

There are two basic methods of zinc-chalcogenides doping with transition-metal ions. The first one is doping during the growing process from vapor phase and the second one is diffusive doping. In [4] the ZnSe:Fe and ZnSe:Ni single crystals were obtained from a vapor phase by free growth on a single crystal substrate with the use of chemical transport in hydrogen.

The advantage of the diffusion doping is the exact adjusting of profile and level of doping. In [2] the ZnSe:Fe crystals are obtained by the doping from a solid phase metallic source (a metallic layer). The diffusion doping in the iron vapor is carried out in [5]. Duration of diffusion process and small iron impurity concentrations in the obtained crystals are the lacks of these diffusion doping methods.

In this study we describe the diffusion technique of doping which allows to obtaining zinc-chalcogenides single crystals with predicted iron and nickel-impurity concentration. The structure of optical absorption spectra has been studied and identified in the visible region. Basing on the optical absorption edge shift, the nickel and iron concentration has been determined. The analysis of the relative optical density profile in the visible region enabled us to calculate the diffusivity of nickel and iron in ZnS, ZnSe, ZnTe crystals.

The purpose of this study is the development of the diffusion technique of zinc-chalcogenides crystals doping with iron and nickel and the determination of the diffusivity.

1 EXPERIMENTAL

The samples for the study were prepared by nickel and iron diffusion doping of pure ZnS, ZnSe and ZnTe

single crystals. The undoped crystals were obtained by free growth on a ZnSe single crystal substrate with the (111) growth plane. The method and the main characteristics of the ZnS, ZnSe and ZnTe crystals were described in details in [6]. Selection of temperature profiles and design of the growth chamber excluded the possibility of contact of the crystal with chamber walls. The dislocation density in obtained crystals was no higher than 10^4 cm^{-2}.

The ZnS:Ni, ZnSe:Ni and ZnTe:Ni crystals were doped by diffusion of impurity from the metallic nickel layer deposited on the crystal surface in the He + Ar atmosphere. The crystals were annealed at the temperatures T_a = 1020−1270 K. The diffusion process time was about 5 hours. After annealing the crystals changed the color: the crystals ZnS:Ni got a yellow color, ZnSe:Ni was light-brown, and ZnTe:Ni was dark-brown.

The first experiments with Fe diffusion were carried out according to a procedure similar for Ni diffusion. The crystals were doped via impurity diffusion from a metal Ni layer deposited on the crystal surface in an evacuated quartz cell. It was found that at 1220 K, the metal Ni layer ~10 mkm dissolved completely in the crystals in the span of no longer than 30 min. The optical absorption spectra showed that the obtained crystals were lightly doped. However, these crystals were found to be convenient objects for studying the optical absorption spectra.

To obtain heavily doped crystals the diffusion by impurity from metal powderlike Fe in He + Ar atmosphere was carried out. In order to avoid etching of crystals, powderlike ZnSe in the ratio 1:2 was added to the Fe powder. Crystals were annealed in evacuated quartz cells at temperatures from 1120 to 1320 K. The duration of the diffusion process was 10−30 hours. After annealing the ZnS:Fe crystals acquired a yellow-brown color, ZnSe:Fe was red-brown, and the ZnTe:Fe crystals were dark-brown.

The diffusion of nickel and iron was carried out under conditions, where the impurity concentration in the source (the metallic nickel layer) remained almost constant. In this case, the solution of the Fick diffusion equation for the one dimensional diffusion has the form

$$\tilde{N}(x,t) = C_0 \left(1 - erf \frac{x}{\sqrt{4Dt}}\right), \qquad (1)$$

where C_0 is the activator concentration near the surface, the symbol "erf" designates the error function (the Gauss function), D is the diffusivity, x is the coordinate, and t is the time.

The optical density spectra in the visible region were measured by means of an MDR-6 monochromator with diffraction gratings 1200 lines/mm. A FEU-100 photomultiplier was used as a light flow receiver. The optical density spectra were measured at 77 and 300 K.

To measure the diffusion profile of the impurities, a thin (0.2–0.4 mm) plate of the crystal was cleaved in the plane parallel to the direction of the diffusion flow. The measurements of the optical density profile of the Ni and Fe-doped crystals were carried out using an MF-2 microphotometer. This device provides the optical density measurement with the step 10 mkm in the direction of the diffusion flow. In this case, the integrated optical density in the spectral range 2.0–2.8 eV was measured.

2. OPTICAL DENSITY SPECTRA IN THE VISIBLE REGION

The optical density spectra (D* — optical density) of the ZnS:(Fe,Ni), ZnSe:(Fe,Ni), ZnTe:(Fe,Ni) crystals have been measured. The iron and nickel doping of crystals results in the absorption edge shift toward lower energies. The shift value increases with annealing temperature. The band gap varies due to the Coulomb interaction between impurity states. Thus correlation between ΔE_g (in meV) and impurity concentration N (in sm^{-3}) is determined by the relation:

$$\Delta E_g = -2 \cdot 10^5 \left(\frac{3}{\pi}\right)^{1/3} \frac{eN^{1/3}}{4\pi\varepsilon_0\varepsilon_s}, \qquad (2)$$

Table 1

Results of calculation of doping impurities concentrations in crystals under investigation.

Annealing temperature, T_a, K	Impurity concentration, cm^{-3}					
	Ni-doped crystals			Fe-doped crystals		
	ZnS:Ni	ZnSe:Ni	ZnTe:Ni	ZnS:Fe	ZnSe:Fe	ZnTe:Fe
1020	---	---	$3 \cdot 10^{17}$	---	---	---
1070	---	$2 \cdot 10^{17}$	$4 \cdot 10^{18}$	---	---	$2 \cdot 10^{17}$
1120	$4 \cdot 10^{17}$	$2 \cdot 10^{18}$	$6 \cdot 10^{19}$	---	---	$3 \cdot 10^{18}$
1170	$2 \cdot 10^{19}$	$4 \cdot 10^{19}$	---	$2 \cdot 10^{16}$	$3 \cdot 10^{16}$	$4 \cdot 10^{19}$
1220	$5 \cdot 10^{19}$	$8 \cdot 10^{19}$	---	$2 \cdot 10^{17}$	$2 \cdot 10^{17}$	$8 \cdot 10^{19}$
1270	$2 \cdot 10^{20}$	10^{20}	---	$7 \cdot 10^{17}$	$8 \cdot 10^{17}$	---
1320	---	---	---	$9 \cdot 10^{18}$	$2 \cdot 10^{18}$	---

where e, electron charge, ε_s is the static permittivity of ZnS, ZnSe or ZnTe. Using the shift of the band gap, we calculated the nickel and iron concentration in the studied crystals (see Table 1).

In the visible spectral region the crystals doped with nickel feature had series of absorption lines, caused by the intrastate transitions from the lower $^3T_1$(F)-state to the excited G-states in the limit of the Ni^{2+} ion.

The crystals doped with iron in the visible region are characterized by the series of absorption lines, which are due to intrastate transitions from the basic state ^5E(F) on the high-power excited states of Fe^{2+} ion. The absorption spectra of undoped ZnSe crystals and ZnSe:Fe and ZnSe:Ni crystals, doped at temperature 1170 K presented in Fig. 1 as an example. The investigation of optical properties of zinc chalcogenides doped with Fe and Ni were described in details in [7,8].

3. DETERMINATION OF NICKEL AND IRON DIFFUSIVITY IN THE ZNS, ZNSE, ZNTE CRYSTALS

The presence of the absorption bands in the visible range (Fig. 1) indicates the possibility of determining the diffusion profile of the impurity by measuring the relative optical density (Δ). This magnitude is the function of the coordinate x in the direction of the diffusion flux; it is determined by the relation
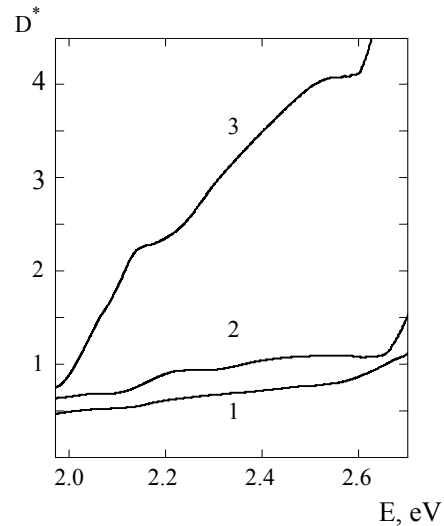
Fig. 1. Spectra of the optical-density D* in the visible region of (1) ZnSe, (2) ZnSe:Fe and (3) ZnSe:Ni crystals.

$$\Delta = \frac{D^*(x) - D^*(\infty)}{D^*(0) - D^*(\infty)}, \qquad (3)$$

where $D^*(x)$ is the optical density of the crystal as a function of the coordinate x, $D^*(0)$ is the optical density of the crystal in the near surface layer with the coordinate $x = 0$, and $D^*(\infty)$ is the optical density of the crystal in the region where the impurity concentration is negligibly low (crystal is undoped). The selected definition

of the relative optical density allows us to compare the dependence $\Delta(x)$ with the concentration profile of the impurity $C(x)/C_0$ calculated by formula (1).
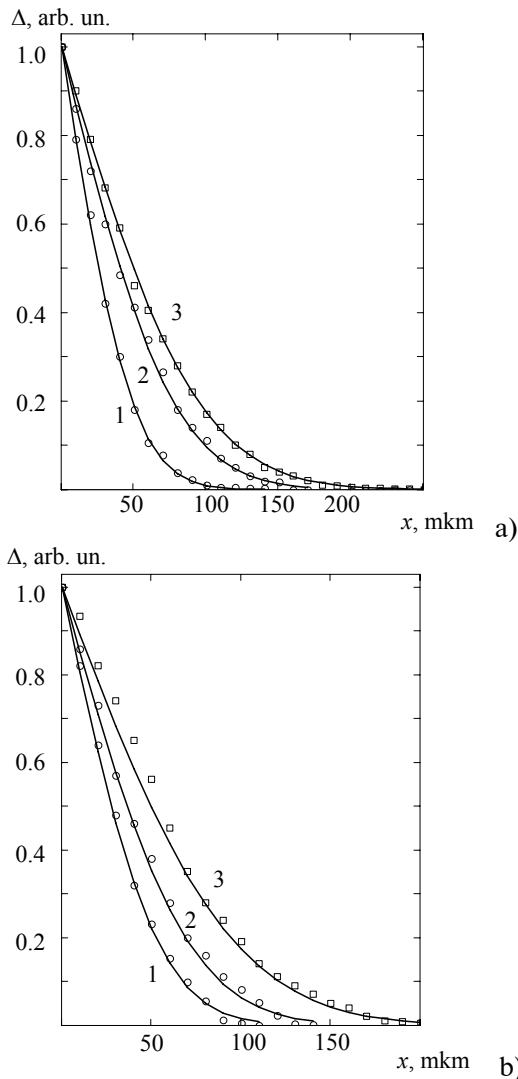
Fig. 2. Profiles of relative optical density (points in the curves) and diffusion profiles (solid lines) of Ni impurity in the ZnTe:Ni crystals (a) and Fe impurity in the ZnTe:Fe crystals. The diffusion temperature is 1070 (1), 1120 (2), 1170 K(3).

In Fig. 2. we show relative optical density profiles (points on curves) and diffusive profiles (solid lines) of nickel impurities in the ZnTe:Ni crystals and iron in the ZnTe:Fe crystals. By means of selection of diffusivity in (1), we obtained good agreement between profiles of the relative optical density and impurities concentration in investigated crystals. The diffusivities of Ni and Fe in the ZnS, ZnSe, ZnTe crystals at temperatures $T_a=1020-1320$ K were calculated similarly. In the Table 2 presented the nickel and iron diffusivities in the investigated crystals at the temperature $T_a=1220$ K. It is established that nickel diffusivities are two orders of magnitude higher than iron diffusivities in all types of the investigated crystals.

The temperature dependence of the difusivities (fig. 3) is described by the Arrhenius equation

$$D(T) = D_0 \exp\left(-\frac{E_a}{kT}\right) \qquad (4)$$
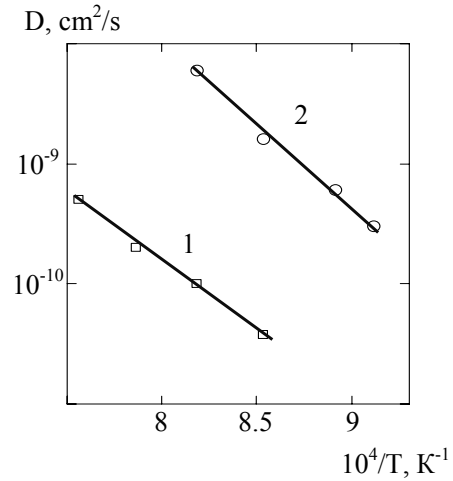
Fig. 3. The temperature dependences of iron diffusivities in ZnS:Fe crystals (1) and nickel diffusivities in ZnS:Ni (2) crystals.

Thus, from temperature dependences of nickel and iron diffusivities the diffusion process activation energies E_a and the preexponential factor D_0 in the Arrhenius equation were calculated for the proper crystals (see Table 2). Comparing obtained the diffusion process activation energies, it was established that in the ZnSe crystals both for nickel impurity and for the iron impurity the diffusion process activation energy has maximal value.

Table 2

The results of diffusion process investigations

Type of the crystal	Ni-doping			Fe-doping		
	D, cm²/s at 1220 K	D_0, cm²/s	E_a, eV	D, cm²/s at 1220 K	D_0, cm²/s	E_a, eV
ZnS	$4 \cdot 10^{-7}$	10^3	2.6	$8 \cdot 10^{-11}$	0.16	2.2
ZnSe	$7 \cdot 10^{-7}$	$8.8 \cdot 10^6$	3.5	$1 \cdot 10^{-10}$	$3.3 \cdot 10^3$	2.9
ZnTe	$8 \cdot 10^{-7}$	0.03	1.5	$4 \cdot 10^{-9}$	$5.6 \cdot 10^{-3}$	1.6

It evidences that in crystals ZnSe diffusion of transitional metal ions is due to dissociative mechanism. High activation energies of 4.45 eV and 3.8 eV were obtained for a diffusive process in the ZnSe:Cr and ZnSe:Co crystals [9,10].

4. CONCLUSION

The investigations enable us to draw the following conclusions.

The diffusion nickel and iron doping technique is developed for ZnS, ZnSe, ZnTe single crystals. Concentrations of doping impurities in the investigated crystals are determined.

It is shown that the diffusion profile of a nickel and iron impurities can be determined by measuring the relative optical density of crystals in the visible region.

The nickel and iron diffusivities in ZnS, ZnSe, ZnTe crystals are calculated in the temperature range of 1020−1320 K. The analysis of the temperature dependences $D(T_a)$ enables us to determine the activation energies E_a of diffusion processes in the proper crystals and the factors D_0 from the Arrhenius equation.

References

1. Fedorov V. V., Mirov S. B. et. al. 3.77–5.05-μm tunable solid-state lasers based on Fe^{2+}-doped ZnSe crystals operating at low and room temperatures // Journal of quantum electronics — 2006. — V.42, №9. — P. 907–917.

2. Кулешов Н. В., Щербицкий В. Г., Кисель В.Э, Левченко В. И., Постнова Л. И. Fe^{2+}:ZnSe — новый материал для пассивных затворов лазеров с длиной волны излучения 3 мкм // Сборник докладов Международной научной конференции "Актуальные проблемы физики твердого тела" ,2001, с.21.

3. J. Kreissl, H. — J. Schulz Transition-metal impurities in II-VI semiconductors:characterization and switching of charge states // J. Cryst. Growth. — 1996. — V. 161. — P. 239–249.

4. Воронов А. А., Козловский В. И., Коростелин Ю. В., Ландман А. И., Подмарьков Ю. П., Фролов М. П., Лазерные характеристики кристалла Fe:ZnSe в диапазоне температур 85—255 K // Квант. Электроника. — 2005 В. 35, № 9. — С.809–812.

5. Demirbas U., Sennaroglu A., Somer M. Synthesis and characterization of diffusion-doped Cr2+:ZnSe and Fe2+:ZnSe // OpticalMaterial s — 2006. — V. 28 P. 231–240

6. Korostelin Yu.V., Kozlovsky V. I., Nasibov A. S., Shapkin P. V. Vapour growth of II-VI solid solution single crystals // J. Cryst. Growth. — 1996. — V. 159. — P. 181–185.

7. Ваксман Ю. Ф., Ницук Ю. А., Яцун В. В., Насибов А. С., Шапкин П. В. Получение и оптические свойства кристаллов ZnSe:Ni // ФТП. — 2010. — Т. 44, В. 2. — С. 149–153.

8. Ваксман Ю. Ф., Ницук Ю. А., Яцун В. В., Насибов А. С., Шапкин П. В. Оптическое поглощение и диффузия железа в монокристаллах ZnSe //ФТП. — 2010. — Т. 44, В. 4. — С. 463–466.

9. Ваксман Ю. Ф., Павлов В. В., Ницук Ю. А., Пуртов Ю. Н., Насибов А. С. Шапкин П. В. Оптическое поглощение и диффузия хрома в монокристаллах ZnSe // ФТП. — 2005. — Т. 39, №4. — С. 401–404.

10. Ваксман Ю. Ф., Павлов В. В., Ницук Ю. А., Пуртов Ю. Н., Насибов А. С., Шапкин П. В. Получение и оптические свойства монокристаллов ZnSe, легированных кобальтом //ФТП. — 2006. — Т.40, №.7. — С. 815–818.

UDC 621.315.592

Yu.F.Vaksman, Yu.A.Nitsuk, V. V. Yatsun, Yu. N. Purtov

DIFFUSION OF TRANSITION-METAL IONS (FE, NI) IN ZINC CHALKOGENIDES

Abstract

The ZnS, ZnSe, ZnTe single crystals doped with iron and nickel are investigated. The diffusion doping is carried out from metallic nickel and powderlike iron in helium and argon atmosphere. The optical density spectra are investigated in the wavelength range of 2–3.8 eV. From the value of the absorption edge shift, the nickel and iron concentrations in crystals under investigation is determined. It is shown that nickel and iron doping results in appearance of absorption lines in the visible spectral region.

The nickel and iron impurity diffusion profile is determined by measuring the relative optical density of crystals in the visible spectral region. The diffusivities of nickel and iron in ZnS, ZnSe, ZnTe crystals are calculated at temperatures of 1020–1320 K.

Key words: zink chalkogenides, diffusion doping, optical-density, diffusivity.

УДК 621.315.592

Ю. Ф. Ваксман, Ю. А. Ницук, В. В. Яцун, Ю. Н. Пуртов

ДИФФУЗИЯ ИОНОВ ПЕРЕХОДНЫХ МЕТАЛЛОВ (FE, NI) В ХАЛЬКОГЕНИДАХ ЦИНКА

Резюме

Исследованы монокристаллы ZnS, ZnSe, ZnTe, легированные железом и никелем. Диффузионное легирование осуществлялась из металлического никеля и порошкообразного железа в атмосфере гелия и аргона. Исследованы спектры оптической плотности в области энергий 2–3.8 эВ. По величине смещения края поглощения определены концентрации никеля и железа в исследуемых кристаллах. Показано, что легирование никелем и железом приводит к появлению полос поглощения в видимой области спектра.

Диффузионный профиль примеси никеля и железа определен путем измерения относительной оптической плотности кристаллов в видимой области спектра. Рассчитаны коэффициенты диффузии никеля и железа в кристаллах ZnS, ZnSe, ZnTe при температурах 1020–1320K.

Ключевые слова: халькогениды цинка, диффузионное легирование, оптическая плотность, коэффициенты диффузии.

УДК 621.315.592

Ю. Ф. Ваксман, Ю. А. Ніцук, В. В. Яцун, Ю. М. Пуртов

ДИФУЗІЯ ІОНІВ ПЕРЕХІДНИХ МЕТАЛІВ (FE, NI) В ХАЛЬКОГЕНІДАХ ЦИНКУ

Резюме

Досліджено монокристали ZnS, ZnSe, ZnTe, леговані залізом та нікелем. Дифузійне легування виконувалось з металевого нікелю та порошкоподібного заліза в атмосфері гелію та аргону. Досліджено спектри оптичної густини в області енергій 2–3.8 eB. За величиною зсуву краю поглинання визначені концентрації нікелю і заліза в досліджуваних кристалах. Показано, що легування нікелем і залізом призводить до виникнення смуг поглинання в видимій області спектру.

Дифузійний профіль домішок нікелю і заліза визначено шляхом вимірювання відносної оптичної густини кристалів в видимій області спектру. Розраховані коефіцієнти дифузії нікелю і заліза в кристалах ZnS, ZnSe, ZnTe при температурах 1020–1320K.

Ключові слова: халькогеніди цинку, дифузійне легування, оптична густина, коефіцієнти дифузії.

V. V. KOVALCHUK, O. V. HRABOVSKIY, YU.S.CHIZHIKOV

State Institute of Measuring Technique, Kuznechnaya, 15, tel. 7266850,
e-mail: lslvv@rambler.ru

THE OPTICAL PROPERTIES OF THE CLUSTERS AT THE SOLID STATE MATRIX

In this article the results of the experimental and theoretical investigation of polyhedral submicron particles (later referred as PSP), in particular, Si-atomic clusters (ACs) are surrounded by solid state matrix. The article presents optical spectra of Si_nY_m — ACs.

The smaller electronegativity of silicon will affect the bond polarity and ionicity, which will in turn have a major influence on the bond lengths involving silicon. Steric effects caused by bulky substituents will, on the one hand be less important than in the carbon analogues because of the longer bond lengths, but, on the other hand, will have a greater effect because of the lower barrier to distortion. One of the striking differences between silicon and carbon atoms is the ease of formation of hypervalent species with silicon. Five- and six-coordinate silicon compounds are stable and the role of d orbitals in the bonding of silicon in these compounds is a subject of continuing debate [1−3]. On the other hand, synthesis of the polyhedral silicon compounds due to their high symmetry is a great challenge since it could lead to novel physical and chemical properties unexpected from the carbon compounds. And such synthesis is possible until recently [4,5,10]. In the last two decade we have been witnessing an explosion of information on the geometry of submicron particles (**SP**) (atomic clusters — ACs) extracted from photoluminescence spectra [6−9,20].

In this article the results of the experimental investigation of Si-ACs are summarized together with our DFT theoretical calculations [10]. These are also compared with those for the small and more ACs analogues. Comparison of the experimental geometry with optimized calculated geometry is given. The article covers Si_nY_m morphology and adsorption spectra, where Y are substituent's simulating of the solid state matrix surrounding. In this refrain, we stress that the Si-ACs may be either tri-, tetra-, penta- or hexacoordinate and Y may have different coordination numbers [11,12]. For each type of Si-Y bond, typical and exceptional compounds are shown and the relevant geometric parameters are listed at the [10]. Our simulation package contains the tools which are necessary for the investigation and visualization of the results generated by the calculation program-packages (CPP) such as a) PDFT, b) POTENTIAL, c) GEOMETRY.

The theoretical method used in the present work is the parameterized density functional scheme of that allows for full relaxation of covalent systems with no symmetry constraints. To study the dynamics of the Si-ACs we offer the approximate calculation scheme. This is the density-functional theory (DFT) in the realization of Kohn and Sham (KS), using a few empirical parameters [4]. This method, which named parameterized DFT- PDFT, is based on the Hartree-Fock scheme plus a proper treatment of the electron correlation. The use of only a few parameters minimizes the effort for the determination of the parameters; it yields a close relation to full ab initio DFT schemes (for example, GAMESS [13]). This is guarantee of the good "transferability" of the parameters, going from one system to another. The use of some approximations in connection with a few empirical parameters makes the scheme computation extremely fast. PDFT allows also the study of dynamical processes through the coupling with molecular dynamics (MD). The method of simulation of the inter-PSP interaction is based on the MD description. The main idea our description leads to the estimation of the energetically characteristics of the Si-ACs which contain from some to several tens atoms. The closely packed ACs were tested and investigated in [10]. The MD is particularly suitable for finding minimum configurations for ACs. When applied to the bulk phases of Si, MD-PDFT has reproduced binding energy differences between the high-pressure metallic phases and the diamond phase in excellent agreement with the schemes based on the local density approximation (LDA) [11,12]. GEOMETRY-package (GP) is a geometrical program based on 3D-representation of the investigation of ACs -structures. The GP generates detailed and easily interpretable and aesthetically appealing graphics representing models of molecular structures and related properties. The package offers a high level of interactivity through the use of the mouse and via a large set of menus and submenus, organized in such a way so as to enable users to learn rapidly the basic operations leading to efficient visualization. For all the menu items, a help facility has been implemented. Various representation options and attributes may be selected for adapting the visual output to personal needs and preferences: the molecular structures may be represented as discrete dots, and the global appearance may be modified via attributes such as back ground appearance, perspective or orthogonal projection and others. The purpose of the GP is the interactive visual representation of three-dimensional models of molecular structures and properties for research. Due to the flexibility of the data- and program-structure, various chemical systems ranging from small compounds (clusters) to

large macromolecules may be investigated, additional interfaces and tools can easily be implemented.

The first optical spectra have been recorded for neutral Si-ACs containing 18−41 atoms [20]. These spectra reveal (Fig.1) a surprise: minute silicon clusters have numerous strong sharp absorption's which do not shift in energy-over entire cluster size range. Results are totally unexpected since theoretical calculations predict by PDFT a wide variation in structure over the size range of the Si-ACs. Fig. 1, show that the spectra can be divided into two parts. The first lies at energies above 3 eV. Here the peaks result from transitions which are rate limited by one-photon absorption's. Many of these peaks exhibit saturation power dependencies even at the lowest laser fluencies that we are able to use for our experiments, e.g., at 3,68 eV in Fig. 2. The second part of these spectra lies below 3 eV where various peaks in the spectra arise from multiple photon excitations. Furthermore, these peaks ride on broad background absorption. The power dependencies of these peaks, e.g., at 1,98 and 2,58 eV in Fig. 1, have slopes which are less than the expected photon order, indicating that the broad background absorption results from transitions which are rate limited by one-photon transitions.
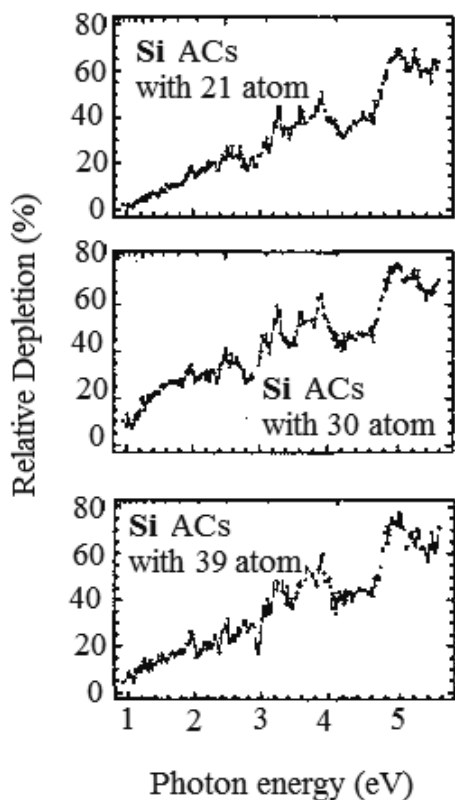
Fig 1. Photo dissociation spectra of the atomic clusters

The tiny pieces of silicon where most of the atoms are on the surface should be greatly reconstructed from bulk silicon [10,11]. Yet, the optical signature of these clusters has much in common with that of crystalline silicon. The most startling finding is that the absorption spectra for all investigated clusters are essentially identical furthermore, we have obtained partial spectra of Si-ACs smaller than Si_{18} and larger than Si_{41}. These preliminary survey data indicate that the spectral signature common to Si_{18} — Si_{41} grows in at about Si_{18} and persists for sizes up to at least 70 atoms. This

spectral similarity is completely unexpected from both a molecular and a bulk perspective. In both cases, Si_{18} this size range are expected to undergo rapid structural changes because of the large surface/interior atom ratio. From a molecular point of view, these clusters span a sufficiently large size range to have structural differences, which should show up in their optical spectra. Our theoretical studies have explored the geometries of small silicon clusters [l0]. The differing calculated methodologies find that the Si-ACs should be strongly reconstructed from bulk silicon, but morphology of its are different. The nature of this reconstruction remains open to intense debate. Some calculations predict that silicon clusters in our size range have tetrahedral bonded network structures whereas others predict more compact structures.

The optimized ACs of tetrasilatetrahedrane (Si_4H_4), hexasilaprismane (Si_6H_6) and octasilacubane (Si_8H_8) at the PDFT level were calculated. The Si-Si bond lengths in Si_4H_4 are shorter than the single bond length of 2,352 A calculated for $H_3Si-SiH_3$, and it increases in the order Si_4H_4 (2,314 A) < Si_6H_6 (2,359 A and 2.375 A) < Si_8H_8 (2,396 A). It is interesting that the Si-Si bond lengths are shorter in the three-membered rings than in the four-membered rings, as is also calculated for the monqcyclic rings: cyclotrisilane (2,341 A) vs cyclotetrasilane (2,373 A). This trend is enhanced in the heavier compounds. However, bond lengths are not necessarily correlated with bond strengths; the bonds in three-membered rings are weaker than those in four-membered rings. This is because the heavier atoms are forced to hybridize to a considerable extern in order to achieve and maintain the three-membered skeletons of a given symmetry a large energy loss. To compensate for this energy loss, the bond lengths between skeletal atoms shorten in order to form bonds as effectively as possible. However, the cost for hybridization is too large to be offset just by bond shortening, leading to higher strain and weaker bonds in the three-membered rings. As a result of the high strain and weak bonds, the heavier polyhedral compounds consisting of only three-membered rings easily undergo bond stretching or bond breaking.

The structural parameters of the octasilacubane (Si_8H_8) at the matrix surrounding are listed in the **tabl. 1**. Octasilacubanes (Si_8H_8) bearing alkyl, aryl and silyl substituents of various sizes were calculated using the semiempirical *MIEHT*-α method [19] and PDFT approach [10]. X-ray structures are available for Y = 2,6-$Et_2C_6H_3$, CMe_2CHMe_2 and t-Bu [18]. Both the calculated and the X-ray structures show almost perfect cubic skeletons. In addition, the experimental skeletal Si bond lengths are reasonably well reproduced by the calculations, taking into account the overestimation of the Si-Si bond distances by *ca* 0,05 A. As **tabl. 1** shows O_h, symmetry of Si_8H_8 is lowered as the substituents become more bulky. Nevertheless, all of the calculated structures still retain relatively high symmetry in contrast with the avialable experimental structures in crystals. This suggests that packing forces significantly affect the favourable conformations of bulky substituents around the cubane skeleton, probably because the energy loss due to the conformational changes is very small.

Table 1

Symmetries, Si-Si-bond lengths, charges and HOMO energies of octasilacubane derivatives (Si_8Y_8) (symbol * denotes calculated by PDFT scheme; in brackets are results from MIEHT-α using basis STO/DZ)

Substitutions (Y)	Symmetry	$r_{Si-Si}, \overset{0}{A}$	Charge on the skeletal Si atoms	$HOMO, eV$ (HF/DZ)
H	O_h	$2,400 * (2,34)$	$0,044 *$	$-9,7 *(-8,23)$
$t-Bu$	D_2	$2,445$ [7]	$0,264$ [7]	$-8,68$ [7]
CMe_2CHMe_2	D_2	$2,462$ [6]	$0,242$ [6]	$-8,54$ [6]
$Si(SiH_3)_3$	D_2	$2,410 *$	$0,0244 *$	$-9,2 *$
SiH_3	O_h	$2,401 * (2,36)$	$-0,211 *$	$-9,5 *(-8,31)$
SiF_3	O_h	$2,390 * (2,35)$	$-0,540 *$	$-9,8 *(-10,42)$

The prismanes with Si and Ge skeletons are yellow to orange. These prismanes have absorptions tailing into the visible region. For example, Si_6H_6 has an absorption band with a maximum at 241 *nm* tailing to *ca* 500 *nm*. The absorption band of Ge_6Y_6 ($Y = 2,6-i-Pr_2C_6H_3$) has a maximum at 261 *nm*, which is red-shifted compared to that of Ge_6Y_6 because of the higher-lying orbitals of the Ge-Ge bonds [13]. Hexasilaprismane Si_6Y_6 is photosensitive. On irradiation in solution at low temperature with light having wavelength 340−380 *nm*, new absorption bands appeared at 335, 455 and 500 *nm* assignable to the absorption bands of hexasila-Dewar benzene. Upon excitation of these bands with wavelengths longer than 460 *nm*, Si_6Y_6 was immediately regenerated. A single chemical species was produced during the photochemical reaction since the bands of Si_6Y_6 (with single Si-Si-bonds) and those assigned to Si_6Y_6 (with double Si-Si-bonds) appeared and disappeared simultaneously (**Fig.2**). The folding angle of the parent hexasila-Dewar benzene (Si_6H_6) with C_{2v} symmetry is 120° at the PDFT level. The through-space interaction between the Si=Si double bonds splits the π-MOs into bonding (π_S) and antibonding (π_*) sets, as shown our calculations. Likewise, their π -MOs split into

π_S^* and π_A^*. The allowed transitions from π_S to π_S^* and from π_A to π_A^* correspond to the experimental absorption bands at 455 and 335 *nm*, respectively. The lowest energy transition from π_A to π_S^* is forbidden. However, it is allowed if the C_{2v} symmetry is lowered. The relatively weak absorption at 500 *nm* is assigned to the transition. The activation parameters for the isomerization of Si_6Y_6 (with double Si-Si-bonds) to Si_6Y_6 (with single Si-Si-bonds) are $Å_a = 0,595$ *eV*. The small $Å_a$ value is consistent with the high reactivity of Si=Si double bonds.

The lowest energy absorption is forbidden when the cubane has high symmetry, but becomes weakly allowed when the symmetry is lowered. MIEHT-α calculations [10] show that the spectrum shape in the low energy region depends strongly on the substituent's.

The kinetic stability of tetrasilatetrahedrane (Si_4H_4), hexasilaprismane (Si_6H_6) and octasilacubane (Si_8H_8) depends strongly on the steric bulkiness of the substituents (matrix). The silyl-substituted Si_nY_m (Y= $t-Bu$) is stable in an inert atmosphere, but is oxidized in air to give colourless solids. The 1,1,2-trimethylpropyl-substituted Si_nY_m (Y= CMe_2CHMe_2) is very stable even in air and survives for two weeks in the solid state.
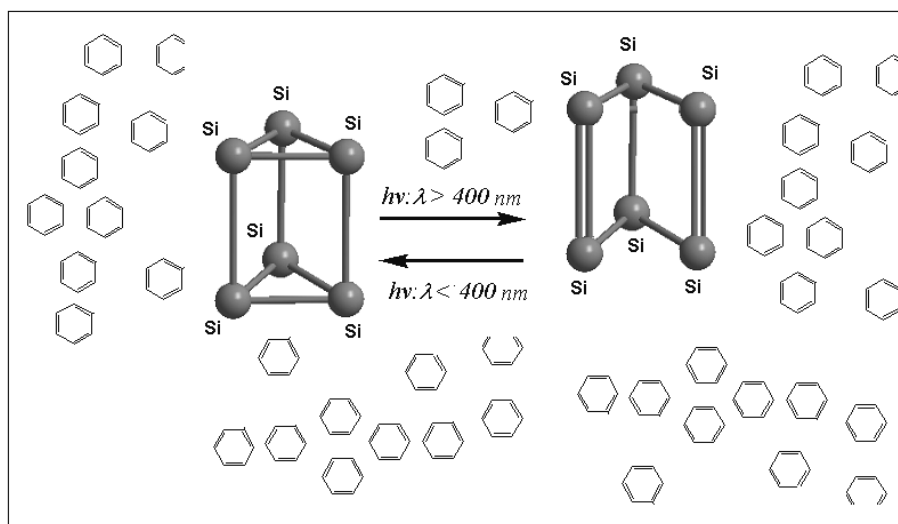
FIGURE 2. Light transition for two type of the cluster Si_6H_6 in matrix surrounding (hexane) (PDFT-model for the clusters and SW — approach for the matrix)

Most probably, the, small HOMO-LUMO gap of 13 makes it possible that the Si=Si double bonds undergo formally symmetry forbidden [2+2] thermal

reaction. Benzene is a key intermediate in the reductive oligomerization of $RCl_2SiSiCl_2R$ and $RSiCl_3$ (R = $2,6-i-Pr_2C_6H_3R$) [16,17]. All cubanes of Si, Ge and Sn

are coloured from yellow to purple [**18**]. The silyl-substituted octasilacubane (Si_8Y_8, $Y=t-Bu$) was synthesized as bright yellow crystal. A diffuse reflection absorption of Si_8H_8 is red-orange. The UV/Vis spectrum of Si_8Y_8 ($Y=CMe_2CHMe_2$) exhibits absorption bands at 252,350 *nm* and around 500 *nm* [**18**]. Aryl-substituted octasilacubane were prepared by the dechlorinative reactions of $ArCl_2SiSiCl_2Ar$ and of $ArSiCl_3$ and was isolated as orange crystal with $Mg/MgBr_2$ reagent [**17**]. The spectrum depends on the type of the aryl substituent. The absorption band at around 240 *nm* is attributecl To the *a-a** transition, while the absorption at around 280 nm is caused by transition from a *a-n* mixing between the orbitals of the Si-Si *a* bonds and the aromatic it orbitals.

SUMMARY

The mechanism by which Si_nY_m with chloral atoms is formed is not clear, but the first step involves the electrophilic attack by PCl_5 on the strained Si-Si bond, followed by an intramolecular skeletal rearrangement. Bromo and iodo derivatives of Si_nY_m are also formed by the reactions of Si_8Y_8 with Br_2 and with I_2. Octasilacubanes were used as a model in an attempt to understand the optical properties of porous silicon because both porous silicon and octasilacubane show a broad photoluminescence spectra and large Stokes shifts. Si_8Y_8, $Y=t-Bu$, for example, shows an absorption edge at *ca* 3,2 eV and a broad photoluminescence spectrum with a peak at 2,50 eV. At the [10] more detail information of the processes of matrix influence on the polyhedral ac are gives.

Deep thanks to Prof. Dr. M. Drozdov for the helpful comments of some calculation results.

References

1. Keghelian P., Melinon P., Perez A. Properties of silicon and silicon-carbon cluster assembled films // Nono Structured Materials. — 1999. — v. 12. — P.277−280
2. Dresselhaus M. S., Dresselhaus G., Eklund P. C. Science of Fullerenes and Carbon Nanotubes: San Diego:Academic Press, 1996. — P.24−229
3. Drozdov V. A., Kovalchuk V. V. Electronic Processes in nanostructures with silicon subphase// J.of Phys. Studies. — 2003. — Vol.4,№ 7. — P.393−401
4. Kovalchuk V. V. Cluster morphology of silicon nanoparticles // Semiconductor Physics, Quantum Electronics & Opto-electronics. — 2007. — v. 10, № 4. P. 81−86
5. Watanabe M. O., Miyazaki T., Kanayama T. Deposition of structure-controlled hydrogenated Si clusters on Si(111) surface // Book of Abstracts 9th International Symp. on Small Particles and Inorganic Clusters. — Lausanne (Switzerland). — 1998. — P.10.50
6. Kamenutsu Y., Suzuki K., Kondo M. Luminescence properties of a cubic silicon cluster octasilacubane // Phys. Rev. — 1992. — B 51. — P.10666−10669
7. Furukawa K., Fujino M., Matsumoto N. Comment on "Crystal structure and optical properties of polymorphic octasilacubane" //Appl.Phys.Lett. — 1995. — v.66, № 10. — P.1291
8. Kanzawa Y., Kageyama, Takeoka S., Fujii M., Hayashi S., Yamamoto K. Size-dependent near-infrared photoluminescence spectra of Si nanocrystal embedded in SiO_2 matrices // Sol.St.Com. — 1997. — v.102. — P.533−537
9. Chen X., Zhao J., Wang G., Shen X. The effect of size distributions of Si nanoclusters on photoluminescence from ensembles of Si nanoclusters//Phys.Lett.A. — 1996. — v.212. — P.285−289
10. Kovalchuk V. V. Cluster modification semiconductor's heterostructures. — K. Hi-Tech, 2007. — P.309
11. Chelikowsky J., Phillips J. C., Kamal M., Strauss M. Surface and thermodynamic force fields for silicon clusters and bulk phase // Phys.Rev.Lett. — 1999. — v.62, №3. — p.292−295
12. Honea E. C., Ogura A., Murray C. A., Raghavachari K., Sprenger W., Jarrold M., Brown W. L. Raman spectra of size-selected silicon clusters and comparison with calculated structures// Nature. — 1998. — v.366. — P.42−44
13. General Atomic and Molecular Electronic Structure System / Schmidt M. W., Baldrige K. K., Boatz J. A., and others // J. Comp. Chem. — 1999- № 14. — P.1347−1363.
14. Conrad D., Scheerschidt K., Goesele U. Molecular dynamics simulations of silicon wafer bonding // Appl.Phys.A. — 1999. — v.62. — P.7−12
15. Sekiguchi A, Sakurai H. Cage and cluster compounds of silicon, germanium, and tin //Advances in organometallic chemistry. — 1999. — V.37. — P.1−38
16. Wiberg N., Finger C. M.M., Auer H., Polborn K. Supersilylated disilenes, cyclotrisilanes, cyclotetrasilanes and tetrahedrosilanes: Production, structures and formation // J. Organometallic Chem. — 1996. — v.521 (1−2). P.377−386
17. Sita L.R, Kinoshita I. Decakis (2,6-diethylpheniyl) decastanna [5] prismane−characte-rization and molecular structure // J.of the Am.Soc. — 1999. — v. 113 (5)- P. 1856−1857
18. Sita L.R, Kinoshita I. Octakis (2,6-diethylpheniyl) Octastannacubanne // Organometallics. — 2000. — v.9 (11). — P.2865−2867
19. Kovalchuk V. V., Chislov V. V., Yanchuk V. A. Cluster model of the real silicon surface //Phys. Stat. Sol.(b). — 1998. — v.187, № 2. — p.47−51
20. Rinnen K. D., Mandich M. L. Spectroscopy of neutral silicon clusters, $si_{18}-si_{41}$: spectra are remarkably size independent// Phys.Rev. — 1999. — v.69,№12. — P.2167−2169

V. V. Kovalchuk, O. V. Hrabovskiy, Yu.S.Chizhikov

THE OPTICAL PROPERTIES OF THE CLUSTERS AT THE SOLID STATE MATRIX

Abstract.
In this article the results of the experimental and theoretical investigation of polyhedral submicron particles (later referred as PSP), in particular, Si-atomic clusters (ACs) are surrounded by solid state matrix. The article presents optical spectra of Si_nY_m — ACs.
Key words: atomic cluster, optical spectra, electronic structure

В. В. Ковальчук, О. В. Грабовский, Ю. С. Чижиков

ОПТИЧЕСКИЕ СПЕКТРЫ КЛАСТЕРОВ В ТВЕРДОТЕЛЬНОЙ МАТРИЦЕ

Резюме

Представлены результаты экспериментальных и теоретических исследований полиэдрических субмикронных частиц (ПСЧ), в частности, Si-атомных кластеров (АК) в твердотельном матричном окружении. Приведены оптические спектры Si_nY_m — АК.

Ключевые слова: атомные кластеры, оптические спектры, электронная структура.

В. В. Ковальчук, О. В. Грабовський, Ю. С. Чіжиков

ОПТИЧНІ СПЕКТРИ КЛАСТЕРІВ У ТВЕРДОТІЛЬНІЙ МАТРИЦІ

Резюме

Наведено результати експериментальних і теоретичних досліджень поліедричних субмікронних частинок (ПСЧ), зокрема, Si-атомних кластерів (АК), таких як тетраедр, гексагональна призма, куб у матричному оточені. Представлені оптичні спектри Si_nY_m — ПСЧ.

Ключові слова: атомні кластери, оптичні спектри, електронна структура.

UDC 539.142 : 539.184

T. A. FLORKO

Odessa State Environmental University

THEORETICAL DETERMINATION OF THE RADIATIVE TRANSITION PROBABILITIES IN SPECTRA OF Ne-LIKE MULTICHARGED IONS

On the basis of a new scheme within a gauge-invariant quantum electrodynamics (QED) perturbation theory it is carried out calculating energies and transition probabilities for some E1, M1, E2 and other transitions in spectra of the Ne-like multicharged ions.

The experimental and theoretical studying of the radiation transition characteristics of a whole number of atomic systems, which are interesting and perspective from the point of view of the quantum electronics and photoelectronics, is in last years of a great importance (c.f.[1−42]). It is also very important for search the optimal candidates and conditions for realization of the X-ray lasing. Especial interest attracts studying the Ne-like multicharged ions. Neon-like ions play an important role in the diagnostics of a wide variety of laboratory and astrophysical plasmas. Primarily because of its importance to astrophysical plasmas, one of the most thoroughly studied neon-like ions is Fe^{16+}. For this ion, there has been a long series of the Hartree-Fock (HF), Dirac-Fock (DF), relativistic perturbation theory (PT) etc. Neon-like Kr, Br, Ni is also important, especially as a diagnostic for tokamak plasmas [1−5,8−15]. Although there was some early work on the HF studying spectra o these ions though an accuracy of these calculations is not high. The well-known multi-configuration HF and DF (MCDF) approaches are widely used in calculations of the atoms and ions [3,8−11]. It provides the most reliable version of calculation for atomic systems. Nevertheless, as a rule, detailed description of the method for studying role of the relativistic, gauge-invariant contributions, nuclear effects is lacking. Serious problems are connected with correct definition of the high-order correlation corrections, QED effects etc. The further improvement of this method is connected with using the gauge invariant procedures of generating relativistic orbital basis's and more correct treating the nuclear and QED effects [1,2,19−26]. Here we present a new, relativistic approach (detailed description see ion refs. [36−39]) to description of the forbidden radiative transitions characteristics in spectra of the heavy atoms and multicharged ions. New method is based on the energy approach and gauge-invariant QED perturbation theory (PT) formalism with using the optimized one-quasi-particle representation and prйcised accounting for the exchange-correlation effects [19−25,31,33−35]. There are carried out the calculations of energies, probabilities and oscillator strengths for the radiative (E1,M1, E2 etc) transitions in spectra of ions of the isoelectronic sequences NeI. Earlier it has been carried theoretical studying of the energies, oscillator strengths [36−38] of the Zn-like multicharged ions and some heavy lanthanide atoms.

Let us describe in brief the important moment of our theoretical approach. As usually, the wave functions zeroth basis is found from the Dirac equation solution with potential, which includes the core ab initio potential, electric, polarization potentials of nucleus (the Gaussian form for charge distribution in the nucleus is used). All correlation corrections of the PT second and high orders (electrons screening, particle-hole interaction etc.) are accounted for. The wave function for a particular atomic state

$$\Psi(\Gamma PJM) = \sum_{r}^{NCF} c_r \Phi(\gamma_r PJM) \qquad (1)$$

is obtained as the above described self-consistent solutions of the Dirac−Fock type equations. Configuration mixing coefficients c_r are obtained through diagonalization of the Dirac Coulomb Hamiltonian

$$H_{DC} = \Sigma_i\, c\alpha_i\, p_i + (\beta_i\text{-}1)c^2 - V_c\,(r|nlj) +$$

$$V_{ex} - V_{nucl}\,(r|R) + \Sigma_{i>j} \exp(i\omega r_{ij})(1\text{-}\alpha_1\alpha_2)/r_{ij} \qquad (2)$$

In this equation the potential:

$$V(r) = V_c\,(r|nlj) + V_{ex} + V_{nucl}\,(r|R). \qquad (3)$$

This potential includes the electrical and polarization potentials of the nucleus. The part V_{ex} accounts for exchange inter-electron interaction. The main exchange effect are taken into account in the equation. The rest of the exchange-correlation effects are accounted for in the first two PT orders by the total inter-electron interaction [20−22,31,35,37]. The effective electron core density (potential V_c) is defined by iteration algorithm within gauge invariant QED procedure [22]. Following to refs.[2,22], let us in brief note the key moments.

Consider the one-quasiparticle system. A quasi-particle is a valent electron above the core of closed electron shells or a vacancy in the core. In the lowest second order of the EDPT a non-zeroth contribution to the imaginary part of electron energy Im δE (the radiation decay width) is provided by relativistic exchange Fock diagram. In the fourth order of the QED PT there are diagrams, whose contribution into the ImδE accounts for the core polarization effects. It is on the electromagnetic potentials gauge (the gauge non-invariant contribution). Let us examine the multielectron atom with one quasi-particle in the first excited state, connected with the ground state by

the radiation transition. In the zeroth QED PT approximation we, as usually (c.f.[2,21,37]),use the one electron bare potential $V_N(r) + V_C(r)$, with $V_N(r)$ describing the electric potential of the nucleus, $V_C(r)$, imitating the interaction of the quasi-particle with the core. The core potential $V_C(r)$ is related to the core electron density $\rho_C(r)$ in a standard way. The latter fully defines the one electron representation. Moreover, all the results of the approximate calculations are the functionals of the density $\rho_C(r)$. In ref.[22] the lowest order multielectron effects, in particular, the gauge dependent radiative contribution for the certain class of the photon propagator calibration is treated. This value is considered to be the typical representative of the electron correlation effects, whose minimization is a reasonable criterion in the searching for the optimal one-electron basis of the PT. The minimization of the density functional Im δE_{ninv} leads to the integral differential equation for the ρ_c, that can be solved using one of the standard numerical codes. In ref. [22] authors treated the function ρ_c in the simple analytic form with the only variable parameter b and substituted it to (6). More accurate calculation requires the solution of the integral differential equation for the ρ_c [2,37].

The probability is directly connected with imaginary part of electron energy of the system, which is defined in the lowest order of perturbation theory as follows:

$$\text{Im}\Delta E(B) = -\frac{e^2}{4\pi} \sum_{\substack{\alpha>n>f \\ [\alpha<n\le f]}} V_{\alpha n \alpha n}^{|\omega_{\alpha n}|},\qquad (4)$$

where $\sum\limits_{\alpha>n>f}$ – for electron and $\sum\limits_{\alpha<n\le f}$ – for vacancy. The potential V is as follows:

$$V_{ijkl}^{|\omega|} = \iint dr_1 dr_2 \Psi_i^*(r_1)\Psi_j^*(r_2)\frac{\sin|\omega|r_{12}}{r_{12}}$$
$$(1-\alpha_1\alpha_2)\Psi_k^*(r_2)\Psi_l^*(r_1).\qquad (5)$$

The separated terms of the sum in (5) represent the contributions of different channels and a probability of the dipole transition is:

$$\tilde{A}_{\acute{a}_n} = \frac{1}{4\acute{\delta}}\cdot V_{\acute{a}_n \alpha_n}^{|\acute{u}_{\acute{a}_n}|}\qquad (6)$$

The corresponding oscillator strength : $gf = \lambda_g^2 \cdot \Gamma_{\alpha_n} / 6.67\cdot10^{15}$, where g is the degeneracy degree, λ is a wavelength in angstroms (Å). Under calculating the matrix elements (5) one could use the angle symmetry of the task and write the expansion for potential $\sin|\omega|r_{12}/r_{12}$ on spherical functions as follows:

$$\frac{\sin|\omega|r_{12}}{r_{12}} = \frac{\pi}{2\sqrt{r_1 r_2}}\times$$
$$\times\sum_{\lambda=0}^{\infty}(\lambda)J_{\lambda+\frac{1}{2}}(|\omega|r_1)J_{\lambda+\frac{1}{2}}(|\omega|r_2)P_\lambda(\cos \mathbf{r_1 r_2}),\quad (7)$$

where J –is the Bessel function of first kind and $(\lambda) = 2\lambda + 1$. This expansion is corresponding to usual multipole one for probability of radiative decay. Substitution of the expansion (7) to matrix element of interaction gives as follows:

$$V_{1234}^{\omega} = \left[(j_1)(j_2)(j_3)(j_4)\right]^{\frac{1}{2}}\times$$
$$\times\sum_{\lambda\mu}(-1)^{\mu}\begin{pmatrix} j_1 j_3 & \lambda \\ m_1 - m_3 & \mu \end{pmatrix}\times\text{Im}\,Q_\lambda(1234);$$
$$Q_\lambda = Q_\lambda^{\text{Qul}} + Q_\lambda^{\text{Br}}.\qquad (8)$$

where j_i are the entire single electron momentums, m_i — their projections; Q_λ^{Qul} is the Coulomb part of interaction, Q_λ^{Br} - the Breit part. The detailed expressions for these parts are received and presented in refs. [2,19–22].

The full probability of the λ -pole transition is usually represented as a sum of the electric (a multipole expansion) $A_\lambda^E = P_\lambda^E$ and magnetic (a multipole expansion) $A_\lambda^M = P_\lambda^M$ parts. More over, one could show that the corresponding expressions for probabilities of the electric and magnetic λ -pole transition $\gamma \to \delta$ in a case of the radiative decay of the one-quasiparticle states are equal:

$$P_\lambda^E(\gamma \to \delta) = 2(2j+1)Q_\lambda^E(\gamma\delta;\gamma\delta)$$
$$Q_\lambda^E = Q_\lambda^{Cul} + Q_{\lambda,\lambda-1}^{Br} + Q_{\lambda,\lambda+1}^{Br}$$
$$P_\lambda^M(\gamma \to \delta) = 2(2j+1)Q_\lambda^M(\gamma\delta;\gamma\delta)$$
$$Q_\lambda^M = Q_{\lambda,\lambda}^{Br}.\qquad (9)$$

In the numerical calculations the transition probability , as usually, is expanded to the series on the known parameter $\alpha\omega$ as follows:

$$Q_\lambda^{Qul} \approx (\alpha\omega)^{(\lambda)}, \quad Q_{\lambda,\lambda-1}^{Br} \approx (\alpha\omega)^{\lambda},$$
$$Q_{\lambda\lambda}^{Br} \approx (\alpha\omega)^{\lambda+3}, \quad Q_{\lambda,\lambda+1} \approx (\alpha\omega)^{\lambda+5}.\qquad (10)$$

In a case of the two-quasi-particle states (this case of the Ne-like ions, where the excited states are represented as stales with the two quasiparticles — electron and vacancy above the closed shells core $1s^2 2s^2 2p^6$) the corresponding probability has the following form (say, transition: $j_1 j_2[J] \to \bar{j}_1 j_2[\bar{J}]$):

$$P(\lambda \mid j_1 j_2[J], \bar{j}_1 j_2[\bar{J}]) =$$
$$= (\bar{J})\begin{Bmatrix} \lambda...J...\bar{J} \\ j_2...\bar{j}_1...j_1 \end{Bmatrix} P(\lambda \mid 1\,\bar{1})(\bar{j}_1),\qquad (11)$$

where the electric and magnetic parts are defined above.

The calculations were divided into two stages (with using the PC atomic code "Superatom-ISAN") [2,8,9,18–25]. In the first stage, the radial wave functions were generated in small multiconfiguration expansions. The spectroscopic orbitals required to form a reference wave function were obtained with a minimal configuration expansion, with full relaxation. Then virtual orbitals were generated in five consecutive steps. At each step, the virtual set has been extended by one layer of virtual orbitals. A layer is defined as a set of virtual orbitals with different angular symmetries. In the present letter, five layers of virtual orbitals of each of the s, p, d, f symmetries were generated. At each step, the configuration expansions were limited to single and double substitutions from valence shells to all new orbitals and to all previously generated virtual layers. The initial shapes of radial orbitals were obtained in the V_c potential. The important effects of

the polarization interaction of external electrons and their mutual screening were taken into account, according to ref.[2−4].

In tables 1 and 2 we present the pprobabilities of the radiation transitions between levels of the configurations $2s^2 2p^5 3s,3d,4s,4d$ and $2s2p^6 3p,4p$ in the Ne-like ions of the Ni XIX and Br XXVI (in s^{-1}; total angle moment J=1): a — the MCDF method; b- relativistic PT with the empirical zeroth approximation (RPT-MP); c1 — our QED PT data (without correlation corrections); c2 — our QED PT data (with an account for the correlation corrections); exp. — experimental data [1−4,8−11,15,18,20,21].

Analysis of the obtained data allows to make the following conclusions. Firstly, one can see that our approach provides physically reasonable agreement with experiment and significantly more advantage able in comparison with standard Dirac-Fock method and little better than the RPTMP method, though the last (RPTMP) results hitherto are considered as the most acceptable (see refs. [13−18]). Secondly, we have checked that the results for the transition probabilities, obtained within our approach in different photon propagator gauges (Coulomb, Babushkin, Landau gauges) are practically equal, that is provided by using an effective QED energy procedure [22].

Table 1

Probabilities of radiation transitions between levels of the configurations $2s^2 2p^5 3s,3d,4s,4d$ and $2s2p^6 3p,4p$ in the Ne-like ion of Ni XIX (in s^{-1}; total angle moment J=1): a — the MCDF method; b- relativistic PT with the empirical zeroth approximation (RPTMP); c1 — our QED PT data (without correlation corrections); c2 — our QED PT data (with an account for the correlation corrections); exp. — experimental data [1−4,8−11,15,18,20,21].

Level J=1	Exp.	a-MCDF	b-RPTMP	c1-QED PT	c2-QED PT
$2p_{3/2}3s_{1/2}$	7.6+11	9.5+11	1.3+12	9.7+11	8.1+11
$2p_{1/2}3s_{1/2}$	6.0+11	1.8+12	1.0+12	7.6+11	6.2+11
$2p_{3/2}3d_{3/2}$	1.4+11	2.2+11	1.5+11	1.7+11	1.4+11
$2p_{3/2}3d_{5/2}$	1.2+13	2.1+13	1.2+13	1.5+13	1.2+13
$2p_{1/2}3d_{3/2}$	3.2+13	4.8+13	3.6+13	4.0+13	3.3+13
$2s_{1/2}3p_{1/2}$	-	-	8.5+11	9.5+11	8.1+11
$2s_{1/2}3p_{3/2}$	-	-	5.1+12	5.6+12	4.7+12
$2p_{3/2}4s_{1/2}$	3.3+11	-	3.6+11	4.1+11	3.4+11
$2p_{1/2}4s_{1/2}$	2.0+11	-	3.0+11	3.1+11	2.4+11
$2p_{3/2}4d_{3/2}$	4.5+10	-	5.2+10	5.4+10	4.8+10
$2p_{3/2}4d_{5/2}$	8.3+12	-	8.3+12	9.2+12	8.2+12
$2p_{1/2}4d_{3/2}$	8.1+12	-	7.9+12	8.9+12	8.0+12
$2s_{1/2}4p_{1/2}$			-	6.3+11	5.7+11
$2s_{1/2}4p_{3/2}$			-	2.7+12	2.4+12

Table 2

Probabilities of radiation transitions between levels of the configurations $2s^2 2p^5 3s,3d,4s,4d$ and $2s2p^6 3p,4p$ in the Ne-like ion of Br XXVI (in s^{-1}; total angle moment J=1): a — the DF method; b- RPTMP; c1,2 — our QED PT data (without and with account for correlation corrections); exp. — experimental data [1−4,8−11,15,18,20,21].

Level J=1	Exp.	a-MCDF	b-RPTMP	c1-QED PT	c2-QED PT
$2p_{3/2}3s_{1/2}$	4.5+12	6.2+12	4.4+12	5.5+12	4.4+12
$2p_{1/2}3s_{1/2}$	3.1+12	4.8+12	2.8+12	3.6+12	2.7+12
$2p_{3/2}3d_{3/2}$	2.8+11	3.9+11	2.9+11	3.5+11	2.8+11
$2p_{3/2}3d_{5/2}$	6.1+13	8.0+13	6.3+13	7.5+13	6.1+13
$2p_{1/2}3d_{3/2}$	8.6+13	9.5+13	8.7+13	9.9+13	8.6+13
$2s_{1/2}3p_{1/2}$	3.9+12	-	4.2+12	4.7+12	4.0+12
$2s_{1/2}3p_{3/2}$	1.4+13	-	1.5+13	1.8+13	1.4+13
$2p_{3/2}4s_{1/2}$	1.1+12	-	1.2+12	1.5+12	1.1+12
$2p_{1/2}4s_{1/2}$	2.1+12	-	2.5+12	2.8+12	2.3+12
$2p_{3/2}4d_{3/2}$	2.8+10	-	7.3+10	6.9+10	6.3+10
$2p_{3/2}4d_{5/2}$	-	-	2.8+13	2.7+13	2.3+13
$2p_{1/2}4d_{3/2}$	2.0+13	-	2.2+13	2.3+13	2.0+13
$2s_{1/2}4p_{1/2}$	2.5+12	-	-	2.9+12	2.6+12
$2s_{1/2}4p_{3/2}$	7.1+12	-	-	8.9+12	8.0+12

Thirdly, calculation has confirmed the great role of the inter electron correlation effects of the second and higher PT orders, namely, effects of the inter electron polarization interaction and mutual screening. In fig.1 we present the calculated by us Z-dependences of the M1 forbidden transition probabilities A from levels $2s_{1/2}3s_{1/2}$ (J=1) (curve 1), $2p_{3/2}3p_{3/2}$ (J=1) (curve 2), $2p_{3/2}3p_{1/2}$ (J=1) (curve 3), $2p_{1/2}3p_{1/2}$ (J=1) (curve 4), $2p_{1/2}3p_{3/2}$ (J=1) (curve 5), $2s_{1/2}3d_{3/2}$ (J=1) (curve 6) into the ground state of Ne-like ions.

The observed non-regularities are explained by the complex character of the configuration interac-

tions and increased significant role of the relativistic and exchange-correlation effects. In conclusion let us note that a significant part of the quite exact spectral probabilities data is firstly obtained and can be used in different applications, including astrophysics, plasma physics and chemistry, atomic optics, laser physics, quantum electronics, physics of the Sun and aurora phenomena etc [1−3,14,15,18,19,25,31,40−42].
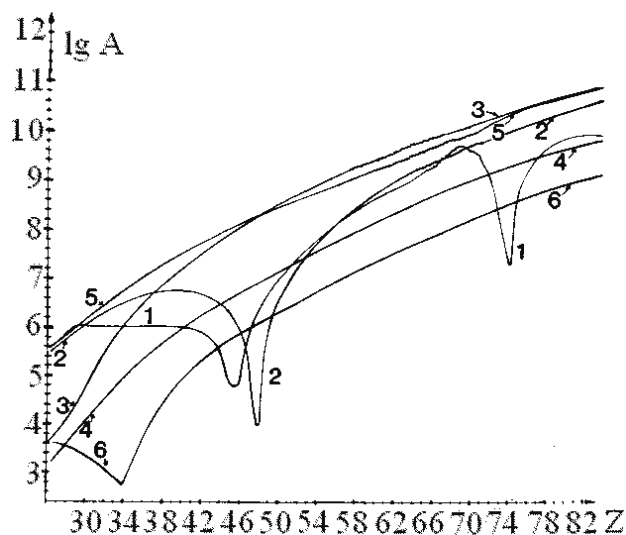
Fig.1. Z-dependences of the M1 forbidden transition probabilities A from levels $2s_{1/2}3s_{1/2}$ (J=1) (curve 1), $2p_{3/2}3p_{3/2}$ (J=1) (curve 2), $2p_{3/2}3p_{1/2}$ (J=1) (curve 3), $2p_{1/2}3p_{1/2}$ (J=1) (curve 4), $2p_{1/2}3p_{3/2}$ (J=1) (curve 5), $2s_{1/2}3d_{3/2}$ (J=1) (curve 6) into the ground state of Ne-like ions..

ACKNOWLEDGEMENTS

References

1. Grant I. P., Relativistic Quantum Theory of Atoms and Molecules. — Oxford, 2008. — 650P.
2. Glushkov A. V., Relativistic Quantum Theory. Quantum, mechanics of Atomic Systems. — Odessa: Astroprint, 2008. — 900P.
3. Froese Fischer C., Tachiev G., Breit−Pauli energy levels, lifetimes, and transition probabilities for the beryllium-like to neon-like sequences //Atomic Data and Nuclear Data Tables. — 2004. — Vol.87. — P.1−184.
4. Mandelstam S. L., Aglitsky E. V., Antsiferov P. S., Panin A. M., X-ray spectra of Ne-like Ba, La, Ce and Pr ions/ // Canad. Journ.of Phys.1994. — Vol.62,N10. — P.1923−1930
5. Safronova U. I., Safronova M. S., Third-order relativistic many-body calculations of energies, transition rates, hyperfine constants, and blackbody radiation shift in $^{171}Yb^+$// Phys. Rev. A. — 2009. — Vol.79. — P.022512
6. Safronova U. I., Safronova A. S., Hamasha, S.M., Beiersdorfer P., Relativistic many-body calculations of multipole (E1, M1, E2, M2, E3, and M3) transition wavelengths and rates between 31−1 41P excited and ground states in nickel-like ions/.//Atomic Data and Nuclear Data Tables. — 2006. — Vol.92. — P.47−104

7. Safronova M. S., Johnson W. R., Safronova U. I., Cowan T., Relativistic many-body theory calculation of the Stark-induced amplitude of 6p-7p transition in thalium//Phys. Rev.A. — 2006. — Vol.74. — P.022504 (8p.).
8. Glushkov A. V., Ivanova E. P., Theoretical Study of Multicharged Ions Spectra of F- and Ne- Isoelectronic Sequence//Spectroscopy of multicharged ions. Ed. Safronova U. I.. — Moscow: Nauka, 1996. — P.5−195.
9. Ivanova E. P., Gogava A. D., Calculation of Na-like spectra−satellites to 2−3 transitions in Ne-like ions//Spectroscopy of highly-ionized atoms. Ed. Safronova U. I.. — Moscow: Nauka, 1998. — P.212−256.
10. Safronova U. I., Cowan T.,Safronova M. S., Relativistic many-body calculations of electric dipole lifetimes, transition rates,oscillator strengths for 2l⁻¹3l' states in Ne-like ions // J.Phys.B:At.Mol.Opt.Phys. — 2005. — Vol.38. — P.2741−2763.
11. Semenov R. I., Kapel'kina E. L., Tsygankova G. A., Tsygankov M. A., Semiempirical calculation of atomic Characteristics of the 2p53d,4d, 2p5ns (n=3−10) configurations of Ne// Opt. Spectr. — 2005. — Vol.99,N4. — P.536−539.
12. Glushkov A. V., Ambrosov S. V., Loboda A. V., Gurnitskaya E. P., Prepelitsa G. P., Consistent QED approach to calculation of electron-collision excitation cross-sections and strengths: Ne-like ions // Int. Journ.Quant.Chem. — 2005. — Vol.104, N4 . — P. 562−569
13. Jamieson M. J., Drake G. W.F., Dalgarno A., Variational calculation of the dynamic polarizabilities of rare-earth metal atoms/ //Phys.Rev. A. — 1995. — Vol.51. — P.3358−3370.
14. Bekov G. I., Vidolova-Angelova E., Ivanov L. N., Letokhov V. S., Mishin B., Laser spectroscopy of low two-timed excited auto ionization states for ytterbium atom//JETP. — 1981. — Vol.80. — P.866−878.
15. Berry H., Desesquelles J., Cheng K. T., Schektman R. Dielectronic satellite spectrum of neon-like ions from beam-foil experiment//Phys.Rev.a. — 1998. — Vol.18,N2. — P.546−551;
16. Kunisz M. D., Coulomb approximation oscillator strengths for some transitions in rare earths//Acta Phys.Polon. — 1992. — Vol.62. — P.285−296.
17. Ostrovsky V. N., Sheynerman S. A., Radiative transitions in the external shells of Hg⁺ion//Opt.Spectr. — 1989. — Vol.67. — P.16−22.
18. Ivanova E. P., Zinoviev N. A., The possibility of X-ray lasers based on inner-shell transitions of Ne-like ions/ // Phys. Lett.A. — 2000− V.274 − P.239−246.
19. Ivanova E. P., Ivanov L. N. Modern Trends in Spectroscopy of Multicharged Ions// Physics Rep. — 1991. — Vol.166,N6. — P.315−390.
20. Glushkov A. V., Ivanova E. P. Theoretical Study of Multicharged Ions Spectra of F- and Ne- Isoelectronic Sequence// J.Quant.Spectr. Rad.Transfer. — 1986. — Vol.36, N2. — P.127−145.
21. Ivanova E. P., Ivanov L. N., Glushkov A. V., Kramida A. E. High order corrections in the Relativistic Perturbation Theory with the model Zeroth Approximation, Mg-like and Ne-like ions //Phys.Scripta −1995. — Vol.32,N4. — P.512−524.
22. Glushkov A. V., Ivanov L. N. Radiation Decay of Atomic States: atomic residue and gauge non-invariant contributions // Phys. Lett.A. — 1992. — Vol.170,N1. — P.33−37
23. Glushkov A. V. Negative Ions of inert Gases// Pis'ma to JETP. — 1992. — T.55,N2- C.104−107; JETP Lett. — 1999. — Vol.55,N2. — P.97−100
24. Glushkov A. V., Ambrosov S. V., Loboda A. V., Chernyakova Yu.G., .Svinarenko A. A., Khetselius O.Yu, QED calculation of the superheavy elements ions: energy levels, radiative corrections and hfs for different nuclear models// Nucl. Phys.A.: Nucl.and Hadr. Phys. — 2004. — Vol. 734. — P.21−28.
25. Glushkov A. V.,Malinovskaya S. V., Svinarenko A. A., Chernyakova Yu.G., QED Calculation of Electron Satellites Spectra in Intense Laser Field in Multicharged Ion// Int.J.Quant.Chem. — 2004. — Vol.99,N5. — P.673−678.
26. Sobel'man I. I. Introduction to theory of atomic spectra. — Moscow: Nauka, 1997.
27. Bunyakova Yu.Ya., Florko T. A., Glushkov A. V., Prepelitsa G. P., Laser photoemission analysis of the fractal parameters for aerosol environment: New data processing system// Photoelectronics. — 2006 . — N15. — P.48−50.

28. Bieron J., Froese-Fischer C., Fritzsche S., Pachucki K., Lifetime and hyperfine structure of the $^3D_2$ state of radium //J. Phys.B:At.Mol.Opt.Phys. — 2004. — Vol.37. — L305–311

29. Khetselius O. Y., Hyperfine structure of radium// Photoelectronics. — 2005. — Vol.14. — P.83–85.

30. Gurnitskaya E. P., Heavy ion storage ring experimental and theoretical determination of the lifetimes for the iron ion levels// Photoelectronics. — 2005. — Vol.14. — P.50–54.

31. Glushkov A. V., Ambrosov S. V., Loboda A. V., Gurnitskaya E. P., Khetselius O.Yu., QED calculation of heavy multicharged ions with account for correlation, radiative and nuclear effects// Recent Advances in Theor. Phys.& Chem. Systems (Springer). — 2006. — Vol.15. — P.285–300.

32. Ostrovsky V. N., Sheynerman S. A. Radiation transitions in the external shells of ion Hg$^+$// Opt. Spectr. — 1999. — Vol.67. — P.16–22

33. Glushkov A. V., New method of accounting for polarization effects in determination of probabilities of the atomic transitions// Opt. Spectr. — 1997. — Vol.71. — P.395–397.

34. Glushkov A. V., Relativistic calculation of oscillator strengths in multicharged ions with single electron above closed shells core// Opt. Spectr. — 1999. — Vol.72. — P.542–547..

35. Khetselius O.Yu., Relativistic Perturbation Theory Calculation of the Hyperfine Structure Parameters for Some Heavy-Element Isotopes//Internat. Journal of Quantum Chemistry. — 2009. — Vol.109,N14. — P. 3330–3335.

36. Florko T. A., Loboda A. V., Svinarenko A. A., Sensing forbidden transitions in spectra of some heavy atoms and multicharged ions: new theoretical scheme/ Sensor Electronics and Microsyst. Techn. — 2009. — N3. — P.21–26.

37. Glushkov A. V., Florko T. A., Khetselius O.Yu., Malinovskaya S. V., Mischenko E. V., Svinarenko A. A., Optimized perturbation theory scheme for calculating the interatomic potentials and hyperfine lines shift for heavy atoms in the buffer inert gas//Internat. Journal of Quantum Chemistry. — 2009. — Vol.109. — P.3325–3329.

38. Florko T. A., Theoretical determination of oscillator strengths of some transitions in rare-earth atom of Eu//Photoelectronics. — 2007. — N16. — P.98–101.

39. Florko T. A., Gurnitskaya E. P., Polischuk V. N., Seredenko S. S., Dipole transitions of rare earth atoms in inert medium in a weak electromagnetic field and quasimolecular term//Photoelectronics. — 2007. — N16. — P.26-

40. Glushkov A. V., Malinovskaya S. V., Ambrosov S. V. Spectroscopy of Neutral and Highly-ionized Atoms: Calculation of the Oscillator Strengths for Na- and Fr-like Ions// Atomic Spectra and Oscillator Strengths for Astrophysical and Laboratory Plasmas. — Meudon: Publications de l'Observatoire de Paris. — 1996. — P.96–99.

41. Віймонт E., Fivet V., Quinet P., Relativistic Hartree−Fock and Dirac−Fock atomic structure calculations in Fr-like ions Ra$^+$, Ac^{2+}, Th^{3+} and U^{5+}// J.of Physics B: Atom. Mol. Opt. Phys. — 2004. — Vol.37. — P.4193–4202.

42. Quinet P., Argante C., Fivet V., Terranova C., Yushchenko A. V., Віймонт E., Atomic data for radioactive elements Ra I, Ra II, Ac I and Ac II and application to their detection in HD 101065 and HR 465 // Astr.& Astrophys. — 2007. — Vol.474,N1. — P.307–314

UDC 539.142 : 539.184

T. A. Florko

THEORETICAL DETERMINATION OF THE RADIATIVE TRANSITION PROBABILITIES IN SPECTRA OF NE-LIKE MULTICHARGED IONS

Abstract.
On the basis of a new scheme within a gauge-invariant QED perturbation theory it as been carried out calculating the energies and transition probabilities for some E1, M1, E2 and other transitions in spectra of Ne-like multicharged ions.
Key words: theoretical spectroscopy, multicharged ion, radiative transition

УДК 539.142 : 539.184

Т. А. Флорко

ТЕОРЕТИЧНОЕ ОПРЕДЕЛЕНИЕ ВЕРОЯТНОСТЕЙ РАДИАЦИОННЫХ ПЕРЕХОДОВ В СПЕКТРАХ NE-ПОДОБНЫХ МНОГОЗАРЯДНЫХ ИОНОВ

Резюме.
Выполнен расчет энергий и вероятностей E1, M1, E2 и др. радиационных переходов в спектрах Ne-подобных многозарядных ионов на основе новой релятивистской схемы в рамках калибровочно-инвариантной КЭД теории возмущений.
Ключевые слова: теоретическая спектроскопия, многозарядный ион, радиационный переход

УДК 539.142 : 539.184

Т. О. Флорко

ТЕОРЕТИЧНЕ ВИЗНАЧЕННЯ ІМОВІРНОСТЕЙ РАДІАЦІЙНИХ ПЕРЕХОДІВ У СПЕКТРАХ NE-ПОДІБНИХ БАГАТОЗАРЯДНИХ ІОНІВ

Резюме.
Виконано розрахунок енергій і ймовірностей E1, M1, E2, інших радіаційних переходів у спектрах Ne-подібних багатозарядних іонів на основі нової релятивістської схеми у межах калібровочно-інваріантної КЕД теорії збурень.
Ключові слова: теоретична спектроскопія, багатозарядний іон, радіаційний перехід

YE. V. BRYTAVSKYI, YU. N. KARAKIS, M. I. KUTALOVA, G. G. CHEMERESYUK

Odessa I. I. Mechnikov National University, ,
2, Dvorianskaya str., Odessa 65082, Ukraine. Tel. +38 048 — 7266356.
Fax +38 048 — 7266356, E-mail: wadz@mail.ru

REVERSIVE SPECTRAL CHARACTERISTICS IN IR-QUENCHING RANGE OF PHOTOCURRENT. THE CASE OF INTERACTING HOLES.

The interaction processes between the basic and excited states of sensitization centres were investigated by reversive procedure. It was stated that all the observed effects can be explained by stimulated level of hole trap occupation and changes in thermal redistribution of captured carriers taking into account that the band scheme was corrected.

Spectral characteristics of semiconductor samples were measured experimentally beginning from the small wavelengths up to the longer ones. Under investigation of intrinsic conductivity the abovementioned procedure gives no influence on experimental result. But this statement is not valid when the processes connected with captures in holes are studied.

Under such procedure the processes for occupation — devastation of holes take place with additional period. Firstly, large concentration of non-equilibrium carriers is created under excitation by wavelengths from intrinsic absorption band. The piece of the mentioned carriers settle in holes. Under rather high intensities of light and velocity of light wavelength change one can create such conditions when the hole by the moment of its excitation is found completely occupied with non-equilibrium charge, independently on the pre-history of processes flowed.

It is convenient. In this case the photoresponse is found large at the expense of considerable carrier release that makes easy to determine the basic parameter — activation energy, i.e. hole depth, that is identical both for equilibrium charge and for non-equilibrium one.

But the processes connected with concentrations of charge carriers on holes that existed there primarily before light exposure can not be examined. At the expense of large number of non-equilibrium charges entering such processes are completely disrupted.

One should wait relaxation times under illumination by each wavelength out of various spectra ranges when the conception about the direction of its change to raise or to decrease lost. Each wavelength of light applied causes the independent effect which is not connected with the foregoing exposure.

In case when equilibrium processes in crystals are studied in participation of holes, one should use the reverse change in radiation wavelength from the greater values (infrared) up to small ones (visible range). In this case the light acts only as the instrument for excitation. Concentration of captured charge existed in holes is only read out with help of light when carriers from holes are excited.

We note that the new conditions take place. Probably this is the reason that such procedure to change spectral content of excitation has been narrow extended.

The carriers shifted from bound to free state are non-equilibrium by definition, but their concentration under usually applied high excitation levels is determined by equilibrium charge located in holes before illumination.

The conditions with interacting holes system, as in our case, between basic and excited states of R-centres are complicated. The long-wave light effect is found to be symmetrical in this time. Under any excitation flow the levels are activated in turn. The direction to change wavelength (from long to short waves or from short to long waves) defines only the order to activate holes — either at first they are activated from narrower excited state and then from the deeper excited one, or vice versa. In the latter case, one should take into account that the part of IR-radiation quanta with energy 1,1 eV (for cadmium sulphide) can excite R-centres in depth 0,9 eV forming hot free holes.

In all variants of current formation in semiconductor crystal, the universality of reversive procedure allows to carry out measurements both traditionally under steady-state conditions and in dynamic regime under different velocity of changes in exciting light wavelength.

The comparison of traditional, steady-state measurements and the procedure under different velocities $\frac{d\lambda}{dt}$ allows to note the following particularities:

1. Firstly, both procedures do not contradict each other . On the contrary, steady-state procedure should be understood as particular case of measurements with null rate $\frac{d\lambda}{dt} = 0$. The possibilities cleared to carry out the analysis under the other magnitudes $\frac{d\lambda}{dt}$ are lacked.

2. The steady-state procedure for measurements of reach photocurrent operates good for significantly occupied holes which concentration is high. The low charge accumulated in holes and/or their low concentration are more typical. The processes connected with this component on photocurrent formation influence only during earlier seconds of exposure. The analysis does not observe them from photocurrent steady-state value because they have been already absent there.

Under dynamic measurements the role of relaxation changes. It stops to be opponent and becomes ally. Under measurements, particularly quick studies, with large values of $\frac{d\lambda}{dt}$ relaxation phenomena effect on photocurrent behavior. When results are compared under different values of $\frac{d\lambda}{dt}$ and then different degrees of relaxation influence, one can show up these mechanisms and, finally, holes parameters and conclude that these mechanisms are forming.

3. Non-equilibrium carriers interchange and balance their energy with lattice during very short time of $10^{-3} - 10^{-1}$ s [1]. As result, the contributions of equilibrium and non-equilibrium carriers in current can not be divided under steady-state measurements. If dark current is formed exclusively at the expense of charge equilibrium component, it is customary to consider that the value of light current is connected only and exclusively with non-equilibrium charges. This can be come true for high levels of exposure but not correct for low illumination. Later we show that the procedure of studies proposed, particularly within maximum rates $\frac{d\lambda}{dt}$, remove these contradictions.

4. When capturing holes interact, as in our case, between basic and excited state of R-centres, the processes of charge redistribution should occur rather quickly because this is one and the same centre geometrically. The carriers have not waste time to drift from one centre to the other. We should note that the particularities of these processes remain unexplored now. And the procedure of high rate measurements for $\frac{d\lambda}{dt}$ in IR-region can be the effective instrument of such studies.

The investigation of phenomena occurred under different order of excitation clear the opportunity that has not been applied earlier to precise the particularities of processes flowed.

Semiconductor single crystal cadmium sulphide was chosen for investigation as the model material. Its advantages are the following: firstly, high photosensitivity (photoresponse — up to eight orders); secondly, IR-quenching of photocurrent characteristic for rather narrow class of materials; thirdly, it is wideband semiconductor ($E_g \sim 2,42$ eV), that allows to carry out investigations within wide range of wavelengths from visible area up to 1600 μm.

The range of applied excitation energies is called the area of interacting holes in the sense that interaction to R and R'-levels is excitation of physically single centre in contrast to the common situation with different groups of centres observed in [2,3].

If the model of Bube was realized at activation of R-centres [4], the significant variations between direct and backward spectral dependencies Q(λ) should not appeared. The basic state with activation energy 1,1 eV is primarily excited when illumination wavelength changes from small values to the greater ones. And the occupation of these state by holes decreases respectively. If excitation with energy 0,9 eV is carried out later, the number of activated holes can not be so large

and longwave maximum Q(λ) can be observed higher than shortwave one.

The higher rate of wavelength change the stronger decrease in maximum within the range 1400 μm in comparison with maximum 1000 μm. This should take place as result of the following causes. Firstly, the steady-state (but non-equilibrium — intrinsic light effects) occupation of R and R'-centres has no time to restore. Secondly, in order that hole excited by longwave light may transfer to free state, it needs to absorb photon, that needs time. The analogous ratio of Q(λ) maxima heights should be observed under reverse change of wavelength — from large values to small ones.

Thermal excitation (according to Bube theory) influences only on R'-centres, whereas capture cross-section for R and R'-centres is similar. As result, steady-state concentration of holes on R'-centres should be considerably lower than on R-levels. Under quick change of wavelength we read out this picture and longwave maximum should locate lower.

At slow decrease in wavelength of quenching light the situation should have time to equalize slightly at the expense of holes departure from R-centres when light passes energy within the range of ~ 0,9 eV. This process is spread in time that is enough to realize the competitive process — holes created by intrinsic light in valence-band are captured. So, the height of shortwave maximum Q(λ) should prevail. But the other situation is realizes experimentally. At any exposure regimes the maximum of spectral characteristics Q(λ) in 1000 μm area was observed lower than at λ≈1400 μm.

In whole spectral distribution of quenching coefficient at increase of excitation wavelength Q(λ↑) and at its decrease Q(λ↓) for different rates $\frac{d\lambda}{dt}$ is shown in Fig. 1. For steady-state curve we used measurements with relaxation up to 20 minutes in each point to avoid transient processes [5,6]. The sample is exposured for a long time in each cycle at spectrum edges at 1000 and 1600 μm to preserve the inter-influence of curves.

The reverse curves for $\frac{d\lambda}{dt}$ ~1 μm/s that causes the most distinctive modifications is shown in Figure 1. The characteristic changes observed in curve of photocurrent quenching along the whole range of applied rates (from 0,33 up to 2,5 μm/s) are brought together in Table 1.

In order to make the observation more useful we show the corrected shape of band-diagram with both states of R-centres [7] (Fig. 2).

VARIANT A:

Value Q in each of maxima is proportional to the number of holes knocked out by light, correspondingly, for shortwave maximum — from basic state of R-centres and for longwave maximum — from excited state. At increase of wavelength in quenching range beginning from 900 μm the exciting light influences firstly on the deeper basic level (see Fig. 2). The initial

occupation of this centre is the same as in steady-state measurements, but the number of activated holes is found smaller because the total time of its exposure is lower depending on rate $\frac{d\lambda}{dt}$. So the value $Q_{max1}(\lambda\uparrow)$ is found lower than the steady-state one. If excitation is carried our from long waves up to short ones, the excited state R' is devastated preliminary. As result of increase in holes number there the flow of thermally excited holes from the basic state raises (in Fig. 2 named as kT). And as result occupation of R-centres is found lower and value $Q_{max1}(\lambda\downarrow)$ becomes smaller when light wavelength decreases up to numbers of order 1000 μm. The optimum rate exists when the discordance $\Delta Q = Q_{max1}(\lambda\uparrow) - Q_{max1}(\lambda\downarrow)$ is the highest accordingly to the model developed in [2,3]. In our case it is approximately 1 μm/s. At further rate increase the discordance decreases because at direct change λ has no time to excite R-state and at reverse change — R'.
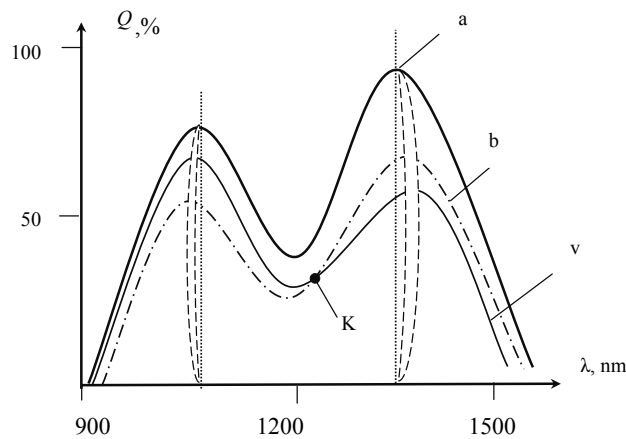
Figure 1. Spectral distribution of quenching at measurements in steady-state conditions (a), at decrease of wavelength (b) and at its increase (v) with rate 1 nm/s.
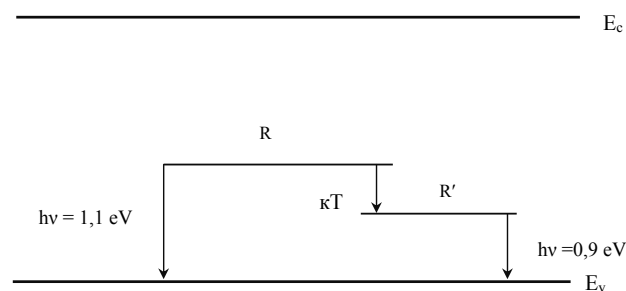
Figure 2. Band diagram of sensitized semiconductor.

VARIANT B:

Now the excitation by long waves meets firstly unexcited occupation of R' states and the value of maximum $Q_{max2}(\lambda\downarrow)$ is defined only by the time of exposure on excited states R' and then rate $\frac{d\lambda}{dt}$. At direct measurements with increase of wavelength the mentioned process has one more cause [2]. Excitation of R-states has occurred before. If raise of hole thermal inflow was characteristic for *Variant A*, now

it causes its decrease. Occupation of R'-centres is found lower, namely, $\Delta Q = Q_{max2}(\lambda\downarrow) - Q_{max2}(\lambda\uparrow)$. Let's note the characteristic peculiarity. As $\Delta Q = Q_{max1}(\lambda\uparrow) - Q_{max1}(\lambda\downarrow)$ is correct for the left maximum, according to Bolzano-Cauchy theorem curves $Q(\lambda\uparrow)$ and $Q(\lambda\downarrow)$ should cross without fail. Really, we have observed this effect at any change rates of light wavelength, at all intensities of illumination. This is shown by point "K" in Fig. 1. The similar nuance is the peculiarity of applied procedure and it can not be observed in traditional measurements.

Table 1

The analyses of characteristic changes for curves of Fig. 1 for different rates of changes on wavelength of quenching light.

Coordinate axis / Position of maximum	Y-ordinate (value of quenching Q, %)	X-abscissa (wavelength of irradiation λ)
Shortwave maximum of quenching (1000 – 1100 μm)	**A.** With increase of rate $\frac{d\lambda}{dt}$, the discordance $\Delta Q = Q_{max1}(\lambda\uparrow) - Q_{max1}(\lambda\downarrow)$ increases, reaching the greater values approximately at 1 μm/s, and the decreases anew.	**C.** Both values — $Q_{max1}(\lambda\downarrow)$ and $Q_{max1}(\lambda\uparrow)$ shifted to short wavelengths comparatively with steady-state maximum, but $Q_{max1}(\lambda\downarrow)$ shifted considerably. With increase of rate $\frac{d\lambda}{dt}$ these deviations firstly decrease reaching the greater values approximately at 1 μm/s, and then decrease.
Longwave maximum of quenching (1300 – 1400 μm)	**B.** With increase of rate $\frac{d\lambda}{dt}$, the discordance $\Delta Q = Q_{max2}(\lambda\downarrow) - Q_{max2}(\lambda\uparrow)$ increases, reaching the greater values approximately at 1 μm/s, and the decreases anew.	**D.** Both values $Q_{max2}(\lambda\downarrow)$ и $Q_{max2}(\lambda\uparrow)$ shifted to the greater wavelengths comparatively with the steady-state maximum but $Q_{max2}(\lambda\uparrow)$ shifted considerably. With increase of rate $\frac{d\lambda}{dt}$ these deviations firstly increase reaching the greater values approximately at 1 μm/s, and the decreases anew.

VARIANT C:

Values $Q_{max1}(\lambda\uparrow)$ and $Q_{max1}(\lambda\downarrow)$ changes down differently. Curve $Q(\lambda\uparrow)$ connected with undisturbed occupation of basic states and show simple scaling of steady-state short-wave maximum $Q(\lambda)$. Both its slopes undergo rather the same decrease. The right slope is bigger because some shift of capture-devastation equilibrium is characteristic for measurements with wavelength longer than maximum one. The abovementioned shift is caused by exciting light itself when measurements at wavelengths shorter than 1000 μm were carried out. As result the maximum $Q_{max1}(\lambda\uparrow)$ slightly shifts to the left. The picture changes at measurements when light wavelength decreases. As is was mentioned previously, excited level devastated preliminary. Thermal excitation from R-centres raised and their occupancy decreases. This can be seen clearly at longwave slope of maximum than at shortwave one be-

ing studied later. As result the maximum loses its symmetry and depending on rate $\frac{d\lambda}{dt}$ significantly shifted to the left. Obviously this effect will decay with increase in change rate of light wavelength because light has time to knock out the smaller number of holes with decrease in time of influence on the centre.

The total behavior shortwave maxima coordinates $Q_{max1}(\lambda\downarrow)$ and $Q_{max1}(\lambda\uparrow)$ in Fig. 1 depending on applied rate $\frac{d\lambda}{dt}$ is shown by the section of dotted lines. It characterises as half-moon which right side is formed by maxima coordinates $Q_{max1}(\lambda\uparrow)$, and left side — by maxima $Q_{max1}(\lambda\downarrow)$.

VARIANT D:

The similar semi-moon with right convex forms for longwave maximum. Now the curve $Q_{max2}(\lambda\uparrow)$ decreases non-symmetrically because the basic level was devastated preliminary, thermal transmission from R to R' decreased and this is cleared significantly on the left slope of dependence $Q(\lambda\uparrow)$. We note that the whole variety of curve family in Fig. 1 can be explained applying one mechanism [2,3] — raise or decrease in thermal excitation of holes from basic to excited states depending on direction of changes in light wavelength.

Namely, the presence of simultaneous effects allows to consider the existence of such channel for intercentre redistribution of charge concentrations to be proved. Its observation became possible owing to reversive method of excitation applied.

References

1. Бонч-Бруевич В. Л., Калашников С. Г. Физика полупроводников // М.: Изд-во "Наука" — 1999. — 672 с.
2. Brytavskyi Ye.V., Karakis Yu.N. "Spectral characteristics of semiconductors with sensitivity centres at reverse excitation"// International Conference of Students and Young Scientists in Theoretical and Experimental Physics HEUREKA -2009. Book of abstracts. May 20 — 22б Lviv, Ukraine.
3. Є. В. Британський, Ю. Каракис "Особливості спектрального розподілу фотоструму в умовах реверсного збудження". // Вісник Львівського університету. Серія Фізична. 2009 р. С. 237 — 243.
4. Бьюб Р. Фотопроводимость твёрдых тел // М.: Изд-во ин. лит. — 2002. — 558 с.
5. Каракис Ю. Н., Затовская Н. П., Зотов В. В., Куталова М. И. Особенности релаксации фототока в кристаллах сульфида кадмия с запорными контактами // 1-а Українська наукова конференція з фізики напівпровідників. Одеса, 10- 14 вересня 2002р. Тези доповідей. Т.2. с.138.
6. Karakis Yu.N., Borschak V. A., Zotov V. V., Kutalova M. I. Relaxation characteristics of cadmium sullphide crystals with IR-quenching // Photoelectronics. — 2002. — No. 11. — P.51—55.
7. Novikova M. A., Karakis Yu. N., Kutalova M. I. Particularities of current transfer in the crystals with two types of recombination centers // Photoelectronics. — 2005. — № 14. — P. 58 — 61.

Ye. V. Brytavskyi, Yu. N. Karakis, M. I. Kutalova, G. G. Chemeresyuk

REVERSIVE SPECTRAL CHARACTERISTICS IN IR-QUENCHING RANGE OF PHOTOCURRENT. THE CASE OF INTERACTING HOLES

Abstract
The interaction processes between the basic and excited states of sensitization centres were investigated by reversive procedure. It was stated that all the observed effects can be explained by stimulated level of hole trap occupation and changes in thermal redistribution of captured carriers taking into account that the band scheme was corrected.
Key words: spectral characteristics, photocurrent, holes.

Каракис Ю. Н.,Бритавский Е. В., Куталова М. И., Чемересюк Г. Г.

РЕВЕРСИВНЫЕ СПЕКТРАЛЬНЫЕ ХАРАКТЕРИСТИКИ В ОБЛАСТИ ИК-ГАШЕНИЯ ФОТОТОКА. СЛУЧАЙ ВЗАИМОДЕЙСТВУЮЩИХ ЛОВУШЕК

Резюме
Исследованы процессы взаимодействия между основным и возбуждённым состоянием очувствляющих центров с применением реверсивного метода. Установлено, что все наблюдаемые эффекты могут быть объяснены стимулированным уровнем заполнения дырочных ловушек и изменением термического перераспределения захваченных носителей с учётом откорректированной зонной схемы.
Ключевые слова: спектральные характеристики, фототок, ловушка.

Каракіс Ю. Н., Бритавський Е. В., Куталова М. І., Чемересюк Г. Г.

РЕВЕРСИВНІ СПЕКТРАЛЬНІ ХАРАКТЕРИСТИКИ У ОБЛАСТІ ІЧ-ГАСІННЯ ФОТОСТРУМУ. ВИПАДОК ВЗАЄМОДІЮЧИХ ПАСТОК

Резюме
Досліджені процеси взаємодії між основним і збудженим станом чутливих центрів з використанням реверсивного засобу. Доведено, що всі спостережені ефекти можуть бути пояснені стимульованим рівнем заповнення діркових пасток та зміною термічного перерозподілу захоплених носіїв з урахуванням відкорегованої зонної схеми.
Ключові слова: спектральні характеристики, фотострум, пастки.

L. V. NIKOLA, A. V. IGNATENKO, A. N. SHAKHMAN

I. I. Mechnikov Odessa National University,
Odessa State Environmental University,
Kherson State University

RELATIVISTIC THEORY OF THE AUGER (AUTOIONIZATION) DECAY OF EXCITED STATES IN SPECTRA OF MULTICHARGED IONS

Relativistic method of calculating the characteristics of the Auger decay in the atomic spectra, based on the S-matrix Gell-Mann and Low formalism, is used for estimating the transition energies and autoionization probabilities in spectra of the Fe ion with one vacancy above the core $1s^22s^22p^63s^23p^6$.

1. The Auger decay is related to very key channel of decay of the excited atomic (molecular) states and attracts a great interest because of the importance for different applications in a plasma physics, physics of the ionized gases, quantum optics and photoelectronics [1−16]. When calculating the Auger decay characteristics it is usually used the two-step model [1−5]. Since the vacancy lifetime in an inner atomic shell is rather long (about 10^{-17} to 10^{-14}s), the atom ionization and the Auger emission are considered to be two independent processes. In the more correct dynamic theory of the Auger effect [1−5] the processes are not believed to be independent from one another. The fact is taken into account that the relaxation processes due to Coulomb interaction between electrons and resulting in the electron distribution in the vacancy field have no time to be over prior to the transition. In fact, a consistent Auger decay theory has to take into account correctly a number of correlation effects, including the energy dependence of the vacancy mass operator, the continuum pressure, spreading of the initial state over a set of configurations etc. [1−6]. Note that the effects are not described adequately to date, in particular , within the Auger decay theory [1−3]. One could remind that the inner shell excitation relaxes via resonant Auger electron or fluorescent photon emission. For example, the resonant Auger spectra of the halogens and noble gases were for the first time reported by Eberhardt *et al* and since then the resonant Auger spectra of noble gases have been studied extensively both experimentally and theoretically [1−8]. In particular, argon (chlorine) and corresponding like ions have attracted a lot of interest.

The most widespread theoretical studying is based on using the multi-configuration Dirac−Fock (MCDF) calculation [1−8]. The theoretical predictions based on MCDF calculations have been carried out within different approximations and remained hitherto non-satisfactory in many relations. Earlier [8−10] it has been proposed relativistic perturbation theory (PT) method of the Auger decay characteristics for complex atoms, which is based on the Gell-Mann and Low S-matrix formalism energy approach) and QED PT formalism [11−14]. The novel element consists in an using the optimal basis of the electron state functions derived from the minimization condition for the calibration-non-invariant contribution (the second order PT polarization diagrams contribution) to the imaginary part of the multi-electron system energy already at the first non-disappearing approximation of the PT [13]. Earlier it has been applied in studying the Auger decay characteristics for a set of neutral atoms, quasi-molecules and solids. Besides, the ionization cross-sections of inner shells in various atoms and the Auger electron energies in solids (*Na,Si etc*) were estimated. Here we will apply this approach to studying the autoionization decay probabilities in spectra of the multicharged ions on example of the Fe ion with one vacancy above the core $1s^22s^22p^63s^23p^6$.

2. Let us describe briefly the key aspects of the relativistic method to autoionization and Auger decay probabilities. Within the frame of PT approach [8,11,14] to the Auger effect description, the Auger transition probability and, accordingly, the Auger line intensity are

defined by the square of an electron interaction matrix element having the form:

$$V^{\omega}_{1234} = \left[(j_1)(j_2)(j_3)(j_4)\right]^{1/2} \times$$

$$\times \sum_{\lambda\mu}(-1)^{\mu}\begin{pmatrix} j_1 j_3 & \lambda \\ m_1 - m_3 & \mu \end{pmatrix} \times \operatorname{Re} Q_{\lambda}(1234);$$

$$Q_{\lambda} = Q_{\lambda}^{\mathrm{Qul}} + Q_{\lambda}^{\mathrm{Br}}. \qquad (1)$$

The terms $Q_{\lambda}^{\mathrm{Qul}}$ and $Q_{\lambda}^{\mathrm{Br}}$ correspond to subdivision of the potential into Coulomb part $cos|\omega|r_{12}/r_{12}$ and Breat one, $cos|\omega|r_{12}\alpha_1\alpha_2/r_{12}$. The real part of the electron interaction matrix element is determined using expansion in terms of Bessel functions: :

$$\frac{\cos|\omega|r_{12}}{r_{12}} = \frac{\pi}{2\sqrt{r_1 r_2}} \times$$

$$\times \sum_{\lambda=0}(\lambda)J_{\lambda+1/2}\left(|\omega|r_<\right)J_{-\lambda-1/2}\left(|\omega|r_>\right)P_{\lambda}(\cos \mathbf{r}_1\mathbf{r}_2). \quad (2)$$

where J is the 1st order Bessel function, $(\lambda)=2\lambda+1$. The Coulomb part $Q_{\lambda}^{\mathrm{Qul}}$ is expressed in terms of radial integrals R_{λ}, angular coefficients S_{λ} [4,11]:

$$\mathrm{Re}\,Q_\lambda^{\mathrm{Qul}} = \frac{1}{Z}\,\mathrm{Re}\,\big\{R_l\,(1243)S_\lambda\,(1243)+$$

$$+R_\lambda\,(1\tilde{2}4\tilde{3})S_\lambda\,(1\tilde{2}4\tilde{3})+R_\lambda\,(1\tilde{2}4\tilde{3})S_\lambda\,(1\tilde{2}4\tilde{3})+$$

$$+R_\lambda\,(1\tilde{2}\tilde{4}\tilde{3})S_\lambda\,(1\tilde{2}\tilde{4}\tilde{3})\big\} \tag{3}$$

As a result, the Auger decay probability is expressed in terms of $\mathrm{Re}\,Q_\lambda(1243)$ matrix elements :

$$\mathrm{Re}\,R_\lambda\,(1243)=$$

$$= \iint dr_1 r_1^2 r_2^2 f_1\,(r_1)f_3\,(r_1)f_2\,(r_2)f_4\,(r_2)Z_\lambda^{(1)}\,(r_<)Z_\lambda^{(1)}\,(r_>). \tag{4}$$

where f is the large component of radial part of single electron state Dirac function and function Z is :

$$Z_\lambda^{(1)} = \left[\frac{2}{|\omega_{13}|\alpha Z}\right]^{\lambda+\frac{1}{2}}\frac{J_{\lambda+\frac{1}{2}}\,(\alpha|\omega_{13}|r)}{r^\lambda\Gamma\left(\lambda+\frac{3}{2}\right)}.$$

The angular coefficient is defined by standard way [8]. The other items in (3) include small components of the Dirac functions; the sign "∼" means that in (3) the large radial component f_i is to be changed by the small g_i one and the moment l_i is to be changed by $\tilde{l}_i = l_i - 1$ for Dirac number $ӕ_i > 0$ and $l_i + 1$ for $ӕ_i < 0$. The Breat interaction is known to change considerably the Auger decay dynamics in some cases (c.f. [4]). The Breat part of Q is defined as the sum:

$$Q_\lambda^{\mathrm{Br}} = Q_{\lambda,\lambda-1}^{\mathrm{Br}} + Q_{\lambda,\lambda}^{\mathrm{Br}} + Q_{\lambda,\lambda+1}^{\mathrm{Br}}, \tag{5}$$
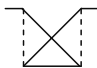
where the contribution of our interest is determined as:

$$Q_\lambda^{\mathrm{Br}} = \frac{1}{Z}\,\mathrm{Re}\,\big\{R_\lambda\,(12\tilde{4}\tilde{3})S_\lambda^l\,(12\tilde{4}\tilde{3})+$$

$$+R_\lambda\,(1\tilde{2}43)S_\lambda^l\,(1243)+R_l\,(1\tilde{2}4\tilde{3})S_\lambda^l\,(12\tilde{4}\tilde{3})+$$

$$+R_l\,(1\tilde{2}4\tilde{3})S_\lambda^l\,(1\tilde{2}4\tilde{3})\big\} \tag{6}$$

The Auger width is obtained from the adiabatic Gell-Mann and Low formula for the energy shift [13].

The contribution of the $A_d = $ ⬭ diagram to the Auger level width with a vacancy $n_\alpha l_\alpha j_\alpha m_\alpha$ is:

$$\sum_\lambda \frac{2}{(\lambda)(j_\alpha)}\sum_{\beta\gamma\le f}\sum_{k>f}Q_\lambda\,(\alpha k\gamma\beta)Q_\lambda\,(\beta\gamma k\alpha), \tag{7}$$

while contribution of the $A_{\mathrm{ex}} = $ ⧖ one is:

$$\frac{2}{(j_\alpha)}\sum_{\lambda_1\lambda_2}\sum_{\beta\gamma\le f}\sum_{k>f}Q_{\lambda_1}\,(\alpha k\gamma\beta)Q_{\lambda_2}\,(\beta\gamma k\alpha)\begin{Bmatrix} j_\alpha & j_\gamma & \lambda_2 \\ j_k & j_\beta & \lambda_1 \end{Bmatrix}. \tag{8}$$

The formulas (7),(8) define the full Auger level width. The partial items of the $\sum_{\beta\gamma}\sum_k$ sum answer to contributions of $\alpha^{-1}\to(\beta\gamma)^{-1}K$ channels resulting in formation of two new vacancies $\beta\gamma$ and one free electron k: $\omega_k = \omega_\alpha + \omega_\beta - \omega_\alpha$. The final expression for the width in the representation of jj-coupling scheme of single-electron moments has the form:

$$\Gamma(2j_1^o l_1^o, 2j_2^o l_2^o; J) = 2\sum_{j_k l_k}|\Gamma(2j_1^o l_1^o, 2j_2^o l_2^o; 1l_o, kjl)|^2 \tag{9}$$

Here the summation is made over all possible decay channels. The basis of electron state functions was defined by the solution of Dirac equation (integrated numerically using the Runge-Cutt method). The calculation of radial integrals $\mathbf{Re}R_\lambda(1243)$ is reduced to the solution of a system of differential equations [4]:

$$\left. \begin{aligned} y_1' &= f_1 f_3 Z_\lambda^{(1)}\,(\alpha|\omega|r)r^{2+\lambda}, \\ y_2' &= f_2 f_4 Z_\lambda^{(1)}\,(\alpha|\omega|r)r^{2+\lambda}, \\ y_3' &= [y_1 f_2 f_4 + y_2 f_1 f_3]Z_\lambda^{(2)}\,(\alpha|\omega|r)r^{1-\lambda}. \end{aligned} \right\} \tag{10}$$

In addition, $y_3(\infty)=\mathbf{Re}R_\lambda(1243)$, $y_1(\infty)=X_\lambda(13)$. The system of differential equations includes also equations for functions $f/r^{|ӕ|-1}$, $g/r^{|ӕ|-1}$, $Z_\lambda^{(1)}$, $Z_\lambda^{(2)}$. The formulas for the auger decay probability include the radial integrals $R_\alpha(\alpha k\gamma\beta)$, where one of the functions describes electron in the continuum state. When calculating this integral, the correct normalization of the function Ψ_k is a problem. The correctly normalized function should have the following asymptotic at $r\to 0$ [4]:

$$\left.\begin{aligned} f \\ g \end{aligned}\right\} \to (ëù)^{-\frac{1}{2}}\begin{cases} \left[ù + (áZ)^{-2}\right]^{-\frac{1}{2}}\sin(kr+ä), \\ \left[ù - (áZ)^{-2}\right]^{-\frac{1}{2}}\cos(kr+ä). \end{cases} \tag{11}$$

When integrating the master system, the function is calculated simultaneously:

$$N(r)=$$

$$= \left\{\pi\omega_k\left[f_k^2\left[\omega_k + (\alpha Z)^{-2}\right] + g_k^2\left[\omega_k + (\alpha Z^{-2})\right]\right]\right\}^{\frac{1}{2}}.$$

It can be shown that at $r\to\infty$, $N(r)\to N_k$, where N_k is the normalization of functions f_k, g_k of continuous spectrum satisfying the condition (11).

The energy of an electron formed due to a transition jkl is defined by the difference between energies of an atom with a hole at the j level and double-ionized atom at kl levels in the final state:

$$E_A(jkl,\,^{2S+1}L_J) = E_A^+(j) - E_A^{2+}(kl,\,^{2S+1}L_J) \tag{12}$$

To single out the above-mentioned correlation effects, the equation (12) can be presented as:

$$E_A(jkl,\,^{2S+1}L_J) = E(j) - E(k) - E(l) - \Delta(k,l;\,^{2S+1}L_J) \tag{13}$$

where the item Δ takes into account the dynamic correlation effects (relaxation due to hole screening with electrons etc.). Other details of the method and calculational procedure can be found in refs. [8–14].

3. Now let us describe some calculated data for the transitions energies and autoionization decay probabilities in the spectra of the multicharged ions on example of the Fe ion with one vacancy above the core $1s^2 2s^2 2p^6 3s^2 3p^6$. This ion of a great interest because of the high complexness of the spectrum and great actuality for astrophysical applications [4–7, 15,16]. As the final state of the studied system after autoionization decay is the three-quasiparticle, the general number of the decay channels is sufficiently large, so we are limited only by summarized probability of the autoionization decay for the state $1s^2 2s^2 2p^6 3s^2 3p^6$ with defi-

nite quantum numbers of vacancies n_1l_1 and n_2l_2. The detailed information about total number of channels is presented in ref. [17]. In table 1 we present values of the "i-f" transitions energies, calculated by us within ab initio QED PT, and also results of calculations within the MCDF (by Klapish et al), relativistic PT (RPT) with empirical zeroth approximation (by Ivanov et al) and available experimental data [12,15−17].

Table 1

The "i-f" transitions energies (in 10^2 cm^{-1}) , calculated within ab initio QED PT, MCDF and available experimental data.

N	i	f	Exp.[15]	MCDF	RPT	QED PT
1	$1s2s^22p^63s^23p$	$1s\ ^22s^22p^63s^2$	577000	577500	577200	577148
2	$1s2s^22p^63s^23p^2$	$1s\ ^22s^22p^63s^23p$	575700	576230	575910	575820
3	$1s2s^22p^63s^23p^3$	$1s\ ^22s^22p^63s^23p^2$	574400	575040	574940	574532
4	$1s2s^22p^63s^23p^4$	$1s\ ^22s^22p^63s^23p^3$	573400	573920	574360	573937
5	$1s2s^22p^63s^23p^5$	$1s\ ^22s^22p^63s^23p^4$	572400	572860	573520	572845
6	$1s2s^22p^63s^23p^6$	$1s\ ^22s^22p^63s^23p^5$	571430	571886	572550	572124

Analysis of the data in table 1 allow to make the following conclusions. Firstly, the accurate account of the complicated inter-electron (vacancy) correlations plays a critical role not only for acceptable quantitative agreement between theory and experiment, however, it is of the principal importance for right interpretation of the corresponding transitions in the spectra. Secondly, the presented in ref.[15] interpretation of the experimental highly ionized iron spectra, probably, is not fully correct because of the high complexness these spectra and, besides, using the DF calculation results for the corresponding interpretation. In fact in our opinion, the experimental data, in particular, for the "5" and "6" transitions (see table 1) are probably not correct and corresponding to other transitions. The difference between the RPT and QED PT data is connected with using the a little different basises of the relativistic wave functions. In our ab initio approach calculation it has been used the QED method [13]. In refs. [12,16] it has been used the empirical zeroth approximation, which naturally accounts for the main (not all) part of the inter-particle correlations contribution. In the table 2 we listed the values for probabilities of decay of the FeX states with vacancy $1s_s$, obtained within our approach (QED PT) with using the optimized basises (OB) of the one-quasiparticle wave functions and calculation data within the RPT with empirical zeroth approximation (without optimization of basises (WOB) of the wave functions) [12].

Table 2

Probabilities of decay of the FeX states with vacancy 1s $_s$: QED PT −OB (A- our data); RPT-WOB (B) [12].

n_2l_2			
method	A B	A B	A B	A
n_1l_1	2s	2p	3s	3p
2s	399+14 42+14	131+14 14+15	130+14 14+14	198+14
2p		264+15 28+15	158+14 17+14	722+14
3s			834+12 90+12	243+13
3p				612+13

Note: the mantissa and decimal order of value are given: $42+14=0.42\cdot10^{14}$;

The analysis of the presented data in the table 2 shows that our results are less than the corresponding data from ref. [12,16] at ~5%. This fact can be explained by using the specially optimized basises of the one-quasiparticle wave functions (it is in fact corresponding to degree of account for the multi particle exchange-correlation effects) in our scheme. In refs. [12,16] it had been used the formalism of relativistic PT with the empirical zeroth approximation, and optimization of the one-quasi-particle wave functions basises is not specially fulfilled, though using the empirical information about corresponding one-quasiparticle atomic ion allows indirectly take into account the correlation corrections. The great experience of using the relativistic QED perturbation theory [4,6,11−14] shows that the basis optimization, as a rule, improves averagely the atomic parameters values at 5−20%. Earlier an application of our scheme to studying the Auger decay characteristics for a set of neutral atoms, quasi-molecules and solids, the ionization cross-sections of inner shells in various atoms etc has demonstrated a reasonably well agreement with available sufficiently exact experimental data. So, we believe that the received results should be considered as quite acceptable and very useful for many applications. At last, it is obvious that the further experimental studying of the corresponding spectra is of a great importance.

References

1. Kulekshov V. F., Kukharenko Yu.A., Fridrikhov S. A. et al. Spectroscopy and Electron Diffraction in Solid Surfaces Studies. Nauka: Moscow, 1995.
2. Aberg T., Hewat G. Theory of Auger effect. Springer-Verlag: Berlin, 1999.
3. Amusia M.Ya. Atomic photoeffect. Acad.Press: N. — Y., 1998.
4. Glushkov A. V., Relativistic Quantum Theory. Quantum, mechanics of Atomic Systems. — Odessa: Astroprint, 2008. — 900P.

5. Aglitsky E. V., Safronova U. I. Spectroscopy of Auto-ionization states of atomic systems. Energoatomizd.: Moscow, 1997.

6. Ivanova E. P., Ivanov L. N., Aglitsky E. V., Modern Trends in Spectroscopy of Multicharged Ions// Physics Rep. — 1999. — Vol.166,N6. — P.315—390.

7. Osmekhin S ., Fritzsche S., Grum-Grzhimailo A. N., Huttula1 M., Aksela H., Aksela S., Angle-resolved study of the Ar $2p^{-1}_{1/2}3d$ resonant Auger decay// J. Phys. B: At. Mol. Opt. Phys.. — 2008. — Vol.41. — P.145003.

8. Tjurin A. V., Khetselius O.Yu., Nikola L. V., Sukharev D. E., Sensing the finite size nuclear effect in calculation of the Auger spectra for atoms and solids// Sensor Electr. and Microsyst. Techn. — 2007. — N1. — P.18—21.

9. Nikola L. V., Quantum calculation of Auger spectra for Na, Si atoms and solids// Photoelectronics. — 2007. — N16. — P.102—105.

10. Malinovskaya S. V., Glushkov A. V., Khetselius O.Yu., Loboda A. V., Lopatkin Yu.M., Nikola L. V., et al, Generalized energy approach to calculating electron collision cross-sections for multicharged ions in a plasma: Debye shielding model// Intern.Journ. Quantum Chem. — 2010. — Vol.112. — P.3131—3138.

11. Ivanova E. P., Ivanov L. N., Glushkov A. V., Kramida A. E. High order corrections in the Relativistic Perturbation Theory with the model Zeroth Approximation, Mg-like and Ne-like ions //Phys.Scripta —1995. — Vol.32,N4. — P.512—524.

12. Glushkov A. V., Ivanov L. N., Ivanova E. P., Generalized energy approach to radiation and autoionization decay of the atomic states //Autoionization Phenomena in Atoms. — Moscow Univ. Press, Moscow. — 1996. — P.58—160.

13. Glushkov A. V., Ivanov L. N. Radiation decay of atomic states: Atomic residue and gauge non-invariant contributions // Phys. Lett.A. — 1999. — Vol.170,N1. — P.33—37.

14. Glushkov A. V., Khetselius O.Yu., Gurnitskaya E. P., Loboda A. V., Lovett L., et al, Gauge-invariant QED perturbation theory approach to calculating nuclear electric quadrupole moments, hyperfine structure constants for heavy atoms and ions// Frontiers in Quantum Systems in Chemistry and Physics (Springer). — 2008. — Vol.18. — P.505—558.

15. Klapish M., Schwab J. L., Fraenkel B. S., Oreg J., The 1s-3p K_β-like X-ray spectrum of highly ionized iron//J.Opt.Soc. Am. — 1997. — Vol.67. — P.148—155.

16. Ivanov L. N., Driker M. N., Relativistic perturbation theory for excited states of atomic systems//J.Phys.B. J. Phys. B: At. Mol. Opt. Phys.. — 1998. — Vol.11. — P.1695—1701.

17. Nikola L. V., Data on the Auger and autoionization decay energies and probabilities for Ne-, Cl-and Ar-like ions within relativistic perturbation theory calculation//Preprint NIIF, I. I. Mechnikov Odessa National University. — N1, 2008. — 24P.

UDC 539.184, 539.186

L. V. Nikola, A. V. Ignatenko, A. N. Shakhman

RELATIVISTIC THEORY OF THE AUGER (AUTOIONIZATION) DECAY OF EXCITED STATES IN SPECTRUM OF MULTICHARGED ION

Abstract.
Relativistic method of calculating the characteristics of the Auger decay in the atomic spectra, based on the S-matrix Gell-Mann and Low formalism and QED perturbation theory, is used for estimating the transition energies and autoionization probabilities in spectra of the Fe ion with one vacancy above the core $1s^22s^22p^63s^23p^6$.
Key words: autoionization decay, multicharged ion, relativistic theory

УДК 539.184, 539.186

Л. В. Никола, А. В. Игнатенко, А. Н. Шахман

РЕЛЯТИВИСТСКАЯ ТЕОРИЯ ОЖЕ (АВТОИОНИЗАЦИОННОГО) РАСПАДА ВОЗБУЖДЕННЫХ СОСТОЯНИЙ В СПЕКТРЕ МНОГОЗАРЯДНОГО ИОНА

Резюме.
Релятивистский метод расчета характеристик Оже распада в атомных спектрах, который основывается на S-матричном формализме Гелл-Мана и Лоу и КЭД теории возмущений, использован для оценки энергий переходов вероятностей автоионизационного распада в спектре иона Fe с одной вакансией над остовом $1s^22s^22p^63s^23p^6$.
Ключевые слова: автоионизационный распад, многозарядный ион, релятивистская теория

УДК 539.184, 539.186

Л. В. Нікола, Г. В. Ігнатенко, А. М. Шахман

РЕЛЯТИВІСТСЬКА ТЕОРІЯ ОЖЕ (АВТОІОНІЗАЦІЙНОГО) РОЗПАДУ ЗБУДЖЕНИХ СТАНІВ У СПЕКТРІ БАГАТОЗАРЯДНОГО ІОНУ

Резюме.
Релятивістський метод розрахунку характеристик Оже розпаду в атомних спектрах, який базується на S-матричному формалізмі Гелл-Мана та Лоу і КЕД теорії збурень, використано для оцінки енергій переходів та ймовірностей авто іонізаційного розпаду в спектрі іону Fe з однією вакансією над остовом $1s^22s^22p^63s^23p^6$.
Ключові слова: автоіонізаційний розпад, багатозарядний іон, релятивістська теорія

V. N. PAVLOVICH, T. N. ZELENTSOVA, I. N. SERGA

Institute for Nuclear Researches, National Academy of Sciences of Ukraine, pr Nauki, 47, Kiev, 03116, Ukraine
Odessa National Polytechnical University, Dept. Nuc. Phys., Shevchenko av., 1, Odessa, 65044, Ukraine
e-mail: nucserga@mail.ru

ANALYSIS OF THE ELECTROMAGNETIC AND STRONG INTERACTIONS EFFECTS IN X-RAY SPECTROSCOPY OF HADRONIC ATOMS AND "KAONIC HELIUM PUZZLE"

It is given an analysis of the electromagnetic and strong interactions contributions to the transitions energies in the X-ray spectra of the hadronic atomic systems and kaonic helium puzzle. It is considered an advanced approach to redefinition of the meson-nucleon phenomenological optical model potential parameters and increasing an accuracy of the hadronic transitions energies definition.

As it is known, one of the fundamental questions in the modern hadron's physics is that the hadron masses being much higher than the mass of their quark content. The current mass of the up (u) and down (d) quarks is two orders of magnitude smaller than a typical hadron's mass of about 1 GeV. This extraordinary phenomenon is proposed to originate from spontaneous breaking of chiral symmetry of massless quarks in strong interaction physics [1−5]. At present time one of the most sensitive tests for the chiral symmetry breaking scenario in the modern hadron's physics is provided by studying the exotic hadron-atomic systems. One could turn the attention on the some differences between the pionic and kaonic systems. In the kaonic case one deals with the strangeness sector, and, for example, the strong interaction effect amounts to a very small shift and width in pionic hydrogen of 7 and 1 eV respectively, At the same time in case of the kaonic hydrogen the values are 200 and 240. Nowdays the transition energies in pionic and kaonic atoms are measured with an unprecedented precision and from studying spectra of the hadronic atoms it is possible to investigate the strong interaction at low energies measuring the energy and natural width of the ground level with a precision of few meV [1−20].

In this paper we give an analysis of the electromagnetic and strong interactions contributions to the transitions energies in the X-ray spectra of hadronic atomic systems. Besides, we consider an advanced approach to redefinition of the meson-nucleon phenomenological optical model potential parameters and increasing an accuracy of the hadronic transitions energies definition.

The mechanism of creation of the hadronic atoms is well known now (e.g. [1,2]).. Really, such an atom is formed when a negative kaon (pion) enters a medium, looses its kinetic energy through ionization and excitation of the atoms and molecules and eventually is captured, replacing the electron, in an excited atomic orbit. The further de-excitation scenario includes the different cascade processes such as the Auger transitions, Coulomb de-excitation, scattering etc. When a kaon (pion) reaches a low-n state with the little angular momentum, strong interaction with the nucleus causes its absorption. The strong interaction is the reason for a shift in the energies of the low-lying levels from the purely electromagnetic values and the finite lifetime of the state corresponds to an increase in the observed level width. At present time several highly priicised measurements are carried out for the kaonic (pionic) hydrogen, helium and other elements. The E570 experiment [12] (look figure 1) allowed to make the priicised measurement of the X-ray energies in the kaonic helium atom. For this system during last decades it takes a place very complicated situation. Speech is about a large discrepancy between the theories and experiments on the kaonic helium 2p state. At the beginning of the 1970's and 80's several experimental groups (WG71- Wiegand-Pehl (1971), BT79-Batty et al (1979), BR83- Baird et al (1983) (e.g.[8−15]) declared relatively large repulsive shift (∼ -40 eV), while the physically reasonable optical models calculations give shift less on the order. This sharp disagreement between the experimental and theoretical results received the status of "kaonic helium puzzle". More large shift was predicted in the theory with assuming the existence of the deeply bound kaonic nuclear states. Several theoretical estimates of the last years (look c.g. [12]) did not confirm the large shift in the kaonic helium. The new measurement of the kaonic helium X-ray was performed using the KEK-PS K5 kaon beam channel in 2005. As a target, super fluid liquid helium was used. The kaonic-atom production points were detected by measuring the charged particles produced by the kaon-nucleus reaction using the vertex chambers, and in addition, the stopped-kaon events in the helium target were selected using a counter measuring the kaon velocity. The X-rays from the kaonic atoms and the Ti/Ni calibration foils were detected using 8 SDDs, which have excellent resolution in energy [∼190 eV (FWHM) at 6.5 keV] and timing [∼160 ns (rms)]. In total, about 2000 events of the kaonic helium La X-rays are collected. The fit functions of the X-ray peaks were carefully studied. The function to fit the pileup events were obtained using the flash ADC data, in which the signal shape of the SDDs were recorded. The functions to fit the low-energy tails were deduced from the fit of the Ti/Ni peaks. The possible energy shifts caused by the pion-induced fluorescence X-rays were checked in the measurement of the pion beams at PSI in Switzerland. The systematic error of the fit functions is found to be 2 eV.
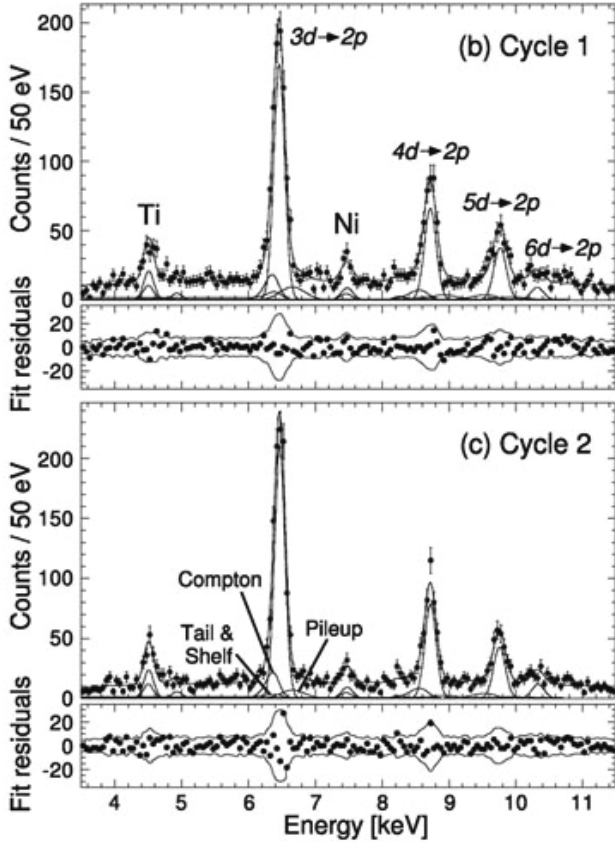
Fig. 1. The experimental kaonic Helium-4 X-ray energy spectra. The kaonic helium 3d-2p, 4d-2p, 5d-2p transitions are clearly observed (from refs. [12])

The most known theoretical models to treating the hadronic atomic systems are presented in refs. [9–11,16–20]. In refs. [16–18] there were developed an effective ab initio schemes to the Klein-Gordon equation solution and further definition of the X–ray spectra for multi-electron kaonic atoms with the different schemes for account for the nuclear, radiative, correlation effects. The theoretical studying the strong interaction shifts and widths from X-ray spectroscopy of kaonic atoms (U, Pb etc) was fulfilled. The most difficult aspects of the theoretical modeling are reduced to the correct description of the kaon (pion)-strong interaction as the electromagnetic part of the problem is reasonably accounted for in models [16–19]. Besides, quite new aspect is linked with the possible, obviously, very tiny electroweak and hyperfine interactions.

All available theoretical models to treating the hadronic (kaonic, pionic) atoms are naturally based on the using the Klein-Gordon equation [5]:

$$m^2 c^2 \Psi(x) = \{\frac{1}{c^2}[i\hbar\partial_t + eV_0(r)]^2 + \hbar^2\nabla^2\}\Psi(x), \quad (1)$$

where c is a speed of the light, h is the Planck constant, and $\Psi_0(x)$ is the scalar wave function of the space-temporal coordinates. Usually one considers the central potential $[V_0(r), 0]$ approximation with the stationary solution:

$$\Psi(x) = \exp(-iEt/\hbar)\phi(x) \qquad (2)$$

where $\phi(x)$ is the solution of the stationary equation.

$$\{\frac{1}{c^2}[E + eV_0(r)]^2 + \hbar^2\nabla^2 - m^2 c^2\}\phi(x) = 0 \qquad (3)$$

Here E is the total energy of the system (sum of the mass energy mc^2 and binding energy ε_0). In principle, the central potential V_0 naturally includes the central Coulomb potential, the vacuum-polarization potential, the strong interaction potential. Standard approach to treating the last interaction is provided by the well known optical potential model (c.g. [11]). Practically in all works the central potential V_0 is the sum of the following potentials. The nuclear potential for the spherically symmetric density $\rho(r|R)$ is:

$$V_{nucl}(r|R) = -((1/r)\int_0^r dr' r'^2 \rho(r'|R) + \int_r^\infty dr' r' \rho(r'|R)) \quad (4)$$

The most popular Fermi-model approximation the charge distribution in the nucleus $\rho(r)$ (c.f.[1,2]) is as follows:

$$\tilde{n}(r) = \tilde{n}_0 / \{1 + \exp[(r - c)/a)]\} \qquad \textbf{(5)}$$

where the parameter $a=0.523$ fm, the parameter c is chosen by such a way that it is true the following condition for average-squared radius: $<r^2>^{1/2}=(0.836 \cdot A^{1/3} + 0.5700)$fm. The effective algorithm for its definition is used in refs. [7,18−20] and reduced to solution of the following system of the differential equations:

$$V'nucl(r,R) = (1/r^2)\int_0^r dr' r'^2 \rho(r',R) \equiv (1/r^2)y(r,R)$$

$$y'(r,R) = r^2 \rho(r,R) \qquad (6)$$

$$\tilde{n}'(r) = (\tilde{n}_0 / a)\exp[(r-c)/a]\{1 + \exp[(r-c)/a]\}^2$$

with the boundary conditions:

$$V_{nucl}(0,R) = -4/(\pi r)$$
$$y(0,R) = 0, \qquad (7)$$
$$\tilde{n}(0) = \tilde{n}_0 / \{1 + \exp[-c/a]\}$$

Another, probably, more consistent approach is in using the relativistic mean-field (RMF) model, which been designed as a renormalizable meson-field theory for nuclear matter and finite nuclei [21−24].To take into account the radiation corrections, namely, the effect of the vacuum polarization there are traditionally used the Ueling potential and its different modifications such as [1−7]. The most difficult aspect is an adequate account for the strong interaction. In a case of the kaonic atomic systems the most popular approach to treating the strong interaction between the nucleus and orbiting kaon is the phenomenological optical potential of model, such as [1,2]:

$$V_N = -\frac{2\pi}{\mu}[1 + \frac{M_K}{M_N}][A_{Kp}\rho_p(r) + A_{Kn}\rho_n(r)], \qquad (8)$$

where M_K and M_N are the kaon and nucleon masses and μ is the kaon-nucleus reduced mass, $\rho_p(r), \rho_n(r)$ are the proton and neutron densities in the nucleus and A_{Kp}, A_{Kn} are the complex effective *Kp* and *Kn* scattering lengths. The known Batty approximation [11] reduces Eq.(10) to the next expression:

$$V_N = -\frac{2\pi}{\mu}[1 + \frac{M_K}{M_N}][a\rho(r)], \qquad (9)$$

where the effective averaged K-nucleon scattering length: $a=[(0.34\pm0.03)+i(0.84\pm0.03)]$ (fm).

The presented value of the length has been indeed chosen to describe the low and middle Z nuclei [11]. The disadvantage of the usually used approach is connected with approximate definition of the proton and neutron densities and using the effective averaged K-nucleon scattering length.

In the pion-nucleon state interaction one should use the following pulse approximation expression for scattering amplitude of a pion on the "i" nucleon [1,2]:

$$f_i(r) = \left\{ b_0' + b_1'(t\tau) + \left[c_0' + c_1'(t\tau) \right] kk' \right\} \delta(r - r_i); \quad (10)$$

Where t and τ are the isospines of pion and nucleon. The nucleon spin proportional terms of the kind $\sigma[kk']$ are omitted. The constants in (10) can be expressed through usual s-wave (α_{2T}) and p-wave $(\alpha_{2T,2J})$ scattering length (T and J -isospin and spin of he system πN. The corresponding parameters in the Compton wave length $\lambdabar_\pi$ terms are as follows:

$$b_0' = (\alpha_1 + 2\alpha_3)/3 = -0.0017\lambdabar_\pi.$$

$$b_0' = (\alpha_3 - \alpha_1)/3 = -0.086\lambdabar_\pi.$$

$$c_0' = (4\alpha_{33} + 2\alpha_{13} + 2\alpha_{31} + \alpha_{11})/3 = -0.208(\lambdabar_\pi)^3.$$

$$c_1' = (2\alpha_{33} - 2\alpha_{13} + \alpha_{31} - \alpha_{11})/3 = -0.184(\lambdabar_\pi)^3.$$

The scattering amplitude for pin on a nucleus is further received as a coherent sum of the πN -scattering lengths. рассеяния. In approximation of the only s-wave interaction the corresponding potential can be written in the Dezer form [1,2]:

$$V_N(r) = -2\pi\hbar^2\mu_\pi^{-1} \left[ZA^{-1}a_p + (A-Z)A^{-1}a_n \right] \rho(r). \quad (11)$$

The s-wave lengths of the $\pi^{-1}p$ -scattering $a_p = (2\alpha_1 + \alpha_3)/3$ и $\pi^{-1}n$ - scattering $a_n = \alpha_3$; scattering are introduced to Eq. (11). Because of the equality between $a_n = b_0' + b_1'$ and $a_p = b_0' - b_1'$ (with an opposite sign) the theoretical shift of the s-level with $T=0$ $(A=2Z)$ from Eq. (12) is much less than the observed shift.So, the more correct approximation must take into account the effects of the higher orders.

In whole the energy of the hadronic atom is represented as the sum:

$$E \approx E_{KG} + E_{FS} + E_{VP} + E_N; \quad (12)$$

Here E_{KG} -is the energy of meson (say, kaon) in a nucleus (Z,A) with the point-like charge (dominative contribution in (12)), E_{FS} is the contribution due to the nucleus finite size effect, E_{VP} is the radiation correction due to the vacuum-polarization effect, E_N is the energy shift due to the strong interaction V_N .The last contribution can be defined from the experimental energy values as:

$$E_N = E - (E_{KG} + E_{FS} + E_{VP}) \quad (13)$$

From the other side the strong meson-nucleus interaction contribution can be found from the solution of the Klein-Gordon equation with the corresponding meson-nucleon potential. In this case, this contribution E_N is the function of the potentials (8)-(11) parameters.

Let us further to analyse some theoretical and experimental results and present some proposals on the further improvement of the available theoretical approaches. In table 1 some experimental and theoretical X-ray energies for kaonic helium for the 2−1 transition (in keV), taken from refs. [11−18].

Measured and calculated K-⁴He X-ray energies (eV) of 3d-2p , 4d-2p and 5d-2p transitions

Transition	3d-2p	4d-2p	5d-2p
Experiment [12]	6466,7±2,5	8723,3±4,6	9760,1±7,7
Theory [16]	6463,50	8721,70	9766,80
Theory [17]	6463,00	8722,00	-
Theory [18]	6464,03	8721,10	9766,54

The corresponding strong interaction shift is defined as the obvious difference:

$$\Delta E(2p) = \Delta E(2p\text{-}nd) - \Delta E^{EM}(2p\text{-}nd)$$

It is interesting to give an analysis of the different theoretical and experimental estimates. According to the WG71,BT79,BR83 experiments (look [1,2]) the strong interaction contribution to the transition energy in the K-⁴He is -40eV. The corresponding value from the last E570 experiment is 1.9eV, the model potential theoretical value by Friedman et al is 0.4 eV and by Sukharev et al is 1.57эВ [12,16−19]. Thus, so called the "kaonic helium puzzle" has the physically reasonable resolution. In table 2 the data for Li-,K-,W-,U-kaonic atoms are given (from refs. [11−20]). Note that in table 2 there are presented the electromagnetic (EM) X-ray energies of K⁻ atoms for transitions between circular levels (from res. [11,16−20]) and the kaon mass was assumed to be 493.677±0.013MeV [11]. In table 2 the theoretical (E_c) and measured (E_m) X-ray energies for some kaonic atoms are listed (from refs.[1,16,17,19]).

Calculated (E_c) and measured (E_m) kaonic atoms X-ray energies (in keV)

Nucl.	Transition	E_c [1]	E_c [16]	E_c,[19]	E_c, [17]	E_m
Li	3−2	15.319	15.330	15.335	15.392	15.320 (24) 15.00 (30)
K	5−4	-	105.952	105.962	105.970	105.86 (28)
W	8−7	-	-	346.572	346.54	346.624(25)
W	7−6	-	-	535.136	535.24	534.886(92)

In table 3 we present the calculated (C) and measured (M) strong interaction shifts ΔE and widths G (in keV) for the kaonic atoms X-ray transitions, taken from ref. [1,2,11,16,20].

Table 3

Calculated (C) and measured (M) strong interaction shifts ΔE and widths G for K⁻ -atoms X-ray transitions: a- shift was estimated with Miller et al measured energy [1]; b — shift estimated with Cheng et al measured energy [2]; c — theory [11]; d — theory [20].

Nucl	ΔE_C (d)	G_C (d)	ΔE_C(c)	G_C (c)	ΔE_M	G_M
W, 8−7	0.038	0.072	-0.003	0.065	0.079[c] 0.052[d]	0.070 (15)
W, 7−6	-0.294	3.85	-0.967	4.187	-0.353[c] -0.250[d]	3.72 (35)
Pb, 8−7	0.035	0.281	-0.023	0.271	0.072[c] 0.047[d]	0.284 (14) 0.370 (150)[a]
U, 8−7	-0.205	2.620	-0.189	2.531	0.120[a]; 0.032[b] -0.40[c]; -0.213[d]	2.67(10) 1.50 (75)[a]

The width G is the strong width of the lower level which was obtained by subtracting the electromagnetic widths of the upper and lower level from the measured value. The shift ΔE is defined as difference between the measured E_M and calculated E_{EM} (electromagnetic) values of transition energies. The calculated value is obtained by direct solving the equation (3) with the optical model kaon-nucleon potential. It is easily to understand that when there is the close agreement between theoretical and experimental shifts, the corresponding energy levels are not significantly sensitive to strong nuclear interaction, i.e the electromagnetic contribution is dominative. In the opposite situation the strong-interaction effect is very significant. Further one can perform the comparison of the theoretically and experimentally defined transition energies in the X-ray spectra and further make redefinition of the meson-nucleon model potential parameters using Eqs. (8)-(11). Taking into account the increasing accuracy of the X-ray hadronic atoms spectroscopy experiments, one can conclude that the such a way will make more clear the true values for parameters of the kaon (pion)-nuclear potentials and correct the disadvantage of widely used parameterization of the potentials (8)-(11) from the light nuclei physics.

References

1. Deslattes R., Kessler E., Indelicato P., de Billy L., Lindroth E. , Anton J., Exotic atoms//Rev. Mod. Phys. — 2003. — Vol.75. — P.35−70.
2. Deloff A., Fundamentals in Hadronic Atom Theory, Singapore: World Scientific, 2003. — 352P.
3. Glushkov A. V., Relativistic Quantum Theory. Quantum, mechanics of Atomic Systems. — Odessa: Astroprint, 2008. — 900P.
4. Hayano R. S., Hori M., Horvath D., Widman E., Antiprotonic helium and CPT invariance//Rep. Prog. Phys. — 2007. — Vol.70. — P.1995−2065.
5. Mohr P. J. Quantum Electrodynamics Calculations in few-Electron Systems// Phys. Scripta. — 1993. — Vol.46,N1. — P.44−52.
6. Quiney H. M., Grant I. P. Partial-wave mass renormalization in atomic QED calculation // Phys.Scripta T. — 1999-Vol.46. — P.132−138.
7. Glushkov A. V., Rusov V. D., Ambrosov S. V., Loboda A. V., Resonance states of compound super-heavy nucleus and EPPP in heavy nucleus collisions // New Projects and New Lines of research in Nuclear physics.Eds. Fazio G. and Hanappe F.: Singapore, World Sci. — 2003. — P. 142−154.
8. Gall K. P., Austin E., Miller J. P., et al, Precision measurements of K⁻ and Σ⁻ masses//Phys.Rev.Lett. — 1998. — Vol.60. — P.186−190.
9. Anagnostopoulos D. F., Biri S., Boisbourdain V., Demeter M., Borchert G., Egger J., Fuhrmann H., Gotta D., Gruber A., Hennebach M. et al// Low-energy X-ray standards from pionic atoms//Nucl. Instrum. Methods B. — 2003. — Vol.205. — P.9−18.
10. Anagnostopoulos D. F., Gotta D., Indelicato P., Simons L. M., Low-energy X-ray standards from hydrogenlike pionic atoms//Arxiv: phys. — 2003. — 0312090v1-P.1−4.
11. Batty C. J., Eckhause M., Gall K. P., et al. Strong interaction effects in high Z- K⁻ atoms//Phys. Rev. C. — 1999. — Vol.40. — P.2154−2160.
12. S. Okada, G. Beer, H. Bhang, M. Cargnelli, J. Chiba, Seonho Choi, C. Curceanu, Y. Fukuda, T. Hanaki, R. S. Hayano, M. Iio, T. Ishikawa, S. Ishimoto, T. Ishiwatari, K. Itahashi, M. Iwai, M. Iwasaki, B. Juhasz, P. Kienle, J. Marton, Y. Matsuda, H. Ohnishi, H. Outa, M. Sato, P. Schmid, S. Suzuki, T. Suzuki, H. Tatsuno, D. Tomono, E. Widmann, T. Yamazaki, H. Yimc and J. Zmeskal, Precision measurement of the 3d -> 2p x-ray energy in kaonic ⁴He//Phys.Lett.B. — 2007. — Vol.653, N 5−6. — P. 387−391.
13. Ito T. M., Hayano R. S., Nakamura S. N., Terada T. P., Observation of kaonic hydrogen atom x rays// Phys. Rev. C. — 1998. — Vol.58. — P.2366 − 2382
14. Ishiwatari T. on behalf of the SIDDHARTA Collaboration, Silicon drift detectors for the kaonic atom X-ray measurements in the SIDDHARTA experiment// Nucl.Instr. and Methods in Physics. Research Sec.A. Accelerators, Spectrometers, Detectors and Associated Equipment. — 2007. — Vol.581,N1−2. — P.326−329.
15. M. Cargnelli, T. Ishiwatari, P. Kienle, J. Marton, E. Widmann, J. Zmeskal, G. Beer, A. M. Bragadireanu, T. Ponta, M. Bazzi, M. Catitti, C. Curceanu (Petrascu), C. Guaraldo, M. Iliescu, P. Levi Sandri, V. Lucherini, D. Pietreanu, D. L. Sirghi, F. Sirghi, P. Lechner, H. Soltau, L. Bombelli, C. Fiorini, T. Frizzi, A. Longoni, F. Ghio, B. Girolami, and L. Struder, Kaonic hydrogen X rays — experiments at DAFNE// Proc. KAON Int. Conf., Laboratori Nazionali di Frascati dell'INFN (Rome, Italy). — 2007. — 5P.
16. Santos J. P., Parente F., Boucard S., Indelicato P., Desclaux j.P., X-ray energies of circular transitions and electron scattering in kaonic atoms//Phys.Rev.A. — 2005. — Vol.71. — P.032501.
17. Indelicato P., Trassinelli M., From heavy ions to exotic atoms// arXiv:physics. — 2005. — V1−0510126v1. — 16P.
18. Sukharev D. E., Khetselius O.Yu., Dubrovskaya Yu.V., Sensing strong interaction effects in spectroscopy of hadronic atoms// Sensor Electr. and Microsyst. Techn. — 2009. — N3. — P.16−21.
19. Sukharev D. E., Florko T. A., Khetselius O.Yu., Dubrovskaya Yu.V., Bremsstrahlung and X-ray spectra for kaonic and pionic hydrogen and nitrogen//Photoelectronics. — 2009. — N18. — P.16−20.
20. Sukharev D. E., Khetselius O.Yu., Turin A. V., Florko T. A., Estimating of X-ray spectra for kaonic atoms as tool for sensing the nuclear structure// Sensor Electr. and Microsyst. Techn. — 2009. — N1. — P.30−35.
21. Serot B. D., Walecka J. D. , Advances in Nuclear Physics Vol. 16: The Relativistic Nuclear Many Body Problem. Plenum Press, New York, 1996.
22. Ring P, Schuck P, The Nuclear Many-Body Problem. — Berlin: Springer, 2000.
23. Gambhir Y. K., Bhagwat A., The relativistic mean field and some of its recent applications// Physics of Elem.Part. and Atom.Nucl. — 2006. — Vol.37. — P.366−436.
24. Khetselius O.Yu., Relativistic perturbation theory calculation of the hyperfine structure parameters for some heavy-element isotopes//Int. Journ. of Quantum Chemistry. — 2009. — Vol.109. — P. 3330−3335.

UDC 539.17

V. N. Pavlovich, T. N. Zelentsova, I. N. Serga

ANALYSIS OF THE ELECTROMAGNETIC AND STRONG INTERACTIONS EFFECTS IN X-RAY SPECTROSCOPY OF HADRONIC ATOMS AND "KAONIC HELIUM PUZZLE"

Abstract.
It is given an analysis of the electromagnetic and strong interactions contributions to the transitions energies in the X-ray spectra of the hadronic atomic systems and kaonic helium puzzle. It is considered an advanced approach to redefinition of the meson-nucleon phenomenological optical model potential parameters and increasing an accuracy of the hadronic X-ray transitions energies definition.
Key words: electromagnetic and strong interactions, hadronic atomic systems, X-ray spectra

УДК 539.17

В. Н. Павлович, Т. Н. Зеленцова, И. Н. Серга

АНАЛИЗ ЭФФЕНКТОВ ЭЛЕКТРОМАГНИТНОГО И СИЛЬНОГО ВЗАИМОДЕЙСТВИЙ В РЕНТГЕНОВСКОЙ СПЕКТРОСКОПИИ АДРОННЫХ АТОМОВ И ЗАГАДКА КАОННОГО ГЕЛИЯ

Резюме.
Проанализированы вклады электромагнитного и сильного взаимодействий в энергии переходов в рентгеновских спектрах адрон-атомных систем, а также "загадка каонного гелия". Рассмотрен эффективный подход к переопределению параметров оптического модельного мезон-нуклонного потенциала и увеличению точности определения энергий переходов в рентгеновских спектрах адронных атомов.
Ключевые слова: электромагнитное и сильное взаимодействие, адронные атомные системы, рентгеновские спектры

УДК 539.17

В. М. Павлович, Т. М. Зеленцова, І. М. Сєрга

АНАЛІЗ ЕФЕКТІВ ЕЛЕКТРОМАГНІТНОЇ І СИЛЬНОЇ ВЗАЄМОДІЙ У РЕНТГЕНІВСЬКІЙ СПЕКТРОСКОПІЇ АДРОННИХ АТОМІВ І "ЗАГАДКА КАОННОГО ГЕЛІЮ"

Резюме.
Проаналізовані внески електромагнітної та сильної взаємодій в енергії переходів у рентгенівських спектрах адрон-атомних систем, а також проблема каонного гелію. Розглянуто ефективний підхід до перевизначення параметрів оптичного модель-ного мезон-нуклонного потенціалу і збільшенню точності визначення енергій переходів у рентгенівських спектрах адронних атомів.
Ключові слова: електромагнітна, сильна взаємодія, адронні атомні системи, рентгенівські спектри

UDC 535.42

S. V. AMBROSOV, O. YU. KHETSELIUS, YU. M. LOPATKIN, A. A. SVINARENKO

I. I. Mechnikov Odessa National University, Pastera str., 27, Odessa, 65016, Ukraine
Odessa State Environmental University, Lvovskaya str., 15, Odessa, 65009, Ukraine
Sumy National University
e-mail: quantsvi@mail.ry

LASER PHOTOIONIZATION ISOTOPE SEPARATION TECHNOLOGY AND NEW PRINCIPAL SCHEME FOR γ-LASER ON QUICKLY DECAYED NUCLEAR ISOMERS WITH AUTOIONIZATION SORTING OF HIGHLY EXCITED ATOMS

Optimal scheme of the laser photo-ionization heavy isotopes (isomers) separation technology and the new possible principal scheme of γ-laser on quickly decayed nuclear isomers with autoionization sorting the highly excited heavy atoms are presented.

To number of the very actual problem of modern nuclear technology, quantum and photoelectronics is related a search of the effective methods for isotopes and nuclear isomers separation and obtaining especially pure substances at atomic level. The basis for its successful realization is, at first, carrying out the optimal multi stepped photo-ionization schemes for different elements and, at second, availability of enough effective UV and visible range lasers with high average power [1—27]. The standard laser photo-ionization scheme may be realized with using processes of the two-step excitation and ionization of atoms by laser pulse. The scheme of selective ionization of atoms, based on the selective resonance excitation of atoms by laser radiation into states near ionization boundary and further photo-ionization of the excited states by additional laser radiation, has been at first proposed and realized by Letokhov et al (c.f. ref.[1]). It represents a great interest for laser separation of isotopes and nuclear isomers. The known disadvantage of two-step laser photoionization scheme a great difference between cross-sections of resonant excitation σ_{exc} and photo-ionization σ_{ion} ($[\sigma_{exc}/\sigma_{ion}] > 10^4 \div 10^8$). It requires using very intensive laser radiation for excited atom ionization. The same is arisen in a task of sorting the excited atoms and atoms with excited nuclei in problem of creation of γ-laser on quickly decayed nuclear isomers [1,2].

Originally, Goldansky and Letokhov [3,4] has considered a possibility of creating a γ-laser, based on a recoiless transition between lower nuclear levels and shown that a γ-laser of this type in the 20—60 keV region is feasible. A feature of design is operation based on relatively short-lived isomer nuclear states with lifetime of 0,1 to 10 sec. The authors [3] has estimated the minimal number of excited nuclei required for obtaining appreciable amplification and possibility of producing sufficient amounts of excited nuclei by irradiation of the target with a thermal neutron beam or by resonant γ-radiation. It is important that low-inertia laser selection of a relatively small friction of excited nuclei of a given composition from the target by the two-step method of selective laser photoionization of atoms with excited nuclei by the radiation from two la-

sers is principally possible. But, it is obvious that here there is a problem of significant disadvantage of the two-step selective ionization of atoms by laser radiation method [1,2]. The situation is more simplified for autoionization resonance's in the atomic spectra, but detailed data about characteristics of these levels are often absent (c.f.[2,4,5,12,17]). The key problems here are connected with difficulties of theoretical studying and calculating the autoionization resonance characteristics. In [2,3] it has been presented principally new approach to solving a class of problems treated. In ref. [2,3,14,19—23] new optimal schemes for the laser photo-ionization sensors of separating heavy isotopes and nuclear isomers were proposed. It is based on the selective laser excitation of the isotope atoms into excited Rydberg states and further autoionization and DC electric field ionization mechanisms. To carry out modelling the optimal scheme of the *U* and *Tm* isotopes (nuclei) sensing, the optimal laser action model and density matrices formalism (c.f.[2,14,19—22]) were used. The similar schemes of laser photo ionization method are developed for control and cleaning the semiconductor substances [19]. The optimal laser photo-ionization schemes for preparing the films of pure composition on example of creation of the 3-D hetero structural super lattices (layers of $Ga_{1-x}Al_xAs$ with width 10E and GaAs of 60E) have been proposed and new models of optimal realization of the first step excitation and further ionization of the Ga^+ ions in Rydberg states by electric field are calibrated. In this paper we give the further development of approach to construction for the optimal schemes of the laser photo-ionization isotope separation technology and to creation of new possible principal scheme of γ-laser on quickly decayed nuclear isomers with laser auto-ionization or electromagnetic field ionization sorting the excited atoms.

Let us remind that in a classic scheme the laser excitation of the isotopes and nuclear isomers separation is usually realized at several steps: atoms are resonantly excited by laser radiation and then it is realized photo ionization of excited atoms [1]). In this case photo ionization process is characterized by relatively low cross section $\sigma_{ion} = 10^{-17} - 10^{-18} cm^2$ and one

could use the powerful laser radiation on the ionization step. This is not acceptable from the energetics point of view [2]. The alternative mechanism is a transition of atoms into Rydberg states and further ionization by electric field or electromagnetic pulse. As result, requirements to energetic of the ionized pulse are decreased at several orders. The main feature and innovation of the presented scheme is connected with using the DC electric field (laser pulse) autoionization on the last ionization step of the laser photoionization technology. There is a principal difference of the simple ionization by DC electric filed. The laser pulse ionization through the auto ionized states decay channel has the advantages (more high accuracy, the better energetics, universality) especially for heavy elements and isotopes, where the DC electric field ionization from the low excited states has not to be high effective. This idea is a key one in the realization of sorting the definite excited atoms with necessary excited nuclei of the A^+ kind, obtained by optimal method of selective photo-ionization of the A kind atoms at the first steps. The suitable objects for modelling laser photoionization separation technology are the isotopes of alkali element Cs, lanthanides and actinides. We considered the isotopes of $_{55}Cs_{78}^{133}$ and $_{70}Yb_{101}^{171}$. For example, the resonant excitation of the Cs can be realized by means dye lasers with lamp pumping (two transitions wavelengths are: $6^2S_{1/2} \to 7\ ^2P_{3/2}$ 4555A and $6^2S_{1/2} \to 7\ ^2P_{1/2}$ 4593A) [15]. In table 1 there are listed the energy parameters for different states of the caesium, obtained in the different approximations (from refs. [1,2,23]). It is useful to remind the corresponding hyperfine splitting energy (6 $^2S_{1/2}$, transition 4–3) of Cs: exp. data- $\Delta v(F,F') = 9192,64MHz$; $\Delta E(F,F') = 306,630 \cdot 10^{-3}$ cm^{-1}; theor. data [23] $-\Delta v(F,F') = 9177,80MHz$; $\Delta E(F,F') = 306,135 \cdot 10^{-3}$ cm^{-1} (from ref.[23]).

Table 1

Valent electron ionization energies (in atom. units) of the ^{133}Cs: ε^{RHF} —one-configuration Hartree-Fock data, релятивистского ХФ; $\varepsilon^{RHF} + \delta\varepsilon^{RHF}$ — the same data, but with account for the correlation corrections; ε^{QED} — QED perturbation theory data; ε^{Exp}- experimental data (see text)

State	ε^{RHF}	$\varepsilon^{RHF} + \delta\varepsilon^{RHF}$	ε^{QED}	ε^{Exp}
$6s_{1/2}$	0,12737	0,14257	0,14295	0,14310
$6p_{1/2}$	0,08562	0,09198	0,09213	0,09217
$6p_{3/2}$	0,08379	0,08951	0,08960	0,08964
$7s_{1/2}$	0,05519	0,05845	0,05862	0,05865
$7p_{1/2}$	0,04202	0,04385	0,04391	0,04393
$7p_{3/2}$	0,04137	0,04303	0,04309	0,04310

The next step is in the further excitation to the Rydberg S,P,D states with main quantum number n=31–37 (the optimal value n=35). Final step is the autoionization of the Rydberg excited atoms by a electromagnetic field pulse and output of the created ions. The scheme will be optimal if an atom is excited by laser radiation to state, which has the decay probability due to the autoionization bigger than the radiation decay probability. In figure 1 we present the numeric modelling results of the optimal form of laser pulse in the photoionization scheme with auto-or electric field ionization by solving the corresponding differential equations system [2,3,14,19–22]. The following definitions are used: δ+dashed line is corresponding

to optimal form of laser pulse, curves 1 and 2 are corresponding to populations of the ground and excited states of Cs. The δ-pulse provides maximum possible level of excitation (the excitation degree is about ~0,25; in experiment [1] with rectangular pulse this degree was ~ 0,1). It is in great degree similar to analogous scheme with the DC electric field and stochastic collisional ionization mechanisms [3,15,21,22]. In fig.1 there is also presented the typical behaviour of the ground (curve 1) and highly excited (curve 2) states population. Let us remember data regarding the excitation and the ionization cross sections for studied system: the excitation cross section at the first step of the scheme is ~10^{-11}cm^2; the ionization cross-section from excited 7^2P_2 state: $\sigma_2 = 10^{-16}$cm^2, from ground state $\sigma_2 = 10^{-18}$cm^2 [1]. One can see that the relation of these cross sections is 10^5 and 10^7 correspondingly. This fact provides the obvious non-efficiency of standard photoionization scheme.
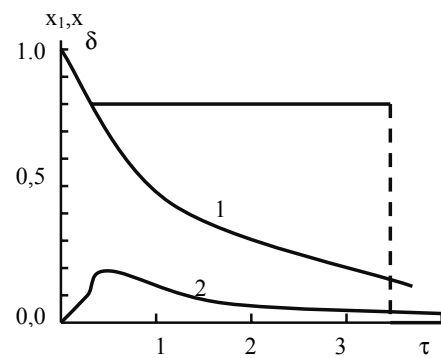
Fig.2. Results of modelling Cs isotopes separation process by the laser photo-ionization method (δ+dashed — laser pulse optimal form; see text)

A use of the autoionization mechanisms at the final step for ionization of the Rydberg excited atoms provides more optimal scheme from energetic point of view. For example, for the $35^2S_{1/2}$ transition the corresponding cross section can reach the value ~10^{-13}cm^2. So, from energetic point of view, this type of ionization can be very perspective alternative to earlier proposed classical two-step and more complicated photoionization schemes (c.f.[3,19–21]). More suitable situation takes a place for the for Yb isotope separation. It is very important that the proposed scheme can be easily implemented to the possible advanced scheme of the γ — laser on quickly decayed nuclear isomers with using laser photoionization sorting excited nuclei M^*_{k+1} with autoionization mechanism through the Rydberg states. Fig.2 easily explains the principal moments of this scheme. It generalizes the known Goldansky-Letokhov [4] and other [2,9,21,22] schemes and has to be more efficient especially from energetics point of view. In this context it is worth to remind very impressive results of the last years, connected with engineering atomic highly excited Rydberg states and correspondingly cooperative laser-gamma-muon-electron- nuclear states (transitions) with the laser (and raser) pulses [24—30]. It is quite possible that cited new effects can be realized in the tasks considered here.

So, the laser photo ionization scheme with autoionization of the highly excited atoms (with optimal set of energetic and radiative parameters: pulse form,

duration, energetic for laser and electric field pulses etc.) could provide significantly more high yield and effectiveness of the whole process of the isotope separation. It is especially worth for implementation to the possible principal scheme of γ -laser on quickly decayed nuclear isomers with autoionization sorting the excited atoms.
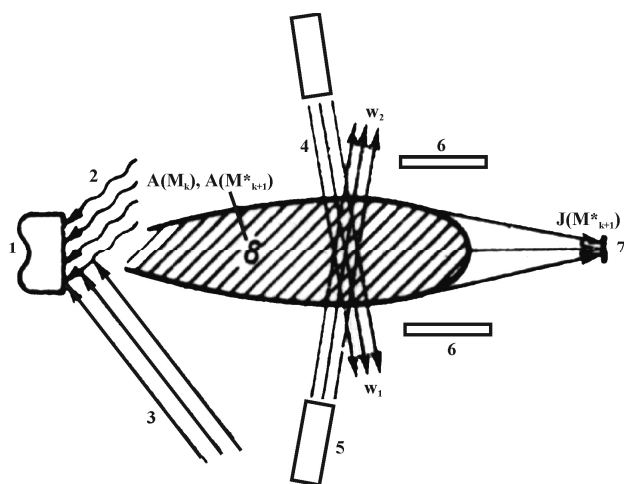
Fig.1. Possible scheme γ — laser on quickly decayed nuclear isomers with using laser photoionization sorting excited nuclei M^*_{k+1} with electric field and auto- and electric field ionization mechanisms: 1 — target of atoms M_k; 2- flux of slow neutrons; 3 — laser ray for evaporation of target; 4 — laser ray for the first step excitation of atoms with excited nucleus $A(M^*_{k+1})$; 5 — laser ray for second-step excitation to highly excited atomic states and Rydberg autoionization by electromagnetic field; 6 — collector system; 7 — atoms with excited nucleus $A(M^*_{k+1})$; 8 — flux of evaporated atoms;

References:

1. Letokhov V. S. Nonlinear Selective Photo-processes in atoms and molecules. — M.,1983. — 408c.

2. Glushkov A. V., Atom in an electromagnetic field. — Kiev: KNT, 2005. — 450P.

3. Glushkov A. V., Ambrosov S. V., Shpinareva I. M., Quantum modelling and optimal governing by selective atomic photoprocesses. — Odessa: TEC, 2002. — 158P.

4. Goldansky V. I., Letokhov V. S. Effect of laser radiation on nuclear decay processes// Sov. Phys. JETP. — 1994. — Vol.67. — P.513–516.

5. Baldwin G. G., Salem J. C., Goldansky V. I., Approaches to the development of gamma ray lasers // Rev.Mod.Phys. — 1999. — Vol.53. — P.687–742

6. Ivanov L. N., Letokhov V. S. Spectroscopy of autoionization resonances in heavy elements atoms// Com.Mod. Phys.D.:At.Mol.Phys. — 1995. — Vol.4. — P.169–184.

7. Glushkov A. V., Ivanov L. N. Radiation Decay of Atomic States: atomic residue and gauge non-invariant contributions // Phys. Lett.A. — 1999-Vol.170,N1. — P.33–37

8. Glushkov A. V.,Ivanov L. N. DC Strong-Field Stark-Effect: consistent quantum-mechanical approach// J.Phys.B: At. Mol. Opt. Phys. — 1999-Vol.26,N16. — P.L379-L386.

9. Glushkov A. V., Ivanov L. N., Letokhov V. S., Nuclear quantum optics// Preprint of Institute for Spectroscopy of the USSR AS, ISAN-N4, 1999. — 16P.

10. Shahbaz A., Muller C., Staudt A., Burvenich T. J., Keitel C. H., Nuclear quantum optics with X-ray laser pulses// Phys.Rev.Lett. — 2007. — Vol.98. — P.263901.

11. Ryabov E. A. Laser separation of isotopes on the basis of IR multi-photon dissociation of molecules//Usp.Phys.Nauk. — 2004. — Vol.174. — P.684–688.

12. Stoll W. Present Status of industrial Isotope separation by laser technology// Atomic and Molecular Pulsed Lasers. — Tomsk: SO RAN, 2001. — P.71.

13. Buchanov V. V., Kazaryan M., Kalugin M., Prokhorov A. M. Laser separation of Silicon Isotopes by the AVLIS Technol-

ogy// Atomic and Molecular Pulsed Lasers. — Tomsk: SO RAN,2001. — P.72.

14. Glushkov A. V., Ambrosov S. V., Non-linear Selective Photoprocesses in Atoms and Molecules and their Optimal Governing. Optimized Isotope Separation Schemes// Atomic and Molecular Pulsed Lasers. — Tomsk: SO RAN, 2001. — P.70.

15. Glushkov A. V., Ambrosov S. V., Ignatenko A. V., Korchevsky D. A., DC strong field Stark effect for non-hydrogenic atoms: New consistent quantum mechanical approach// Int. Journ. of Quantum Chemistry. — 2004. — Vol.99. — P.936–949.

16. Glushkov A. V., Rusov V. D., Ambrosov S. V., Loboda A. V. Resonance states of compound super-heavy nucleus and electron-positron pair production in heavy nucleus collisions //New projects and new lines of research in Nuclear Physics. Eds. G.Fazio and F.Hanappe, Singapore : World Scientific. — 2003. — P.126–142.

17. Glushkov A. V., Ambrosov S. V., Loboda A. V., Gurnitskaya E. P., Prepelitsa G. P., Consistent QED approach to calculation of electron-collision excitation cross-sections and strengths: Ne-like ions // Int. Journ.Quant.Chem. — 2005. — Vol.104, N4 . — P. 562–569.

18. Glushkov A. V., Malinovskaya S. V., Chernyakova Yu.G., Svinarenko A. A., Cooperative Laser- electron-nuclear processes: QED theory of electron satellites spectra for multicharged ion in a laser field//Int.Journ.Quant.Chem. — 2004. — Vol.99. — P.889–898.

19. Glushkov A. V. , Lepikh Ya.I. , Ambrosov S. V., Khetselius O.Yu., New optimal schemes of the laser photoionization technologies for cleaning the semiconductor materials and preparing the films of pure composition at atomic level// Ukrainian Journal of Physics. — 2008. — Vol.53,N10. — P.1017–1022.

20. Ambrosov S. V., New optimal schemes of the laser photo-ionization technologies for cleaning the semiconductor materials and preparing the films of pure composition at atomic level// Functional Materials. — 2003. — V.10,N2. — P.201–205.

21. Ambrosov S. V., Laser photoionization sensor of the separating isotopes and nuclear reactions products: Theoretical foundations of new scheme// Sensor Electr. & Microsyst. Techn. — 2004. — N2. — P.50–57.

22. Ambrosov S. V., Laser photoionization sensor technology and new possible principal scheme for γ -laser on quickly decayed nuclear isomers with electric field sorting of excited atoms//Sensor Electr. and Microsyst.Techn. — 2005. — N3. — P.18–22.

23. Khetselius O.Yu., Relativistic perturbation theory of the hyperfine structure parameters for some heavy-element isotopes//Int. Journ. of Quantum Chemistry. — 2009. — Vol.109,N14. — P. 3330–3335.

24. Kishimoto S., Yoda Y., Kobayashi Y., Kitao S., Haruki R., Masuda R., Seto M., Nuclear excitation by electron transition on ^{197}Au by photoionization around the K-absorption edge// Phys.Rev.C. — 2006. — Vol.74. — P.031301–1-031301–8.

25. Harston M. R., Caroll J. J., Nuclear excitation and de-excitation in resonant electron transition// Laser Physics. — 2004. — Vol.14,N1. — P.1452–1460.

26. Tkalya E. V., Theory of the nuclear excitation by electron transition process near the K edge//Phys.Rev.A. — 2007. — Vol.75. — P.022509.

27. Glushkov A. V., Malinovskaya S. V., Dubrovskaya Yu.V., Vitavetskaya L. A., Quantum theory of cooperative muon-nuclear processes: Discharge of metastable nuclei during negative muon capture// Recent Advances in Theory of Phys. and Chem. Systems (Berlin, Springer). — 2006. — Vol.15. — P.301–328.

28. Glushkov A. V., Khetselius O.Yu., Malinovskaya S. V., Optics and spectroscopy of cooperative laser-electron nuclear processes in atomic and molecular systems — new trend in quantum optics// Europ.Phys.Journ. — 2008. — Vol.T160. — P.195–204.

29. Glushkov A. V., Khetselius O.Yu., Loboda A. V., Svinarenko A. A., QED approach to atoms in a laser field: Multi-photon resonances and above threshold ionization//Frontiers in Quantum Systems in Chemistry and Physics (Berlin, Springer). — 2008. — Vol.18. — P.541–558.

30. Dunning F. B., Mestayer J. J., Reinhold C. O., Yoshida S., Burgdorfer J., Engineering atomic Rydberg states with pulsed electric fields// J. Phys. B: At. Mol. Opt. Phys. — 2009. — Vol.42. — P.022001.

S. V. Ambrosov, O. Yu. Khetselius, Yu. M. Lopatkin, A. A. Svinarenko

LASER PHOTOIONIZATION ISOTOPE SEPARATION TECHNOLOGY AND NEW PRINCIPAL SCHEME FOR γ -LASER ON QUICKLY DECAYED NUCLEAR ISOMERS WITH AUTOIONIZATION SORTING OF HIGHLY EXCITED ATOMS

Abstract
Optimal scheme of the laser photo-ionization heavy isotopes (isomers) separation technology and the new possible principal scheme of γ -laser on quickly decayed nuclear isomers with autoionization sorting the highly excited heavy atoms are presented.
Key words: laser photoionization, isotopes separation, γ -laser on quickly decayed nuclear isomers

С. В. Амбросов, О. Ю. Хецелиус, Ю. М. Лопаткин, А. А. Свинаренко

ЛАЗЕРНО-ФОТОИОНИЗАЦИОННАЯ ТЕХНОЛОГИЯ РАЗДЕЛЕНИЯ ИЗОТОПОВ И НОВАЯ ПРИНЦИПИАЛЬНАЯ СХЕМА γ -ЛАЗЕРА НА БЫСТРОРАСПАДАЮЩИХСЯ ЯДЕРНЫХ ИЗОМЕРАХ С АВТОИОНИЗАЦИОННОЙ СОРТИРОВКОЙ ВЫСОКО ВОЗБУЖДЕННЫХ АТОМОВ

Резюме
Предложены новая схема лазерно-фотоионизационной технологии разделения тяжелых изотопов (изомеров) и новая возможная принципиальная схема γ -лазера на быстрораспадающихся ядерных изомерах с автоионизационной сортировкой высоко возбужденных тяжелых атомов.
Ключевые слова: лазерная фотоионизация, разделение изотопов, γ-лазер на быстро распадающихся ядерных изомерах

С. В. Амбросов, О. Ю. Хецеліус, Ю. М. Лопаткін, А. А. Свинаренко

ЛАЗЕРНО-ФОТОІОНІЗАЦІЙНА ТЕХНОЛОГІЯ РОЗПОДІЛУ ІЗОТОПІВ І НОВА ПРИНЦИПІАЛЬНА СХЕМА γ -ЛАЗЕРА НА ЯДЕРНИХ ІЗОМЕРАХ, ЩО ШВИДКО РОЗПАДАЮТЬСЯ, ІЗ АВТОІОНІЗАЦІЙНОЮ СОРТИРОВКОЮ ВИСОКО ЗБУДЖЕНИХ АТОМІВ

Резюме
Запропоновані нова схема лазерно-фотоіонізаційної технології розподілу важких ізотопів (ізомерів) та нова принципіальна схема γ — лазера на ядерних ізомерах, що швидко розпадаються, із авто іонізаційним сортуванням високо збуджених важких атомів.
Ключові слова: лазерна фотоіонізація, розподіл ізотопів, γ- лазер на ядерних ізомерах, що швидко розпадаються

A. A. DRAGOEV, A. V. MUNTJANU, YU. N. KARAKIS, M. I. KUTALOVA

Odessa I. I. Mechnikov National University,
2, Dvorianskaya str., Odessa 65082, Ukraine. Tel. +38 048 — 7266356.
Fax +38 048 — 7266356, E-mail: wadz@mail.ru

CALCULATION FOR MIGRATION-DEPENDENT CHANGES IN NEAR-CONTACT SPACE-CHARGE REGIONS OF SENSITIZED CRYSTALS

Energy shape for contact barrier to crystal contained R-centers has been calculated. It was shown that migration of sensitizing centers can cause the longtime changes in shape of photocurrent relaxation curves.

Longtime relaxation of photocurrent up to 50—60 minutes was observed in sensitized CdS samples under illumination by intrinsic light 515 μm (Figure 1). It is characteristic that photocurrent became stable within the range of 10 minutes under low illumination. With increase of light flux, the raise of photocurrent is found to be non-proportional. The value of photocurrent increased only several times with raise of exposure level in one order. This situation certifies that several concurring processes take place in the crystal.
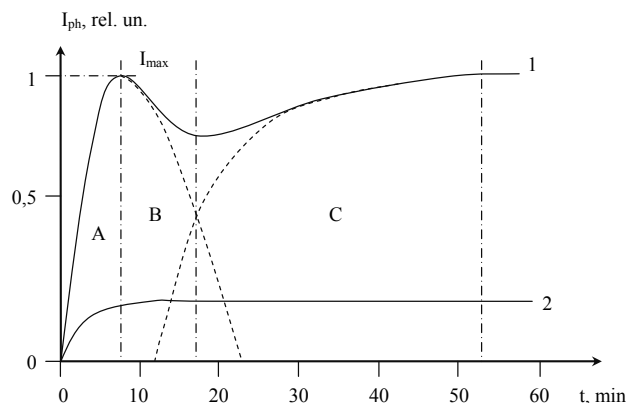
Fig. 1. Relaxation of intrinsic photocurrent at illumination level: (1) — 10—15 lx; (2) — 1—3 lx.

Besides, relaxation was accompanied firstly by decrease of photocurrent during 10—15 minutes in some crystals with rather large distance between contacts (not less than 1 mm). And then the restoration of photocurrent value took place during the period of 40—50 minutes.

The similar times for the flowing processes exclude the electronic explanation only and are the typical for migration-ionic phenomena [1,2]. The transition of impurity ions along crystal lattice is possible already at field intensities $10^4 — 10^5$ V/cm that was shown previously [1,2]. At barrier height of order 1 eV and width ~1 μm it is possible to reach such level of fields in near-contact regions of crystals.

Volt-current characteristics for investigated samples was of symmetric sublinear shape that was typical for back branches of Schottky barriers [3]. It indicates that closing contacts exist in both sides of crystal (Figure 2).

Barrier fields in that time has the directions which promote withdrawal of negatively charged doping to the central part and extraction of positively charged impurity to space-charge regions (SCR) of contacts.
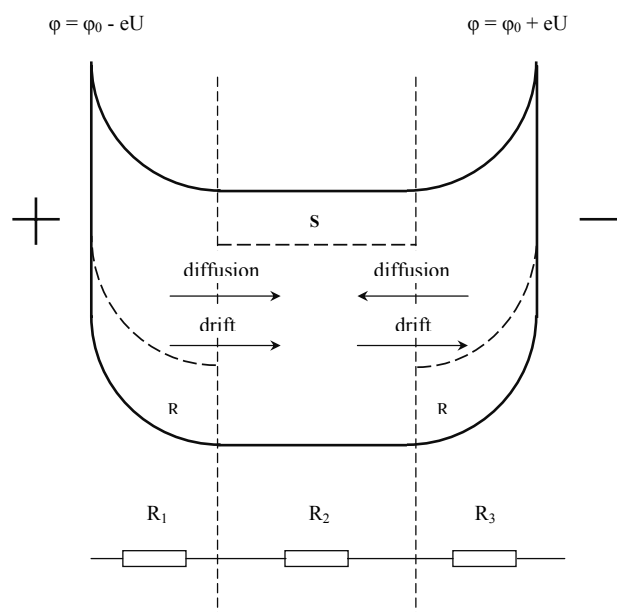
Fig. 2. Migration processes in crystal by electric light and field.

In studies of IR-quenching effect we showed that the samples had rather high concentration of S- and R-centers. But the behavior of these impurities in electric fields is different. Naturally S-center is the complex of sulphur vacancy and interstitial cadmium [4]. It can not have the observable conductivity to move along crystal lattice. As a first approximation for this study we consider that distribution of S-centers remain uniform with electric field strength applied.

On the contrary, R-center is cooper in cadmium sublattice [4] that can move rather easily along crystal.

According to paper [5], R-centers create the levels in the forbidden band with depth of occurrence 0.9—1.1 eV. It is obvious that these centers can capture the intrinsic holes and contain them for a long time. In paper [6] it was shown that R-centers charge positively. In the described conditions their extraction out of the crystal regions with width of diffusion length from barrier internal boundary and accumulation of this impurity in SCR of contacts take place under effect of Schottky barrier fields.

In whole, the distribution of R-center concentration comes to the shape shown in Fig. 2. The part of these centers losses its charge as result of slack recombination processes. So, concentration of charged N_2^+ -centers in near-contact regions under equilibrium conditions is considerably lower than their general concentration N_2.

When the crystal is simultaneously affected by intrinsic light and external voltage (Fig. 1), its internal situation changes. Let's firstly observe the initial state of contacts. In darkness and under condition $N_2^+ < N_{dn}$, the charge in SCR is concentrated in ionized donors. As far as the barrier is closing we neglect the influence of free electric charge. Then $\rho = e N_{dn}^+$.

Distribution of potential in SCR can be found from Poisson equation

$$\frac{d^2\varphi}{dx^2} = \frac{4\pi e^2}{\varepsilon} N_{dn} \ , \tag{1}$$

which standard solution is

$$\varphi(x) = \frac{2\pi e^2}{\varepsilon} N_{dn} (L-x)^2 . \tag{2}$$

Value L in (2) specifies width of SCR at equilibrium height of barrier ϕ_0:

$$L_d = \sqrt{\frac{\varepsilon}{2\pi e^2} \frac{1}{N_{dn}} \varphi_0} \tag{3}$$

At exposure with higher light intensity the condition $N_2^+ < N_{dn}$ is broken. R-centers, already located in SCR and distributed there uniformly, capture the great amount of non-equilibrium holes and completely ionized $N_2^+ = N_2$. We used high-ohmic crystals, therefore, concentration of donors there is not large. Simultaneously the striking effect of IR-quenching indicates the great concentration of R-centers. As result, $N_2^+ = N_2 \gg N_{dn}$.

The positive charge in SCR is observed now in R-centers and equations (2)-(3) are modified :

$$\varphi_b^1(x) = \frac{2\pi e^2}{\varepsilon} N_2 (L-x)^2 ; \tag{4}$$

$$L_b^1 = \sqrt{\frac{\varepsilon}{2\pi e^2} \frac{1}{N_2} (\varphi_0 - eU)} . \tag{5}$$

where ϕ and L were calculated for the case of light values at high intensities. Here we take into account that barrier height decreased up to value $\varphi(0) = \varphi_0 - eU$ under influence of internal voltage. It will be shown below that the changes in second barrier that increased in the same field affected insignificantly.

Equations (3)-(5) make possible to explain the increase of photocurrent within the region "A" in Fig. 1. It is seen that width of barrier (5) in light and because of condition $N_2 \gg N_{dn}$ decreased comparatively to dark value (3). Simultaneously the barrier became lower. Resistance R_1 (Fig. 2) in this part of crystal decreases and the current raises. Because the processes are limited only by the time of capture to holes, the changes take place quickly.

However, the processes that occur in the barrier (in Fig. 2 it is the left one) are more complicated. If the number of light quanta is small the concentration of non-equilibrium holes is created insignificant. In SCR of the contact they distributed according to the law

$$\Delta p(x) = \Delta p \exp\left[\frac{\varphi(x)}{kT}\right], \tag{6}$$

where Δp - concentration of holes near barrier origin; $\varphi(x)$ - potential distribution. As the criterion of low illumination we choose

$$\Delta p \exp\left[\frac{\varphi(x)}{kT}\right] < N_2 . \tag{7}$$

This means that the number of holes is insufficient in any barrier point to occupy all R-centers. In such conditions the positive charge registered is the holes captured at R-centers correspondingly to formula (7):

$$\rho = e N_2^+(x) = e \Delta p \exp\left[\frac{\varphi(x)}{kT}\right]. \tag{8}$$

Then Poisson equation has the form:

$$\frac{d^2\varphi}{dx^2} = \frac{4\pi e^2}{\varepsilon} \Delta p \exp\left[\frac{\varphi(x)}{kT}\right]. \tag{9}$$

or

$$\frac{d^2 z}{dx^2} = A \exp(z) \tag{10}$$

where

$$z = a\varphi ; \quad A = \left(\frac{4\pi e^2}{\varepsilon} \Delta p\right) \frac{1}{kT} ; \quad a = \frac{1}{kT} . \tag{11}$$

Integration of formula (10) gives

$$\left(\frac{dz}{dx}\right)^2 = 2A\left[\exp(z) - 1\right]. \tag{12}$$

Equation (12) requires the numerical integration of formula (7). But it can be simplified. The condition (7) supposes the small number of hole near barrier bottom and, correspondingly, the small charge in sensitizing centers. Otherwise, the remote boundary of the barrier is dependent on ionized donors:

$$\Delta p(L) \exp\left[\frac{\varphi(L)}{kT}\right] < N_{dn}^+ . \tag{13}$$

Here we take into account the low levels of exposure $\Delta p(L) < n_0$ and small potential of barrier $\varphi(L) \to 0$. Thus, the barrier now consists of two parts, the greater one submitted to equation (12), and the boundary is defined by analogy to (2). In order to value the width of SCR for such barrier it is enough to apply (12) in condition $e^z \gg 1$.

Then

$$\frac{dz}{dx} = \pm\sqrt{2A} \exp\left(\frac{z}{2}\right). \tag{14}$$

In whole SCR with increase of x the value φ, and then z too, decays (see Fig. 2, the left barrier). In such situation the sign "+" in equation (14) should be rejected as the symbol without any physical meaning. Then, taking into account (11) we obtain

$$\exp\left(-\frac{\varphi}{2kT}\right) = \sqrt{\frac{2\pi e^2 \Delta p}{\varepsilon kT}}\,(x - L_1) + 1 \,. \qquad (15)$$

Theoretically, there is no difficulty to obtain the explicit shape of potential distribution

$$\varphi = 2kT \ln\left[\frac{1}{1 - \sqrt{\dfrac{2\pi e^2 \Delta p}{\varepsilon kT}}\,(L_1 - x)}\right], \qquad (16)$$

and, owing to condition (7), equation (16) should join to equation (2). But formula (15) is sufficient to value the width of SCR. In the left boundary, when $x = 0$

$$\exp\left(\frac{\varphi_0 - eU}{2kT}\right) = 1 - \sqrt{\frac{2\pi e^2 \Delta p}{\varepsilon kT}}\,L_1 \,. \qquad (17)$$

Here we took into account that voltage decreased barrier height was applied together with light (as shown in Fig. 2). But L_1 is only the part of barrier, although the greater one, that is defined by the charge captured in R-centers

$$L_1 = \frac{1 - \exp\left(-\dfrac{\varphi_0 - eU}{2kT}\right)}{\sqrt{\dfrac{2\pi e^2}{\varepsilon}\Delta p \dfrac{1}{kT}}} \,. \qquad (18)$$

Taking into account equation (5) for greater levels of exposure let's calculate

$$\frac{L_1}{L_b^l} = \frac{1 - \exp\left(-\dfrac{\varphi_0 - eU}{2kT}\right)}{\sqrt{\dfrac{\varphi_0 - eU}{kT}}} \cdot \sqrt{\frac{N_2}{\Delta p}} \cdot \exp\left(\frac{\varphi_0 - eU}{2kT}\right) \quad (19)$$

In other case, applying formula (13) we obtain

$$\frac{L_1}{L_b^l} > \frac{\exp\left(\dfrac{\varphi_0 - eU}{2kT}\right) - 1}{\sqrt{\dfrac{\varphi_0 - eU}{kT}}} \,. \qquad (20)$$

And expression for L_1 being solved for the large barriers, owing to condition $\exp\left[\dfrac{\varphi(x)}{kT}\right] \gg 1$. So, unit in numerator (20) can be removed. It is evident, that any exponent with index exceeding unit is greater than its degree. So, finally we obtain

$$\frac{L_1}{L_b^l} > \sqrt{\frac{\exp\left(\dfrac{\varphi_0 - eU}{kT}\right)}{\dfrac{\varphi_0 - eU}{kT}}} \gg 1 \,.$$

Here L_1 — only the part of barrier under the condition of low illumination level. Finally,
$L_b^l \cdot L_s^l \cdot L^d$, with :l — light, b — big, d — dark

$$\frac{L_s^l}{L_b^l} \gg 1 \,. \qquad (21)$$

It means that at low illuminations the barrier having the same height considerably broadens. This is the second cause for the current to be lower in curve 2 within region "A" of Fig. 1.

We also note that owing to $N_2^+ = N_2 \gg N_{dn}$ the comparison of equations (3) and (5) gives $L^d > L_b^l$. At the same time, any occurrence of the positive charge within SCR in light must decrease its width [3]. So, the logical order of equations (3), (5) и (21) is aligned as follows $L^d > L_s^l > L_b^l$. With illumination the width of SCR decays, the higher light intensity the greater decrease. This is in accordance with equation (18) (Δp in denominator) and with formula (5).

Now let's observe the influence of light on formation of ionic-coordination mechanisms.

The travel of charged R^+-impurity can occur in applied electric field within the times of tens minutes (region "B" of Fig. 2). And the behavior of SCR in both ends of crystals is observed different.

Let the polarity of applied field is such as shown in Fig. 2. Then it must cause the withdrawal of N_2^+-centers from the left barrier and the increase of their concentration owing to drift component in the right barrier. Simultaneously, diffusive withdrawal of N_2^+-centers from both contacts is forming because N_2^+-centers charge in light everywhere. It is seen from Figure 2 that both causes for the left barrier add together but for the right barrier they concur. And application of field and light results in the greater extraction of R-centers from the left contact to the central part, but the height of this contact diminishes by external field. In the right contact the external field would increase the height, but the greater concentration of residual N_2^+-charge decrease it. So, the parameters of the right SCR are controlled by the complex of causes that concur each other. As a first approximation the right SCR should be considered as stable region and changes of Fig. 1 connected only with the left contact. The dominating mechanism for it is expansion that was shown above. The height of this barrier can be also considered stable because the external field decreases it and the departure of R^+-charge — increases.

Thus, the region "B" of Fig. 1 is controlled only by one process — the left SCR expands and its resistance increases but current decays. This process will be the stronger the higher intensity of light. Firstly, concentration of charged centers in this case is greater. Secondly, the barrier is wide for twilight illumination as shown in (21). This just the case when we did not observe the longterm decrease of current in curve 2 of Fig. 1.

We note that the change in polarity of applied voltage does not vary the view. The barriers simply switch places and roles.

The sensitizing centers that extract out of near-contact SCR actuate two more mechanisms outside. Depending on light intensity, large or small concentration of positive charge captured to centers is found in subsurface layer that was shown above. Respectively, these centers by the action of diffusion or drift leave this region that accompany by its expansion. The change in length for the central part of crystal take place at the same time.

As far as the total length of crystal — central part plus two contact regions — remain invariable, the

expansion in of the contact should inevitably result in narrowing of central part. And its electrical resistance (R_2 in Fig. 2) decreases because of the simple reduction in length. But resistance of the whole tandem raises because the part of inter-electrode space replaced by the higher ohmic region of barrier.

This would result in the further stimulation of photocurrent decrease, but this process is put over by the other one. R-centers coming to central part sensitized it. In accordance to paper [8] lifetime of majority carriers can increase up to five orders. We showed [6] that such situation will take place when concentrations of S- and R-centers become approximately equal: $N_2 \sim N_1$.

The increase of lifetime in its turn causes the increase of conductivity

$$\sigma = en\mu = e(f\tau)\mu . \qquad (22)$$

As far as decrease of conductivity with barrier expansion carries out approximately linear and even sublinear, the process (22) is accompanied by avalanche increase of conductivity. And the current in region "C" of Fig. 1 must raise as shown by dotted line. But the term of this process is longer. Firstly, it initiates by several concurring mechanisms in contrast to the region "B" and all the more to region "A" in Fig. 1. Secondly, the simple increase in concentration of sensitizing centers at the bottom of SCR $N_2 \gg N_1$ does not initiate the additional changes. The definite time to distribute groups of R-centers along a crystal is required. Namely this is the cause for asymmetry in well sides at relaxation in Fig. 1.

The abovementioned processes are obviously absent for twilight illumination (curve 2 in Fig. 1). The number of R^+-centers is considerably lower and their doping in central part of crystal is insignificant. Besides, the barrier was considerably wider primarily (see (21)). For comparatively short samples SCR

of contacts can join upon the whole. The sensitizing centers have no space to extract. We connect the absence of current decrease in region "C" of curve 1 (Fig. 1) observed experimentally with the described situation.

In conclusion we note — after finishing all the processes of redistribution for curve 1 in Fig. 1, current becomes stable at the same level in region "C" (I_{max}) as in maximum after termination of capture processes in region "A" that was expected earlier. This can be explained taking into account the following: as many sensitizing centers has left SCR as the equal number of them has finally caused the changes in the central part of crystal

References

1. Виктор П. А. "Некоторые особенности фотопроводимости неоднородных монокристаллов сульфида кадмия". Диссертация на соискание ученой степени кандидата физико-математических наук. Одесса.1999 г. с.140
2. Игнатов А. В. "Исследование влияния ионных процессов на электрические и фотоэлектрические свойства кристаллов сульфида кадмия". Диссертация на соискание ученой степени кандидата физико-математических наук. Одесса. 1999 г. — с.114 .
3. Стриха В. И. "Контактные явления в полупроводниках" — Киев, "Вища школа", 2002 г., с.223
4. Лошкарев В. Е., Любченко А. В., Шейкман М. К. Неравновесные процессы в фотопроводниках — Киев: "Наукова думка", 1999. — с.264.
5. Р. Бьюб "Фотопроводимость твёрдых тел" — Из-во Ин. лит. М., 2002г. с.558.
6. Ye. V.Britavsky, Y. N. Karakis, M. I. Kutalova, G. G. Chemeresyuk "On the charge state of rapid and slow recombination centers in semiconductors"//Photoelectronics, n. 17. 2008. P. 65 — 69.
7. Марсет Санчо Педро. "Исследование переходных процессов в области пространственного заряда гетеропереходов на основе сульфида кадмия". Диссертация на соискание ученой степени кандидата физико-математических наук. Одесса. 1999г. с.138 .
8. А. Роуз. "Основы теории фотопроводимости" — М.: Мир, 1999 — с.192 .

A. A. Dragoev, A. V. Muntjanu, Yu.N. Karakis, M. I. Kutalova

CALCULATION FOR MIGRATION-DEPENDENT CHANGES IN NEAR-CONTACT SPACE-CHARGE REGIONS OF SENSITIZED CRYSTALS

Abstract
Energy shape for contact barrier to crystal contained R-centers has been calculated. It was shown that migration of sensitizing centers can cause the longtime changes in shape of photocurrent relaxation curves.
Key words: cristals, R-centers, photocurrent, relaxation curve.

А. А. Драгоев, А. В. Мунтяну, Ю. Н. Каракис, М. И. Куталова.

РАССЧЁТ МИГРАЦИОННО — ЗАВИСИМОГО ИЗМЕНЕНИЯ ПРИКОНТАКТНЫХ ОПЗ ОЧУВСТВЛЁННЫХ КРИСТАЛЛОВ

Резюме
Рассчитан энергетический профиль контактных барьеров к кристаллу, содержащего R-центры. Показано, что миграция центров очувствления способна вызвать долговременные изменения вида релаксационных кривых фототока.
Ключевые слова: кристалл, R-центры, фототок, релаксационная кривая.

УДК 621.315.592

А. А. Драгоев, А. В. Мунтяну, Ю. Н. Каракис, М. И. Куталова

РОЗРАХУНОК МІГРАЦІЙНО — ЗАЛЕЖНОЇ ЗМІНИ ПРИКОНТАКТНИХ ОПЗ З ПІДВИЩЕНОЮ ЧУТЛИВІСТЮ КРИСТАЛІВ.

Резюме
Розраховано енергетичний обрис контактних бар·єрів до кристалів, в яких знаходяться R — центри. Доведено, що міграція центрів підвищення чутливості спроможна викликати багатотермінові зміни вигляду релаксаційних кривих фотоструму.
Ключові слова: кристал, R- центри, фотострум, релаксаційна крива.

V. A. TARASOV, N. V. MUDRAYA

Odessa National Polytechnical University, Dept. Nucl. Phys., av. Shevchenko, 1, Odessa, 65044, Ukraine
e-mail: quantmud@mail.ru

X-RAY OPTICS AND SPECTROSCOPY OF KAONIC ATOMS: VACUUM POLARIZATION CORRECTION TO TRANSITION ENERGIES

It is given an analysis of the schemes for accounting the radiation corrections due to the polarization of vacuum to the X-ray transitions energies in the spectra of kaonic systems. It is considered a new possible parametric approximation for vacuum polarization potential.

Relatively new direction in the atomic and nuclear physics has obtained a great pulse in the last decades because of the possible great contribution to understanding as theory of strong interactions and nuclear forces as applied applications in a field of creation new X-ray standards [1,2].

It is well known that an exotic (hadronic) atom is usually formed when a particle, with a negative charge and long-enough lifetime, slows down and stops in matter. It can then displace an atomic electron in the atomic system and become bound in a high principal quantum number atomic orbital around the nucleus. The principal quantum number of this highly excited state is of the order of n $=(m/m_e)^{1/2}$, where m and m_e are the masses of the particle and of the electron, respectively [1]. The higher the overlap between the wave functions of the electron and the particle, the more probable is the formation of an exotic atom [1]. The hadronic atoms formed in this way are named after the particle forming them. It the particle is a the negative kaon K-, a meson with a spin-0 and a lifetime of $1.237 \cdot 10^{-8}$ s, a kaonic atom is thus created. In principle, the pionic, muonic and other exotic atomic systems are created by the same way.

Because the particle mass, and thus transition energies are so much higher that the electron's (a kaon is .964 times heavier than an electron), the de-excitation of the exotic atom will start via Auger processes, in a process equivalent to internal conversion for gamma-rays, while the level spacing is small and there are electrons to be ejected, and then via radiative (E1) transitions, producing characteristic X-rays while cascading down its own sequence of atomic levels until some state of low principal quantum number.

Theoretical consideration of the corresponding kaonic atoms has obtained a great pulse in the last decades because of development of the consistent methods of quantum electrodynamics in a theory of relativistic atom [3—5]. As the relativistic and radiative corrections has a critical role as for usual heavy atoms and ions as for the hadronic atoms, implementation of the consistent methods of their prйcised account [1—23] became one of the most important and challenging problems of a theory.

Our aim here to give analysis of the most widespread schemes of the account for the vacuum polarization effect and indicate the most effective ones. Besides, we propose new generalized approach to this topic.

Usually, the vacuum polarization is accounted for in the so called Uehling approximation [3,4], which comes from changes in the bound-kaon wave function, and can be relatively easily implemented in the framework of the resolution of the Klein-Gordon equation using one of the self-consistent methods. For example, speech is about the Dirac-Fock method in the one- or multi-configuration approximations or more sophisticated versions such as many-body relativistic perturbation theory or quantum-electrodynamics perturbation theory [3—5, 10—23]. In practice one only need to add the corresponding Uehling potential to the nuclear Coulomb potential, to get the contribution of the vacuum polarization to the wave function to all orders, which is equivalent to evaluate the contribution of all diagrams with one or several vacuum polarization loop of the well known kind. For the exact signification of these diagrams one could look the corresponding reviews, e.g., [3—5]. The Uehling potential accounts practically for the main contribution due to the vacuum polarization effect. But there are other corrections of the higher orders. In particular, the other two vacuum polarization terms are usually included, namely the Kallen and Sabry term, which contributes to the same order as the iterated Uelhing correction, and the Wichmann and Kroll term, which is calculated by perturbation theory [3—5,10—18,22]. It should be noted that in general theoretical treating of the corresponding vacuum polarization diagrams represents very complicated problem, which hitherto has not the complete solution despite the many impressive attempts to do it.

In the first order of the perturbation theory on the parameter $Z\alpha$ (Z is a charge of a nucleus in the atomic system and α is the fine structure constant) the main vacuum polarization correction to the potential of a nucleus is matrix element of the Uehling potential [3]:

$$\Delta V_{Uh}(r) = -\frac{2\alpha Z\alpha}{3\pi r} \times$$

$$\times \int_m^\infty d\mu \exp(-2\mu r)\left(1 + \frac{m^2}{2\mu^2}\right)\mu^{-2}\left(\mu^2 - m^2\right)^{1/2}. \quad (1)$$

The expression (1) is written for the point nucleus in the atomic system. It is well known that the prйcised consideration of the heavy atomic and hadronic systems must take into account the finite size effect and other nuclear corrections too. An account of the

finite nucleus size effect modifies this expression by the following way [4]:

$$\Delta \tilde{V}_{Uh}(r) = -\frac{2\alpha^2}{3\pi}\int d^3r' \int_m^\infty d\mu \exp(-2\mu|r-r'|)\times$$

$$\times\left(1+\frac{m^2}{2\mu^2}\right)\left(\mu^2-m^2\right)^{1/2}\frac{\rho(r')}{|r-r'|}, \qquad (2)$$

Here $\rho(r)$ is a function of the charge distribution in a nucleus, which is normalized by a standard condition:

$$\int \rho(r)d^3r = Z. \qquad (3)$$

The Ueling potential obviously decreases for $r >> m^{-1}$. Wichmann and Kroll developed the method, which allows to calculate the vacuum polarization effect in all orders on the parameter $\alpha\,(Z\alpha)^n$, and based on the exact electronic propagator in an external field (look details in ref. [2]). In refs. [10,18,19] it has been introduced another representation for the vacuum-polarization potential:

$$\Delta V_{Uh}(r) = -\frac{2\alpha Z\alpha}{3\pi r}\times$$

$$\times\int_m^\infty d\mu \exp(-2\mu r)\left(1+\frac{m^2}{2\mu^2}\right)\mu^{-2}\left(\mu^2-m^2\right)^{1/2} \equiv$$

$$\equiv -\frac{2\alpha}{3\pi r}C(g), \qquad (4)$$

$$g = \frac{r}{\alpha Z}.$$

In ref. [18,19] the alternative approach for definition of the function $C(g)$ was used and based on the asymptotical expressions in two limited cases: :

$$C(g) \to \tilde{C}_1(g) = \ln(g/2)+1.410548-1.037845g \qquad (5a)$$
$$g \to 0$$

$$C(g) \to \tilde{C}_2(g) = -1.8800 \exp(-g)/g^{3/2} \qquad (5b)$$
$$g \to \infty$$

An account for the asymptotical expressions can be realized in Eq. (4) by the following way:

$$\tilde{C}(g) = \tilde{C}_1(g)\tilde{C}_2(g)/\left(\tilde{C}_1(g)+\tilde{C}_2(g)\right) \qquad (6)$$

The error, provided by using the expression (6) is not overcome ~ 2–5% of the general vacuum-polarization shift in he nuclear charge range Z=10–170. The main part of the error is connected with indefiniteness in the definition of the $\tilde{C}_2(g)$ in Eq. (7). More exact approximation of the Ueling potential has been introduced in ref.[21]. The final expressions in this approach for the function $C_2(g)$ are as follows:

$$\tilde{\tilde{C}}(g) = \tilde{C}_1(g)\tilde{\tilde{C}}_2(g)/\left(\tilde{C}_1(g)+\tilde{\tilde{C}}_2(g)\right) \qquad (7a)$$

$$\tilde{\tilde{C}}_2(g) = \tilde{C}_2(g)f(g) \qquad (7b)$$

$$f(g) = \left((1.1022/g - 1.3362)/g + 0.8028\right) \qquad (7c)$$

The using this formula permits one to decrease the calculation errors for this term down to ~1–2%. The error of the usual calculation scheme is ~10% [3,4]. In our opinion the further improvement of the presented expressions can be reached by means additional correction multiplayer, say b, which value is found by means the fitting procedure, for example under application the concrete atomic system. Besides, the same approach had the additional advantage. Really, there is no necessity to define very complicated, higher order contributions of the Wichmann and Kroll type to the general vacuum polarization correction and it is possible indeed to be limited by the generalized Uerling term. One can introduce the generalized determination as $C_2(g) = C_2(g|b)$, where the parameter b can be found within the fitting procedure. As example, in table 1 we list the numerical values of the C(g) function in the Ueling potential as function of the parameter $g = r/\alpha z$ in the four approximations: A- Exact data [18], B- calculation data [18,19], C- calculation data [21] and D- calculation data (this work).

Table 1

The numerical values of the C(g) as function of the parameter $g = r/\alpha z$ in the four approximations: A- Exact data [1], B-calculation data [33], C- calculation data [13] and D- calculation data (this work).

$g = r/\alpha z$	A	B	C	D
1.000	0.1766	0.22	0.177	0.1794
0.750	0.2832	0.28	0.2802	0.2841
0.500	0.4831	0.43	0.4765	0.4830
0.400	0.6160	0.55	0.5976	0.6058
0.300	0.8083	0.73	0.7895	0.8004
0.200	1.1126	1.03	1.1096	1.1213
0.150	1.3472	1.27	1.3386	1.3501

Further as example, we are listing the known data on the energy (in eV) contributions for selected transitions in the kaonic nitrogen [22,23]. According ref. [23], in a case of the 8k-7i, transition the Coulomb contribution value is 2968.4565eV; the vacuum polarization one is 1.8758eV; the relativistic recoil one is 0.0025eV and hyperfine structure one is -0.0009eV (the total value: 2970.4118eV). According ref. [22], in a case of the 8i-7h transition the Coulomb contribution value is 2968.5344eV; the vacuum polarization one is 1.1789eV; the relativistic recoil one is 0.0025eV and hyperfine structure one is -0.0006eV (the total value: 2969.6373eV). In the both papers the different methodises for the vacuum polarization correction have been used. The analysis shows that the parametric approximation iproposed in this paper to estimating the vacuum polarization correction to the transition energy can improve the results of the both approaches averagely on ~0.5–1% without increasing additional numerical efforts.

References

1. Hayano R. S., Hori M., Horvath D., Widman E., Antiprotonic helium and CPT invariance//Rep. Prog. Phys. — 2007. — Vol.70. — P.1995–2065.
2. Deslattes R., Kessler E., Indelicato P., de Billy L., Lindroth E. , Anton J., Exotic atoms//Rev. Mod. Phys. — 2003. — Vol.75. — P.35–70.
3. Grant I., Relativistic Quantum Theory of Atoms and Molecules Theory and Computation, Springer Series on Atomic, Optical, and Plasma Physics. 2007. — Vol.40. — P.587–626.

4. Glushkov A. V., Relativistic quantum theory. Quantum mechanics of atomic systems, Odessa: Astroprint, 2008. — 900P.

5. Braun M. A., Safronova U. I., Gurchumeliya A. D., Relativistic theory of atom. — Moscow: Nauka, 1994. — 280P.

6. Schweppe J., Belkacem A., Blumenfeld L., Clayton N., Feinberg B., Gould H., Kostroum V. E., Levy L., Misawa S., Mowst J. R. and Priuor M. H. Measurement of the Lamb shift in lithiumlike uranium (U^{89+})// Phys.Rev.Lett. — 1999. — Vol.66. — P.1434−1437.

7. Gould H. . Lamb shift measurement in lithiumlike uranium (U^{89+})//Phys.Scripta T. — 1998-Vol.46. — P.61−64.

8. Klaft I.,Borneis S., Engel T., Fricke B., Grieser R., Huber G., Kuhl T., Marx D., Neumann R., Schroder S., Seelig P., Volker L. Precision laser spectroscopy of ground state hyperfine splitting of H-like $^{209}Bi^{82+}$//Phys.Rev.Lett. — 1997. — Vol.73. — P.2425−2427.

9. Von Brentano P., Platte D., Budelsky D., Kremer L., Pross H. J., Scheuer F. Lamb shift experiments with laser resonance method// Phys.Scripta. — 1999. — Vol.46. — 162−166.

10. Mohr P. J. Energy Levels of H-like atoms predicted by Quantum Electrodyna-mics,10<Z<40 // Atom.Data Nucl .Data Tabl. — 19939Vol.24,N2. — P.453−470.

11. Blundell S. A. Ab initio Calculations of QED Effects in Li-like, Na-like and Cu-like Ions// Phys.Scripta. — 1999. — Vol.46,N1. — P.144−150.

12. Persson H., Lindgren L., Salomonson S. A new approach to the electron self-energy calculation// Phys.Scripta.T. — 1999. — Vol.46. — P.125−131.

13. Johnson W. R., Blundell S. A., Sapistein J. Finite basis sets for the Dirac equation constructed from B splines// Phys. Rev.A. — 1998. — Vol.37. — P.307−315.

14. Indelicato P. Relativistic effects in few-electron heavy atoms. Ab initio evaluation of levels energy and transition probabilities// Phys.Scripta T. — 1996. — Vol.65. — P.57−62.

15. Drake G. W. F. High precision calculations and QED effects for two-and three-electron atoms// Phys.Scripta T. — 1999-Vol.46. — P.116−124.

16. Schneider S. M., Greiner W., Soff G. Vacuum-polarization contribution to the hydrogen-structure spliting of H-like atoms// Phys.Rev.A. — 1997. — Vol.50. — P.118−122.

17. Yerokhin V. A., Shabaev V. M. Accurate calculation of self-energy diagrams for high Z He-like atoms//Phys.Lett.A. — 1995-Vol.207. — P.274−280.

18. Ivanova E. P., Ivanov L. N., Aglitsky E. V., Modern Trends in Spectroscopy of Multicharged Ions// Physics Rep. — 1999. — Vol.166,N6. — P.315−390.

19. Ivanova E. P., Ivanov L. N., Glushkov A. V., Kramida A. E. High order corrections in the Relativistic Perturbation Theory with the model Zeroth Approximation, Mg-like and Ne-like ions //Phys.Scripta −1997. — Vol.32,N4. — P.512−524

20. Glushkov A. V., Rusov V. D., Ambrosov S. V., Loboda A. V., Resonance states of compound super-heavy nucleus and EPPP in heavy nucleus collisions // New Projects and New Lines of research in Nuclear physics.Eds. Fazio G. and Hanappe F.: Singapore, World Sci. — 2003. — P. 142−154.

21. Glushkov A. V., Khetselius O.Yu., Gurnitskaya E. P., Loboda A. V., Lovett L., et al, Gauge-invariant QED perturbation theory approach to calculating nuclear electric quadrupole moments, hyperfine structure constants for heavy atoms and ions// Frontiers in Quantum Systems in Chemistry and Physics (Springer). — 2008. — Vol.18. — P.505−558.

22. Santos J. P., Parente F., Boucard S., Indelicato P., Desclaux j.P., X-ray energies of circular transitions and electron scattering in kaonic atoms//Phys.Rev.A. — 2005. — Vol.71. — P.032501.

23. Sukharev D. E., Florko T. A., Khetselius O.Yu., Dubrovskaya Yu.V., Bremsstrahlung and X-ray spectra for kaonic and pionic hydrogen and nitrogen//Photoelectronics. — 2009. — N18. — P.16−20.

V. A. Tarasov, N. V. Mudraya

X-RAY OPTICS AND SPECTROSCOPY OF KAONIC ATOMS: VACUUM POLARIZATION CORRECTION TO TRANSITION ENERGIES

Abstract.

It is given an analysis of the schemes for accounting the radiation corrections due to the polarization of vacuum to the X-ray transitions energies in the spectra of kaonic systems. It is considered a new possible parametric approximation for vacuum polarization potential.

Keywords: X-ray spectroscopy, kaonic atoms, vacuum polarization

В. А. Тарасов, Н. В. Мудрая

РЕНТГЕНОВСКАЯ ОПТИКА И СПЕКТРОСКОПИЯ КАОННЫХ АТОМОВ: ПОПРАВКА ЗА СЧЕТ ПОЛЯРИЗАЦИИ ВАКУУМА К ЭНЕРГИЯМ ПЕРЕХОДОВ

Резюме.

Выполнен анализ процедур учета радиационной поправки на поляризацию вакуума к энергиям рентгеновских переходов в спектрах каонных атомов. Рассмотрено возможное новое параметрическое приближение для вакуум- поляризационного потенциала.

Ключевые слова: рентгеновская спектроскопия, каонные атомы, поляризация вакуума

В. А. Тарасов, Н. В. Мудра

РЕНТГЕНІВСЬКА ОПТИКА І СПЕКТРОСКОПІЯ КАОННИХ АТОМІВ: ПОПРАВКА ЗА РАХУНОК ПОЛЯРИЗАЦІЇ ВАКУУМУ ДО ЕНЕРГІЙ ПЕРЕХОДІВ

Резюме.

Виконано аналіз процедур урахування радіаційної поправки на поляризацію вакууму до енергій рентгенівських переходів у спектрах каонних атомів. Розглянуто можливе нове параметричне наближення для вакуум- поляризаційного потенціалу

Ключові слова: рентгенівська спектроскопія, каонні атоми, поляризація вакууму

SH. D. RURMASHEV, T. N. BUGAEVA, T. I. LAVRENOVA, N. N. SADOVA

Odessa I. I.Mechnikov National University
Odessa, 65026, Ukraine, e-mail: kurm@mail.css.od.ua. Tel. 746–66–58

FEATURES OF INTERACTION OF COMPONENTS IN "GLASS- $Pb_2Ru_2O_{7-x}$, RuO_2" HETERO-PHASE SYSTEMS

Resistance pastes on basis RuO_2 differ by a relative chemical inactivity. Large maintenance of boron oxide and high acidity of glasses are the main reasons of chemical $Pb_2Ru_2O_{7-x}$ decomposition and formation of ruthenium dioxide under annealing of the hetero-phase systems. The increase of resistive layers conductivity with the growth of conduction phase maintenance can be explained by percolation transition because of conducting phase cluster formation in the glass matrix. The increase of conductivity begins at lower concentrations $Pb_2Ru_2O_{7-x}$ with growth of B_2O_3 concentration in glass. The transfer of electrons between separate conducting grains by means of thermo electronic emission with the presence of activating process is the possible current mechanism. Mechanism of electrons tunneling also takes place.

INTRODUCTION

Thick-film technology is one of the basic methods of radio electronic apparatus complex miniaturization. Resistors and conductive elements in the general volume of hybrid integrated elements take large space. Resistance pastes on basis RuO_2 differ by a relative chemical inactivity. They can be made with the wide range of surface resistance, low values of temperature coefficient of resistance (TCR). Dioxide of ruthenium (rutile) does not dissolve in a glass matrix, what allows to promote the temperature of annealing to 1200⁰C and to get resistance compositions properties which insignificantly depend on the annealing profiles. Large positive TCR is compensated due to glass-binding or special alloying additions in small concentrations. With the purpose of economy of expensive pure ruthenium in the paste, ruthenium compounds with appropriate crystalline structure similar to pyrclorine are widely used in resistance pastes $M_2Ru_2O_7$. In particular, the lead ruthenate obtained by sintering at 800−880⁰C of dioxide of ruthenium and oxide or salt of lead mixture is used. Such material has low surface resistance and cubic crystalline structure.

It is known that forming of ruthenic resistors thick films is accompanied by difficult chemical processes [1]. During the paste annealing the interaction between the conductive phase of resistor and glass and binding compound appears. The phase composition of resistor base on $Pb_2Ru_2O_{7-x}$ strongly related to chemical composition of permanent and temporal binding compounds of the resistance paste.

The influence of the glass composition on conductivity of the hetero-phase system of "glass- $Pb_2Ru_2O_{7-x}$, RuO_2" was studied in the present work.

RESULTS AND THEIR DISCUSSION

The $Pb_2Ru_2O_{7-x}$ content and permanent binding compound in the inorganic components of the studied pastes were 30 and 70 w %, correspondently. Resistance films have been obtained by annealing of the pastes, deposited on ceramics at 850 ⁰C. The exposition time at maximal temperature was 15 min.

It was figured out that in pastes containing only $Pb_2Ru_2O_{7-x}$ before annealing, two crystalline phases were observed in X-ray-diagram, corresponding to pyrclorine $Pb_2Ru_2O_{7-x}$ and rutile RuO_2 phases. The appearance of ruthenium dioxide in the layers is impossible to explain by thermal dissociation of initial conduction phase (CCP), because the annealing temperature is not enough for activation of this process. Consequently, RuO_2 appears as a result of chemical reactions via interaction between $Pb_2Ru_2O_{7-x}$ and binding components of resistive paste.

It is known that $Pb_2Ru_2O_{7-x}$ interacts with some metal oxides. This interaction is affected by acid-base transitions and can be realized because acidic properties of those metal oxides are stronger than in case of ruthenium. Therefore, it is possible to conclude that in our case in the permanent binding compound of resistive paste there are components with acid stronger properties than ruthenium. Thus, RuO_2 is formed within chemical reaction, affected by interaction of binding components of the paste with $Pb_2Ru_2O_{7-x}$.

In glass resistors composition there are silicon, aluminum and boron oxides belonging to acid type. In [1] from the method of X-ray-phase analysis results it was published that only B_2O_3 destroys $Pb_2Ru_2O_{7-x}$ completely. We studied pastes based on glasses containing silicon and boron oxides. In fig.1 the change of $Pb_2Ru_2O_{7-x}$ and RuO_2 content in resistors on the basis of the system of "$Pb_2Ru_2O_{7-x}$ — Pb-Si-B- glasses" is presented. It can be seen that with the increase of B_2O_3 content in binding components of resistive paste $Pb_2Ru_2O_{7-x}$ concentration diminishes and RuO_2 in thick films concentration increases. These results are similar to the data, published in [1]. Thus, appearance RuO_2 in resistors is affected by Ru substitution with boron in $Pb_2Ru_2O_{7-x}$.

Instability of $Pb_2Ru_2O_{7-x}$ in resistance pastes results not only from the B_2O_3 presence in glass composition. The process of formation of ruthenium dioxide begins with the certain concentration of boron oxide. Lead ruthenate collapses in resistors with glasses,

which have concentration of acid-type oxides close or higher to lead oxide concentration. In fig.1 $Pb_2Ru_2O_{7-x}$ decomposition of begins at the acid B_2O_3 concentrations about 10...20 %. It was found, that only in glasses with $Pb_2Ru_2O_{7-x}$ content no more than 30% noticeable increase RuO_2 takes place. Consequently, interaction of $Pb_2Ru_2O_{7-x}$ with binding components of the paste starts if the glass contains boron oxide and has certain base properties. The relation of basic and acid components must be less than 1. In our case this value was 0.5.

The content of temporary binding components in the paste composition plays considerable role. The increase of ruthenium dioxide maintenance in the resistors obtained from pastes with organic binding agent based on fat passes through the stage of metallic ruthenium formation with subsequent oxidization to ruthenium dioxide. Therefore, it can be explained that considerable $Pb_2Ru_2O_{7-x}$ decomposition (fig. 1) takes place under the boron oxide concentration up to 20%, while $Pb_2Ru_2O_{7-x}$ maintenance in the initial component is more than 30%. It points to the fact that transition function of lead ruthenate transformation to ruthenium dioxide is partly provided by temporary organic binding agent.
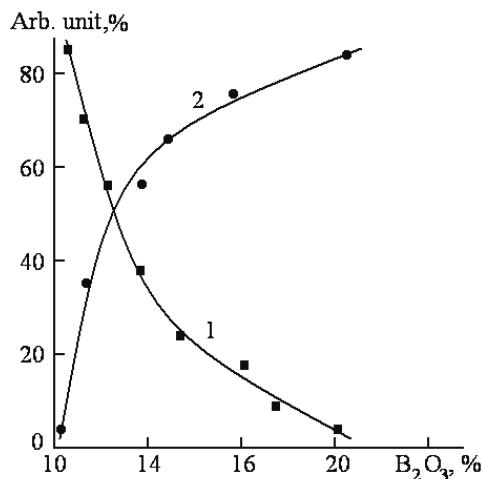

Fig.1. Dependence of CCP percentage content on the concentration B_2O_3 in permanent binding agent. 1 — $Pb_2Ru_2O_{7-x}$; 2 — RuO_2

Electrical properties of the obtained layers were studied. It was found that with the increase of conductive phase-permanent binding agent ration in pastes (CCP:CS) the surface resistance of the films goes down (fig.2) and the TCR values comes from the positive values to negative. Thus, the investigated layers show the features described by classic dependence of the layer properties on its composition for thick-film resistive materials. The dependence is conditioned by diminishing of dielectric layers thickness between the CCP particles and ramification of their cluster chains under decreasing of the bulk part of CS. The change of microstructure of $Pb_2Ru_2O_{7-x}$ and RuO_2 resistors under the increase of CCP maintenance in resistive layers was confirmed by microscopic studies performed before [2]. The resistive elements based on RuO_2 have lower resistance and TRC value is much higher in the positive values region in comparison with thick-film resistors (TFR) based on $Pb_2Ru_2O_{7-x}$ (with the identi-

cal bulk part of CCP). It is explained by higher conductivity of RuO_2 clusters.

Different electrical properties are shown by resistive elements with the identical CCP concentration but with the different dispersion parameter of initial phases. It is explained by influence of CCP and CS particle sizes on microstructure and electrical properties of the hetero-phase systems. It is known that thinner initial powders of ingredients are, i.e. the higher the active surface area, the higher resistivity and smaller and even negative TCR values show thick-film resistors. However, the opposite dependences can take place and [2].
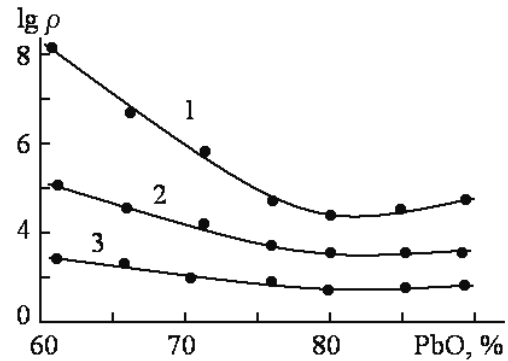
Fig.2 Dependence of surface resistance on PbO contents in two-component glasses composition. $Pb_2Ru_2O_{7-x}$ content in initial composition, %: 1 — 20, 2 — 35, 3 — 50.

Composition varying changes not only acid-basic (chemical) but also physical and chemical properties of CS [3]. Change of PbO/SiO_2 ration in two-component glasses composition causes the change of basicity, and also to decrease of linear expansion temperature coefficient (TCLE). Such change of properties appropriately influences on electrical properties of TFR. Acidity grows with PbO growth, i.e. concentration RuO_2 grows, resistance decreases (fig.2). If this process occurred only as acid-basic interaction, resulting in RuO_2 accumulation in bulk films, their resistance must constantly decline. However, this value doesn't change monotonically with CS composition, but according to dependence with the extreme value (fig. 2). The change of glasses composition can lead to gradual change (diminishing) of internal deformation tension in resistive films, to its removal and even development to opposite direction. Such change of internal tension can be reflected on the change of dielectric barriers thickness between the CCP particles and to be interfered with the processes occurring under TFR forming.

The investigation of concentration dependence of resistive films conductivity showed that the resistive films conductivity considerably grows with the increase of concentration of conducting phase $Pb_2Ru_2O_{7-x}$ up to 30% and higher. Such increase is explained by conductivity percolation transition because of conducting phase cluster formation in a glass matrix. It was emphasized that with growth of B_2O_3 concentration in glass the increase of conductivity begins at the lower $Pb_2Ru_2O_{7-x}$ concentrations because of high-conducting phase RuO_2 concentration increase in the matrix-dispersible system.

The transfer of electrons between separate conducting grains by means of thermo electronic emission

with the presence of activating process was supposed as the conductivity mechanism. The mechanism of electrons tunneling was also considered. A temperature-activating component can appear from the redistribution of charges between the conductivity isles. Tunnel-resonance conductivity is possible because of admixtures presence in the glass matrix.

CONCLUSIONS

Large maintenance of boron oxide and high acidity of glasses are the main reasons of chemical $Pb_2Ru_2O_{7-x}$ decomposition and formation of ruthenium dioxide under annealing of the hetero-phase systems.

The increase of resistive layers conductivity with the growth of conduction phase maintenance can be explained by percolation transition because of conducting phase cluster formation in the glass matrix. The increase of conductivity begins at lower concentrations $Pb_2Ru_2O_{7-x}$ with growth of B_2O_3 concentration in glass.

The transfer of electrons between separate conducting grains by means of thermo electronic emission with the presence of activating process is the possible current mechanism. Mechanism of electrons tunneling also takes place.

References

1. Лозинский Н. С., Груба А. И., Шевцова Н. А., Волков В. И. Химическое взаимодействие в резисторах на основе рутенита свинца // Известия АН СССР, Сер. Неорганические материалы. — 1999. — т.26, №6. Р. 1307–1312.
2. Sh.D.Kurmashev, T. M. Bugaeva, T. I. Lavrenova, N. N. Sadova INFLUENCE OF THE GLASS PHASE STRUCTURE ON THE RESISTANCE OF THE LAYERS IN SYSTEM "GLASS-RuO₂"// Photoelectronics-2009. — V.18. P.99–102.
3. Н. С. Лозинский, А. И. Груба, Л. И. Левченко, О. Н. Гарштя. Влияние компонентов рутенита свинца на параметры керметных резисторов // ТКЭА — 1997. — №4. С.39–46.

SH. D. RURMASHEV, T. N. BUGAEVA, T. I. LAVRENOVA, N. N. SADOVA

FEATURES OF CO-OPERATION OF COMPONENTS IN HETERO-PHASE SYSTEMS OF "GLASS- $Pb_2Ru_2O_{7-x}$, RuO_2"

Abstract

Resistance pastes on basis RuO_2 differ by a relative chemical inactivity Large maintenance of oxide of the coniferous forest and high acidity of glasses, is principal reason of chemical decomposition of $Pb_2Ru_2O_{7-x}$ and formation of dioxide of ruthenium at burning of the hetero-phase systems

As the physical mechanism of current-conduction the transfer of electrons is credible between separate conducting corns by means of thermic-emission emission supposing the presence of activating process.

Key words: RuO_2 resistive pastes, $Pb_2Ru_2O_{7-x}$ compounds, hetero-phase systems.

Ш. Д. Курмашев, Т.,Н. Бугаева, Т. И. Лавренова, Н. Н. Садова

ОСОБЕННОСТИ ВЗАИМОДЕЙСТВАИЯ КОМПОНЕНТОВ В ГЕТЕРОФАЗНЫХ СИСТЕМАХ "СТЕКЛО — - $Pb_2Ru_2O_{7-x}$, RuO_2 "

Резюме

Резистивные пасты на основе RuO_2 отличаются относительной химической инертностью. Большое содержание оксида бора и высокая кислотность стёкол — основная причина химического разложения рутенита свинца и образования диоксида рутенита при обжиге гетерофазных систем.

В качестве физического механизма токопротекания вероятен перенос электронов между отдельными проводящими зёрнами посредством термоэлектронной эмиссии, предполагающей наличие активационного процесса. Также наблюдался механизм. туннелирования электронов

Ключевые слова: рутенит свинца, туннелирование электронов, гетерофазные системы.

Ш. Д. Курмашев, Т.,Н. Буґаєва, Т. И. Лавренова, Н. Н. Садова

ОСОБЛИВОСТІ ВЗАЄМОДІЇ КОМПОНЕНТІВ У ГЕТЕРОФАЗНИХ СИСТЕМАХ "СКЛО — - $Pb_2Ru_2O_{7-x}$, RuO_2 "

Резюме

Резистивні пасти на основі RuO_2 характеризуються відносною хімічною інертністю. Великий склад оксиду бора і висока кислотність скла — основна причина хімічного розкладу рутеніта свинця і утворення діоксида рутеніта при обжигу гетерофазних систем.

В якості фізичного механізму струмопротікання вирогіден перенос электронів проміж окремими провідними зернами за допомогою термоелектронної емісії, при наявності активаційного процесу. Також спостерігався механізм. тунелювання електронів

Ключові слова: рутеніт свинця, тунелювання электронів, гетерофазні системи.

E. V. MISCHENKO

Odessa State Environmental University, L'vovskaya str., 15, Odessa, 65009, Ukraine
e-mail: quantmis@mail.ru

QUANTUM MEASURE OF FREQUENCY AND SENSING THE COLLISIONAL SHIFT OF THE CAESIUM ALKALI ATOM HYPERFINE LINES IN MEDIUM OF HELIUM GAS

Problem of constructing the alkali atom quantum measure of frequency and definition of the collisional shift of the caesium atom hyperfine structure lines in a medium of helium bath gas are considered. At first, within relativistic approach it is studied the interatomic potential and hyperfine structure line collision shift and broadening for the caesium atom in a medium of helium bath gas.

At present time to the important and actual topics of the applied atomic optics, spectroscopy and photoelectronics is related a problem of studying the collisional shifts and broadening of the hyperfine structure lines for heavy elements (alkali, alkali-earth, lanthanides, actinides and others) in an atmosphere of inert gases [1−23]. From the other side, this task is of a great importance for understanding the elementary atomic collisional processes in a low-temperature astrophysical and laboratory plasma physics and plasma-chemistry [2,6,7]. Besides, one could mention also that the heavy atoms are very interesting from the point of view of studying a role of weak interactions in atomic optics. More over, speech is about unprecedented perspectives in order to check precisely a correctness of the Standard model [2,6,22]. Another important topic is related with construction of the quantum frequency measure. For a long time the corresponding phenomenon for thallium atom attracted a special attention because of possibility to create the thallium quantum frequency measure. Alexandrov and co-workers [5] have realized the optical pumping of the thallium atoms on the line of 21GHz, which corresponds to transition between the components of hyperfine structure for the ground state, and have measured the collisional shift of this line due to buffer (bath) gas. Naturally, the inert buffer gases (He, Ar etc.) were used.

The detailed non-relativistic theory of the collisional shift and broadening of the hyperfine structure lines for simple elements (light alkali elements etc.) has been developed by many authors (see discussions in refs. [1−8]). However, consideration of heavy elements faces the serious difficulties [2,3,18,22,23]. Firstly, a critical importance has a correct account for the relativistic and exchange-correlation corrections. From the other side, a great role plays a quality of the electron wave functions. Particularly, calculations of the hyperfine structure line shift and broadening allow one to check the quality of the wave functions and study the contribution of the relativistic and exchange-correlation effects. By the way, in last years the alkali, lanthanide and actinide elements attract a great interest because of their perspectives in many applications, including the sensor physics and atomic optics devices (see refs. [1−7] and references there). It is very curious that until now a consistent, accurate quantum mechanical approach for calculating

key characteristics of the collisional processes was not developed though many different simplified models have been proposed (see, for example [1,4]). The most widespread approach is based on the calculation of the corresponding collision cross-section, in particular, in a case of the van der Waals interaction between colliding particles. However, such an approach does not factually define any difference between the Penning process and resonant collisional one and gives often non-correct results for cross-sections. More consistent method requires data on the process probability $G(R)$ as a function of inter nuclear distance. It should be noted that these data are practically absent at present time.

In this paper the problem of constructing the alkali caesium atom quantum measure of frequency and definition of the collisional shift for the caesium atom hyperfine lines in a medium of bath (He) gas are studied. Earlier developed new, comprehensive relativistic approach [8,18−21] is used to calculate the interatomic potentials, hyperfine structure collision shift and broadening for the Cs atom in a medium of the inert bath gases. The basic expressions for the collision shift and broadening of the hyperfine structure spectral lines are satisfying to the kinetic theory of spectral lines [2,7]. The exchange perturbation theory has been used for calculating the corresponding interatomic potentials. Earlier the approach has been successfully applied to studying the collisional shift of the thallium, rubidium and other atoms hyperfine lines in a medium of the inert (He etc) gases [18−21].

As the detailed description of the used formalism is given in refs. [9−11], below we are limited by presenting the key expressions. First of all, to calculate the collision shift of hyperfine structure spectral lines one could use the following expression known from kinetic theory of spectral line form (see [8,18]):

$$f_p = \frac{\Delta}{p} = \frac{4\pi N_b}{p} \int_0^\infty e^{-U(R)/kT} \left[1 + g(R)\right] \delta\omega(R) R^2 dR \quad (1)$$

where $U(R)$ is the effective potential of the interatomic interaction, which has a central symmetry in a case of the systems $A—B$ (in our case, for example, $B=He; A=Cs$); T- is a temperature, ω_o -is a frequency of the hyperfine transition in the isolated active atom, $\delta\omega(R) = \Delta\omega(R) / \omega_o$ - is the relative local shift of the hy-

perfine structure lines, which is arisen due to the disposition of the active atoms (say, atom of caesium and helium *He*) on a distance R, N_b - is a concentration of the buffer atoms and $\{1+g(R)\}$ is the temperature form-factor. To calculate an effective potential of the interatomic interaction we use a method of the exchange perturbation theory [2,11]. To calculate a local shift one uses a method of exchange perturbation theory (we use the modified version EL-HAV [18]). Within exactness to second order terms on potential of Coulomb interaction of the valent electrons and atomic cores one can write:

$$\delta\omega(R)=\frac{S_0}{1-S_0}+\Omega_1+\Omega_2-\frac{C_6}{R^6}\left(\frac{2}{\overline{E}_a}+\frac{1}{\overline{E}_a+\overline{E}_B}\right), \quad (2)$$

Here C_6 is the van der Waals constant for interaction *A-B (e.g.,* a pair of *Cs-He;* look below*); I*, $E_{1a,b}$ are the ionization potential and excitation energy on the first level for atoms A, B correspondingly; S_0 is the overlapping integral; The value of $\overline{E}_{a,b}$ is defined as follows:

$$\overline{E}_{\alpha,b}=\left(I_{a,b}+E_{1a,b}\right)/2,$$

The values Ω_1, Ω_2 in the expression (2) are the non-exchange and exchange non-perturbation sums of the first order correspondingly, which are defined as follows:

$$\tilde{n}_0=<\Phi_0^1(1)\left|H'_{HF}\right|\Phi_0^{'}(1)>/<\Phi_0^1(1)\left|\Phi_0^{'}(1)\right>$$

$$\Omega_1=\frac{2}{N(1-S_0)\rho_0}\sum_k{}'\frac{\langle\Phi_0^{'}(1)\left|H'_{HF}\right|\Phi_k^{'}(1)\rangle V_{k0}}{E_0-E_k}$$

$$\Omega_2=\frac{2}{N(1-S_0)\rho_0}\sum_k{}'\frac{\langle\Phi_0^{'}(1)\left|H'_{HF}\right|\Phi_k^{'}(1)\rangle U_{k0}}{E_0-E_k}$$

where $\hat{I}'_{HF}$ is the operator of hyperfine interaction, N is the total number of electrons taken into account in calculation; $E_{k'}$, $\Phi_k^{'}(1)=F_{k_a}^{'}(1)\phi_{k_b}(2...N)$ — energy and non-symmetrized wave function of state $k=\{k_a,,k_b\}$ for isolated atoms A and B. The non-exchange matrix element of the Coulomb interatomic interaction is as follows:

$$V_{ko}=<\Phi'_k(1)\,|\,V(1)\,|\,\Phi'_0(1)>.$$

Correspondingly the exchange matrix element is as follows:.

$$U_{k0}=\sum_{i=2}^N\langle\Phi_k^{'}(1)\left|V(i)\right|\Phi_0^{'}(i)\rangle$$

For example, in a case of the system Fr—He the operator V(1) is as follows:

$$V(1)=U_{SCF}(r_{a^2})+U_{SCF}(r_{a^3})-$$

$$-2U_{SCF}(R)+\frac{1}{r_{12}}+\frac{1}{r_{13}}+\frac{1}{r_{b1}}, \quad (3)$$

where $U_{SCF}(r)$ is the self-conjunctive field, created by the Cs core.

Let us return to consideration of the van der Waals constant C_6 for the interatomic A-B interaction. As a rule, one could use the approximate values for the van der Waals constant C_6 etc. Often the sufficiently great

mistake in definition of the van der Waals constants provides non-high accuracy of the inter-atomic potentials calculation and further inaccuracies. The van der Waals constant may be written as follows [2,6]:

$$C_6(L,M)=C_{6,0}(L)-\frac{3M^2-L(L+1)}{(2L-1)(2L+3)}\cdot C_{6,2}(l) \quad , \quad (4)$$

where $C_{6,0}(L)$ is the isotropic component of the interaction and $C_{6,2}(L)$ is the component corresponding to the $P_2(cos\theta)$ term in the expansion of the interaction in Legendre polynomials, where the angle specifies the orientation in the space-fixed frame. The dispersion coefficients $C_{6,0}(L)$ and $C_{6,2}(L)$ may be expressed in terms of the scalar and tensor polarizabilities $\alpha_0(L;iw)$ and $\alpha_2(L;iw)$ evaluated at imaginary frequencies. In particular, for the helium case one may write:

$$C_{6,0}(L)=\frac{3}{\pi}\cdot\int_0^\infty\alpha_0(L;iw)\overline{\alpha}_{He}(iw)dw \quad (5)$$

where $\overline{\alpha}_{He}$ is the dynamical polarizability of helium. The polarizabilities at imaginary frequencies are given in atomic units as follows:

$$\alpha_\|(L,M;iw)=2\sum_{\gamma,M_\gamma}\frac{(E_\gamma-E_L)|<LM\,|\,\hat{z}\,|\,L_\gamma M_\gamma>|^2}{(E_\gamma-E_L)^2+w^2} \quad (6)$$

where E_γ is the energy of the electronically excited state $|L_\gamma M_\gamma>$ and the z axis lies along the internuclear axis. Usually (see [3,4,23]) the non-relativistic Hartree-Fock basises of the wave functions are used. More sophisticated approach is based on using the relativistic Dirac-Fock wave functions (first variant) [8,21]. Another variant is using the relativistic wave functions as the solutions of the Dirac equations with different model potentials and different density functionals (the Kohn-Sham DFT theory) [18,22]. In this paper we have used the basis of relativistic functions, generated by the Dirac equation with the Green-Ivanov-Ivanova model potential [2,11]. The detailed approbation of this model potential in studying spectra and radiative characteristics of the ytterbium and thallium atoms is given in refs. [2,11,14−16,19,20]. In a number of papers it has been rigorously shown that using the optimized basises in calculating the atomic electron density dependent properties has a decisive role (see discussions in refs. [2,18]). Here we will not in details discuss this question.

The ground configuration for the caesium atom is: *[Xe]6s* (term: ^{2}S). In table 1 we list t our theoretical results for the line shift f_p (1/Torr) for the Cs-He pair. The observed value of the line shift (T=323K) and other theoretical results for f_p are given in table 1 too. Other theoretical data are obtained on the basis of the exchange PT with using the wave functions basises in Clementi et al and Hartree-Fock approximations (from refs. [1,2,4,12]).

The important feature of our scheme is a correct account of the correlation and polarization effects with using special effective functionals from [2,11]. A difference between our theoretical data and other calculation data is explained by using the different basises of wave functions and different PT schemes. For other temperatures there are no quite precise data. It is obvious that using the gauge-invariant optimized

basises of the wave functions and correct version of the exchange PT will be necessary in a case of the alkali elements in an atmosphere of more heavy inert gases [18,22,23].

Table 1
Theoretical data for shift f_β (10^{-9} 1/Torr) of the Cs-He system (look text)

System	Cs-He	Cs-He	Cs-He	Cs-He
T, K	Experiment	Our theory	Other Theor. [6]	Other Theor. [6]
223	-	178	-	-
323	135	137	126	109
423	-	123	111	96
523	-	112	100	85
623	-	105	94	78
723	-	98	-	-
823	-	92	-	-

References

1. Freeman A. J., Frankel R. H., Hyperfine interactions. — N-Y.: Plenum, 1997. — 340P.
2. Glushkov A. V., Relativistic and correlation effects in spectra of atomic systems. — Odessa: Astroprint, 2006. — 400P.
3. Chi X., Dalgarno A., Groenenborn G. C., Dynamic polarizabilities of rare-earth-metal atoms and dispersion coefficients for their interaction with helium atoms//Phys.Rev.A. — 2007. — Vol.75. — P.032723.
4. Batygin V. V., Sokolov I. M., Collisional shift and adiabatic broadening of line of the hyperfine transition in the ground state of thallium in an atmosphere of the buffer helium, krypton and xenon//Opt. Spectr. — 1993. — Vol.55. — P.30−38.
5. Alexandrov E. B., Popov V. I., Yakobson N. N., The optical pumping of the thallium atoms on the line of 21GHz// Opt. Spectr. — 1999. — Vol.46. — P.404−408.
6. Grant I., Relativistic Quantum Theory of Atoms and Molecules Theory and Computation, Springer Series on Atomic, Optical, and Plasma Physics. — 2007. — Vol.40. — P.587−626.
7. Sobel'man I. I. Introduction to theory of atomic spectra. — M.: Nauka. — 1997.
8. Mischenko E. V., Loboda A. V., Svinarenko A. A., Dubrovskaya Yu.V., Quantum measure of frequency and sensing collisional shift of the ytterbium hyperfine lines in medium of helium gas// Sensor Electr. and Microsyst. Techn. — 2009. — N1. — P.25−29.
9. Mischenko E. V., Transition energies and oscillator strengths in helium within equation of motion approach with density functional method for effective account of correlation's// Photoelectronics. — 2006 . — N15. — P.58−60.
10. Ivanov L. N., Ivanova E. P. Extrapolation of atomic ion energies by model potential method: Na-like spectra // Atom. Data Nucl .Data Tabl. — 1999-Vol.24,N2. — p.95−101.
11. Kaplan I. G., Theory of intermolecular interactions, Moscow: Nauka, 1995, 400p.
12. Jamieson M. J., Dalgarno A., Aymar M., Tharamel J., A study of exchange interactions in alkali molecular ion dimers with application to charge transfer in cold Cs// J. Phys. B: At. Mol. Opt. Phys. — 2009. — Vol.42. — P.095203.
13. Jamieson M. J., Drake G. W.F., Dalgarno A., Variational calculation of the dynamic polarizabilities of rare-earth metal atoms/ //Phys.Rev. A. — 1995. — Vol.51. — P.3358−3370.
14. Vidolova-Angelova E., Ivanov L. N., Angelov D. A. Autoionization decay of highly excited Rydberg Tm, Yb states// J.Phys.B:At.Mol.Opt.Phys. — 1998. — Vol.21. — P.3877−3890.
15. Vidolova-Angelova E., Ivanova E. P., Ivanov L. N., Energies and widths of autoionization states for ytterbium atom//Opt. Spectr. — 1997. — Vol.50,N2. — P.243−248.
16. Bekov G. I., Vidolova-Angelova E., Ivanov L. N., Letokhov V. S., Mishin V. I., Laser spectroscopy of narrow two-timely excited autoionization states for ytterbium atom// JETP. — 1997. — Vol.80,N3. — P.866−878.
17. Krunisz M. D., Coulomb approximation oscillator strengths for some transitions in rare earths// Acta Phys. Pol.. — 1999. — Vol.A62. — P.285−296.
18. Glushkov A. V., Florko T. A., Khetselius O.Yu., Malinovskaya S. V., Mischenko E. V., Svinarenko A. A., Optimized perturbation theory scheme for calculating the interatomic potentials and hyperfine lines shift for heavy atoms in the buffer inert gas//Internat. Journal of Quantum Chemistry. — 2009. — Vol.109. — P.3325−3329.
19. Glushkov A. V., Khetselius O.Yu., Mischenko E. V., Loboda A. V., Gurnitskaya E. P., Relativistic quantum chemistry of heavy elements: Interatomic potentials and lines shift for systems "Alkali element-Inert gas"// Theory and Applications of Comput. Chem. (AIP). — 2009. — Vol. 1102. — P.172−175.
20. Khetselius O.Yu.,Glushkov A. V., Mischenko E. V., Florko T. A., Gurnitskaya E., Loboda A. V., Sukharev D., Collisional shift of the Tl hyperfine lines in an atmosphere of inert gases// Spectral Line Shapes (AIP). — 2008. — Vol. 15. — P.231−233.
21. Mischenko E. V., Quantum measure of frequency and sensing the collisional shift and broadening of Rb hyperfine lines in medium of helium gas// Photoelectronics. — 2009. — N18. — C.91−96.
22. Khetselius O.Yu., Relativistic Perturbation Theory Calculation of the Hyperfine Structure Parameters for Some Heavy-Element Isotopes//Internat. Journal of Quantum Chemistry. — 2009. — Vol.109,N14. — P. 3330−3335.
23. Buchachenko A. A., Szczesniak M. M., Chalasinski G., Calculation of the Van der Waals coefficients for interaction of rare-earth metal atoms with helium atoms //J.Chem. Phys. — 2006. — Vol.124. — P.114301.

E. V. Mischenko

QUANTUM MEASURE OF FREQUENCY AND SENSING THE COLLISIONAL SHIFT OF THE CAESIUM HYPERFINE LINES IN MEDIUM OF HELIUM GAS

Abstract.
A problem of constructing the caesium quantum measure of frequency and sensing the collisional shift of the caesium hyperfine structure (HFS) lines in a medium of bath (He) gas is treated. Relativistic approach is used in calculating the inter atomic potentials, oscillator strengths, HFS collision shift and broadening.
Keywords: quantum measure of frequency, collisional shift, caesium, helium gas.

УДК539.184

Е. В. Мищенко

КВАНТОВАЯ МЕРА ЧАСТОТЫ И ДЕТЕКТИРОВАНИЕ СТОЛКНОВИТЕЛЬНОГО СДВИГА ЛИНИЙ СВЕРХТОНКОЙ СТРУКТУРЫ АТОМА ЦЕЗИЯ В АТМОСФЕРЕ ГЕЛИЯ

Резюме.
Рассмотрена проблема построения цезиевой квантовой меры частоты и определения столкновительного сдвига линий сверхтонкой структуры атома цезия в атмосфере буферного (гелий) газа. Релятивистский подход использован в расчете межатомных потенциалов, столкновительного сдвига и уширения линий сверхтонкой структуры.
Ключевые слова: квантовая мера частоты, столкновительный сдвиг, цезий, газ гелия

УДК 539.184

О. В. Міщенко

КВАНТОВА МІРА ЧАСТОТИ І ДЕТЕКТУВАННЯ ЗСУВУ ЛІНІЙ НАДТОНКОЇ СТРУКТУРИ АТОМУ ЦЕЗІЯ ЗА РАХУНОК ЗІТКНЕНЬ В АТМОСФЕРІ ГЕЛІЯ

Резюме.
Розглянуто проблему побудови цезієвої квантової міри частоти і визначення зсуву за рахунок зіткнень ліній надтонкої структури атому цезія в атмосфері буферного (гелій) газу. Релятивістський підхід використано у розрахунку міжатомних потенціалів і зсуву та уширення ліній надтонкої структури за рахунок зіткнень.
**Ключові слова**: квантова міра частоти, зсув за рахунок зіткнень, цезій, газ гелія

V. I. MIKHAILENKO, A. A. KUZNETSOVA, G. P. PREPELITSA, A. V. IGNATENKO

Odessa National Maritime Academy,
Odessa State Environmental University

PENNING AND STOCHASTIC COLLISIONAL IONIZATION OF ATOMS IN AN EXTERNAL MAGNETIC FIELD

The basises for the consistent quantum theory of the Penning and stochastic collisional ionization of atoms in an external magnetic field are presented and based on the Schrцdinger equation solution for atom in a magnetic field and Focker-Plank stochastic equation method.

1. A recent progress in modern experimental technique of generation electromagnetic (laser) field stimulates a great attention to the studying elementary atomic collisional processes in plasmas, gases and other mediums at presence of the external field [1−22]. The most interesting and simultaneously very complicated phenomena include the ionization of excited atoms by means of the photon and electron impact, atom-atom or ion-atom collisions). Though there are many theoretical and experimental papers, however some important aspects are remained unclear hitherto. The situation, however, does not look as good for more complex targets, such as ionization of the heavy multielectron system, say, noble gases leaving the ion in the outer $(ns^2np^5)^2P$ or $(nsnp^6)^2S$ states, ionization plus simultaneous excitation of He and other quasi-two-electron targets such as Mg, the role of resonances and auto ionizing states, and the additional complexity when the linear momentum of the incoming projectile and the two outgoing particles (electrons in this paper) are no longer in the same plane. Interestingly, out-of-plane ionization and ionization via auto ionizing states without excitation both seem to be sensitive to higher-order effects, very similar to simultaneous ionization-excitation in coplanar kinematics [4]. Indeed to fulfill an accurate account of the inter electron correlation effects in the atomic collisions is very difficult as these effects and other ones are not adequately described within many simplified models. Situation changes dramatically under consideration of the different atomic collisional processes under availability of the external electromagnetic fields. Even more simple case of the external static electric or magnetic field is remained hitherto quantitatively undeceived.

From this point of view, a great interest attracts a formulation of the consistent quantum theory for the atomic collisional processes in presence of the external magnetic field. [1−5, 11−14]. Let us remind the key interatomic collisional processes, which are of a great interest for many applications, namely:

$$A^*(nl)+B\rightarrow(A+B^+)+e \text{ or} \tag{1}$$

$$A^*(nl)+B\rightarrow(A^+ +B)+e \text{ or} \tag{2}$$

$$A^*(nl)+B\rightarrow AB^+ +e. \tag{3}$$
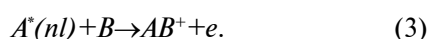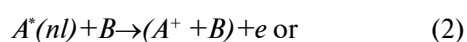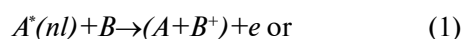
In these formula A^* denotes the atom in an excited state, B^+ is the ionized atom. The process (3) is corre-sponding to the associative ionization. It takes a place when the dissociation energy of molecular ion AB^+ is more than the ionization potential of the excited atom [1,2]. The first process (1) takes a place and runs very effectively in a case when the excitation energy of the A atom is more than the ionization potential of the atom B. Here one can introduce the Penning process, which is corresponding to the situation when the atom A is in the metastable state. The most widespread theoretical schemes for description of the cited processes (look, for example, [1−5,20,21]) are based on the defining the capture cross-section of collisional particles by field of the wan der Waals interaction potential. It should be mentioned several versions of the rectilin-ear classical trajectories model too [1−3,20]. Similar models, however, do not account for any difference between the Penning process and resonant collisional processes. In refs. [17−20] the different new approach-es to the treating elementary atomic processes (1)-(3) are presented. Though the Penning and stochastic collisional ionization of atoms had been a subject of intensive theoretical and experimental interest, how-ever, the available level of modelling in not satisfactory [20]. The modern actual tasks are connected with the external magnetic field on the corresponding Penning and stochastic collisional ionization processes, how-ever, hitherto it is absent any adequate theory. So, the main aim of this work is firstly to present the basises of a consistent theory.

2. In order to take into account an external mag-netic field and construct the corresponding electron wave functions one must start for the treating the Zee-mane problem. It is very important to have the zeroth approximation, which includes an external magnetic field, i.e. the strength of the field is arbitrary. Let us underline that despite a long history since the dis-covery of the Zeemane effect and sufficiently great number papers on atomic systems in an external mag-netic field, hitherto a majority of results are as a little acceptable for many applications as related only the hydrogen atom (look, for instance, [4−6,11−13]). A definite interest has been renewed after discovery of the quantum chaos phenomenon in atomic systems in the static magnetic field [1−13,22]. Below we consider a standard scheme to treating multi-electron atom in a static magnetic field. The purpose is to present the basis scheme for definition of the electron wave func-tions for further using in the collisional task.

As usually, the hydrogen-like Hamiltonian for atom in a magnetic field B has the form as follows:

$$\hat{H} = \frac{1}{2m}(p + \frac{1}{2}\frac{e}{c}[Br])^2 - \frac{e^2}{r}. \qquad (4)$$

Here we did not account for the electron spin, though its account is supposed. Because of the invariance of $\hat{H}$ in relation to rotations around the axe Oz (it is parallel to field B and crossing a nucleus of an atom), naturally z-component of the orbital moment $L_z = hM$ is the conserving variable. In the cylindrical coordinates with axe Oz∥B with account of the trivial dependence of the wave function upon the rotation angle ϕ around the axe z ($\Psi \sim e^{iM\phi}$), one could write the corresponding equation in the form (in atomic units: $e=h=m=1$):

$$\left[\frac{\partial^2}{\partial\rho^2} + \frac{1}{\rho}\frac{\partial}{\partial\rho} + \frac{\partial^2}{\partial z^2} - \frac{M^2}{\rho^2} - 4\gamma^2\rho^2 + \frac{4}{r} + (\frac{E}{R_y} - \gamma M)\right] \times$$
$$\times \Psi(\rho,z) = 0 \qquad (5)$$

Naturally the 2D equation (5) has not an analytical solution as the Coulomb interaction term with $r = (\rho^2 + z^2)^{1/2}$, prevents to the variables separation. It is easily to show that the equation (5) can be rewritten as follows:

$$H\psi(\rho,z) = E\psi(\rho,z) \qquad (6)$$

$$H = -1/2(\partial^2/\partial\rho^2 + 1/\rho\partial/\partial\rho + \partial^2/\partial z^2 - m^2/\rho^2),$$
$$V(\rho,z) = -(\rho^2 + z^2)^{-1/2} + 1/8\gamma^2\rho^2 + \gamma m/2,$$

where $\gamma = B/B_o$ ($B_o = 2,3505\cdot10^9$). The potential $1/8\gamma^2\rho^2$ limits a motion in the direction, which is perpendicular to the B direction. In the region $\gamma \gg 1$ the electron motion along (or perpendicular) magnetic field is defined by the Coulomb interaction (by a size of the cyclotronic orbit $\lambda = (\hbar c/eM)^{1/2}$). The simplified circumstance is that the potential of the longitudinal Coulomb interaction can be received by way of the averaging the total Coulomb potential $e^2(\rho^2 + z^2)^{-1/2}$ on the little radius of the transverse motion. The one-particle energy for given values of magnetic field B is defined as:

$$\varepsilon_{B\mu} = (m_\mu + |m_\mu| + 2s_{z\mu} + 1)\gamma/2 - \varepsilon_\mu \qquad (7)$$

where $\varepsilon\mu$ — one-particle energy (the field is absent), $S_z\mu$ is the spin projection on the axe z. Let us remember that the wave function at absence of the field has the asymptotics as $\exp[-(-2\varepsilon)^{1/2} r]$. When magnetic field is present, the value should be replaced by the ionization energy from the stationary state on the Landau lowest level. In order to find the width of the Zeemane resonance it is necessary to know the imaginary part of state energy in the lowest perturbation theory [4]:

$$Im\ E = G/2 = \pi <\Psi_{Eb}|H|\Psi_{Es}>^2 \qquad (8)$$

with the general Hamiltonian H (G- resonance width). The state functions Ψ_{Eb} and Ψ_{Es} are assumed to be normalized to unity and by the $\delta(k-k')$-condition, accordingly. The necessary electron wave functions in a case of the atom in a static magnetic field are defined by the numerical solution of the corresponding equation (6) (see refs. [4,6,1–13,20]). Further we will suppose

that the corresponding energies and wave functions are found, so let us return to collisional problem.

3. As usually, one can introduce the definition of complete cross section for collisional process (1) as follows:

$$\sigma = \int_0^\infty 2\pi\rho d\rho\{1 - \exp[-\int_{-\infty}^{+\infty} G(R)dt]\} \qquad (9)$$

Here $G(R)$ is a probability of the Auger effect $G(R) = 2\pi|V_{12}|^2 g_2$ (indexes 1 and 2 are relating to states: $A^* + B$ and $A + B^+ + e$; g is a density of the final states; V is operator of interaction between atoms). In a case when ionization process is realized in the repulsive potential of interaction between atoms in the initial channel, the cross-section is:

$$\sigma = (4\pi f_w / v)\int_{R_{tn}}^\infty R^2 G(R)\sqrt{1 - U(R)/E}dR \qquad (10)$$

Here v is the relative velocity of collision, R_{tn} is the minimally possible distance of rapprochement (the turning point); f_w is the probability that the process is permitted on full electron spin of system of the collisional atoms.

Further, as usually, it is necessary to account for a possibility of decay in the second and higher orders of perturbation theory on $V(R)$. Such approach may be used as for the Penning ionization description as for ionization through the wan-der-Waalse capture [3,5]. In the perturbation theory second and higher orders it is introduced the matrix element: $\langle 1|V(R)G_{E_\infty}V(R)...V(R)|2\rangle$ insist of the simple matrix element $\langle 1|V(R)|2\rangle$ in expression for probability of collisional decay. Here [1> ≡ [A*+B> is the initial state, [2> ≡ [A+B^++e> is the final state; G_E is the Green function (see below); $E\infty$ is an energy of quasi-molecule A*B under $R \to \infty$. The latter is corresponding to approximation of the non-interacting atoms.

Naturally it is supposed that the atomic wave functions are constructed within above presented scheme with external magnetic field. Further one can use for operator $V(R)$ the standard expansion on non-reducible tensor operators:

$$V(R) = \sum_{l_1,l_2=1}^\infty V_{l_1 l_2}(n)/R^{l_1+l_2+1} \qquad (11)$$

$$V_{l_1 l_2}(n) = (-1)^{l_2}\sqrt{\frac{(2l_1 + 2l_2)!}{(2l_1)!(2l_2)!}}(C_{l_1+l_2}(n)\{Q_{l_1}^A \otimes Q_{l_2}^B\})\ ,\ n = \frac{R}{R}$$

where $\hat{Q}_{lm}$ is an operator of the 2^l-pole moment of atom and $C_{lm}(n)$ is the modified spherical function. If we suppose that atom A* is in the state with the whole moment J_i and projection on the quantization axe M_i; in the final state the corresponding quantum numbers are $J_f M_f$; The final expression for the full probability of the electron ejection is similar to expressions, obtained in ref. [17,18]:

$$G(R) = \frac{2\pi(2l_1+1)(l_1+1)(2l_1+3)(2l_2+1)(l_2+1)(2l_2+3)}{R^{2l_1+2l_2+8}(2l_i+1)[1+\delta_{l_1 l_2}]^2(2J_i+1)}$$
$$\left|\sum_{p_1 p_2 p_3 l_f}(C_{l_2+1\,0\,l_1+1\,0}^{p_1 0})^2 \times\right.$$

$$\times (2p_2+1)(2p_3+1)\begin{Bmatrix} 1 & l_1 & l_1+1 \\ 1 & l_2 & l_2+1 \\ p_2 & p_3 & p_1 \end{Bmatrix}\left|\sum_{Jl}\begin{Bmatrix} 1 & 1 & p_2 \\ l_f & l_i & l \end{Bmatrix}\right.$$

$$\left[\begin{Bmatrix} l_2 & l_1 & p_3 \\ J_f & J_i & J \end{Bmatrix}\Re_{Jl}^{lf}(l_1,l_2)+\right.$$

$$\left.\left.+(-1)^{l_1+l_2+p_2+p_3}\begin{Bmatrix} l_1 & l_2 & p_3 \\ Jf & Ji & J \end{Bmatrix}\Re_{Jl}^{lf}(l_2,l_1)\right]\right|^2 . \quad (12)$$

Here the reducible matrix elements are represented as:

$$\Re_{Jl}^{lf}(l_2,l_1)=$$

$$=<n_A J_i;O_B l_i\left\|\widehat{Q}_{l_2}^A \widehat{d}^B g_{Jl}^{A*B_0}\widehat{Q}_{l_1}^A \widehat{d}^B\right\|O_A J_f;El_f> \quad (13)$$

Here $d^B=Q^B_1$ is an operator of the dipole moment of atom B, g^{A*B0}_{Jl} is a radial Green function. Because of that the final state of atom $B\,|\,El_f>$ is a state of continuum with scattering phase δ_{lf} then the fine structure of levels in atom B is not accounted. It is possible to show that the similar expression for G can be received from Eq. (8) within energy approach [10,12].

The attractive perspective for realization the stochastic c collisional process is provided by a case when the atom A in process (1) is highly excited (Rydberg state). In principle here the theoretical treating is similar to a case of the external static electric field [5]. The qualitative physical picture is corresponding to a chaotic drift of the Rydberg electron which interacts with the electromagnetic field of dipole (and simultaneously with an external magnetic field). This interesting physical situation can be adequately treated within generalized theory of chaotic drift for the Coulomb electron in the external microwave field (see refs. [4–6,11–13]). The function of distribution $f(n,t)$ of the Rydberg electron on space of effective quantum numbers n should be introduced. The equation of motion of the Rydberg electron has the well known form:

$$\partial f(n,t)/\partial t=\partial/\partial n\,[\Theta(n-N_{min})D(\,R)n^3\,\partial f(n,t)/\partial n\,]-$$

$$-\Theta(n-N_{max})G(n,R)f(n,t) \quad (14)$$

Here $\Theta(n-N_{min})$ is the Heviside function. It served here as additive multiplier in the coefficient of diffusion: Dn^3 and provides freeezing of the stochastic processes in region of the low lying states in accordance with the known Cirikov criterion: $N_{min}<n<N_{max}$. For the Rydberg states $(n>N_{max})$ a direct channel of ionization is opened and the electron ejection takes a place. It is important to note that process will be realized with more probability under availability of the external magnetic field. Naturally, any numerical estimate can be received only on the basis of concrete calculation. It is obvious that the dynamics of the whole process will be very interesting and it is hardly possible to give any exact estimated on the basis of the qualitative conclusions.

4. In this paper we presented the basises of a consistent theory for the Penning and stochastic collisional ionization of atoms in an external magnetic field, which is in fact based on the Schrцdinger equation solution for atom in a magnetic field and Focker-Plank stochastic equation method. In this aspect the theory differs of the analogous approaches [3,5,17–19], where an external field is generally absent or the electric static field is present [5]. Despite an obvious consistency of the presented theory, its practical realization is naturally connected with sufficiently complicated numerical calculations (even accounting availability of such effective numerical codes as "Dirac", "Superatom", Superstructure" and others [4,12,20]). The other problems for the theory realization are discussed in ref. [5]. Nevertheless, in order to demonstrate the important sequences of the theory we will give some qualitative estimates, using the obvious classical particular case of the presented approach, namely, the motion classical rectilinear trajectories approximation [1,3]. As example, we consider the process $He(2^1S_0)+B_0\rightarrow He(1^1S_0)+B^+_0+e^-$ (B_0=H, Na; T=300ºK). The Penning process cross-section is given in the classical limit by a simple formula (in atomic units) [1] :

$$\sigma_P=(\frac{9\pi}{11})(\frac{63\pi}{256v})^{2/11}\Gamma(R^2\Gamma)^{2/11} \quad (15)$$

where $v=\sqrt{2T/\mu}$ - velocity, μ — normalized mass of collided atoms, R — interatomic distance and Γ is the probability (autoionization width). The experimental values of the cited process cross sections (field B=0) are [1,20,21]: σ_p(He-H)=33·10^{-16}cm^2 , σ_p(He-Na)=17·10^{-16}cm^2. As it's indicated in ref. [5], these values are the upper limit of the true ones. The data, provided by the classical model [3,20], are: σ_p(He-H)=(6–8)·10^{-16}cm^2, σ_p(He-Na)=(7–9)·10^{-16}cm^2 (T= 300ºK). The external magnetic field effect on the Penning process parameters can be different in dependence upon the parameter γ. If B is not large (in comparison with standard atomic value), the corresponding effect will not be essential. The simple estimates show [6,9] that during changing the field strength ($\gamma=10^{-5}\rightarrow 10^{-2}$) for both processes the autoionization width can be changed on the three-four times. But, obviously this is a qualitative estimate. The classical model does not give an adequate quantitative description of the process. In a case of the stochastic collisional process, in particular, with Rydberg collided atoms, the external filed effect can essentially change the stochastic mechanism [9,12]. So, in any case an availability of the external magnetic field makes significantly more complicated the physics of the studied collisional processes.

References

1. Chemistry of plasma, Eds. Smirnov B. M., Devdariani A. L. — Moscow, 1989. — Vol.15.
2. Kaplan I. G., Intermolecular interactions. — Moscow: Nauka, 1997. — 380P.
3. Nikitin E. E., Umansky S.Ya., Semiempiril methods of calculating the atomic interaction potentials. . Achievements of science and technique. Serie: Structure of molecules and chemical bond. — Moscow: VINITI, 1999. — Vol.4. — 220P.
4. Ruder H., Wunner G., Herold H., Geyer F. Atoms in Strong Magnetic Fields. — Berlin: Springer-Verlag, 1994. — 384p.
5. Mikhailenko V. I., Kuznetsova A. A., Penning and stochastic collisional ionization of atoms in an external electric field// Sensor Electr. and Microsyst. Techn. — 2009. — N4. — P.12–17.
6. Lisitsa V. S., New in Stark and Zeemane effects for atom of hydrogen//UFN. — 1997. — Vol.153. — P.379–422.

7. Bodo E., Zhang P., Dalgarno A., Ultra-cold ion–atom collisions: near resonant charge exchange// New Journal of Physics. — 2008. — Vol. 10. — P.033024.

8. Jamieson M. J., Dalgarno A., Aymar M., Tharamel J., A study of exchange interactions in alkali molecular ion dimers with application to charge transfer in cold Cs.// J. Phys. B: At. Mol. Opt. Phys. — 2009. — Vol.42. — P.095203

9. Letokhov V. S. Nonlinear selective photo processes in atoms and molecules. — M.: Nauka, 1999. — 408P.

10. Ivanov L. N., Letokhov V. S. Spectroscopy of autoionization resonances in heavy elements atoms// Com.Mod.Phys.D.:At.Mol.Phys. — 1995. — Vol.4. — P.169−184.

11. Dando P. A., Monteiro T. S. Atoms in Static Fields: Chaos or Difraction?// Photonic, Electronic, Atomic Collisions. — Singapore: World Sci.Pub. — 1997. — P.621−630.

12. Atoms and Molecules in Strong External Fields.Eds. Schmelher P., Schweizer W. — N. — Y.: Plenum Press, 1998. — 410p.

13. Glushkov A. V., Atom in electromagnetic field. — Kiev: KNT, 2005. — 400P.

14. Glushkov A. V., Ivanov L. N., DC Strong-field Stark-effect: New consistent quantum-mechanical approach// J.Phys. B: At. Mol. Opt. Phys. — 1999. — Vol.26. — P.L379-L386.

15. Glushkov A. V., Lepikh Ya.I., Fedchuk A. P., Ignatenko A. V., Khetselius O.Yu., Ambrosov S.V , Wannier-Mott excitons and atoms in a DC electric field: photoionization, Stark effect, resonances in the ionization continuum// Sensor Electr. and Microsyst. Techn. — 2008. — N4. — P.5−11.

16. Masnow-Seeuws F., Henriet A., Two-electron calculations for intermediate Rydberg states Na₂: quantum defects/ //J. Phys.B.At.Mol.Phys. — 1998-Vol.21- P.L338−346.

17. Ambrosov S. V. New optimal scheme for gases and isotopes optically discharged separation with Penning and stochastic collisional ionization// Phys. Aerodisp.Syst. — 2003. — N40. — P.340−352.

18. Manakov N. L., Ovsyannikov V. D., Ostrovsky V. N., Yastrebov V. N. Influence of long-acting forces on the Penningionization//Opt. Spectr. 1994. — Vol.56,-P.222−226.

19. Bezuglov N. N., Borodin B. M., Kazansky A. K. et al, Analysis of stochastic equations of the Focker-Plank with valuable boundary conditions in elementary process of collisional ionization//Opt. Spectr. — 2001. — Vol.89. — P.25−33.

20. Photonic, Electronic and Atomic Collisions. Eds. Aumar F., Winter H. — Singapore: World Scientific. — 2007. — 650P.

21. Dupret K., Zakrzewski J., Delande D. Resonances in the diamagnetic Rydberg spectrum: order and chaos// Europhys. Lett. — 1995. — Vol.31,N5−6. — P.251−256.

22. Loboda A. V., Svinarenko A. A., The electron capture processes in the ion-atomic collision system: Energy approach// Sensor Electr. and Microsyst. Techn. — 2009. — N2. — P.30−36

V. I. Mikhailenko, A. A. Kuznetsova, G. P. Prepelitsa, A. V. Ignatenko

PENNING AND STOCHASTIC COLLISIONAL IONIZATION OF ATOMS IN AN EXTERNAL MAGNETIC FIELD

Abstract.
The basises for the consistent quantum theory of the Penning and stochastic collisional ionization of atoms in an external magnetic field are presented and based on the Schrцdinger equation solution for atom in a magnetic field and Focker-Plank stochastic equation method.
Key words: Penning and stochastic collisional ionization, magnetic field

В. И. Михайленко, А. А. Кузнецова , Г. П. Препелица, А. В. Игнатенко

ПЕННИНГОВСКАЯ И СТОХАСТИЧЕСКАЯ СТОЛКНОВИТЕЛЬНАЯ ИОНИЗАЦИЯ АТОМОВ ВО ВНЕШНЕМ МАГНИТНОМ ПОЛЕ

Резюме.
Изложены основы последовательной теории пеннинговской и стохастической столкновительной ионизации атомов при наличии внешнего магнитного поля, базирующейся на решении уравнения Шредингера для атома в магнитном поле и методе стохастического уравнения Фоккера-Планка.
Ключевые слова: пеннинговская, стохастическая столкновительная ионизация, магнитное поле

В. І. Михайленко, Г. О. Кузнецова, Г. П. Препелица, Г. В. Ігнатенко

ПЕННІНГІВСЬКА ТА СТОХАСТИЧНА ЗА РАХУНОК ЗІТКНЕНЬ ІОНІЗАЦІЯ АТОМІВ У ЗОВНІШНЬОМУ МАГНІТНОМУ ПОЛІ

Резюме.
Викладені основи послідовної теорії пеннінгівської та стохастичної за рахунок зіткнень іонізації атомів при наявності зовнішнього магнітного поля, яка базується на рішенні рівняння Шредінгеру для атому у магнітному полі і методі стохастичного рівняння Фоккер-Планка.
Ключові слова: пеннінгівська, стохастична за рахунок зіткнень іонізація, магнітне поле

UDC 541.27

A. P. FEDCHUK, A. V. GLUSHKOV, YA. I. LEPIKH

I. I. Mechnikov Odessa National University,
Odessa State Environmental University

COMBINED ELECTRODYNAMICAL AND QUANTUM — CHEMICAL APPROACHES TO MODELLING THE CATALYTIC ACTIVITY OF METALS, METAL ALLOYS AND SEMICONDUCTORS

The catalytic activity estimating of the metals, binary metallic alloys and semiconductor materials is considered within the combined quantum mechanical and electrodynamics approach in the electron theory of catalysis.

INTRODUCTION

A study of catalytic activity for metals, metallic alloys and semiconductors is of a great importance for different practical applications, for example, during the elaboration of electrochemical solid-state energy sources, planning the efficacy of semiconductor sensors and naturally developing advanced chemical industry technologies etc [1−19]. It is known [2,3,8−10], that the components concentration's change in metallic alloys could result in drastic variation of catalytic activity as well as of electrochemical properties. The same effect is characteristic for semiconductors when some impurities are introduced inside the pure material. Generally speaking catalysis on semiconductors is more widespread phenomenon that it seems at first sight. Really, a majority of metals is usually covered by semiconductor film [5,7]. In the contact with pure surface the oxygen, hydrogen and nitrogen are quickly absorbed by a surface even under low temperatures. The attempts of comprehensive quantitative description of the metal-like systems (metallic alloys, heavily doped semiconductors) electronic structure including the description of processes on electrodes' surfaces of the electrochemical solid-state energy sources and naturally electrochemical and catalytic processes have been undertaken in a number of papers (see refs.in [1−26]).

Naturally a mechanism of heterogeneous catalytic process can be understood under obligatorily treating intermediate stages, namely, stages of adsorption and desorption [1,2]. Generally speaking, as any chemical process, the heterogeneous catalytic process has the electron mechanism in the end. Any heterogeneous reaction can be interpreted as the process based on radical mechanism. Radicals and ion-radicals appear on the surface under chemosorption and provide the radical mechanism of the heterogeneous reactions. But, naturally it doesn't mean that non-radical mechanisms are excluded. The catalytic reaction path through one-electron charged intermediates (ion-radicals) is not the main mechanism in heterogeneous catalysis but, of course, is possible in some special cases. As example, above the cited approaches to adsorption and catalysis one could mention a group of the conceptual models which are based on using the density functional formalism [14−16]. There is a great num-ber of papers (see [1−5, 16−19,26]), where the catalysis and electrochemical problems are considered within *ab initio* quantum chemistry methods. Using these methods allowed to get very useful information about processes considered, however, some quite important moments of the physical and chemical nature of these processes often remain up to known degree veiled. Besides, one could mention well known calculation difficulties of description of the catalysis processes within *ab initio* quantum chemistry methods [1−5,8−13]. Simplification of the corresponding calculation schemes leads to a loss of the quantitative accuracy for phenomenon description and, generally saying, to qualitatively invalid conclusions in many cases. Naturally, a great interest attracts a development of more physical and calculationally economical model approaches to a catalysis problem. In this sense, as alternative, one could indicate more simplified (from the calculation point of view), but quite effective electrodynamical and quantum-chemical modeling models for description of the catalytic processes (see [8−10, 20−22]). Above cited approaches it should be separately mentioned a group of papers, which are devoted to simple homogeneous phone models by Lang-Kohn, Bardeen, Theophilou, Vannimenus-Budd, Norskov-Lundqvist-Hjelmberg et al and base on an conception of the Kohn-Sham density functional theory (look a detailed review of the corresponding models and results in refs.[1−5,15−19,26]).

At present time there is a great number of experimental papers (see refs. [1−3,5−7]), where it has been shown that the electronic processes in metallic and semiconductor materials provide their electric, optical and magnetic properties and simultaneously the catalytic ones. Though now it is clear that activation of reagents in heterogeneous catalysis is associated, as a common rule, with surface adsorption but not with deep penetration into the solid matrix. Nevertheless, there is a certain parallelism between electronic and catalytic properties of the material. To find a link between these two groups of properties is a main aim of the electron theory of catalysis. Naturally here one could mention the pioneering papers in a field of electron theory of catalysis by Hauffe et al (Germany), Boudart, Voltz, Taylor et al (USA), Germain , Claudel et al (France), Pisarzhevsky, Wolkenstein, Lyashenko, Terenin, Lidorenko (USSR) et al (see reviews [1−

10,26]). On the one hand, the electron theory of catalysis is based on the modern theory of chemical bond, but on the other hand its fundament is modern theory of solids. It is well known that the theory of chemical bond has to do with the transformations of molecules on the surface and the theory of solids treats the processes inside material. The theory of chemisorption and heterogeneous catalysis has to do with the transformations of the surface molecules each connecting the crystal and forming a united system. As a rule, the electron theory of catalysis like other modern variants of the catalysis theory are not alternative and do not compete with each other. As a matter of fact, these theories describe different aspects of the process and surely differ only by the conceptual approach to the problem. Here we consider a problem of catalytic activity definition for metals, binary metallic alloys and semiconductor materials and present the basises of a new approach to electronic theory of catalysis, which is based on using the electrodynamical and quantum-mechanical models [8−10, 20−22].

1. LINK BETWEEN THE FERMI LEVEL POSITIONS ON SURFACE AND INSIDE THE MATERIAL

Now it is obvious that the catalytic properties of metals and semiconductors are directly connected with electronic processes which occur inside and on the surface of the materials and provide these properties in the end. The role of catalyst results in generation of the surface radicals, which are arisen due to the free valences of catalyst on the surface and forming during reaction. Naturally the free valences on the surface exhaust very slowly as the valences supply on the surface from the volume. Appearance of the radical or ion-radical forms is connected with a role of the crystal lattice free electrons and holes during chemosorption. Say, a semiconductor in the catalytic process has a role not only inert layer (where the chemical reaction runs) but as an active e participant of the process too. More over it can by one of the components in the intermediate stages of the reaction. In any case, the catalytic properties of semiconductor are defined by their nature and electron structure and a mechanism of the catalytic action is in definite degree inside the material too. One could mention that introduction of the impurities inside the semiconductor changes its catalytic properties [5,7]. More over, now it is well established a certain correlation between the material electroconductivity, the output work (forbidden band width in the energy spectrum of semiconductor) and its catalytic properties (the adsorption ability of material too). An effect of the light (laser radiation) on semiconductor leads to internal photoelectric effect and changing its adsorption and catalytic activity. One could note that the Fermi level position defines the adsorption and catalytic activity of the surface in relation to molecules of the given kind under other equal conditions. Naturally, the Fermi level position on the surface is dependent upon its position inside the crystal. Surely there is a direct link between the surface and bulk properties of materials. The factors, which shift the Fermi level inside, say, in the semiconductor, influence on its surface

properties too. Naturally, special case is a case of the large density of the surface states.

The chemosorption ability of the surface, a degree of its charging, a reactive ability of the chemisorbed particles etc are directly defined by the Fermi level position on the surface of crystal (say, a distance between the Fermi level and the conductivity band bottom: E_F^s). Let us denote the position of the Fermi level inside the crystal as E_F^v . The direct link between the values E_F^s and E_F^v can be obtained from the condition of the electric neutrality of crystal:

$$\sigma + \int_0^\infty \rho(x)dx = 0 , \qquad (1)$$

where σ is a density of the surface charge and ρ is a density of the volume charge in the plane, say x (the material occupies the semispace x>0). Further one could write as follows:

$$\sigma = \sigma(P,T;E_F^s) , \qquad (2)$$

where P is a pressure, T is a temperature. Naturally, if all surface charge is provided only by the chemisorbed particles (say, the same kind), then the expression for σ has more complicated form (see refs. [2,5,7]). The second item in Eq. (1) is the function of E_F^s and E_F^v :

$$\int_0^\infty \rho(x)dx = R(T;E_F^s;E_F^v) . \qquad (3)$$

In result one can write the obvious relationship, which gives a direct link between E_F^s and E_F^v :

$$\sigma(P,T;E_F^s) + R(T;E_F^s;E_F^v) = 0 \text{ or } E_F^s = f(P;T;E_F^v) \quad (4)$$

This equation establishes correlation between the surface and bulky properties of the material (semiconductor etc.). Let us further to introduce new advanced electrodynamical and quantum-mechanical models in the electron theory of catalysis for metals, metal alloys and semiconductors.

2. ELECTRODYNAMICAL AND QUANTUM-MECHANICAL APPROACHES FOR METALS AND METALLIC ALLOYS

It is well known [23,24] that the electron structure of a metallic system in the simple approximation can be approximated by a set of isotropic s-d energy bands. The static dielectric permeability is represented as follows:

$$\varepsilon = 1 + \varepsilon_{ss} + \varepsilon_{dd} + \varepsilon_{sd} + \varepsilon_{ds} , \qquad (5)$$

where ε (ij) describes the contribution into ε due to the i-j transitions. In approximation of the free electrons the expression for ε_{ss} looks as:

$$\varepsilon_{ss} = 2\pi v_s (E_F)k^{-2}\{1+[4(k_F^s)^2 -$$
$$-k^2]\ln\left|(2k_F^s + k)/2k_F^s - k\right|/4k_F^s k\}. \qquad (6)$$

.where $k=q \cdot a_B$, q is the wave number, a_B is the Bohr radius, $q_F = (3\pi^2 z_i /\Omega)^{1/3}$; z_i is a number of electrons in "i" band; $v_i(E_F) = N_i(E_F)a_B^2 e$, $N_i(E_F)$ is a density of states on the Fermi surface in "i" band. The corresponding expression for ε_{dd} is as follows:

$$\varepsilon_{dd} = 2\pi v_d(E_F)k^{-2}|M_{dd}|^2 \{1 + [4(k_F^d)^2 - $$
$$-k^2]\ln|(2k_F^d + k)/2k_F^d - k)|/4k_F^d k\} \quad (7)$$

Here the matrix element M_{dd} is defined by the superposition of the wave functions for d electrons. The contribution ε *(ds)* is important only for systems containing the precious metals. This contribution is defined as follows:

$$\mathring{a}_{ds} = [2m_s k_d e^2 f_c / \eth h^2 k^2] \times$$
$$\times \{1 + [4(k_d)^2 - k^2]\ln|(2k_d + k)/2k_d - k)|/4k_d k\}. \quad (8)$$

where m_s is the effective mass of electron in the conductivity band; k_d, f_c are the numeral parameters [23,24]. Usually the contribution ε_{ds} in Eq. (5) for transition metals is about several percents. The effective potential, which imitates an effect of metallic potential field on the hydrogen atom (for process $H=H^+ + e^-$) is defined as follows:

$$\ddot{O}(r) = -\frac{2e^2}{\pi r}\int_0^\infty \frac{\sin kr}{k\varepsilon(k)}dk \quad (9)$$

Further it is supposed that a problem considered has the spherical symmetry and crystal potential is fully screened by the conductivity electrons. Substitution of (5) to (9) leads to the expression:

$$\Phi(r) = -(e^2 a/r)\exp[-\alpha R]\cos[\alpha R] \quad (10)$$

where

$$\alpha = [\pi^{-1}12(k_F^s)^2]^{-1/4} \times$$
$$\times \{v_s(E_F) + (k_F^d/k_F^s)v_d(E_F) + f_c(k_F^d/k_F^s)^2 v_s(E_F)\}^{1/4},$$
$$R = 2q_F^s r \ , \ a = (k_F^s)^{-1}$$

Further the key idea is as follows. We find the numerical solution of the Schrodinger equation for the hydrogen atom in a field $\Phi(r)$ and obtain the corresponding spectrum of states, which could be continual or discrete in dependence upon the critical parameter $\zeta^{-1} = \alpha/a$ [8–10]. Such a problem for the potential (10) has been in details considered by Bonch-Bruevich and Glasko, Marinov and Popov and reconsidered by Lidorenko etal (look the reviews in [8–10,23,25,26]). In fig.1 the corresponding parameters α and a for a number of metals are presented [8]. The spectrum is continual, if $\zeta < 0,362$ and the corresponding material is a catalyst for the hydrogen ionization [27,28] reaction.

If $\zeta > \zeta o$, the spectrum is discrete (metal or metal alloy does not demonstrate catalytic activity for cited reaction). In refs. [9,10] such an approach has been successfully applied to studying the catalytic properties of the metals in relation to reaction of the hydrogen ionization and obtained a good agreement with the known experimental data [1,5–7].

Let us consider further more interesting case of the binary metallic alloys and present the corresponding model. In the binary metallic alloy the Fermi level position E_F as well as the corresponding state density $v(E_F)$, accompanied with electronic structure parameters α and a are changing under change of the admixture concentration c. To define the cited changing it is quite correct to use the Thomas-Fermi approach [23]. We suppose that the admixture's atoms volume has the

spherical form. The radius R_c is connected with concentration by the formula:

$$(qR_c)^{-3} = (qr_s)^{-3}c ,$$

where r_s — the electron gas characteristic parameter. Let us remind that $(qr_s)^{-3} \sim 0.01 - 0.05$ for the typical metals. For screened potential $V(r)$ near the admixture (if $|\Delta E_F - V| < E_F$), the corresponding Poisson equation looks as:

$$\Delta V(r) = q^2 \{V(r) - \Delta E_F\} \quad (11)$$
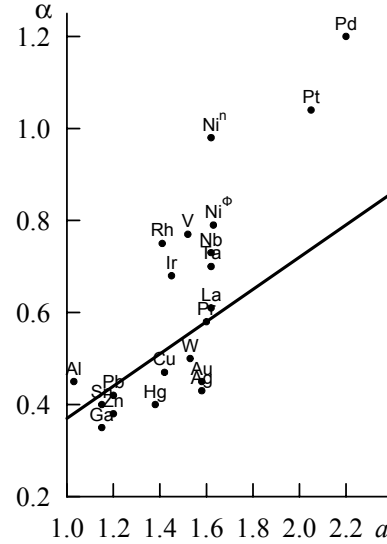
Fig.1. A diagram of parameters α, a for a number of metals

Elementary solution of equation (7) with the boundary conditions:

$$(dV/dr)_{Rc} = 0 , V(R_c) = 0, V \to -Z_v e/r , r \to 0$$

(here Z_v is a difference of the components valences) is defined as:

$$V(r,R_c) - \Delta E_F = [-Z_v e/r]\{qR_c ch[q(R_c - r)] +$$
$$+sh[q(R_c - r)]\}/[qR_c ch(qR_c) + sh(qR_c)] \quad (12)$$

Second boundary condition provides the expression for Fermi level shift in dependence upon the concentration c:

$$\Delta E_F = Z_v e^2 q /[qR_c ch(qR_c) + sh(qR_c)]. \quad (13)$$

So, for the binary metallic alloy, the value $v(E_P)$ is substituted by the value $v(E_P) = v(E_P) + \Delta v(E_P)$ [9]. In fact the parameters, which define the catalytic activity for metallic compounds, are directly dependent upon the components concentration. As example of the models application for definition of the catalytic activity of metallic alloy in relation of the hydrogen ionization reaction let us consider the alloy Ni-Cu. In fig.2 a dependence of the Fermi level shift ΔE_F in the alloy Ni-Cu upon the Cu concentration c (in atomic units) is presented and calculated according to Eq. (13).

The estimate shows that the alloy Ni-Cu with a small concentration of Cu (till 16%) is a good catalyst for the hydrogen ionization reaction, however situation is changed in the opposite direction with a growth of ζ. This is in acceptable agreement with the experimental data [1,5–7].

Fig. 2. A dependence of the Fermi level shift ΔE_F in the alloy Ni-Cu upon Cu concentration c (in atomic units) [9]

3. ELECTRODYNAMICAL AND QUANTUM-MECHANICAL MODEL FOR SEMICONDUCTOR

Now, we consider similar to above described one approach to description of catalytic processes on semiconductors and determine a connection between the semiconductors electron structure parameters and their catalytic activity in the relation to simple model reaction of the $H = H^+ + e$ type. Above proposed model is transformed through the following way. In order to describe the electronic structu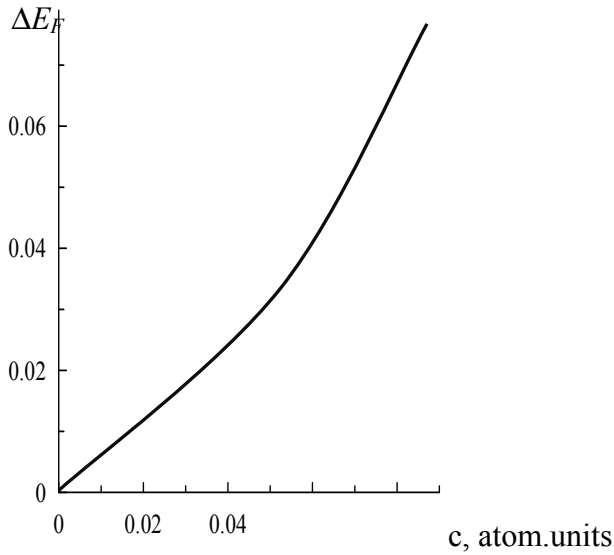re of semiconductor let us use the known Resta model [39] in the Thomas-Fermi theory for semiconductors (see [8]). We consider the model semiconductor as the electron gas with non-perturbed density n_0. The corresponding Poisson equation is as follows:

$$V(r) = q \{V(r) - A\},$$

where $q = 4k_F / \pi a_B$ and A is a constant. Let us suppose that there is the finite screening radius R near the probing charge Z_e and $n(R) = n_0$. Then a constant A is equal $V(R)$. Beyond the radius R the point charge Z_e potential is equal to:

$$V(R) = -Ze^2 / [\varepsilon(0) r], \; r > R,$$

where $\varepsilon(0)$ is a static dielectric permeability. Independent solution for the Poisson equation have the following form: $Ze^2 exp[qr]/r$. So, the general expression for potential energy is:

$$V(r) = - Ze^2 /r \{C_1 exp(-qr) +$$
$$+ C_2 exp(qr)\} + A, \; r < R \qquad (14)$$

Taking into account the continuity condition, boundary condition ($V(r) \rightarrow 0, \; r \rightarrow 0$), the expression for V (r) looks as follows:

$$V(r) = -\{Ze^2 /r\}\{ sh[q(R-r)]/ sh[qR] -$$
$$- Ze / \varepsilon(0)R, \; r < R \qquad (15)$$

The continuity condition for electric field under $r = R$ allows to define a link between the screening parameter and ε (0) as:

$$\varepsilon (0) = sh[qR]/qR.$$

If $\varepsilon(0) > 1$, R is equal to finite value comparable with distance to the nearest atoms (for example, for NiO, CuO, ZnO, ZnS, ZnTe semiconductors this value is 4.8−6.1E) [6]. The Schrodinger equation solution with potential (15) allows to define the corresponding energy spectrum in dependence upon the parameters $\varepsilon(0)$, $k_F (E_F)$ and then to find a link between the semiconductors electron structure parameters and their catalytic activity likely above described approach. Let us note here that a problem of definition of the hydrogen atom state energies in the static screened potential (in particular, the potential of the Debye type) approximation is well known in a theory of plasma and considered in many papers (see [23−26]). However, the potential (15) in this task is firstly considered by us. As an example of the approach application, we have carried out an estimate of the catalytic activity for the CuO, ZnO semiconductors in the hydrogen ionization (oxidation) reaction. Our estimate (the considered case for semiconductors is corresponding to the numerical estimate $\zeta < \zeta o$ for metals) shows that the ground level of the hydrogen atom in a case of the CuO and ZnO semiconductors is in a continuum, i.e. the known Mott effect has a place here [30]. In their turn this means that the the CuO and ZnO semiconductors are good catalysts for the hydrogen ionization reaction. This is in an excellent agreement with the known experimental data [1,5−7]. We believe that the simplified model for semiconductors may be naturally improved, but the key idea remains the same.

CONCLUSIONS

We presented the combined approach to estimating the catalytic activity of the metallic and semiconductor materials in the electron theory of catalysis, which is based on the combined quantum-mechanical and electrodynamical models. We have shown that even in the zeroth approximation very useful information about catalytic activity of the studied materials for some model reactions can be obtained within quite simple and physically reasonable approach. The catalytic properties of the semiconductor and metallic materials are directly connected with electronic processes which occur inside and on the surface of the materials and provide these properties in the end. In fact, our approach can be considered as an effective zeroth approximation in the electron theory of catalysis. It can also provide an evaluation of the charge exchange processes on a surface and, in such a way, could be used for the semiconductor sensors efficiency prediction for the given type reactions. Naturally, some additional factors such as the electrolyte influence, surface effects, the electrodes potential, the electrolyte type, electron concentration in the surface layer and many others [1−10] should be taken into account. Let us underline that very important and positive feature of the approach is clear quantitative physical correlation

between the electron structure parameters for metallic and semiconductor materials and their catalytic properties. On the other hand, naturally, the presented approach is the semi-quantitative one in more degree and surely can not provide a full quantitative description of the catalysis properties for any substances in relation to any reactions. More over it would be very useful further to link the elaborating approach with recent theory of the catalysis on the metals and semiconductors (not only by means of the eq. (3,4) and similar sufficiently complicated relationships) in order to provide more consistent, combined quantitative description of the complicated reactions on metals, metallic alloys, semiconductors. In any case we believe that the presented conception can be very useful in dealing with new challenges in the modern theory of catalysis, connected with direct electric or laser field effect on the catalytic processes on the surface of metallic and semiconductor materials (by means of the photoeffect, the Szilard-Chalmers type effects etc) and governing by these processes, carrying out new biocatalysts and studying related topics, searching new classes of the nanocluster catalysts) etc (see refs. in [31,32]). It is self-understood that the corresponding potentials should be modified in a case of the nano-cluster films (semiconductor heterostructures and superlattices; the Stark effect in nanocluster films). In this essence earlier developed quantum-mechanical methods (see [27,28]) can be easily and naturally combined with the presented approach.

References

1. Waite, R.E.; Bockris, J.; Conway, B. E. Modern Aspects of Electrochemistry (N-Y., Plenum Press) 1999, Vol.21; Fundamentals of Electrochemical Deposition, The Electrochemical Society Series, Ed. Paunovic, M. (N. — Y., John Wiley & Sons, Inc.) 2006.
2. Thomas, J.M.; Thomas, W. J. Principles and Practice of Heterogeneous Catalysis (N. — Y., Wiley-VCH) 1996; Richards, R. Surface and Nanomolecular Catalysis (N. — Y., CRC Press) 2006.
3. Stampfl C., Kreuzer H., Payne S., Scheffler M., Challenges in predictive calculations of processes at surfaces: surface thermodynamics and catalytic reactions//Appl. Phys. A. — 1999. — Vol.69. — P. 471–480.
4. Da Silva J. L.F., Stampfl C., Scheffler M., Adsorption of Xe Atoms on Metal Surfaces: New Insights from First-Principles Calculations//Phys.Rev.Lett. — 2003. — Vol.90. — P. 066104.
5. Austin, S. Material Solid State Batteries (Singapore, World Scientific) 1996; Electronic Phenomena in Adsorption and Catalysis on Semiconductors and Dielectrics, Springer Series in Surface Sciences, Eds. Kiselev, V. F.; Krylov, O.V. (Berlin, Springer) 1997, Vol.7.
6. Wolkenstein, F. F. Electron Processes on surface of semiconductors under chemosorbtion (Moscow, Pub. Nauka) 1991; Meylikhov, E.Z.; Lazarev S. D., Electrophysical properties of semiconductors (Moscow, Pub.Nauka) 1997.
7. Royter, V. A. Catalytic properties of substances (Moscow, Pub. Nauka) 1998.
8. Glushkov A. V., Kondratenko P. A., Lepikh Ya.I. , Fedchuk A. P., Svinarenko A. A., Lovett L., Electrodynamical and quantum — chemical approaches to modelling the electrochemical and catalytic processes on metals, metal alloys and semiconductors//Int. Journ. of Quantum Chemistry. — 2009. — Vol.109,N14. — P.3473–3481.
9. Glushkov A. V., Electron theory of Catalysis on Metallic Alloys: Electrodynamical model// Electrochemistry. — 1999. — Vol.27,N1. — P. 131–133; Electron theory of Catalysis on Metals: Quantum Chemical model// Electrochemistry. — 1998-Vol.29,N3. — P.369–376.
10. Glushkov A. V., Lepikh Ya.I., Fedchuk A. P., Khetselius O.Yu.,Electrodynamical and quantum –chemical modelling the electrochemical and catalytic processes on metals and semiconductors: Lanthanide perovskites// Photoelectronics. — 2008. — N17. — P.89–94.
11. Wilson, S. Handbook on Molecular Physics and Quantum Chemistry (Chichester, Wiley) 2007, 650p.; Glushkov, A. V. Relativistic Quantum Theory. Quantum Mechanics of Atomic Systems (Odessa, Astroprint, Odessa) 2008, 900p.
12. Slater, J. C. The self-Consistent Field Method for molecules and solids: Quantum theory of molecules and solids (N. — Y., McGraw-Hill) 1999.
13. Glushkov A. V., Parkhomenko V. D., Tcybulev P. N., Belous M. V., Katashinsky A. K., Bound States in Catalysis: New electrodynamical & quantum chemical models in electron theory of catalysis// Uzhgorod Univ. Sci. Herald. Series. Physics. — 2000. — Vol.8,N2. — P.361–365.
14. Kohn W., Sham L., Quantum density oscillations in an inhomogeneous electron gas//Phys. Rev.A. — 1995. — Vol.137. — P.1697–1710.
15. Advanced Topics in Theoretical Chemical Physics, Progress in Theoretical Chemistry and Physics, Eds. Maruani, J.; Lefebvre, R.; Brдndas, E. (Berlin, Springer) 2004, Vol.12.
16. The Fundamentals of Electron Density, Density Matrix and Density Functional Theory in Atoms, Molecules and the Solid State, Progress in Theoretical Chemistry and Physics, Eds. Gidopoulos, N.I., Wilson, S. (Berlin, Springer) 2004, Vol.14.
17. Li, W. — X.; Stampfl, C.; Scheffler, M., Why is a Noble Metal Catalytically Active? The Role of the O-Ag Interaction in the Function of Silver as an Oxidation Catalyst//Phys. Rev. Lett. — 2003. — Vol.90. — P.256102
18. Piccinin, S.; Stampfl, C.; Scheffler, M., First-principles investigation of Ag-Cu alloy surfaces in an oxidizing environment//Phys. Rev. B. — 2008. — Vol.77. — P.075426.
19. Masnou F., Philips N., Valiron P., Model potential calculations of the molecular system Na-Ne//Phys.Chem.Lett. — 1998. — Vol.41,N3. — P.395–398.
20. Glushkov A. V., Fedchuk A. P., Khetselius O.Yu., Heavy Elements , Relativistic SOC Effects in Catalysis Processes// Proc. European Science Foundation REHE School and Workshop on "Spin-Orbit Coupling in Chemical Reactions", (Poland), 1998. — P.11.
21. Glushkov A. V., A new approach in Electron theory of Catalysis: Electrodynamical and QuantumChemical models.Catalysis modeling in Plasma Chemical Reactors// Proc. 220th National Meeting of American Chemical Society: Catalysis and Plasma Technologies, Washington, (2000). — P. 221–224.
22. Glushkov A. V., New Approach in Electron Theory of Catalysis: Electrodynamical and Quantum Mechanical Models for binary metallic alloys// Proc.12th International Congress on Catalysis, Granada (Spain), 2000. — P.Th31.
23. Lundqvist, S.; March, N. Theory of Inhomogeneous Electron Gas (N-Y., Plenum Press) 1993,Ch.5.
24. Pines, D.; Nozieres, F. Theory of quantum liquids (N. — Y., Benjamin) 1966.
25. Two-dimensional electron systems. Eds. Maradulin, A.; Lozovik, Yu.E. (Amsterdam, North-Holland) 1996.
26. Kraeft, W. — D.; Kremp, D.; Ebeling, W.; Ropke G. Quantum statistics of charged particle systems (Berlin, Akad. — Verlag) 1996.
27. Glushkov A. V., Ivanov L. N., DC Strong-Field Stark-Effect: consistent quantum-mechanical approach // J.Phys.B:At. Mol.Opt.Phys. — 1999. — Vol.26,N16. — P.L379–389.
28. Glushkov A. V., Ambrosov S. V., Ignatenko A. V., Korchevsky D. A., DC Strong Field Stark Effect for Non-hydrogenic Atoms: Consistent Quantum Mechanical Approach // Int.Journ.Quant.Chem. — 2004. — Vol.99,N5. — P.936–939.
29. Resta, R., Density functionals in theory of semiconductors// Phys.Rev.B. — 1997. — Vol.16. — P.2717–2726.
30. Mott, N.F.; Metal-Insulator transitions, London, Taylor & Francis, 1994.
31. Glushkov A. V., Khetselius O.Yu., Malinovskaya S. V., New laser-electron nuclear effects in the nuclear γ transition spectra in atomic and molecular systems// Frontiers in Quantum Systems in Chemistry and Physics (Springer). — 2008. — Vol.18. — P.523–540.
32. Glushkov A. V., Khetselius O.Yu., Malinovskaya S. V., Optics and spectroscopy of cooperative laser-electron nuclear processes in atomic and molecular systems — New trend in quantum optics// Europ.Phys.Journ. ST. — 2008. — Vol.160,N1. — P.195–204.

A. P. Fedchuk, A. V. Glushkov, Ya.I. Lepikh

COMBINED ELECTRODYNAMICAL AND QUANTUM — CHEMICAL APPROACHES TO MODELLING THE CATALYTIC ACTIVITY OF METALS, METAL ALLOYS AND SEMICONDUCTORS

Abstract.
The catalytic activity definition for metals, binary metallic alloys and semiconductor materials is considered within the combined quantum mechanical and electrodynamics approach in the electron theory of catalysis.
Key words: catalytic properties, metals, binary metallic alloys, semiconductors

А. П. Федчук, А. В. Глушков, Я. И. Лепих

ЭЛЕКТРОДИНАМИЧЕСКИЙ И КВАНТОВОХИМИЧЕСКИЙ ПОДХОД К МОДЕЛИРОВАНИЮ КАТАЛИТИЧЕСКОЙ АКТИВНОСТИ МЕТАЛЛОВ, СПЛАВОВ

И ПОЛУПРОВОДНИКОВ

Резюме.
Изложен комбинированный электродинамический и квантово-химический подход в электронной теории катализа к моделированию электрохимических свойств и каталитической активности металлов, металлических сплавов и полупроводниковых материалов.
Ключевые слова: квантово-химический подход, каталитические свойства, металлы, металлические сплавы, полупроводники

О. П. Федчук, О. В. Глушков, Я. І. Лепіх

ЕЛЕКТРОДИНАМІЧНИЙ І КВАНТОВОХІМІЧНИЙ ПІДХІД ДО МОДЕЛЮВАННЯ КАТАЛІТИЧНОЇ АКТИВНОСТІ МЕТАЛІВ, СПЛАВІВ І НАПІВПРОВІДНИКІВ

Резюме.
Викладено комбінований електродинамічний та квантово-хімічний підхід в електронній теорії каталізу до моделювання електрохімічних властивостей та каталітичної активності металів, металічних сплавів і напівпровідникових матеріалів.
Ключові слова: квантово-хімічний підхід, каталітичні властивості, метали, металічні сплави, напівпровідники

T. N. ZELENTSOVA, T. B. TKACH, A. N. SHAKHMAN, I. N. SERGA

Odessa National Polytechnical University, Dept. Nucl. Phys., Shevchenko Av., 1, Odessa, 65044, Ukraine
Odessa State Environmental University, L'vivskaya str., 15, Odessa, 65009, Ukraine
Kherson State University
e-mail: nucserga@mail.ru

ENERGY APPROACH TO POSITRON COLLISIONAL EXCITATION AND IONIZATION OF MULTIELECTRON RYDBERG ATOMS

Within the energy approach (S-matrix formalism) it is presented a new basis approach to positron collisional ionization of the Rydberg multi-electron atoms in the quantum defect approximation.

1. INTRODUCTION

In this paper we firstly give the QED interpretation of the such physically interesting and very complicated phenomenon as positron collisional excitation and ionization of the multi-electron atoms in Rydberg states. Considered will be processes, which lead to single (outer shell) ionization of the multielectron atom. Positron impact can lead to ionization via two reaction channels usually called break up (of the atom into an electron and ion) and transfer of one atomic electron to the projectile to form positronium. The most accurate positron ionization cross sections for example, for helium are presented in [1] and analysed in comparison with that for electron impact ionization. It should be noted that the features of particular interest are the merging of the cross sections above 600 eV when the first Born approximation is valid, the positron cross section exceeding the electron cross section at medium energies and a cross over of the cross section curves near threshold.

Let us remember that the modern quantum theory of atomic systems can be considered as a fundamental basis for treating a wide cycle of phenomena, including the excitation, photoionization, radiation and autoionization decay etc. [1−21]. In the last years a great success has been achieved in the applied atomic , nuclear, and laser physics, quantum and photo-electronics. Naturally, for more than 80 years, the theory of collisional ionization was developing and considering mainly the ground states and lowest excited states in usual neutral atoms, beginning from the hydrogen one. But a great progress in experimental laser physics and appearance of the so called tunable lasers allow to get the highly excited Rydberg states of atoms. In fact this is a beginning of a new epoch in the atomic physics regarding the Rydberg atoms [1−8]. The experiments with Rydberg atoms had very soon resulted in the discovery of an important ionization mechanism, provided by unique features of the Rydberg atoms. Relatively new topic of the modern theory is connected with consistent treating the positron-collisional ionization of the Rydberg atoms [1−5]. From the theoretical point of view, the positron collisional effect can essentially affect on the Rydberg states in atoms. In the last years there is appearing a sufficiently great number of papers devoted to the electron collisional ionization of the Rydberg atoms within the non-relativistic

and relativistic approaches (look refs. [1−21]). Usually the standard methods of atomic physics, including the Hartree-Fock, Dirac-Fock, different model potential schemes, R-matrix and energy approaches etc [1−4] were used in order to define the electron-collisional ionization characteristics of neutral and even Rydberg atoms. In our opinion the significant advantage of the simple model potential and quantum defect approached (non-relativistic schemes) in comparison with other methods and, particularly, other model potentials is the possibility of presenting analytically, in terms of the hypergeometric functions, the quantitative characteristics for arbitrarily high orders, related to both bound−bound and bound−free transitions. From the other side, the heavy Rydberg atomic systems and corresponding collisional phenomena should be considered within strictly relativistic theory. Here we present new combined quantum defect method and energy approach to definition of the positron-collisional excitation and ionization characteristics of the Rydberg atoms. The important feature of new theory is implementation of the quantum defect approximation to the S-matrix energy formalism. This provides sufficiently correct and simultaneously simplified numerical procedure to definition of the corresponding collisional ionization properties. Naturally, the similar formulation is in many aspects similar to the corresponding electron impact ionization phenomenon. More over, as starting basis we use the energy approach to QED theory of multi-particle relativistic atoms by Glushkov-Ivanov [4, 11,12] and earlier developed by us theory of the electron-Rydberg atoms collisional phenomena [20,21].

2. POSITRON COLLISIONAL IONIZATION OF THE RYDBERG ATOMS: ENERGY APPROACH

As in refs. [13,14,20], for definiteness, we consider the highly excited Rydberg states $1s^2 2s^2 2p^5 nl$ (n>>3) of the Ne-like ion, which can be treated as two-quasi-particle (2QP) states. It is usually accepted, as the bare potential, a potential including the electric nuclear potential V_N and some parameterized potential V_C, that imitates the interaction of closed-shell electrons with quasi-particles. The parameters of the model

bare potential are chosen so as to generate accurate eigen-energies of all one-quasi-particle (1QP) states, i.e. $2s2p^6$, $2s^22p^5$ states of the F-like ion and $2s^22p^6nl$ states of Na-like ions, with the same nucleus. Usually the experimental one-quasi-particle energies are used for determination of parameters of the model potential (look refs. [4,10,11]). Naturally (look below) the quantum defect approximation is very effective here as it provides the hydrogen-like approximation for the corresponding wave functions.

The energy approach in scattering theory [4,11–14] and the masters formulas are applicable here, but there is a key difference. Consider as an example, the positron-collisional excitation of the Rydberg Ne-like ion: $((2j_{iv})^{-1}3j_{ie}[J_iM_i], \varepsilon_{in}) \rightarrow (\Phi_o, \varepsilon_{sc})$. Here Φ_o is the state of the ion with closed shells (ground state of the Ne-like ion); J_i is the total angular moment of the initial target state; indices *iv, ie* are related to the initial states of vacancy and electron; indices ε_{in} and ε_{sc} are the incident and scattered energies, respectively to the incident positron and scattered positron (electron). It is convenient to use the second quantization representation. In particular, the initial state of the system "atom plus free electron" can be written as

$$|I> = a_{in}^+ \sum_{m_{iv}, m_{ie}} a_{ie}^+ a_{iv} \Phi_o C_{m_{ie}, m_{iv}}^{J_i, M_i} \qquad (1)$$

Here $C_{m_{ie}, m_{iv}}^{J_i, M_i}$ is the Clebsh-Gordan coefficient. Final state is: $|F> = a_{sc}^+ \Phi_o$, where Φ_o is the state of an ion with closed electron shells (ground state of Ne-like ion), $|I>$ represents three-quasiparticle (3QP) state , and $|F>$ represents the one-quasiparticle (1QP) state. For the state (1) the scattered part of energy shift *Im ΔE* appears first in the PT second order in the form of integral over the scattered positron energy ε_{sc}:

$$\int d\varepsilon_{sc} G(\varepsilon_{iv}, \varepsilon_{ie}, \varepsilon_{in}, \varepsilon_{sc}) / (\varepsilon_{sc} - \varepsilon_{iv} - \varepsilon_{ie} - \varepsilon_{in} - i0) \quad (2)$$

with

$$Im\Delta E = \pi G(\varepsilon_{iv}, \varepsilon_{ie}, \varepsilon_{in}, \varepsilon_{sc}) \qquad (3)$$

Here *G* is a definite squired combination of the two-electron matrix elements (2). The value $\sigma = -2 Im\Delta E$ represents the collisional cross-section if the incident positron eigen-function is normalized by the unit flow condition and the scattered particle eigenfunction is normalized by the energy δ function. The collisional strength $\Omega(I \rightarrow F)$ is connected with the collisional cross section σ by expression (c.f. [4,14]):

$$\sigma(I \rightarrow F) =$$
$$= \Omega(I \rightarrow F) \cdot \pi / \{(2J_i + 1)\varepsilon_{in}[(\alpha Z)^2 \varepsilon_{in} + 2]\} \qquad (4)$$

Here and below the Coulomb units are used; 1 C.u. $\approx 27,054 Z^2$ eV, for energy; 1 C.u.$\approx 0,529 \cdot 10^{-8}/Z$ cm, for length; 1 C.u. $\approx 2,419 \cdot 10^{-17}/Z^2$ sec for time. The collisional de-excitation cross section is:

$$\sigma(IK \rightarrow 0) =$$
$$= 2\pi \sum_{j_{in}, j_{sc}} (2j_{sc} + 1)\{\sum_{j_{ie}, j_{iv}} <0|j_{in}, j_{sc}|j_{ie}, j_{iv}, J_i > B_{ie,iv}^{IK}\}^2 \quad (5)$$

Here $B_{ie,iv}^{IK}$ is a real matrix of eigen-vectors coefficients, which is obtained after diagonalization of the secular energy matrix. The amplitude like combination in (8) has the following form:

$$<0|j_{in}, j_{sc}|j_{ie}, j_{iv}, J_i >=$$
$$= \sqrt{(2j_{ie} + 1)(2j_{iv} + 1)}(-1)^{j_{ie}+1/2} \times \sum_\lambda (-1)^{\lambda + J_i} \times$$
$$\times \{\delta_{\lambda, J_i} / (2J_i + 1)Q_\lambda(sc, ie; iv, in) +$$
$$+ \begin{bmatrix} j_{in}...j_{sc}...J_i \\ j_{ie}...j_{iv}.....\lambda \end{bmatrix} Q_\lambda(ie; in; iv, sc)\} \qquad (6)$$

In (6) values Q_λ are defined in ref. [4]. For the collisional excitations from ground state (inverse process) one must consider $a_{in}^+ \Phi_0$ as the initial state and

$$|F> = a_{sc}^+ \sum_{m_{fe}, m_{fv}} a_{fe}^+ a_{fv} \Phi_o \tilde{C}_{m_{fe}, m_{fv}}^{J_f, M_f} \quad (7)$$

as a final state. The cross-section is as follows:

$$\sigma(0 \rightarrow IF) = 2\pi(2J_f + 1) \sum_{j_{in}, j_{sc}} (2j_{sc} + 1) \cdot$$
$$\cdot \{\sum_{j_{fe}, j_{fv}} B_{fe,fv}^{FK} < j_{fe}, j_{fv}J_f | j_{in}, j_{sc} | 0 >\}^2 \qquad (8)$$

To calculate the corresponding parameters, one should use the relativistic expressions for quantum defect approximation wave functions. As it was indicated, the heavy Rydberg atomic systems should be considered within strictly relativistic theory.

3. QUANTUM DEFECT APPROXIMATION FOR RYDBERG ATOMS

In order to simple and accurately treat the Rydberg multi-electron atoms it is useful to apply the known quantum defect approximation by Seaton et al (see refs. [1. 20,21]) and implement it to the scheme for calculation the collisional excitation (ionization) cross-sections. Let us give the master formulas of this approximation in application to our task. The general expression for the wave function can be presented in a standard form as follows:

$$\Psi(\Gamma PJM) = \sum_r^{NCF} c_r \Phi(\gamma_r PJM) \qquad (9)$$

which should be received from the self-consistent solutions of the Dirac type quantum-defect equations. Configuration mixing coefficients c_r are usually obtained through diagonalization of the Dirac-Coulomb Hamiltonian, which is chosen by us in the following form [4]:

$$H_{DC} = \Sigma_i [c\alpha_i p_i + (\beta_i - 1)c^2 -$$
$$- V(r|nlj)] + \Sigma_{i>j} \exp(i\omega r_{ij})(1 - \alpha_1 \alpha_2)/r_{ij} \qquad (10)$$

where α_i, β are the Dirac matrices. The potential in H_{DC} contains the electrical potential of a nucleus, the electron self-consistent potential and the potential of exchange inter-electron interaction. In the quantum defect approximation the one-particle wave functions are found from solution of the relativistic Dirac equation, which can be written in the central field in a two-component (*f,g*) form [4]:

$$f' = -(\chi + |\chi|)f/r - \alpha ZVg - (\alpha Z E_{n\chi} + 2/\alpha Z)g \quad (11)$$

$$g' = (\chi - |\chi|)g/r - \alpha ZVf + \alpha Z E_{n\chi} f \qquad (12)$$

Here the Coulomb units (C.u.) are used; $E_{n\chi}$ is one-electron energy without the rest energy and other notations are standard. In the quantum defect approximation to describe a spectrum of the Rydberg atom it is usually used the simple formula:

$$E_{alk} = -\frac{1}{2n_{eff}^2} = -\frac{1}{2(n-\delta_l)^2} \ , \ n \in N \qquad (13)$$

where n_{eff} — effective quantum number, δ_l — quantum defect, which is dependent upon the orbital quantum number. Usually to reach a high accuracy in definition of the quantum defect it is used an expansion (the known Ritzs formula):

$$\delta_l = \delta_l^{(0)} + \sum_{i=1}^{M} \delta_l^i E^i \qquad (14)$$

From the physical point of view, for the bound states a quantum defect defines an effect of the non-Coulomb part of the atomic potential in multi-electron system. For the scattering states a role of the quantum defect belongs to the asymptotic phase shift τ. According to the Siton theorem , a link between phase shift and quantum defect is given by [1]:

$$\tau = \delta_l \cdot \pi \qquad (15)$$

Further it is non-difficult to present the Dirac equations (11) or (12) in the quantum defect approximation. Really, in this case the potential $V_{at} = -1/r$ for $r > r_0 > 0$ (r_0 is a radius of the atomic core, for example in the F-,Ne-,Na-like ions). Naturally for the bound states the corresponding components, for example, $F(r) \to 0$ under $r \to \infty$. For large values of r the corresponding functions are satisfying to the asymptotics as follows:

$$f(E,l,r) \to u(m.l.r)\sin(\pi m) - v(m,l,r)e^{i\pi m} \ , \ (16a)$$

$$g(E,l,r) \to -u(m.l.r)\sin(\pi m) + v(m,l,r)e^{i\pi(m+1/2)} \quad (16b)$$

where u,v are respectively exponentially increasing and decreasing functions. Naturally to get asymptotically exponentially decreasing function a multiplier u in (16) must reach to zero, i.e. it is correct a condition:

$$\sin(\tau + \pi m) = \sin(\tau + \pi\sqrt{-1/2E}\,) = 0 \qquad (17)$$

Finally for the bound state, the correctly normalized solution is as follows:

$$F_{l,E_{alk}}(r) = \cos(\pi\delta_l)s_l(E_{alk},r) + \sin(\pi\delta_l)c_l(E_{alk},r) \quad (18)$$

where $E_{alk} = E$ and the functions s_l, c_l represent the normalized (on energy) regular and non-regular Coulomb functions. Further using the quantum defect approximation functions in the energy approach scheme to calculating the positron-collisional excitation (ionization) of the Rydberg atoms is the same as in the initial version of the method [4] (see also details in refs. [20,21]).

4. CONCLUSIONS

Thus, here we have presented a new combined quantum defect method and energy approach to definition of the positron-collisional excitation and ionization characteristics of the Rydberg atoms. The key feature of the presented basis theory is an implementation of the quantum defect approximation into the frames of the S-matrix energy formalism to positron-Rydberg muilti-electron atom collisional system. Obviously, this will provide sufficiently correct and simultaneously simplified numerical procedure to definition of the corresponding collisional excitation and ionization properties and thus it is represented significantly more advantagable in comparison with the cumbersome Hartree-Fock and Dirac-Fock methods [1−4]. Naturally, from the one side, the task considered has to be more simple in comparison the similar electron-collisional problem (absence of the exchange) [1−4,6,7,20], but, from another side, one should take into account different channels of decay, including the transferring one ionized atomic electron to the projectile to form positronium (look, for example, [1,2,5]). As result, a theoretical description of the multi-body collisional system and correspondingly some expressions will become more complicated.

In conclusion the authors would like to thank Professors V. D.Rusov, A. V. Glushkov, V. N. Pavlovich, V. N. Vysotsky for useful comments.

References

1. Atoms in astrophysics, Eds. Burke P. G., Eissner W. B., Hummer D. G., Persival L. C. — N. — Y., Plenum Press. — 1994. — 340P.
2. Photonic, Electronic and Atomic Collisions. Eds. F.Aumar, H.Winter, World Sci., Singapore. — 2007. — 650P.
3. Grant I. Relativistic Quantum Theory of Atoms and Molecules. — Oxford, 2007–650P.
4. Glushkov A. V., Relativistic quantum theory. Quantum mechanics of atomic systems. — Odessa: Astroprint, 2008. — 900P.
5. Mukherjee T., Sarkar N. K., Ro-vibrational close coupling study of positron−hydrogen molecule scattering using the parameter-free model correlation polarization potential// J. Phys. B: At. Mol. Opt. Phys. — 2008. — Vol.41. — P.125201.
6. Rosenberg L., Relativistic theory of electron-impact ionization//J. Phys. B: At. Mol. Opt. Phys. — 2010. — Vol.43. — P.065203.
7. Archubi C D , Montanari C. C., Miraglia J. E., Many-electron model for multiple ionization in atomic collisions// J. Phys. B: At. Mol. Opt. Phys.. — 2007. — Vol.40. — P.943–954.
8. Grutter M., Zehnder O., Softley T. P., Merkt F., Spectroscopic study and multichannel quantum defect theory analysis of the Stark effect in Rydberg states of neon// J. Phys. B: At. Mol. Opt. Phys. — 2008. — Vol.41. — P.115001. — 11p.
9. Zelentsova T. N., Perelygina T. B., Thermal photoionization of the Rydberg atoms by the blackbody radiation: New relativistic approach// Sensor Electr. and Microsyst. Techn. — 2009. — N4. — P.11–16.
10. Ivanova E. P., Ivanov L. N., Aglitsky E. V., Modern Trends in Spectroscopy of multi-charged IonsPhysics Rep. — 1998. — Vol.166,N6. — P.315–390
11. Glushkov A. V., Ivanov L. N. Radiation Decay of Atomic States: atomic residue and gauge non-invariant contributions // Phys. Lett.A. — 1997-Vol.170,N1. — P.33–37.
12. Glushkov A. V., Energy Approach to Resonance states of compound super-heavy nucleus and EPPP in heavy nucleus collisions// Low Energy Antiproton Physics. AIP Serie. — 2005. — Vol.796. — P.206–210.
13. Glushkov A. V., Rusov V. D., Ambrosov S. V., Loboda A. V. Resonance states of compound super-heavy nucleus and EPPP in heavy nucleus collisions // In: New projects and new lines of research in nuclear physics.Eds. G.Fazio, F.Hanappe, Singapore : World Scientific. — 2003. — P.126–132.
14. Glushkov A. V., Ambrosov S. V., Loboda A. V., Gurnitskaya E. P., Prepelitsa G. P., Consistent QED approach to

calculation of electron-collision excitation cross-sections and strengths: Ne-like ions // Int. Journ.Quant.Chem. — 2005. — Vol.104, N4 . — P. 562−569.

15. Zelentzova T. N., Malinovskaya S. V., Dubrovskaya Yu.V., The atomic chemical environment effect on the β decay probabilities: Relativistic calculation//Bulleten of Kiev Univ. Serie Phys. — Math. — 2004. — №4 . — C.427−432.

16. Benvenuto F., Casati G., Shepelyansky D., Rydberg Stabilization of atoms in strong fields: "magic" mountain in chaotic sea// Z.Phys.B. — 1999. — V.94. — P.481−486.

17. Safronova U. I., Safronova M. S., Third-order relativistic many-body calculations of energies, transition rates, hyperfine constants, and blackbody radiation shift in ^{171}Yb$^+$//Phys. Rev. A. — 2009. — Vol.79. — P.022512.

18. Dorofeev D. L., Zon B. A., Kretinin I. Y., Chernov V. E., Method of the quantum defect Green's function for calculation of dynamic atomic polarizabilities// Opt. Spectr. — 2005. — Vol. 99. — P. 540−548.

19. Badnell N. R., Calculations for electron-ion collisions and photoionization processes for plasma modeling// J.Phys. CS. — 2007. — Vol.88. — P.012070−1--012070−8.

20. Zelentsova T. N., Lopatkin Yu.M., Nikola L. V., Perelygina T. B., Seredenko S. S., Energy approach to collisional ionization of the Rydberg atoms: Quantum defect approximation// Sensor Electr. and Microsyst. Techn. — 2010. — N1. — P.14−18.

21. Zelentsova T. N., Perelygina T. B., Thermal photoionization of the Rydberg atoms by the blackbody radiation: New relativistic approach// Sensor Electr. and Microsyst. Techn. — 2009. — N4. — P.5−11.

T. N. Zelentsova, T. B. Tkach, A. N. Shakhman, I. N. Serga

ENERGY APPROACH TO POSITRON COLLISIONAL EXCITATION AND IONIZATION OF MULTIELECTRON RYDBERG ATOMS

Abstract.
Within the energy approach (S-matrix formalism) it is presented a new basis approach to positron collisional ionization of the Rydberg multi-electron atoms in the quantum defect approximation .
Key words: positron collisional ionization, energy approach, Rydberg atoms

Т. Н. Зеленцова, Т. Б. Ткач, А. Н. Шахман, И. Н. Серга

ЭНЕРГЕТИЧЕСКИЙ ПОДХОД К ОПИСАНИЮ ПОЗИТРОН-СТОЛКНОВИТЕЛЬНОЙ ИОНИЗАЦИИ МНОГОЭЛЕКТРОННЫХ РИДБЕРГОВСКИХ АТОМОВ

Резюме.
В рамках энергетического подхода (S-матричный формализм) изложены основы нового теоретического метода описания позитрон-столкновительной ионизации многоэлектронных ридберговских атомов в приближении квантового дефекта.
Ключевые слова: позитрон- столкновительная ионизация, энергетический подход, ридберговские атомы

Т. М. Зеленцова, Т. Б. Ткач, А. М. Шахман, І. М. Сєрга

ЕНЕРГЕТИЧНИЙ ПІДХІД ДО ОПИСУ ІОНІЗАЦІЇ ЗА РАХУНОК ЗІТКНЕННЯ З ПОЗИТРОНОМ БАГАТОЕЛЕКТРОННИХ РІДБЕРГІВСЬКИХ АТОМІВ

Резюме.
В межах енергетичного підходу (S-матричний формалізм) викладені основи нового теоретичного методу опису іонізації багатоелектронних рідбергівських атомів за рахунок зіткнення з позитроном у наближенні квантового дефекту.
Ключові слова: іонізація за рахунок зіткнення з позитроном, енергетичний підхід, рідбергівські атоми

D. E. SUKHAREV, YU. V. DUBROVSKAYA, A. A. SVINARENKO

Odessa National Polytechnic University, Dept. Nucl. Phys., Shevchenko Av., 1
Odessa State Environmental University
e-mail: quantsvi@mail.ru

SENSING STRONG INTERACTION EFFECTS IN X-RAY SPECTROSCOPY OF KAONIC ATOMS

The theoretical studying the strong interaction shifts and widths from X-ray spectroscopy of some kaonic atomic systems is fulfilled. Sensing the strong interaction effects and theoretical estimating spectra of kaon atoms is considered as a new tool for studying nuclear structure and strong K-nucleus interaction.

1. INTRODUCTION

At present time studying the hadronic, in particular, kaonic atomic systems (pionic, muonic etc atoms) is of a great importance for further the development of atomic and nuclear theories and sensing the nuclear structure (fundamental kaon, pion-nucleus strong interactions) and carrying out new low-energy X-ray standards [1−16]. Besides, it is attractable due to the possibilities to evaluate the kaon etc mass using high accuracy X-ray spectroscopy. The spectroscopy of kaonic hydrogen allows to study the strong interaction at low energies by measuring the energy and natural width of the ground level with a precision of few meV [1−5]. The collaborators of the E570 experiment [6,7] measured X-ray energy of a kaonic helium atom, which is an atom consisting of a kaon (a negatively charged heavy particle) and a helium nucleus. Batty et al [4] had performed theoretical and experimental studying the strong- interaction effects in spectra of high Z kaonic atoms. These authors had applied the naпve phenomenological optical model estimates. Now new exciting experiments are been preparing in order to make sensing the strong interaction effects in other hadronic atoms. It is known that the shifts and widths due to the strong interaction can be systematically understood using phenomenological optical potential models. Nevertheless, one could mention a large discrepancy between the theories and experiments on the kaonic helium 2p state. A large repulsive shift (about -40 eV) has been measured by three experimental groups in the 1970's and 80's, while a very small shift (< 1 eV) was obtained by the optical models calculated from the kaonic atom X-ray data with Z>2 [1−6]. This significant disagreement (a difference of over 5 standard deviations) between the experimental results and the theoretical calculations is known as the "kaonic helium puzzle". A possible large shift has been predicted using the model assuming the existence of the deeply bound kaonic nuclear states. However, even using this model, the large shift of 40 eV measured in the experiments cannot be explained. A re-measurement of the shift of the kaonic helium X-rays is one of the top priorities in the experimental research activities. In the theory of the kaonic and pionic atoms there is an important task, connected with a direct calculation of the X-ray transition energies within consistent relativistic quantum mechanical atomic and nuclear theory methods. The standard way is based on solution of the Klein-Gordon equation, but there are many important problems connected with accurate accounting for as kaon-nuclear strong interaction effects as QED radiative corrections (first-ly, the vacuum polarization effect etc.) [1−5]. This topic has been a subject of intensive theoretical and experimental interest (see [12−20]). In refs. [5,10] it has been developed an effective ab initio scheme to the Klein-Gordon equation solution and further definition of the X−ray spectra for multi-electron kaonic atoms with an account of the nuclear, radiative effects. The theoretical studying the strong interaction shifts and widths from X-ray spectroscopy of kaonic atoms (U, Pb etc) was fulfilled. In this paper, which goes on our work [5,10,21], we study some transitions in the X-ray spectra of lithium, sodium etc.

2. THE KLEIN-GORDON EQUATION APPROACH IN THE KAONIC ATOM THEORY

As the key moments of the used approach to studying the spectra for multi-electron kaonic atoms with an account of nuclear and radiative effects are earlier in details described [10,21]), here we are limited only by the master equations. The wave functions of the zeroth approximation for kaonic atoms are found from the Klein-Gordon equation [5]:

$$m^2 c^2 \Psi(x) = \{\frac{1}{c^2}[i\hbar\partial_t + eV_0(r)]^2 + \hbar^2\nabla^2\}\Psi(x), \quad (1)$$

where h is the Planck constant, c the velocity of the light and the scalar wavefunction $\Psi_0(x)$ depends on the space-time coordinate x = (ct,r). Here it is considered a case of a central Coulomb potential ($V_0(r)$, 0). A usually, We consider here the stationary solution of Eq. (1). In this case, we can write:

$$\Psi (x) = \exp(-iEt/\hbar)\phi(x) \quad (2)$$

and Eq. (1) becomes:

$$\{\frac{1}{c^2}[E + eV_0(r)]^2 + \hbar^2\nabla^2 - m^2 c^2\}\phi(x) = 0 \quad (3)$$

where E is the total energy of the system (sum of the mass energy mc² and binding energy ε_0). In principle,

the central potential V_0 should include the central Coulomb potential, the vacuum-polarization potential as well as the kaon-nucleus strong interaction potential (optical model potential). Earlier we have calculated some characteristics of hydrogen-like and other multi-electron ions with using the nuclear charge distribution in the form of a uniformly charged sphere and Gaussian form (c.f. [19–21]). The advantage of the Gaussian form nuclear charge distribution is provided by using the smooth function instead of the discontinuous one as in the model of a uniformly charged sphere [22]. It is obvious that it simplifies the calculation procedure and permits to perform a flexible simulation of the real distribution of the charge in a nucleus. In last years to define the nuclear potential it is usually used the Fermi model for the charge distribution in the nucleus $\rho(r)$ (c.f.[21]):

$$\tilde{n}(r) = \tilde{n}_0 / \{1 + \exp[(r-c)/a)]\} \qquad (4)$$

where the parameter $a=0.523\ fm$, the parameter c is chosen by such a way that it is true the following condition for average-squared radius: $<r2>1/2=(0.836 \cdot A1/3 + 0.5700)fm$. Further let us present the formulas for the finite size nuclear potential and its derivatives on the nuclear radius. If the point-like nucleus has the central potential $W(R)$, then a transition to the finite size nuclear potential is realized by exchanging W(r) by the potential [18]:

$$W(r|R) = W(r)\int_0^r dr\, r^2 \rho(r|R) + \int_r^\infty dr\, r^2 W(r)\rho(r|R). \quad (5)$$

We assume it as some zeroth approximation. Further the derivatives of various characteristics on R are calculated. They describe the interaction of the nucleus with outer electron; this permits recalculation of results, when R varies within reasonable limits. The Coulomb potential for the spherically symmetric density $\rho(r|R)$ is:

$$V_{nucl}(r|R) = -((1/r)\int_0^r dr'\, r'^2 \rho(r'|R) + \int_r^\infty dr'\, r'\rho(r'|R) \quad (6)$$

It is determined by the following system of differential equations [18]:

$$V'nucl(r,R) = (1/r^2)\int_0^r dr'\, r'^2 \rho(r',R) \equiv (1/r^2) y(r,R)$$

$$y'(r,R) = r^2 \rho(r,R) \qquad (7)$$

$$\tilde{n}'(r) = (\tilde{n}_0/a)\exp[(r-c)/a]\{1+\exp[(r-c)/a]\}^2$$

with the boundary conditions:

$$V_{nucl}(0,R) = -4/(\pi r)$$

$$y(0,R) = 0\,, \qquad (8)$$

$$\tilde{n}(0) = \tilde{n}_0 / \{1 + \exp[-c/a]\}$$

The new important topic is connected with a correct accounting the radiation QED corrections and, first of all, the vacuum polarization correction. Procedure for an account of the radiative QED corrections in a theory of the multi-electron atoms is given in detail in refs. [5,18]. Regarding the vacuum polarization

effect let us note that this effect is usually taken into account in the first PT order by means of the Uehling potential:

$$U(r) = -\frac{2\alpha}{3\pi r}\int_1^\infty dt\, \exp(-2rt/\alpha Z)(1+1/2t^2)\frac{\sqrt{t^2-1}}{t^2} \equiv$$

$$\equiv -\frac{2\alpha}{3\pi r}C(g), \qquad (9)$$

where $g = \frac{r}{\alpha Z}$. In our calculation we usually use more exact approach. The Uehling potential, determined as a quadrature (9), may be approximated with high precision by a simple analytical function. The use of new approximation of the Uehling potential [18] permits one to decrease the calculation errors for this term down to 0.5 — 1%. Besides, using such a simple analytical function form for approximating the Uehling potential allows its easy inclusion into the general system of differential equations.

3. ESTIMATE OF THE STRONG INTERACTION EFFECT CONTRIBUTION

As it is well known, the nuclear absorption is defined by the strength of the strong interaction and overlapping the kaonic atomic wave function with the nuclear ones. The widespread approach to treating the strong interaction between the nucleus and orbiting kaon is in using the phenomenological optical potential of the following form [1,5,10]:

$$V_N = -\frac{2\pi}{\mu}[1+\frac{M_K}{M_N}][A_{Kp}\rho_p(r)+A_{Kn}\rho_n(r)], \quad (10)$$

where μ is the kaon-nucleus reduced mass, M_K and M_N are the kaon and nucleon masses, $\rho_p(r), \rho_n(r)$ are the proton and neutron densities in the nucleus and A_{Kp}, A_{Kn} are the corresponding complex effective *Kp* and *Kn* scattering lengths. It si well known the Batty simplifying assumption of the following kind [4]:

$$V_N = -\frac{2\pi}{\mu}[1+\frac{M_K}{M_N}][a\rho(r)]\,,$$

where *a* is the effective averaged K-nucleon scattering length. Batty et al had analyzed the previous kaon data and found the acceptable value for the a length is as follows [4]:

$$a=[(0.34\pm0.03)+i(0.84\pm0.03)]\ (fm).$$

The presented value of the length a has been indeed chosen to describe the low and middle Z nuclei [4]. The disadvantage of the usually used approach is connected with approximate definition of the proton and neutron densities and using the effective averaged K-nucleon scattering length. More correct approach is in the relativistic mean-field (RMF) model for the ground-state calculation of the nucleus. The RMF model has been designed as a renormalizable meson-field theory for nuclear matter and finite nuclei [20]. The realization of nonlinear self-interactions of the scalar meson led to a quantitative description of nuclear ground states. As a self-consistent mean-field

model (for a comprehensive review see ref. [19,20]), its ansatz is a Lagrangian or Hamiltonian that incorporates the effective, in-medium nucleon-nucleon interaction. As a Kohn-Sham scheme, the RMF model can incorporate certain ground-state correlations and yields a ground-state description beyond the literal mean-field picture. RMF models are effective field theories for nuclei below an energy scale of 1GeV, separating the long- and intermediate-range nuclear physics from short-distance physics, involving, i.e., short-range correlations, nucleon form factors, vacuum polarization etc, which is absorbed into the various terms and coupling constants. In our opinion, the most effective parameterization is available in the NL3-NLC scheme (see details in refs. [5,20]), which is used by us.

4. RESULTS AND CONCLUSIONS

In ref. [5,21] we have listed some calculation data for a set of kaonic atom (H, N, U, Pb etc)transitions. Here we present the same data for the Li-,K-, and W- systems. In table 1 we present the calculated electromagnetic (EM) X-ray energies of kaonic atoms for transitions between circular levels. The transitions are identified by the initial (n_i) and final (n_f) quantum numbers. The calculated values of transition energies are compared with available measured (E_m) and other calculated (E_c) values [1−7]. In a case of the close agreement between theoretical and experimental data, the corresponding levels are less sensitive to strong nuclear interaction. In the opposite case one could point to a strong-interaction effect in the exception cited above.

Table 1

Calculated (E_c) and measured (E_m) kaonic atoms X-ray energies (in keV)

Nucl.	Transition	E_c,our theor	E_c, [4]	E_c [6]	E_c [7]	E_m
Li	3−2	15.335	15.392	15.319	15.330	15.320 (24) 15.00 (30)
K	5−4	105.962	105.970	-	105.952	105.86 (28)
W	8−7	346.572	346.54	-	-	346.624(25)
W	7−6	535.136	535.24	-	-	534.886(92)

Note: the kaon mass was assumed to be 493.677±0.013MeV [11].

In table 2 we present the calculated (C) and measured (M) strong interaction shifts ΔE and widths G (in keV) for the kaonic atoms X-ray transitions. The subscripts M and C stands for measured and calculated values correspondingly. The width G is the strong width of the lower level which was obtained by subtracting the electromagnetic widths of the upper and lower level from the measured value. The shift ΔE is defined as difference between the measured E_M and calculated E_{EM} (electromagnetic) values of transition energies; the calculated value is obtained by direct solving the equation (1) with kaon-nuclear potential. Besides, the measured values by Miller et al and Cheng et al (from refs. [1,4] are listed in table 2 too. It should be noted that Cheng et al did not make any energy calibration above the 511 e^+ annihilation and Batty et al [4] indicated that the corresponding difference between the energy values is not serious. In whole this work allows to conclude that the measured strong interaction parameters are reasonably well reproduced by the Klein-Gordon theory.

Table 2

Calculated (C) and measured (M) strong interaction shifts ΔE and widths G for the kaonic atoms X-ray transitions: a- the shift was estimated with Miller et al measured energy (see [1]); b — the shift was estimated with Cheng et al measured energy (see [1]); c — the shift by Batty et al [4]; d — this work;

Nucl	$ΔE_C$ (d)	G_C (d)	$ΔE_C$ (c)	G_C (c)	$ΔE_M$	G_M
W, 8−7	0.038	0.072	-0.003	0.065	0.079[c] 0.052[d]	0.070 (15)
W, 7−6	-0.294	3.85	-0.967	4.187	-0.353[c] -0.250[d]	3.72 (35)

References

1. Deloff A., Fundamentals in Hadronic Atom Theory, Singapore: World Scientific, 2003. — 352P.
2. Hayano R. S., Hori M., Horvath D., Widman E., Antiprotonic helium and CPT invariance//Rep. Prog. Phys. — 2007. — Vol.70. — P.1995−2065.
3. Deslattes R., Kessler E., Indelicato P., de Billy L., Lindroth E. , Anton J., Exotic atoms//Rev. Mod. Phys. — 2003. — Vol.75. — P.35−70.
4. Batty C. J., Eckhause M., Gall K. P., et al. Strong interaction effects in high Z- K⁻ atoms//Phys. Rev. C. — 1999. — Vol.40. — P.2154−2160.
5. Khetselius O.Yu., Turin A. V., Sukharev D. E., Florko T. A., Estimating of X-ray spectra for kaonic atoms as tool for sensing the nuclear structure// Sensor Electr. and Microsyst. Techn. — 2009. — N1. — P.30−35.

6. Okada S., Beer G., Bhang H., et al, Precision measurement of the 3d→2p x-ray energy in kaonic ⁴He//Phys.Lett.B. — 2007. — Vol.653, N 5−6. — P. 387−391.
7. Ito T. M., Hayano R. S., Nakamura S. N., Terada T. P., Observation of kaonic hydrogen atom x rays// Phys. Rev. C. — 1998. — Vol.58. — P.2366 − 2382
8. Ishiwatari T. on behalf of the SIDDHARTA Collaboration, Silicon drift detectors for the kaonic atom X-ray measurements in the SIDDHARTA experiment// Nucl.Instr. and Methods in Physics. Research Sec.A. Accelerators, Spectrometers, Detectors and Associated Equipment. — 2007. — Vol.581,N1−2. — P.326−329.
9. Glushkov A. V., Makarov I. T., Nikiforova E. S., Pravdin M. I., Sleptsov I.Ye., Muon component of EAS with energies above 10¹⁷eV//Astropart.Phys. — 1995. — Vol.4. — P.15−22
10. Glushkov A. V., Khetselius O.Yu., Gurnitskaya E. P., Loboda A. V., Sukharev D. E., Relativistic Quantum Chemistry of Heavy Ions and Hadronic Atomic Systems: Spectra and

Energy Shifts// Theory and Applications of Computational Chemistry (AIP). — 2009. — Vol.1. — P.131–134.

11. Santos J. P., Parente F., Boucard S., Indelicato P., Desclaux j.P., X-ray energies of circular transitions and electron scattering in kaonic atoms//Phys.Rev.A. — 2005. — Vol.71. — P.032501.

12. Mohr P. J. Quantum Electrodynamics Calculations in few-Electron Systems// Phys. Scripta. — 1999. — Vol.46,N1. — P.44–52.

13. Grant I., Relativistic Quantum Theory of Atoms and Molecules Theory and Computation, Springer Series on Atomic, Optical, and Plasma Physics. 2007. — Vol.40. — P.587–626.

14. Quiney H. M., Grant I. P. Partial-wave mass renormalization in atomic QED calculation // Phys.Scripta T. — 1993. — Vol.46. — P.132–138.

15. Wilson S., Recent Advances in Theoretical Physics and Chemistry Systems//Recent Advances in Theor. Phys. and Chem. Systems (Springer). — 2006. — Vol.15. — P.11–45.

16. Glushkov A. V., Energy Approach to Resonance states of compound super-heavy nucleus and EPPP in heavy nucleus collisions// Low Energy Antiproton Phys. (AIP). — 2005. — Vol.796. — P.206–210.

17. Glushkov A. V., Rusov V. D., Ambrosov S. V., Loboda A. V., Resonance states of compound super-heavy nucleus and EPPP in heavy nucleus collisions // New Projects and New Lines of research in Nuclear physics.Eds. Fazio G. and Hanappe F.: Singapore, World Sci. — 2003. — P. 142–154.

18. Glushkov A. V., Relativistic quantum theory. Quantum mechanics of atomic systems, Odessa: Astroprint, 2008. — 900P.

19. Glushkov A. V., Lovett L., Khetselius O.Yu., Gurnitskaya E. P., Dubrovskaya Yu.V., Loboda A. V., Generalized multiconfiguration model of decay of multipole giant resonances applied to analysis of reaction (μ-n) on the nucleus ^{40}Ca// International Journal of Modern Physics A. Particles and Fields. — 2009. — Vol. 24. — P.611–615.

20. Serot B. D., Walecka J. D. , Advances in Nuclear Physics Vol. 16: The Relativistic Nuclear Many Body Problem. Plenum Press, New York, 1996.

21. Sukharev D. E., Florko T. A., Khetselius O.Yu., Dubrovskaya Yu.V., Bremsstrahlung and X-ray spectra for kaonic and pionic hydrogen and nitrogen//Photoelectronics. — 2009. — N18. — P.16–20.

UDC 539.182

D. E. Sukharev, Yu.V. Dubrovskaya, A. A. Svinarenko

SENSING STRONG INTERACTION EFFECTS IN X-RAY SPECTROSCOPY OF HADRONIC ATOMS

Abstract.
The theoretical studying the strong interaction shifts and widths from X-ray spectroscopy of kaonic atoms is fulfilled. Sensing the strong interaction effects and theoretical estimating spectra of kaonic atomic systems can be considered as a new tool for studying nuclear structure and strong K-nucleus interaction.
Key words: strong interaction effects, spectroscopy, kaonic atoms

УДК 539.182

Д. Е. Сухарев, Ю. В. Дубровская, А. А. Свинаренко

ДЕТЕКТИРОВАНИЕ ЭФФЕКТОВ СИЛЬНОГО ВЗАИМОДЕЙСТВИЯ В РЕНТГЕНОВСКОЙ СПЕКТРОСКОПИИ АДРОННЫХ АТОМОВ

Резюме.
Выполнено теоретическая оценка сдвигов и ширин уровней, обусловленных эффектами сильного взаимодействия, в рамках рентгеновской спектроскопии каонных атомов. Детектирование эффектов сильного взаимодействия и оценка спектров каонных атомов являются одним из новых подходов к определению ядерной структуры и параметров сильного каон-ядерного взаимодействия.
Ключевые слова: эффекты сильного взаимодействия, спектроскопия, каонные атомы

UDC 539.182

Д. Є. Сухарев, Ю. В. Дубровська, А. А. Свинаренко

ДЕТЕКТУВАННЯ ЕФЕКТТІВ СИЛЬНОЇ ВЗАЄМОДІЇ У РЕНТГЕНІВСЬКІЙ СПЕКТРОСКОПІЇ АДРОННИХ АТОМІВ

Резюме.
Виконано теоретичну оцінку зсувів і ширин рівнів, які обумовлені ефектами сильної взаємодії, в межах рентгенівської спектроскопії каонних атомів. Детектування ефектів сильної взаємодії і теоретична оцінка спектрів каонних атомів є одним з нових підходів до визначення ядерної структури і параметрів сильної каон- ядерної взаємодії.
Ключові слова: ефекти сильної взаємодії, спектроскопія, каонні атоми.

UDC 539.186

YU.G. CHERNYAKOVA, L. A. VITAVETSKAYA, T. A. FLORKO, E. V. MISCHENKO, G. P. PREPELITSA

Odessa State Environmental University

ESTIMATING THE TOKAMAK PLASMA PARAMETERS BY MEANS HIGH RESOLUTION THEORETICAL X-RAY SPECTROSCOPY METHOD

A high resolution theoretical spectroscopy scheme is used for sensing and diagnostics the tokamak plasma parameters. There are obtained the theoretical values for the wavelengths and other atomic characteristics of satellite spectrum for the He-like ions from Ar^{16+} to V^{22+}, which are compared with other theoretical results and the tokamak de Fontenau-aux-Roses measurements data.

In last years a great attention is turned to problems of experimental and theoretical study of high temperature multi-charged ions plasma and developing the new diagnostics methods (c.f. [1−4]). Similar interest is also stimulated by importance of carrying out the approaches to determination of the characteristics for multi-charged ions plasma in thermonuclear (tokamak) reactors, searching new mediums for X-ray range lasers. The X-ray laser problem has stimulated a great number of papers devoting to development of theoretical methods for the modeling the elementary processes in a collisionally pumped plasma.

A great progress in development of laser technique, tokamaks and accelerators experiments resulted to a new class of problems in the plasma physics and correspondingly diagnostics of their parameters. The electron temperatures and particle confinement times in tokamak plasmas permit the ionization of the heavy impurity elements up to the helium-like (eventually hydrogen-like) charge state. High resolution spectroscopy of the line emission of these ions has become a powerful technique for determining the electron and ion temperatures T_e and T_i, the macroscopic plasma movement and dynamics of the plasma impurity transport. Experimental measurements have beer carried out by means of Bragg crystal spectrometers, high quality spectral analysis for diagnostic-relevant impurities at several large tokamaks: Ti^{20+} and Fe^{24+} (Princeton Large Torus), Cr^{22+} (tokamak de Fontenau-aux-Roses=TFR) etc [1−4]. The TFR measurements of the plasma parameters and wavelengths, atomic characteristics of satellite spectrum of the He-like ions from Ar^{16+} to Mn^{23} (Ar, Sc, V,Cr, Mn) are accurately carried out and presented in ref. [2].

Two key theoretical problems must be solved in order to develop a special code and to predict necessary plasma parameters needed for sensing the plasma parameters. First one is a highly accurate definition of the rate coefficients for elementary processes in the plasma that are responsible for the forming emission lines spectra. The second problem is connected with necessity of development new adequate calculation schemes for defining the wavelengths, level populations, inversions, line intensities etc. at definite plasma parameters. Despite of great number papers, devoting to solving cited problems (c.f. [1−10] and references in them), they are at present time quite far from final adequate solution. The most consistent approach to considered problems solving must base on the quantum electrodynamics (QED) [6−10]. In ref. [9−11] two new consistent QED versions for calculations of the spectroscopic characteristics of the multicharged ions in plasma have been developed, based on the QED perturbation theory formalism [12]. In ref. [11] some illustrations regarding sensing the tokamak plasma parameters (electron temperature etc.) and calculation results for wavelengths atomic characteristics of satellite spectrum of the He-like ions were presented and compared with the experimental data of the tokamak de Fontenau-aux-Roses measurements. Here we use more sophisticated theory [11], however, it takea into account the QED corrections according the methodics [3,6,12].

Let us describe the key moments of the used theory for definition of the spectroscopic characteristics for multicharged ions in plasma [9,11]. Both theoretical spectroscopy perturbation theory (PT) schemes allow calculating spectra and spectroscopic characteristics of neutral atoms, multicharged ions with account of relativistic, correlation, nuclear, QED effects. The version [11] allows to take into account the QED, radiative effects; version [9] allows to account for the correlation effects and should be used in calculation of not very heave atomic systems. It does not account for the QED effects. The wave functions zeroth basis is found from the Dirac equation solution with potential, which includes the core ab initio potential, electric, polarization potentials of nucleus (the gaussian form for charge distribution in the nucleus is used). All correlation corrections of the PT second and high orders (electrons screening, particle-hole interaction etc.) are accounted for. The nuclear potential is provided by choice of the charge distribution in the nucleus as the Gaussian function:

$$\rho\left(r|R\right)=\left(4\gamma^{3/2}/\sqrt{\pi}\right)\exp\left(-\gamma r^2\right)$$

Here $\gamma = 4/\pi R^2$; R is an effective nucleus radius, defined as: $R = 1.60 \times 10^{-13} z^{1/3}$ (cm). The Coulomb potential for spherically symmetric density $\rho\left(r|R\right)$ is:

$$V_{nucl}\left(r|R\right)=-\left(\left(1/r\right)\int_0^r dr'r'^2\rho\left(r'|R\right)+\int_r^\infty dr'r'\rho\left(r'|R\right)\right)$$

Let us consider the Li-like ion as example. One can write the DF-like equations for a three-electron

system $1s^2nlj$. Formally they fall into one-electron Dirac equations for the orbitals $1s, nlj$ with potential:

$$V(r)=2V(r|1s)+V(r|nlj)+V_{ex}+V(r|R).$$

This potential includes the electrical and polarization potentials of the nucleus. The part V_{ex} accounts for exchange inter-electron interaction. The main exchange effect will be taken into account if in the equation for the $1s$ orbital we assume $V(r)=V(r|1s)+V(r|nlj)$ and in the equation for the nlj orbital $V(r)=2V(r|1s)$. The rest of the exchange-correlation effects are accounted for in the first two PT orders by the total inter-electron interaction [11,12]. The core electron density is defined by iteration algorithm within gauge invariant QED procedure [13]. Other details of the calculation procedure, including definition of the matrix elements of the QED PT with effective account of the exchange-correlation effects can be found in ref. [9−11]. In order to take into account the Breit and QED corrections we used the approach and the corresponding data from refs. [3,6,12].

The spectral lines we are concerned with here are the characteristic lines w,x,y,z, ($1s2^1S_0-1s2p$ $^1P_1$, $^3P_2$, $^3P_1$, $1s2s$ $^3S_1$) of the helium-like ion and associated satellite lines of the Li-like type $1s^22l-1s2l2p$ produced by dielectronic recombination to, or inner-shell exci-

tation of , the lithium-like ion. The most prominent helium-like and satellite lithium-like lines are given in tables 1 and 2. The corresponding alternative data from refs. [2,11] are presented too. With respect to the intensities of the spectral lines one should note that the line, say, q (see table 1) is mainly due to collisional excitation of the lithium-like ion (c.f.[2,4,5]). Neglecting recombination and cascade effect for w, the ratio of the local emissivities of these lines is $\varepsilon_q/\varepsilon_w \sim 2/3 n_{Li}/n_{He}$, where n_{Li} and n_{He} are the densities of the Li- and He-like ions, respectively (from optically thin plasmas the ratio of the line-of-sight integrated emissivities is observed) [2]. For a satellite (s) line which is excited mainly by dielectronic recombination from the He-like to the Li-like ion one can write [11] :

$$\varepsilon_s/\varepsilon_w = F_1(s, T_e)F_2^*(s)/C_w(T_e),$$
$$F_1(s, T_e)=(1,65\cdot10^{-22})T_e^{-3/2}exp(-E_s/T_e)$$

where E_s and T_e are in eV; $F_2^*(s)$ is a line-specific intensity factor given in table 1; $C_w(T_e)$ is the rate coefficient (in cm^3/s) for collisional excitation of line w; E_s is the difference in energy of the satellite state in the recombined ion and the ground state in the recombining ion [2−4]. The $\varepsilon_s/\varepsilon_w$ ratio may be used as a diagnostic for the electron temperature (provided the electron velocity distribution in Maxwellian).

Table 1

Calculated wavelengths and satellite intensity factors (λ in E; F_2^* in 10^{13} s^{-1}): Ar

Line	Array	λ [2]	λ [11]	λ, present	F_2^*
w	$1s2p\,^1P_1 - 1s2^1S_0$	3,9457	3,9461	3,9460	-
x	$1s2p\,^3P_2 - 1s2^1S_0$	3,9632	3,9636	3,9634	-
s	$1s2s2p\,^2P_{3/2} - 1s^22s\,^2S_{1/2}$	3,9648	3,9652	3,9650	1,80
t	$1s2s2p\,^2P_{1/2} - 1s^22s\,^2S_{1/2}$	3,9660	3,9665	3,9662	3,36
m	$1s2p^2\,^2S_{1/2} - 1s^22p\,^2P_{3/2}$	3,9629	3,9634	3,9632	2,60
y	$1s2p\,^3P_1 - 1s2^1S_0$	3,9671	3,9674	3,9672	-
q	$1s2s2p\,^2P_{3/2} - 1s^22p\,^2S_{1/2}$	3,9784	3,9787	3,9785	0,98
k	$1s2p^2\,^2D_{3/2} - 1s^22p\,^2P_{1/2}$	3,9875	3,9878	3,9876	16,67
r	$1s2s2p\,^2P_{1/2} - 1s^22s\,^2S_{1/2}$	3,9808	3,9811	3,9809	2,75
a	$1s2p^2\,^2P_{3/2} - 1s^22p\,^2P_{3/2}$	3,9831	3,9835	3,9834	3,48
j	$1s2p^2\,^2D_{5/2} - 1s^22p\,^2P_{3/2}$	3,9917	3,9923	3,9919	22,93
z	$1s2sp\,^3S_1 - 1s2^1S_0$	3,9916	3,9919	3,9918	-

Table 2

Calculated (this paper) wavelengths and satellite intensity factors (λ in E; F_2^* in 10^{13} s^{-1}): Sc, V

Line	Array	λ (Sc)	F_2^* (Sc)	λ (V)	F_2^* (V)
w	$1s2p\,^1P_1 - 1s2^1S_0$	2,8697	-	2,3788	-
x	$1s2p\,^3P_2 - 1s2^1S_0$	2,8805	-	2,3866	-
s	$1s2s2p\,^2P_{3/2} - 1s^22s\,^2S_{1/2}$	2,8816	2,47	2,3878	2,57
t	$1s2s2p\,^2P_{1/2} - 1s^22s\,^2S_{1/2}$	2,8828	6,78	2,3887	8,98
m	$1s2p^2\,^2S_{1/2} - 1s^22p\,^2P_{3/2}$	2,8811	3,57	2,3876	4,17
y	$1s2p\,^1P_1 - 1s2^1S_0$	2,8844	-	2,3908	-
q	$1s2s2p\,^2P_{3/2} - 1s^22p\,^2P_{1/2}$	2,8901	0,48	2,3941	0,21
k	$1s2p^2\,^2D_{3/2} - 1s^22p\,^2P_{1/2}$	2,8951	25,90	2,3976	30,82
r	$1s2s2p\,^2P_{1/2} - 1s^22s\,^2S_{1/2}$	2,8926	3,93	2,3969	4,89
a	$1s2p^2\,^2P_{3/2} - 1s^22p\,^2P_{3/2}$	2,8930	6,48	2,3962	8,78
j	$1s2p^2\,^2D_{5/2} - 1s^22p\,^2P_{3/2}$	2,8989	35,54	2,4011	43,30
z	$1s2sp\,^3S_1 - 1s2^1S_0$	2,9002	-	2,4029	-

In ref. [2,11] it was indicated that the $\varepsilon_q/\varepsilon_w$ ratio increases very rapidly with increasing nuclear charge Z due to mainly the Z^4 dependence of the radiative transition probability A_r in the expansion $F_2^*(s)$. It is instructive to make use of a z-scaling law for the $C_w(T_e)$ of two elements A and B as [2]:

$$C_w^A(T_e)=\gamma^{3/2}C_w^B(\gamma^2, T_e)$$

where $\gamma=(Z_B-0,5)/(Z_A-0,5)$. In table 1 we present the calculated wavelengths and satellite intensity factors (λ in E; F_2^* in 10^{13} s^{-1}) for the multicharged ion of Ar. The corresponding data have been received on the basis of calculations within the multi-configuration intermediate-coupling scheme with a statistical Thomas-Fermi potential (ref. [2]) and our scheme (with account for the Breit and QED corrections). In a

whole, an account of the radiative corrections leads to some changing the wavelengths. A detailed comparison with experiment [2] shows that our data are a little in more good agreement with experimental data than data [2,11]. In table 2 we present the calculated in this paper wavelengths and satellite intensity factors (λ in E; F_2^* in 10^{13}s^{-1}) for the multicharged ion of Sc and V. One could guess that an account of the Breit and radiative corrections is naturally important in spectroscopy of satellite lines. Numerical evaluation for the most prominent satellite line j (see table 1) shows that $\varepsilon_j/\varepsilon_w \sim z^n$, where n=7,08 (n is very weakly T_e dependent between 1000 and 2000 eV). The evaluated value of the electron temperature is 1550 eV, which is in a physically reasonable with the experimental values [2].

So, the carried out calculation of the wavelengths and atomic characteristics of satellite spectrum of the He-like ions from Ar^{16+} to V^{22+} and evaluation of the TFR plasma parameters (electron temperature) shows that theoretical spectroscopy scheme, based on the using QED PT method of calculating the multicharged ions spectroscopic characteristics with account the radiative corrections should be widely used for diagnostics the tokamak plasma parameters.

References

1. Rosmej F. B., Hoffman D. H., Geissel M. et al, Advanced X-ray diagnostics based on an observation of high-energy Rydberg transitions from autoionizing levels in dense laser-produced plasmas// Phys. Rev.A. — 2001-Vol.63. — P.063409–063418.

2. TFR group, Cornille M., Dubau J., Loulergue M. Chare-dependent wavelengths shifts and line intensities in the dielectronic satellite spectrum of helium-like ions// Phys.rev.A. — 1995. — Vol.32,N5. — P.3000–3010.

3. Aglitsky E. V., Safronova U. I. Spectroscopy of autoionization states of atomic systems. — Moscow: Nauka, 1995.

4. Chenais-Popovics C., Rancu O., Renaudin P., Gauthier J. C. X-ray Spectroscopy of Laser-Produced Hot Dense Plasmas// Phys.Scripta. — 1996. — Vol.65,N1. — 163–168.

5. Seely J. F., Ekberg J. O. Brown C. M. et al, Laser −Produced Spectra and QED Effects for Fe-, Co-, Cu-, Zn-like ions of Au, Pb, Bi,Th, U// Phys.Rev.Lett. — 1996. — Vol.57,N23. — P.2924–2926.

6. Mohr P. J. Quantum Electrodynamics Calculations in few-Electron Systems// Phys.Scripta. — 1998-Vol.46,N1. — P.44–52.

7. Blundell S. A. Ab initio Calculations of QED Effects in Li-like, Na-like and Cu-like Ions// Phys.Scripta. — 1998. — Vol.46,N1. — P.144–150.

8. Ivanova E. P., Ivanov L. N. Modern Trends in Spectroscopy of Multicharged Ions// Physics Rep. — 1999. — Vol.166,N6. — P.315–390.

9. Chernyakova Yu.G., Prepelitsa G. P., Shumlyansky I. I. Satellite structure of the emission lines of the Cu plasma in a low inductive vacuum spark// Photoelectronics. — 2002. — Vol.11. — P.59–61.

10. Chernyakova Yu.G., Relativistic perturbation theory calculation of the satellite structure of the 2−3 Ne-like lines// Uzhgorod Univ.Sci.Herald.Ser.Phys. — Math. — 2001. — Vol.10. — P.331–335

11. Chernyakova Yu.G., Ignatenko V. M.,Vitavetskaya L. A., Sensing the tokamak plasma parameters by means high resolution x-ray theoretical spectroscopy method: new scheme// Sensor Electr. & Microsyst. Techn. — 2004. — N2. — P.20–24

12. Glushkov A. V., Relativistic Quantum Theory. Quantum, mechanics of Atomic Systems. — Odessa: Astroprint, 2008. — 900P.

Yu.G. Chernyakova, L. A. Vitavetskaya, T. A. Frorko, E. V. Mischenko, G. P. Prepelitsa

ESTIMATING THE TOKAMAK PLASMA PARAMETERS BY MEANS HIGH RESOLUTION THEORETICAL X-RAY SPECTROSCOPY METHOD

Abstract.

A high resolution theoretical spectroscopy scheme is used for sensing and diagnostics the tokamak plasma parameters. There are obtained the theoretical values for the wavelengths and other atomic characteristics of satellite spectrum for the He-like ions from Ar^{16+} to V^{22+}, which are compared with other theoretical results and the tokamak de Fontenau-aux-Roses measurements data.

Key words: tokamak plasma, parameters sensing, theoretical spectroscopy method

Ю. Г. Чернякова, Л. А. Витавецкая, Т. А. Флорко, Е. В. Мищенко, Г. П. Препелица

ОЦЕНКА ПАРАМЕТРОВ ПЛАЗМЫ ТОКАМАКА НА ОСНОВЕ МЕТОДА ТЕОРЕТИЧЕСКОЙ РЕНТГЕНОВСКОЙ СПЕКТРОСКОПИИ ВЫСОКОГО РАЗРЕШЕНИЯ

Резюме.

Метод теоретической рентгеновской спектроскопии высокого разрешения использован для оценки и диагностики параметров плазмы токамака. Получены теоретические значения длин волн и др. атомных характеристик сателлитного спектра Не-подобных ионов от Ar^{16+} до V^{22+}, которые сравниваются с имеющимися теоретическими данными и данными измерений на токамаке de Fontenau-aux-Roses.

Ключевые слова: плазма токамака, метод детектирования, теоретическая спектроскопия

УДК 539.186

Ю. Г. Чернякова, Л. А. Вітавецька, Т. О. Флорко, О. В. Міщенко, Г. П. Препелица

ОЦІНКА ПАРАМЕТРІВ ПЛАЗМИ ТОКАМАКА НА ОСНОВІ МЕТОДУ ТЕОРЕТИЧНОЇ РЕНТГЕНІВСЬКОЇ СПЕКТРОСКОПІЇ ВЫСОКОГО РОЗРІШЕННЯ

Резюме.

Метод теоретичної рентгенівської спектроскопії високого розрішення використано для оцінки та діагностики параметрів плазми токамака. Отримані теоретичні значення довжин хвиль та інших атомних характеристик сателітного спектру He-подібних іонів від Ar^{16+} до V^{22+} , які порівнюються з наявними теоретичними даними і даними вимірювань на токамаці de Fontenau-aux-Roses.

Ключові слова: плазма токамака, метод детектування, теоретична спектроскопія

110

O. YU. KHETSELIUS, A. V. LOBODA, YU. M. LOPATKIN, YU. V. DUBROVSKAYA

I. I. Mechnikov Odessa National University, Pastera str., 27, Odessa, 65016, Ukraine
Odessa State Environmental University,
Sumy National University
e-mail: nuclei08@mail.ru

RELATIVISTIC APPROACH TO THE RECOIL INDUCED EXCITATION AND IONIZATION OF IONS DURING CAPTURE OF NEUTRON

The relativistic energy approach is adapted to description of the recoil-induced excitation and ionization in atoms due to a neutron capture. The data for transition probabilities to different electronic states, induced by a neutron capture, are presented for some ions.

The paper is devoted to carrying out new adequate consistent relativistic approach to the recoil-induced excitation and ionization in atoms and ions due to the neutron capture and alpha-particle. In last years a development of methods of the laser spectroscopy allowed observing and further using the little changes in structure of atomic and molecular spectra resulted from the corresponding alteration of the internal state of a nucleus or because of the cooperative neutron-electron-gamma-nuclear processes, including the neutron capture [1−20]. The neutron capture phenomenon is responsible for complicated and rich physics of the different excitation and ionization processes in the electron shells of the atoms and ions [1−8]. The first references to the neutral recoil are originated from the known classical papers by Migdal and Levinger (look the detailed description of the history and corresponding models in refs. [1,2]), who evaluated approximately the ionization of an atom undergoing a sudden recoil in due to neutron impact and in a radioactive disintegration respectively. Gol'dansky-Letokhov-Ivanov have estimated an influence of the electron shell on velocity of recharging the metastable nucleus during the muon and neutron capture within simple qualitative models [2,3] and found the cited effect to be very small. The neutral recoil situation differs radically from processes involving a charged particle for which the sudden recoil approximation is often invalid (look, for example, refs. [1−3, 10−14]). An attractive situation arises under the transition to heavy multicharged ions because of changing the energy and geometric parameters of the electron shell. The character of interaction with a nucleus may change strongly, opening new channels of electron-nuclear processes [7−9]. Such effects as the electron-positron pair production (during the nucleus recharging) etc. are added to traditional channels of the nucleus excited state decay Here one could mention the processes of capture of neutron or alpha particle by atom or ion [1,2,4]. It is easily imagine a situation when this process becomes by energetically possible only after removal of the strongly bound electron in the initial state. It is known that it's possible the transfer of part of a nuclear energy to the atom or molecule electron shells under radiating (absorption) the γ quanta by a nucleus.

The different simple models (look, for example, refs. [1−4, 5−9,13−19]) were developed to evaluate the different cooperative processes channels, in particular, excitation or ionization of an atom, the electronic redistribution of an atom induced a sudden recoil of its nucleus occurring when a neutral particle is either emitted (γ-radioactivity) or captured (neutron capture for instance). The consistent QED approach to cited processes has been developed in refs. [9−12,19−21].

Here we adapt a relativistic energy approach [10,11,19−22] to the recoil-induced excitation and ionization in atoms (ions) due to the neutron capture. As method of calculation of the correlated electron wave functions, we use the QED perturbation theory (PT) on inter electron interaction [24−27].

Let us describe the key moments for the quantum approach to the recoil-induced excitation and ionization in atoms due to some particle capture [11−13]. The initial state of system being a discrete state, it is clear that two phenomena can occur after the momentum transfer to the final nucleus: an excitation to a final discrete state of the daughter system or an ionization, the final state lying in the continuum. The transition amplitude matrix element is given by the overlap between initial state (nuclear charge Z) and final state (nuclear charge Z') in a Galilean boost of velocity v. The overlap in the momentum space is as follows:

$$\int d\vec{p}\ \Phi_i(\vec{p}, Z)\Phi_f^*(\vec{p}+\vec{k}, Z') \qquad (1)$$

where subscript i, f represent the set of quantum numbers of the initial and final states and $\hbar k = mv$ is the recoil momentum of electron accompanying the resulting nucleus and having kinetic energy equal to $(ka_0)^2 Ry$. The energy E_R of the recoiling nucleus of mass M_R is:

$$E_R = \frac{M_R}{m_e}(k\,a_0)^2 R_{yd} \qquad (2)$$

The function $\Phi_i(\vec{p}, Z)$ is related to the function $\Psi_i(r, Z)$ as:

$$\Phi_i(\vec{p}, Z) = (2\pi)^{-\frac{3}{2}}\int d\vec{r}\,e^{-i\vec{p}\cdot\vec{r}}\,\Psi_i(\vec{r}, Z) \qquad (3)$$

So, using these relations the overlap is defined by:

$$b_{if} = \int d\vec{r}\ \Psi_i(\vec{r}, Z)e^{-i\vec{k}\cdot\vec{r}}\Psi_f^*(\vec{r}, Z') \qquad (4)$$

The probability of populating state f starting from state i is given by $P_{if} = |b_{if}|^2$. As we are dealing in multi-

electron systems, one can write the wave function of system as:

$$\psi(\gamma L S M_L M_S) = \sum_i a_i \Phi(\gamma_i L S M_L M_S) \qquad (5)$$

The extension of eq.(4) to two-electron system is:

$$b_{if} = \int d\vec{r}_1 \int d\vec{r}_2 \Psi_i(\vec{r}_1;\vec{r}_2;Z)e^{-ik(z_1+z_2)}\Psi_f^*(\vec{r}_1,\vec{r}_2;Z') \qquad (6)$$

where the Oz-axis of the coordinate system is chosen along the $\boldsymbol{k}$ direction. The two-electron recoil operator $R=exp[-ik(z_1+z_2)]$ matrix element between the correlated electronic wave functions of the form (5) is written in standard form [1,22]:

$$(\overline{\Psi}(\gamma'L'S'M_S')\,|\,R\,|\,\Psi(\gamma L S M_L M_S)) =$$
$$= (\Psi(\gamma L S M_L M_S)\,|\,R^*\,|\,\overline{\Psi}(\gamma'L'S'M_L'M_S')) =$$
$$= \sum_{i,j} a_i^* \overline{a}_j \left\langle \Phi(\gamma_i L S M_L M_S)\,|\,R^*\,|\,\overline{\Phi}(\gamma_j L'S'M_L'M_S')\right\rangle \quad (7)$$

It could be reduced to the direct and exchange contributions:

$$\frac{1}{\sqrt{(1+\delta_{\rho_a l_a \rho_b l_b})(1+\delta_{\rho_c l_c \rho_d l_d})}} \times$$
$$\times [R\,(ab,\,cd) + (-1)^{l_a+l_b-L-S}\,R(ba,\,cd)] \qquad (8)$$

where $R(ij,\,rt) \equiv \langle (\rho_i l_i)_1 (\rho_j l_j)_2 L S M_L M_S\,|\,R^*\,|$

$$\overline{(\rho_r l_r)_1 (\rho_l l_l)_2}L'S'M_L'M_S'\rangle$$

The plane wave function development can be used for each one-electron recoil operator:

$$R = e^{-ik(z_1+z_2)} = \sum_{l,l'=0}^{\infty} (-i)^{l+l'}(2l+1)(2l'+1)\times$$
$$\times j_l(kr_1)j_{l'}(kr_2)C_0^{(l)}(1)C_0^{(l')}(2) \qquad (9)$$

where $C_m^{(l)} = \sqrt{(4\pi)/(2l+1)}Y_{lm}$. The one-electron reduced matrix element brings some simplification taking the target in its ground state $1s^2\,^1S$:

$$\langle (\rho_i l_i)_1 (\rho_j l_j)_2\,^1S_{00}\,|\,R^*\,|\,\overline{(\rho_r l_r)_1 (\rho_l l_l)_2}\,^1L_{00}'\rangle = (-1)^{l_r-l_l}$$

$$\sqrt{2L'+1}\sum_{l,l'}^{\infty} i^{l+l'}(2l+1)(2l'+1)\sum_{m=-l_{min}}^{+l_{min}} (l_i\,\|\,C^{(l)}\,\|\,l_r)(l_j\,\|\,C^{(l')}\,\|\,l_l)$$

$$\times \begin{pmatrix} l_i & l_j & 0 \\ m & -m & 0 \end{pmatrix}\begin{pmatrix} l_r & l_l & L' \\ m & -m & 0 \end{pmatrix}\begin{pmatrix} l_i & l & l_r \\ -m & 0 & m \end{pmatrix}$$

$$\begin{pmatrix} l_j & l' & l_l \\ m & 0 & -m \end{pmatrix}$$

$$\times \int_0^\infty dr P_{\rho_r l_r}(r)j_l(kr)\overline{P_{\rho_r l_r}}(r)\int_0^\infty dr P_{\rho_l l_j}(r)j_{l'}(kr)\overline{P_{\rho_l l_l}}(r) \quad (10)$$

All notations in eq. (10) are standard. The matrix element on correlated electron functions is calculated according to the formula:

$$\sum_{f,i}|<\Psi_f\,|\,R\,|\,\Psi_i>|^2 = \sum_{f_1,f_2}|<\Phi_{f1f2}\,|\,R\,|\,\Phi_{i1i2}>| +$$
$$+\sum_{n_1 n_2}\frac{<\Phi_{f1f2}\,|\,V\,|\,\Phi_{n1n2}><\Phi_{n1n2}\,|\,R\,|\,\Phi_{i1i2}>}{E_{n_1 n_2}^0 - E_{f_1,f_2}^0} + \dots \quad (11)$$

where E^0 and Φ are the eigen values and eigen functions of the Coulomb hamiltonian, V is operator of the electrostatic interaction between electrons; its matrix elements are equal to difference between direct and exchange integrals. Such an approach allows accounting for the inter-electron correlation in the initial and final states with high degree of accuracy. [25–27].

It should be strictly noted that, generally speaking, the presented above formulas are acceptable for treating the non-relativistic atomic systems (say, hydrogen, helium etc). Consistent and qualitatively adequate description of the cooperative processes in multicharged ions (essentially relativistic systems) requires using the the QED formalism, in particular, the relativistic energy approach, based on the S-matrix Gell-Mann and Low formalism and QED PT (the basises are in details presented in refs. [10,11,19], look standard QED [20–23]). To calculate transition amplitude it is necessary to use the basis's of the correlated relativistic Dirac bi-spinors. To construct such basis we use formalism of the QED PT on the inter-electron interaction [9,21,24].

In the QED PT the matrix elements of the interaction operator between two-electron states give the standard contribution of the first order (energy matrice M):

$$M_1^{(2)} = \left\langle n_1 l_1 j_1 \quad n_2 l_2 j_2\,[J]\|V_{int}\|n_4 l_4 j_4 \quad n_3 l_3 j_3\,[J]\right\rangle =$$
$$= P_1 P_2 (-1)^{1+j_2+j_4+J}\times$$
$$\times\left[(2j_1+1)(2j_2+1)(2j_3+1)(2j_4+1)\right]^{1/2}\times$$
$$\times\sum_{i,k}\sum_a \begin{Bmatrix} j_i j_k J \\ j_2 j_1 a \end{Bmatrix}\left(\delta_{i,3}\delta_{k,4}+(-1)^J\delta_{i,4}\delta_{k,3}\right)Q_a \quad (12)$$

where, as usually, $P_1 = \begin{cases} 1 & \text{for } n_1 l_1 j_1 \neq n_2 l_2 j_2 \\ \frac{1}{2} & \text{for } n_1 l_1 j_1 = n_2 l_2 j_2 \end{cases}$,

$$P_2 = \begin{cases} 1 & \text{for } n_3 l_3 j_3 \neq n_4 l_4 j_4 \\ \frac{1}{2} & \text{for } n_3 l_3 j_3 = n_4 l_4 j_4 \end{cases}$$

The variable Q_a ($Q_\lambda = Q_\lambda^{Qul} + Q_\lambda^{Br}$) contains the Coulomb and Breit parts and is standardly expressed through the radial integrals R_λ and angle coefficients S_λ., The detailed expressions can be found, for example, in ref. [24]. In particular, one could write for the Coulomb part (in the Coulomb units)

$$Q_\lambda^{Qul} = \frac{1}{Z}\left\{R_l(1243)S_\lambda(1243)+R_\lambda(\tilde{1}24\tilde{3})S_\lambda(\tilde{1}24\tilde{3})\right.$$
$$\left.+R_\lambda(\tilde{1}\tilde{2}4\tilde{3})S_\lambda(\tilde{1}\tilde{2}4\tilde{3})+R_\lambda(\tilde{1}\tilde{2}4\tilde{3})S_\lambda(\tilde{1}\tilde{2}4\tilde{3})\right\} \quad (13)$$

Here there used the notations: the large component of the Dirac wave function is denoted as 1 (2,3,4), the little component — as $(\tilde{1}\tilde{2}4\tilde{3})$, i.e. with "wave" symbol. For example, one of the integrals in Eq. (13) is as follows:

$$R_\lambda(1243) =$$
$$= \iint dr_1 r_1^2 r_2^2 f_1(r_1)f_3(r_1)\times$$
$$\times f_2(r_2)f_4(r_2)Z_\lambda^{(1)}(r_<)Z_\lambda^{(1)}(r_>). \qquad (14)$$

$$Z_\lambda^{(1)} = \left[\frac{2}{|\omega_{13}|\alpha Z}\right]^{\lambda+\frac{1}{2}} \frac{J_{\lambda+\frac{1}{2}}(\alpha|\omega_{13}|r)}{r^\lambda \Gamma\left(\lambda+\frac{3}{2}\right)}.$$

The Breit part is as follows [24]:

$$Q_\lambda^{Br} = Q_{\lambda,\lambda-1}^{Br} + Q_{\lambda,\lambda}^{Br} + Q_{\lambda,\lambda+1}^{Br}, \qquad (15)$$

where

$$Q_\lambda^{Br} = \frac{1}{Z}\,\mathrm{Re}\,\Big\{R_\lambda\left(12\tilde{4}\tilde{3}\right)S_\lambda^l\left(12\tilde{4}\tilde{3}\right)+$$

$$R_\lambda\left(\tilde{1}\tilde{2}43\right)S_\lambda^l\left(1243\right)+R_l\left(\tilde{1}2\tilde{4}3\right)S_\lambda^l\left(\tilde{1}2\tilde{4}3\right)+$$

$$+R_l\left(1\tilde{2}4\tilde{3}\right)S_\lambda^l\left(1\tilde{2}4\tilde{3}\right)\Big\} \qquad (16)$$

Further it should be mentioned that the angle part of the matrix element $S(1243)$ is factorized on the indexes 1, 3 and 2, 4 and can be presented by the following way:

$$\left.\begin{array}{l} S_\lambda^{(1)}(1243) = (\lambda)(-1)^{\lambda+l+1}\,S_\lambda^l(13)S_\lambda^l(24),\\[4pt] S_\lambda^{(1)}(13) = (-1)^{j_3+j_3}\,(ll_1l_3)\times\\[4pt] \times\begin{pmatrix} j_3 & j_1 & \lambda \\ -\frac{1}{2} & \frac{1}{2} & 0 \end{pmatrix}\left\{\dfrac{1}{\sqrt{2\lambda(\lambda+1)}}\times\right.\\[8pt] \left[(-1)^{j_1+j_3+\lambda}\,(j_3)+(j_1)\right]\begin{pmatrix} \lambda & 1 & l \\ -1 & 1 & 0 \end{pmatrix}+\\[8pt] \times +(-1)^{j_3+j_1+\lambda}\begin{pmatrix} \lambda & 1 & l \\ 0 & 0 & 0 \end{pmatrix}\Big\}. \end{array}\right\} \qquad (17)$$

The available in Eq. (17) $3j$ symbols are expressed by the known standard analytical formulas.

We have performed studying the transition probabilities to different electronic states, which are induced during the capture of a neutron by the ^{3}He, ^{39}Ar^{16+} ions. The atom ^{4}He resulting from the neutron capture by ^{3}He recoils with a 99keV energy. The higher recoil energy 1,6MeV is corresponding to K=3,99. According to ref. [12], at K=1 the total population of the three first series ^{1}S, ^{1}P and ^{1}D reaches as much as ~98%. The dominating channel is excitation to discrete state (57%) and then the channel for ionization of one electron (38%). It differs from situation of higher recoil energies, as then the double-ionization processes become dominant. We will not present the probabilities data as the relativistic values are practically identical to results by Glushkov et al and Wauters et al, where non-relativistic approaches (PT and B-spline approach) are used to define the correlated wave functions [12,14]. Thus, the relativistic effects have to be not important for He atomic system. The relativistic effects however became important for heavy multicharged He-like ions. In a case of He-like ion ^{139}Ar^{16} the binding energy of electrons is much higher in comparison with neutral He. We firstly carried out the calculation of the transition probabilities for this ion and defined (look table 1) that at K=5 the total population of the three first series ^{1}S, ^{1}P and ^{1}D reaches as much as ~69% and it differs drastically from situation of the neutral He.

Table 1
Transition probabilities (in %) to different electronic states by capture of a neutron by ^{139}Ar^{16+}

Final States	ΣP (K=5)			
	^{1}S	^{1}P^0	^{1}D	^{1}S+^{1}P+^{1}D
Discrete states	56,6595	11,8841	0,3318	68,8754
Autoionizing states	0,5811	0,2508	1,0094	1,8413
Ionization of one electron	2,7214	18,9950	6,3182	28,0346
Double ionization	0,3306	0,3361	0,5815	1,2482
SUM	60,2926	31,4660	8,2409	99,9995

It has been found that at relatively high recoil energies ~28% probability transfer from the discrete spectrum population mechanism to single-ionization. It is relatively new situation in the recoil induced ionization of the atomic systems by a neutron capture. Obviously, the experimental studying the processes considered and determination of the corresponding probabilities in a case of the high Z-charged ions is of a great importance.

References

1. Dykhne A. M., Yudin G., Sudden perturbations and quantum evolution. — Moscow: UFN, 1999.
2. Glushkov A. V., Khetselius O.Yu., Lovett L., Electron-β-Nuclear Spectroscopy of Atoms and Molecules and Chemical Environment Effect on the β-Decay parameters// Advances in the Theory of Atomic and Molecular Systems. Series: Progress in Theoretical Chemistry and Physics, Eds. Piecuch P., Maruani J., Delgado-Barrio G., Wilson S. (Berlin, Springer). — 2009. — Vol. 20. — P. 125–172.
3. Glushkov A. V., Khetselius O.Yu., Malinovskaya S. V., Optics and spectroscopy of cooperative laser-electron nuclear processes in atomic and molecular systems — New trend in quantum optics// Europ.Phys.Journ. — 2008. — Vol. T160,N1. — P.195–204.
4. Bohr O., Motelsson B., Structure of Atomic Nucleus. — N. — Y.: Plenum, 1975.
5. Letokhov V. S., Laser Spectroscopy. — N. — Y.: Acad.Press., 1977; Letokhov V. S., Nonlinear selective photo-processes in atoms and molecules. — Mocow: Nauka, 1993. — 408P.
6. Letokhov V. S., Using lasers in the atomic, nuclear and molecular physics// Apllication of Lasers in Atomic, Nuclear, Molecular Physics. Eds. Prokhorov A. M., Letokhov V. S. — M.:Nauka,1999. — P.401–454; Singapore: World Sci.,1999. — P.413–464.
7. Goldansky V. I., Letokhov V. S. Effect of laser radiation on nuclear decay processes// Sov. Phys. JETP. — 1999. — Vol.67. — P.513–516
8. Ivanov L. N., Letokhov V. S. Spectroscopy of autoionization resonances in heavy elements atoms// Com.Mod.Phys.D.:At. Mol.Phys. — 1999-Vol.4. — P.169–184.
9. Glushkov A. V., Ivanov L. N., Ivanova E. P., Generalized energy approach to radiation and autoionization decay of the atomic states //Autoionization Phenomena in Atoms. — Moscow Univ. Press, Moscow. — 1999. — P.58–160; Glushkov A. V., Ivanov L. N., Letokhov V. S., Nuclear quantum optics// Preprint ISAN N4, Moscow-Troitsk, 1997. — 16P.
10. Glushkov A. V., Ivanov L. N. Radiation Decay of Atomic States: atomic residue and gauge non-invariant contributions // Phys. Lett.A. — 1999. — Vol.170,N1. — P.33–37.
11. Glushkov A. V., Energy Approach to Resonance states of compound super-heavy nucleus and EPPP in heavy nucleus collisions// Low Energy Antiproton Physics. — 2005. — Vol.796. — P.206–210.
12. Glushkov A. V., Malinovskaya S. V., Gurnitskaya E. P., Khetselius O.Yu.,Dubrovskaya Yu.V., Consistent quantum theory of the recoil induced excitation and ionization in atoms

during capture of neutron// J.Phys.C. — 2006. — Vol.35. — P.425−430.

13. Vysotskii V. I., The problem of controlled spontaneous nuclear γ-decay: theory of controlled excited and radioactive nuclei γ-decay//Phys.Rev.C. — 1998. — Vol.58-P. 337−350.

14. Wauters L., Vaeck N., Godefroid M., van der Hart H. W., Demeur M., Recoil-induced electronic excitation and ionization in one-electron and two-electron ions// J.Phys.B. — 1997. — Vol.30. — P.4569−4589.

15. Harston M. R., Carroll J. J., Nuclear excitation and de-excitation in resonant electronic transitions// Laser Phys. — 2004. — Vol.14. — P.1452−1463.

16. Burvenich T. J., Evers J., Keitel C. H., Dynamic nuclear Stark shift in superintense laser fields// Phys.Rev.C. — 2006. — Vol.74. — P.044601.

17. Palffy A., Sheid W., Harman Z., Theory of nuclear excitation by electron capture for heavy ion// Phys.Rev.A. — 2006. — Vol.73. — P.012715.

18. Kishimoto S., Yoda Y., Kobayashi Y., Kitao S., Haruki R., Masuda R., Seto M., Nuclear excitation by electron transition on ^{197}Au by photoionization around the K-absorption edge// Phys.Rev.C. — 2006. — Vol.74. — P.031301.

19. Glushkov A. V., Rusov V. D., Ambrosov S. V., Loboda A. V., Resonance states of compound super-heavy nucleus and EPPP in heavy nucleus collisions // New Projects and New Lines of research in Nuclear physics.Eds. Fazio G. and Hanappe F.: Singapore, World Sci. — 2003. — P. 142−154.

20. Glushkov A. V., Khetselius O.Yu., Loboda A. V., Gurnitskaya E. P., Florko T. A., Sukharev D. E.,.Lovett L., Gauge-invariant QED perturbation theory approach to the nuclear electric quadrupole moments, hyperfine structure constants for heavy atoms and ions// Frontiers in Quantum Systems in Chem. and Phys. (Springer). — 2008. — Vol.18. — P.505−522.

21. Glushkov A. V., Relativistic Quantum Theory. Quantum, mechanics of Atomic Systems. — Odessa: Astroprint, 2008. — 900P.

22. Grant I. Relativistic Quantum Theory of Atoms and Molecules. — Oxford, 2007−650P.

23. Dyall K., Faegri K.Jr., Introduction to relativistic quantum theory. — Oxford, 2007. — 590P.

O.Yu. Khetselius, A. V. Loboda, Yu.M. Lopatkin, Yu.V. Dubrovskaya

RELATIVISTIC APPROACH TO THE RECOIL INDUCED EXCITATION AND IONIZATION OF IONS DURING CAPTURE OF NEUTRON

Abstract.
The relativistic energy approach is adapted to description of the recoil-induced excitation and ionization in atoms due to a neutron capture. The data for transition probabilities to different electronic states, induced by a neutron capture, are presented.
Key words: atom ionization probability, capture of neutron, energy approach

О. Ю. Хецелиус, А. В. Лобода, Ю. М. Лопаткин, Ю. В. Дубровская

РЕЛЯТИВИСТСКИЙ ПОДХОД К ОПИСАНИЮ ЭФФЕКТОВ ВОЗБУЖДЕНИЯ И ИОНИЗАЦИИ В ИОНАХ ВСЛЕДСТВИЕ ЗАХВАТА НЕЙТРОНА

Резюме.
Релятивистский энергетический подход адаптирован к задаче описания возбуждения и ионизации в атомах и ионах, индуцированных отдачей вследствие захвата нейтрона. Представлены данные вероятностей переходов в различные электронные состояния, индуцированные захватом нейтрона, для ряда ионов.
Ключевые слова: вероятность ионизации, захват нейтрона, энергетический подход

О. Ю. Хецеліус, А. В. Лобода, Ю. М. Лопаткін, Ю. В. Дубровська

РЕЛЯТИВІСТСЬКИЙ ПІДХІД ДО ОПИСУ ЕФЕКТІВ ЗБУДЖЕННЯ ТА ІОНІЗАЦІЇ В ІОНІХ ЗАВДЯКИ ЗАХОПЛЕННЮ НЕЙТРОНУ

Резюме.
Релятивістський енергетичний підхід адаптовано до опису збудження та іонізації в атомах та іонах, індукованих віддачею завдяки захопленню нейтрону. Представлені дані ймовірностей переходів у різні електронні стани, які індуковані захопленням нейтрону, для ряду іонів.
Ключові слова: імовірність іонізації, захоплення нейтрону, енергетичний підхід

UDC 539.186

A. P. FEDCHUK, A. V. GLUSHKOV, YA.I. LEPIKH, A. V. LOBODA, YU. M. LOPATKIN, A. A. SVINARENKO

I. I. Mechnikov Odessa National University
Odessa State Environmental University,
Sumy National University
e-mail: dirac13@mail.ru

THE GREEN'S FUNCTIONS AND DENSITY FUNCTIONAL APPROACH TO VIBRATIONAL STRUCTURE IN THE PHOTOELECTRON SPECTRA OF CARBON OXIDE MOLECULE

The combined theoretical approach to vibrational structure in photoelectron spectra (PES) of molecules, which is based on the density functional theory (DFT) and the Green's-functions (GF) approach, is used for quantitative treating the carbon oxide molecule PES.

INTRODUCTION

The GF method is very well known in a quantum theory of field, quantum electrodynamics, quantum theory of solids. This approach naturally provided the known progress in treating atoms, solids and molecules, as it has been shown in many papers (c.f.[1–15]). The experimental PES spectra of molecules usually show a pronounced vibrational structure [5–6]. Many papers have been devoted to treatment of the vibrational spectra by construction of potential curves for the reference molecule (the molecule which is to be ionized) and the molecular ion. Usually the electronic GF is defined for fixed position of the nuclei. The cited method, however, requires as input data the geometries, frequencies, and potential functions of the initial and final states. Since in most cases at least a part of these data are unavailable, the calculations have been carried out with the objective of determining the missing data by comparison with experiment. To avoid this difficulty and to gain additional information about the ionization process, Cederbaum et al [11] extended the GF approach to include the vibrational effects and showed that the GF method allowed *ab initio* calculation of the intensity distribution of the vibrational lines etc. For large molecules far more approximate but more easily applied methods such as DFT [16,17] or from the wave-function world the simplest correlated model MBPT are preferred [2,8,10]. Indeed, in the last decades DFT theory became by a great, quickly developing field of the modern computational chemistry of molecules. Here the combined theoretical approach [12–15] to vibrational structure in PES of molecules, which is based on the DFT and the GF approach, is used for quantitative treating the carbon oxide molecule. The density of states, which describe the vibrational structure in PES, is calculated with using combined DFT-GF approach. It is important that calculation procedure is significantly simplified with using DFT formalism. This simplification allowed to get the first important results in a laser-electron-γ nuclear spectroscopy of molecules [14], namely, results on the electron-vibration-rotation-γ nuclear satellite lines.

The density of states in one-body and many-body problem.

Quasiparticle Fermi-liquid density functional theory

As usually (see details in refs. [2,8,11,14]), the quantity which contains the information about the ionization potentials (I.P.) and molecular vibrational structure due to quick ionization is the density of occupied states:

$$N_k(\epsilon) = (1/2\pi\hbar)\int dt\, e^{ih^{-1}\epsilon t}\langle\psi_0|a_k^t(0)a_k(t)|\psi_0\rangle, \quad (1)$$

where $|\Psi_0\rangle$ is the exact ground state wave function of the reference molecule and $a_k(t)$ is an electron destruction operator, both in the Heisenberg picture. For particle attachment the quantity of interest is the density of unoccupied states:

$$N_k(\epsilon) = (1/2\pi\hbar)\int dt\, e^{ih^{-1}\epsilon t}\langle\psi_0|a_k(t)a_k^t(0)|\psi_0\rangle \quad (2)$$

Usually in order to calculate the value (1) states for photon absorption one should express the Hamiltonian of the molecule in the second quantization formalism. The Hamiltonian is as follows:

$$H = T_E(\partial/\partial x) + T_N(\partial/\partial X) + $$
$$+ U_{EE}(x) + U_{NN}(X) + U_{EN}(x, X), \quad (3)$$

where T_E and T_N are the kinetic energy operators for electrons and nuclei, and U represents the interaction; U_{EE} represents the Coulomb interaction between electrons, etc; x (X) denotes electron (nuclear) coordinates. As usually, introducing a field operator $\Psi(R,\theta,x) = \sum \varphi_i(x,R,\theta)a_i(R,\theta)$ with the Hartree-Fock (HF) one–particle functions $\phi_i(\in_i(R)$ are the one-particle HF energies and f denotes the set of orbitals occupied in the HF ground state; R_0 is the equilibrium geometry on the HF level) and dimensionless normal coordinates Q_s one can write the standard Hamiltonian as follows [11,15]:

$$H = H_E + H_N + H_{EN}^{(1)} + H_{EN}^{(2)}, \quad (4)$$

$$H_E = \sum_i \epsilon_i(R_0)a_i^t a_i + \frac{1}{2}\sum V_{ijkl}(R_0)a_i^t a_j^t a_l a_k - $$
$$- \sum_{i,j}\sum_{k\in f}[V_{ikjk}(R_0) - V_{ikkj}(R_0)]a_i^t a_j,$$

$$H_N = \hbar\sum_{s=1}^{M}\omega_s(b_s^t b_s + \frac{1}{2}),$$

$$H_{EN}^{(1)} = 2^{-1/2} \sum_{s=1}^{M} \left(\frac{\partial^{o}_{i}}{\partial Q_s} \right)_0 (b_s + b_s^t)[a_i^t a_i - n_i] +$$

$$+ \frac{1}{4} \sum_i \sum_{s,s'=1}^{M} \left(\frac{\partial^2 {}^{o}_{i}}{\partial Q_s \partial Q_{s'}} \right)_0 (b_s + b_s^t)(b_{s'} + b_{s'}^t)[a_i^t a_i - n_i],$$

$$H_{EN}^{(2)} = 2^{-3/2} \sum \sum_{s=1}^{M} \left(\frac{\partial V_{ijkl}}{\partial Q_s} \right)_0 (b_s + b_s^t) \times$$

$$\times [\delta v_1 a_i^t a_j^t a_k + \delta v_2 a_i a_k a_k a_i^t + 2\delta v_3 a_j^t a_k a_l a_i^t] +$$

$$\frac{1}{8} \sum \sum_{s,s'=1}^{M} \left(\frac{\partial^2 V_{ijkl}}{\partial Q_s \partial Q_{s'}} \right)_0 (b_s + b_s^t) \times$$

$$\times (b_{s'} + b_{s'}^t)[\delta v_1 a_i^t a_j^t a_k + \delta v_2 a_i a_k a_k a_i^t + 2\delta v_3 a_j^t a_k a_l a_i^t],$$

with $n_i = 1$ (0), $i \in f$ ($i \notin f$), $\delta\sigma_f = 1$ (0), $(ijkl) \in \sigma_f$, where the index set v_1 means that at least φ_k and φ_l or φ_i and φ_j are unoccupied, v_2 that at most one of the orbitals is unoccupied, and v_3 that φ_k and φ_j or φ_l and φ_j are unoccupied. Here for simplicity all terms leading to anharmonicities are neglected. The ω_s are the HF frequencies; b_s, b_s^t are destruction and creation operators for vibrational quanta as

$$Q_s = (1/\sqrt{2})(b_s + b_s^t), \quad \partial / \partial Q_s = (1/\sqrt{2})(b_s - b_s^t) \quad (5)$$

The interpretation of the above Hamiltonian and an exact solution of the one-body HF problem is given in refs. [5,6]. The HF-single-particle component H_0 of the Hamiltonian (4) is as follows:

$$H_0 = \sum_i \epsilon_i (R_0) a_i^t a_i + \sum_{s=1}^{M} \hbar\omega_s (b_s^t b_s + \frac{1}{2}) +$$

$$+ \sum_{s=1}^{M} \sum_i 2^{-1/2} \left(\frac{\partial^{o}_{i}}{\partial Q_s} \right)[a_i^t a_i - n_i](b_s + b_s^t)_0 +$$

$$+ \sum_{s,s'=1} \sum_i \frac{1}{4} \left(\frac{\partial^2 {}^{o}_{i}}{\partial Q_s \partial Q_{s'}} \right)_0 [a_i^t a_i - n_i](b_s + b_s^t)(b_{s'} + b_{s'}^t) \quad (6)$$

Correspondingly in the one-particle picture the density of occupied states is given by

$$N_k^0(\epsilon) = \frac{1}{2\pi\hbar} \int_{-\infty}^{\infty} dt e^{i\hbar^{-1}(\epsilon - \epsilon_k)t} \langle 0| \, e^{\pm i\hbar^{-1}\tilde{H}_{0}^t} \, |0\rangle, \quad (7)$$

$$\tilde{H}_0 = \sum_{s=1}^{M} \hbar\omega_s b_s^t b_s + \sum_{s=1}^{M} g_s^k (b_s + b_s^t) +$$

$$+ \sum_{s,s'=1}^{M} \gamma_{ss'}^k (b_s + b_s^t)(b_{s'} + b_{s'}^t) \quad (8)$$

$$g_s^i = \pm \frac{1}{\sqrt{2}} \left(\frac{\partial^{o}_{i}}{\partial Q_s} \right)_0, \quad \gamma_{ss'}^i = \pm \frac{1}{4} \left(\frac{\partial^2 {}^{o}_{i}}{\partial Q_s \partial Q_{s'}} \right)_0. \quad (9)$$

Introducing new operators

$$c_s = \sum_{l=1}^{M} (\lambda_1^{sl} b_l + \lambda_2^{sl} b_l^t) \quad (10)$$

with real coefficients λ_1^{sl}, λ_2^{sl}, defined in such a way that $\tilde{H}_0$ in new operators is

$$\tilde{H}_0 = \sum_{s=1}^{M} \hbar\tilde{\omega}_s c_s^t c_s + \sum_{s=1}^{M} \hat{g}_s (c_s + c_s^t) + k. \quad (11)$$

eq. (7) is as follows:

$$N_k^0(\epsilon) = \sum_{n_1 \cdots n_M} |\langle \hat{n} \, |U \, |0\rangle|^2 \times$$

$$\times \delta(\epsilon - \epsilon_k \pm \Delta\epsilon_k \pm n \cdot \hbar\hat{\omega}) \quad (12)$$

where δ function in (12) naturally contains the information about adiabatic ionization potential and the spacing of the vibrational peaks; $|\langle \hat{n} \, |U \, |0\rangle|^2$ is the well-known Franck-Condon factor.

In a diagrammatic method to get function $N_k(\epsilon)$ one should calculate the GF $G_{kk'}(\epsilon)$ first [1,3,11,18]:

$$G_{kk'}(\epsilon) = -i\hbar^{-1} \int_{-\infty}^{\infty} dt e^{i\hbar^{-1}\epsilon t} \times$$

$$\times \langle \psi_0| \, T\{ \, a_k(t) a_k^t(0) \, \} \, |\psi_0\rangle \quad (13)$$

and the function $N_k(\epsilon)$ can be found from the relation

$$\pi N_k(\epsilon) = a \, \text{Im} \, G_{kk}(\epsilon - ai\eta), \quad a = -sign\epsilon_k. \quad (14)$$

Choosing the unperturbed Hamiltonian H_0 to be $H_0 = \sum_i \epsilon_i a_i^t a_i + H_N$ one finds the GF. In the known approximation GF is as follows:

$$G_{kk'}^{OB}(t) = \pm\delta_{kk'} i \exp\left[-in^{-1}(\epsilon_k \mp \Delta\epsilon)t \right] \times$$

$$\times \sum_n |\langle \hat{n}_k |U_k|0\rangle|^2 \exp(\pm in_k \cdot \hat{\omega}_k t), \quad (15)$$

The corresponding Dyson-like equation ($\Sigma = \hat{O}$) is as follows:

$$G_{kk'}(\epsilon) = G_{kk'}^{OB}(\epsilon) + \sum_{kk'} G_{kk}^{OB}(\epsilon) \Phi_{kk'} G_{k'k'}(\epsilon) \quad (16)$$

$$\Phi_{kk'}(\epsilon) = \sum_{\substack{i,j \in F \\ l \notin F}} \sum_{n_i, n_j, n_l} \frac{(V_{klij} - V_{klij}) V_{k'lij} U_{n_i i} U_{n_j j} U_{n_l l}}{\epsilon + E_l - E_i - E_j} +$$

$$+ \sum_{\substack{i,j \in F \\ l \notin F}} \sum_{n_i, n_j, n_l} \frac{(V_{klij} - V_{klij}) V_{k'lij} U_{n_i i} U_{n_j j} U_{n_l l}}{\epsilon + E_l - E_i - E_j}$$

where $U_{n_i i} = |\langle \hat{n}_i |U_i|0\rangle|^2$ and $E_i = \epsilon_i \mp \Delta\epsilon_i \mp h\hat{n}_i \cdot \hat{\omega}_i$ (17)

The direct method for calculation of $N_k(\epsilon)$ as the imaginary part of the GF includes a definition of the vertical I. P. (V. I. P.s) of the reference molecule and then of $N_k(\epsilon)$. The zeros of the functions

$$D_k(\epsilon) = \epsilon - \left[\epsilon^{op} + \Sigma(\epsilon) \right]_k, \quad (18)$$

where $(\epsilon^{op} + \Sigma)_k$ denotes the k-th eigenvalue of the diagonal matrix of the one-particle energies added to matrix of the self-energy part, are the negative V. I. P. 's for a given geometry. One can write [11,13]:

$$(V.I.P.)_k = -(\epsilon_k + F_k),$$

$$F_k = \Sigma_{kk}\left(-(V.I.P.)_k \right) \approx \frac{1}{1 - \partial\Sigma_{kk}(\epsilon_k)/\partial_\epsilon} \Sigma_{kk}(\epsilon_k). \quad (19)$$

Expanding the ionic energy E_k^{N-1} about the equilibrium geometry of the reference molecule in a power series of the normal coordinates of this molecule leads to a set of linear equations in the unknown normal coordinate shifts δQ_s, and new coupling constants are then:

$$g_1 = \pm \left(1/\sqrt{2} \right) \left[\partial(\epsilon_k + F_k)/\partial Q_l \right]_0 \quad (20)$$

$$\gamma_{ll'} = \pm\left(\frac{1}{4}\right)\left[\partial^2\left(\epsilon_k + F_k\right)/\partial Q_l / \partial Q_{l'}\right]_0$$

The coupling constants g_l and $y_{ll'}$ are calculated by the well-known perturbation expansion of the self-energy part using the Hamiltonian H_{EN} of Eq. (3). In second order one obtains:

$$\sum\nolimits_{kk}^{(2)}(\epsilon) = \sum_{\substack{i,j \\ s\notin F}}\frac{\left(V_{ksij}-V_{ksji}\right)V_{ksij}}{\epsilon+\epsilon_s-\epsilon_i-\epsilon_j} + \sum_{\substack{i,j \\ s\notin F}}\frac{\left(V_{ksij}-V_{ksji}\right)V_{ksij}}{\epsilon+\epsilon_s-\epsilon_i-\epsilon_j} \quad (21)$$

and the coupling constant g_p can be written as

$$g_l \approx \pm\frac{1}{\sqrt{2}}\frac{\partial\epsilon_k}{\partial Q_l}\frac{1+q_k\left(\partial/\partial\epsilon\right)\sum_{kk}\left[-(V.I.P.)_k\right]}{1-\left(\partial/\partial\epsilon\right)\sum_{kk}\left[-(V.I.P.)_k\right]}, \quad (22)$$

$$q_k = \frac{\displaystyle\sum\frac{\left(V_{ksij}-V_{ksji}\right)^2}{\left[-(V.I.P.)_k+\epsilon_s-\epsilon_i-\epsilon_j\right]^2}\left[\frac{\partial\epsilon_s}{\partial Q_l}-\frac{\partial\epsilon_i}{\partial Q_l}-\frac{\partial\epsilon_j}{\partial Q_l}\right]}{\displaystyle\frac{\partial\epsilon_k}{\partial Q_l}\sum\frac{\left(V_{ksij}-V_{ksji}\right)^2}{\left[-(V.I.P.)_k+\epsilon_s-\epsilon_i-\epsilon_j\right]^2}} \quad (23)$$

It is suitable to use further the pole strength of the corresponding GF:

$$\rho_k = \left\{1-\frac{\partial}{\partial\epsilon}\sum\nolimits_{kk}\left[-(V.I.P.)_k\right]\right\}^{-1}; 1\ge\rho_k\ge 0, \quad (24)$$

$$g_l \approx g_l^0\left[\rho_k+q_k\left(\rho_k-1\right)\right], \quad g_l^0 = \pm 2^{-1/2}\partial\epsilon_k/\partial Q_l \quad (25)$$

Below we give the DFT definition of the pole strength corresponding to V. I. P.'s and confirm the earlier data [11−15]: $p_k\approx 0,8-0,95$. The coupling constant is:

$$\gamma_{ll} = \gamma_{ll}^0\left(\frac{g_l}{g_l^0}\right)+\frac{1}{4}\sqrt{2}g_l^0\frac{\partial}{\partial Q_l}\left(\frac{g_l}{g_l^0}\right) \quad (26)$$

Further we consider the quasiparticle Fermi-liquid version of the DFT, following to refs. [18−20]. The master equation can be derived using an expansion for self-energy part Σ into set on degrees of x, $\epsilon-\epsilon_F$, $p^2-p_F^2$ (here ϵ_F and p_F are the Fermi energy and pulse correspondingly):

$$\left[p^2/2-\sum_\alpha Z_\alpha/r_\alpha+\sum\nolimits_0(x)+p(\partial\sum/\partial p^2)p\right]\Phi_\lambda(x) =$$
$$= (1-\partial\sum/\partial\epsilon)\epsilon_\lambda\Phi_\lambda(x) \quad (27)$$

The functions Φ_λ in (27) are orthogonal with a weight $\rho_k^{-1}=a^{-1}=[1-\partial\Sigma/\partial\epsilon]$. Now one can introduce wave functions of the quasiparticles $\varphi_\lambda=a^{-1/2}\Phi_\lambda$, which are, as usually, orthogonal with weight 1. The equations (27) can be obtained on the basis of variational principle, if we start from a Lagrangian of a system L_q (DF). It should be defined as a functional of quasiparticle densities:

$$\nu_0(r) = \sum_\lambda n_\lambda\,|\Phi_\lambda(r)|^2,$$

$$\nu_1(r) = \sum_\lambda n_\lambda\,|\nabla\Phi_\lambda(r)|^2,$$

$$\nu_2(r) = \sum_\lambda n_\lambda[\Phi_\lambda^*\Phi_\lambda - \Phi_\lambda^*\Phi_\lambda].$$

The densities ν_0 and ν_1 are similar to the HF electron density and kinetical energy density correspondingly; the density ν_2 has no an analog in the HF or DFT theory and appears as result of account for the energy dependence of the mass operator Σ. A Lagrangian L_q can be written as a sum of a free Lagrangian and Lagrangian of interaction: $L_q = L_q^0 + L_q^{int}$, where a free Lagrangian L_q^0 has a standard form:

$$L_q^0 = \int dr\sum_\lambda n_\lambda\Phi_\lambda^*(i\partial/\partial t-\epsilon_p)\Phi_\lambda, \quad (28)$$

The interaction Lagrangian is defined in the form, which is characteristic for a standard (Kohn-Sham [16]) DFT (as a sum of the Coulomb and exchange-correlation terms), however, it takes into account for the energy dependence of a mass operator Σ:

$$L_q^{int} = L_K-\frac{1}{2}\sum_{i,k=0}^2\int\beta_{ik}F(r_1,r_2)\nu_i(r_1)\nu_k(r_2)dr_1dr_2 \quad (29)$$

where β_{ik} are some constants (look below), F is an effective potential of the exchange-correlation interaction. The Coulomb interaction part L_K looks as follows:

$$L_K = -\frac{1}{2}\int[1-\sum\nolimits_2(r_1)]\nu_0(r_1)[1-$$
$$-\sum\nolimits_2(r_2)]\nu_0(r_2)/|r_1-r_2|\,dr_1dr_2 \quad (30)$$

where $\Sigma_2=\partial\Sigma/\partial\epsilon$. In the local density approximation the potential F can be expressed through the exchange-correlation pseudo-potential V_{xc} as follows [20]:

$$F(r_1,r_2)=\delta V_{xc}/\delta\nu_0\cdot\delta(r_1-r_2).$$

Further, one can get the following expressions for $\Sigma_i = -\delta L_q^{int}/\delta\nu_i$:

$$\Sigma_0 = (1-\Sigma_2)V_K+\Sigma_0^{ex}+\frac{1}{2}\beta_{00}\delta^2 V_{XC}/\delta\nu^2\nu_0^2+$$
$$+\beta_{00}\delta V_{XC}/\delta\nu_0\nu_0+\beta_{01}\delta V_{XC}/\delta\nu_0\nu_1+$$
$$\beta_{01}\delta^2 V_{XC}/\delta\nu_0^2\cdot\nu_0\nu_1+\beta_{02}\delta^2 V_{XC}/\delta\nu_0^2\cdot\nu_0\nu_2+$$
$$+\beta_{02}\delta V_{XC}/\delta\nu_0\cdot\nu_2 \quad (31)$$

$$\Sigma_1 = \beta_{01}\delta V_{XC}/\delta\nu_0\cdot\nu_0+\beta_{12}\delta V_{XC}/\delta\nu_0\cdot\nu_2+\beta_{11}\delta V_{XC}/\delta\nu_0\cdot\nu_1$$

$$\Sigma_2 = \beta_{02}\delta V_{XC}/\delta\nu_0\cdot\nu_0+\beta_{12}\delta V_{XC}/\delta\nu_0\cdot\nu_1+\beta_{22}\delta V_{XC}/\delta\nu_0\cdot\nu_2$$

Here V_K is the Coulomb term, Σ_0^{ex} is the exchange term. Using the known canonical relationship, one can derive the quasiparticle Hamiltonian, which is corresponding to L_q:

$$H_q = H_q^0+H_q^{int} = H_q^0-L_K+$$
$$+\frac{1}{2}\beta_{00}\delta V_{XC}/\delta\nu_0\cdot\nu_0^2+\beta_{01}\delta V_{XC}/\delta\nu_0\cdot\nu_0\cdot\nu_1+$$
$$+\frac{1}{2}\beta_{11}\delta V_{XC}/\delta\nu_0\cdot\nu_1^2-\frac{1}{2}\beta_{22}\delta V_{XC}/\delta\nu_0\cdot\nu_2^2 \quad (32)$$

Further let us give the short comment regarding constants β_{ik}. Indeed, in some degree they have the same essence as the similar constants in the well-known Landau Fermi-liquid theory and the Migdal finite Fermi-systems theory. Regarding universality of β_{ik}, indeed, as we know now, the total universality

of the constants in the last theories is absent, though a range of its changing is quite small [18]. In any case it requires a careful check. Obviously, the terms with constants β_{01}, β_{11}, β_{12}, β_{22} should be neglected (at least in the zeroth approximation in comparison with others), so they can be equal to 0. The value of β_{00} is dependent on definition of V_{xc}. If as V_{xc} it is used one of the DFT exchange-correlation potentials from, then without losing a community of statement, $\beta_{00}=1$. The constant β_{02} can be in principle calculated by analytical way, but it is very useful to remember its connection with a spectroscopic factor F_{sp} of the system [18]:

$$F_{sp} = \left\{ 1 - \frac{\partial}{\partial \in} \sum_{kk} \left[-(V.I.P.)_k \right] \right\} \qquad (33)$$

One can see that this definition is corresponding to the pole strength of the corresponding Green's function [2,11]. As potential V_{xc} we use the Gunnarsson-Lundqvist exchange-correlation functional [17]:

$$V_{XC}(r) = -(1/\pi)[3\pi^2 \cdot \rho(r)]^{1/3} -$$
$$-0,0333 \cdot \ln[1 + 18,376 \cdot \rho^{1/3}(r)] \qquad (34)$$

Using the above written formula, one can simply define the values (24), (33).

RESULTS AND CONCLUSIONS

In ref. [15] the above presented combined approach has been applied to analysis of the photoelectron spectrum for the sufficiently complicated from the theoretical point of view N_2 molecule, where the known Koopmans' theorem even fails in reproducing the sequence of the V. I. P.'s in the PE spectrum (c.f.[5−7]). It is stressing, however it has been possible to get the full sufficiently correct description of the diatomics PES already in the effective one-quasiparticle approximation [11,13]. Another essential aspect is sufficiently simple calculational procedure, provided by using the DFT. Moreover, here the cumbersome calculation is not necessary, if the detailed Hartree-Fock (Hartree-Fock-Rothaan) data (separate HF-potential curves of molecule and ion) for the studied diatomic molecule are available. The carbon oxide molecule, which is considered in this paper, has been naturally studied in many papers. (see [3−8]). In full analogy with the molecule of N_2 [15] it is easily to estimate the pole strengths p_k and the values q_k. When the change of frequency due to ionization is small, the density of states can be well approximated using only one parameter g:

$$N_k(\in) = \sum_{n=0}^{\infty} e^{-s} \frac{S^n}{n!} \delta(\in - \in_k + \Delta \in_k + n \cdot \hbar\hat{\omega}),$$
$$S = g^2 (\hbar\omega)^{-2} \qquad (35)$$

In case the frequencies change considerably, the intensity distribution of the most intensive lines can analogously be well approximated by an effective parameter S. In fig.1 it is presented the experimental [5,6] PES for the CO molecule together with the theoretical one, calculated with g^0 and Eq. (35).
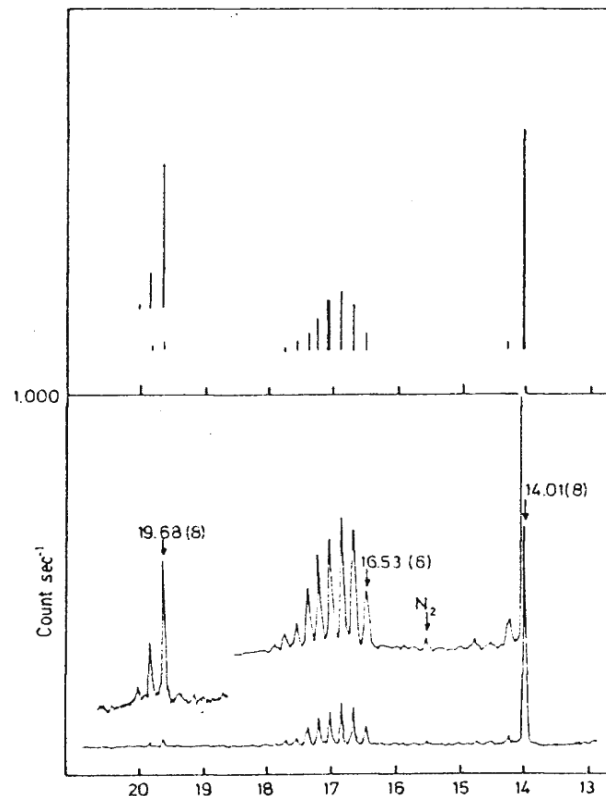

Fig.1. Experimental and calculated (the uppermost spectrum is calculated with S^0 and Eq. (35)) photoelectron spectrum of the CO molecule (see text).

We will mean that S^0 denotes the constant S calculated with g^0 and S^{exp} denotes the value derived from the experimental spectrum. The deviations of the one-particle constants g^0 from the experimental ones are practically fully arisen due to the correlation effects. In table 1 we listed the experimental and calculated (our data) values of S.

Table I

Experimental and calculated (our data) values of

S^0			S^{exp}		
5σ	1π	4σ	5σ	1π	4σ
0.045	2.394	0.262	0.04	2.30	0.27[b]

One could guess that there a physically reasonable agreement between the theoretical and experimental results for all three bands. It should be noted that more sophisticated calculation by Cederbaum et al [11] gives the theoretical value S(4,5σ), which is practically identical to the experimental values, however the value S(1π)=2.59 is in some degree different from S^{exp}. This example also confirms that quite simple theory become an effective tool in interpreting the vibrational structure of the molecular PES, especially taking into account an essential simplification (implementation of the DFT scheme) of the standard Green's function approach. At last, we should note that the presented combined GF-DFT approach can be very helpful for multi-atomic molecules, especially for larger ones, when full *ab initio* calculations can be not available.

References

1. Thouless D J, Quantum Mechanics of Many-Body Systems (Academic, N. — Y., 1991).
2. Wilson W., Handbook on Molecular Physics and Quantum Chemistry, Chichester: Wiley, 2003. — 680P.
3. Lindgren I., Morrison M., Atomic Many-Body Theory. — Berlin: Springer, 1996. — 370P.
4. Abrikosov A., Gorkov L., Dzyaloshinskii E., Quantum Field Theoretical Methods in Statistical Physics Oxford: Pergamon, 1995. — 400P.
5. Turner D. W., Baker C., Baker A. D., Brunrile C. R., Molecular photoelectron spectroscopy. — N. — Y.: Wiley, 1999
6. Herzberg G., Molecular Spectra and Molecular Structure-Moscow: Mir, 1997. — Vol.1.
7. Cade D. E., Wahl A. L., Hartree-Fock-Roothaan wave functions for diatomic molecules// Atomic Data and Nucl. Data Tabl. — 1994. — Vol.13,N4. — P.2339−2389.
8. Bartlett R. J., Musiał M. N., Coupled-cluster theory in quantum chemistry//Rev. Mod. Phys. — 2007. — Vol.79. — P.291−328.
9. Dorofeev D., Zon B. A., Kretinin I., Chernov V. E., Method of quantum defect Green's function for calculation of dynamic atomic polarizabilities// Optics and Spectr. — 2005. — Vol. 99. — P.540−548.
10. Ivanova E. P., Ivanov L. N., Aglitsky E. V., Modern Trends in Spectroscopy of multi-charged Ions// Physics Rep. — 1998. — Vol.166,N6. — P.315−390.
11. Кцppel H., Domcke W., Cederbaum L. S., Green's function method in quantum chemistry// Adv. Chem. Phys. — 1999. — Vol.57. — P.59−132.
12. Glushkov A. V., An effective account for energy effects of exchange and correlation in a theory of multi-electron systems//Journ. Struct. Chem. — 1999. — Vol.31,N4. — P.3−7.
13. Glushkov A. V., New approach to theoretical definition of ionization potentials for molecules on the basis of Green's function method//Journ.of Phys.Chem. — 1998. — Vol.66. — P.2671−2677.
14. Glushkov A. V., Malinovskaya S. V., Loboda A. V., Shpinareva I. M., Prepelitsa G. P., Consistent quantum approach to new laser-electron-nuclear effects in diatomic molecules // J.Phys.Cs. — 2006. — Vol.35. — P.420−424.
15. Glushkov A. V., Lepikh Ya.I., Fedchuk A. P., Loboda A. V., The Green's functions and density functional approach to vibrational structure in the photoelectron spectra of molecules//Photoelectronics. — 2009. — N18. — P.119−127.
16. Kohn W., Sham L. J. Quantum density oscillations in an inhomogeneous electron gas//Phys. Rev. A. — 1995. — Vol.137,N6. — P.1697−1706.
17. The Fundamentals of Electron Density, Density Matrix and Density Functional Theory in Atoms, Molecules and the Solid State, Eds. Gidopoulos N. I., Wilson S. — Amsterdam: Springer, 2004. — Vol.14. — 244P.
18. Glushkov A. V., Relativistic and correlation effects in spectra of atomic systems. — Odessa: Astroprint. 2006. — 450P.
19. Ivanova E. P.,Ivanov L. N., Glushkov A. V.,Kramida A. E., High-order corrections in relativistic perturbation theory with the model zeroth approximation, Mg-like and Ne-like ions //Physica Scripta. — 1999. — Vol.32(4). — P.512−524.
20. Glushkov A. V., An universal quasiparticle energy functional in a density functional theory for relativistic atom//Optics and Spectr. — 1999. — Vol.66,N1-P.31−36.

A. P. Fedchuk, A. V. Glushkov, Ya.I. Lepikh, A. V. Loboda, Yu. M. Lopatkin, A. A. Svinarenko

THE GREEN'S FUNCTIONS AND DENSITY FUNCTIONAL APPROACH TO VIBRATIONAL STRUCTURE IN THE PHOTOELECTRON SPECTRA OF CARBON OXIDE MOLECULE

Abstract.
The combined theoretical approach to vibrational structure in photoelectron spectra (PES) of molecules, which is based on the density functional theory (DFT) and the Green's-functions (GF) approach, is used for quantitative treating the carbon oxide molecule PES.
Key words: photoelectron spectra of molecules, Green's functions, density functional theory

А. В. Глушков, Я. И. Лепих, А. П. Федчук, А. В. Лобода, Ю. М. Лопаткин, А. А. Свинаренко

МЕТОД ФУНКЦИЙ ГРИНА И ФУНКЦИОНАЛА ПЛОТНОСТИ В ОПРЕДЕЛЕНИИ КОЛЕБАТЕЛЬНОЙ СТРУКТУРЫ ФОТОЭЛЕКТРОННОГО СПЕКТРА МОЛЕКУЛЫ СО

Резюме.
Комбинированный теоретический метода описания колебательной структуры для фотоэлектронных спектров молекул, который базируется на методе функций Грина и теории функционала плотности (ТФП), применен к количественному описанию фотоэлектронного спектра молекулы СО
Ключевые слова: фотоэлектронный спектр молекул, метод функций Грина, теория функционала плотности

О. В. Глушков, Я. І. Лепіх, О. П. Федчук, А. В. Лобода, Ю. М. Лопаткін, А. А. Свинаренко

МЕТОД ФУНКЦІЙ ГРІНА І ФУНКЦІОНАЛУ ГУСТИНИ У ВИЗНАЧЕННІ ВІБРАЦІЙНОЇ СТРУКТУРИ ФОТОЕЛЕКТРОННОГО СПЕКТРУ МОЛЕКУЛИ СО

Резюме.
Комбінований теоретичний метод опису вібраційної структури для фотоелектронних спектрів молекул, який базується на методі функцій Гріна і теорії функціоналу густини, застосовано до кількісного опису фотоелектронного спектру молекули СО.
Ключові слова: фотоелектронний спектр молекул, метод функцій Гріна, теорія функціонала густини

V. A. SMYNTYNA, O. A. KULINICH, I. R. IATSUNSKYI, I. A. MARCHUK

I. I. Mechnikov Odessa National University, e-mail: yatsunskiy@gmail.com

FACTORS INFLUENCING THE YIELD STRESS OF SILICON

Factors influencing the yield stress of silicon are investigated with advanced research methods. It is shown that elastic stresses which are concentrated at the structural defects (dislocation, crystalline grain boundary, dendrite and lamella) will influence on the yield stress of silicon.

1. INTRODUCTION

Further micro- and nano-miniturization of electronics elements produces enhanceable requirements to the semiconductor quality and to the technology. As it is known, sources of structural defects in semiconductors are stresses. Plastic deformation is always characterized by the yield stress. The stress level at which a material no longer behaves elastically, but instead experiences a small plastic deformation is known as the yield stress (point) or a plasticity threshold — τ_k . The great number of research papers is devoted to the problem of defect formation and, in particular, the yield point of monocrystallin silicon and systematize in monographs (see, e.g. [1, 2]). However, not all factors influencing the yield stress of silicon are sufficiently detailed investigated. This fact has conditioned the problem statement of the given work devoted to the investigation of the structural defects in silicon wafers and their influence on the yield point.

2. EXPERIMENTAL DETAILS

We studied Cz-Si wafers of different orientation, N-, P- type with $\rho = 4 — 10$ (Ohm·cm).

The following methods and equipment were used for researching the silicon wafers:

— method of selective chemical etching by Sirtle or Secco; Sirtle chemical selective etchant (50 g CrO3 + 100 ml H_2O + 100 ml HF (46 %)) is used to etch close-packed silicon planes (111) with the etching speed of about (2—3) µm/min. Knowledge of the etching speed enabled us to control the depth of analysis from the surface into the bulk of the silicon wafer.

— scanning electron microscopy (SEM), by means of scanning electron microscope analyzer "Cam Scan-4D" with a system of the energetic dispersive analyzer "Link-860" (with the usage of "Zaf" program, mass sensitivity of the device is 0.01 %, beam diameter ranges from $5 \cdot 10^{-9}$ to $1 \cdot 10^{-6}$;

— optical methods of researches with the usage of metallographic microscope "MMP-2P";

— Auger spectrometer LAS-3000 (beam diameter — 5 microns).

The technique of experiments consisted of the following: the selective chemical etching method allows one to carry out the level-by-level analysis of silicon by etching layers and to reveal defects simultaneously. Af-

ter selective chemical etching application, the surface of wafers was investigated on deficiency with the usage of metallographic optical microscope "MMP-2P". To improve the defects image quality and to obtain the possibility of making the quantitative analysis of impurity, we applied such methods of analysis as scanning electron microscopy with energetic dispersive analyzers and Auger spectrometer.

3. RESULTS AND DISCUSSION

It is known**,** that stresses and deformations exceeding a plasticity threshold are the source of structural defects in solids. In case of a defectless material the yield stress depends on electrophysical and elastic parameters and other conditions (temperature, pressure, etc.). Alternative, the magnitude of a plasticity threshold can essentially vary. The relationship between the stress and strain that the material displays is known as a stress-strain curve (Fig. 1).
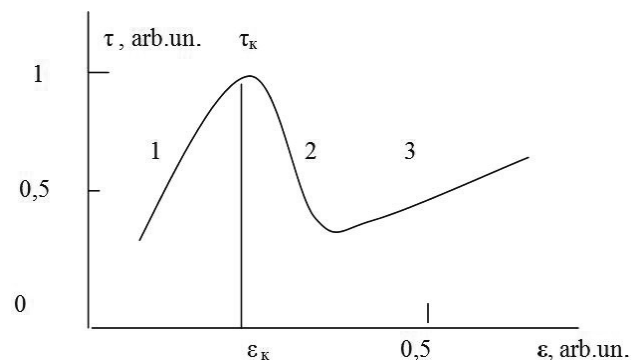

Fig.1. The quality stress-strain curve.

It is unique for each material and is found by recording the amount of deformation (strain) at distinct intervals of tensile or compressive loading. Up to this amount of stress, stress is proportional to strain (Hooke's law), so the stress-strain graph is a straight line, and the gradient will be equal to the elastic modulus of the material (region 1, Fig.1). Second region of stress-strain curve describe the increasing of dislocation density due to the formation of new dislocations and dislocation multiplication (region 2, Fig.1). At sufficiently large strains, the stress in materials increases with strain in a nonlinear manner, this is called hardening. On further straining, the material breaks (region 3, Fig.1) [2].

According to the Frank-Read source mechanism, presence of point defects of various type changes elastic parameters of crystals that at external actions leads to formation of structural defects. Thus, in this theory key parameter influencing the yield stress is the density of point defects [3].

Figure 2 illustrates the dislocation multiplication due to scribing of silicon wafers at a room temperature. Mechanical stresses are passed round approximately in the radial direction from a scribe channel because this direction is possible to relate with dislocations and areas with the changed mechanical potential and which can be related to Frank — Read sources. In the context of Alexander — Haasen model the dislocation multiplication happens by their recrawlings to the subsequent reproduction [4]. However, the problem related to the impurity atmosphere effecting on the yield stress will stand aside. According to models of static and dynamic dislocation "ageing", impurity atmospheres interacting with dislocations, create starting stresses, which are necessary for overcoming to shift dislocation from a place [5]. Such interaction, also, creates the additional retardation rationing an impellent at dislocations moving. The dynamic "ageing" leads to astable dislocation jump moving and dislocation multiplication owing to their brakes-off from the impurities. The offered models well present some experimental data, according to which, increasing of initial dislocation density can lower the yield stress, however the presence of the impurity atmospheres increases the yield stress [6, 7].

Fig.2. The SEM image of dislocation multiplication.

Elastic stresses are accumulated around the dislocation core during dislocation formation (Fig. 1, a region 2). For single crystalline silicon the yield stress (τ_κ), depending on orientation and other parameters, being over the range $\tau_k = (5 \cdot 10^8 - 2 \cdot 10^9)\,N/cm^2$ at magnitudes of the relative strains $\varepsilon_k = (10^{-5} - 2 \cdot 10^{-4})$ [8]. If the average distance between the 60° dislocations is 10^{-5} m, the relative strains counted by formula $\varepsilon = (b/D)k$, where D — average distance between dislocations, b-magnitude of a vector Burgers projection, $k \approx 0.5$, is equal $2.7 \cdot 10^{-5}$, i.e. is in the second region (fig. 1). Such relative strains are starting on further mechanical and thermal affecting. Dangling bonds are shaped around the dislocation core due to presence of compression and extension zone. These cause atomic bonds weakening and change the local threshold of plasticity.

The yield stress depends on temperature [5]. The yield stress decrease is caused by the temperature increasing. At temperatures $1000-1200^0$ C (the high-temperature oxidation) the yield stress falls down in $50-60$ times. Thus, presence of strains around dislocations and temperature increase can lower the yield stress of single crystalline silicon.

The impurity atmosphere around dislocations can result not only "ageing", but also generates compensation stresses and strains. Impurity atoms accumulate around dislocations in an extension zone if impurity atom radius more than radius of silicon atom. Thus there is a decrease of stresses and strains localized around dislocations. Impurity atoms accumulate in a compression zone if the radius of impurity atom is less, than radius of silicon atom. In this case there is a decrease of strains and stresses. Figure 3 shows the electronic image of 60° dislocation received on a surface p-Si (10 (100)) which come out after 2 minutes etching (Sacco etchant). The picture is received in a conductance mode.
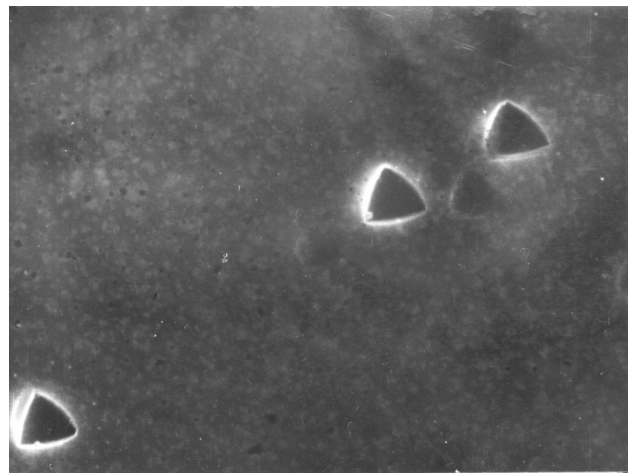

Fig.3. The SEM image of dislocations 1x3000 (conductance mode).

The X-Ray analysis of light areas of dislocation has shown presence of oxygen atoms (oxygen concentration is 6 atomic percents) (fig. 4). Oxygen atoms are located in interstitial position of a silicon crystal lattice, and being in an inactive electrical state. Oxygen atoms decrease stresses and strains localized around dislocation due to radius of oxygen atom more than radius of silicon atom occupying a position in an extension zone of dislocation. This causes that silicon crystal lattice begin more hardening and increase the yield stress.

If oxygen atoms create in dislocation-free silicon uncontrollable impurities in the form of interstitial position atoms accumulations or an accumulation of oxygen precipitates, it occurs the relative strains which it is possible to count approximately (taking into account known restrictions on sp^3-hybridizations), according to expression $\varepsilon = \omega C$ (Vegard's law), where ω — Vegard's coefficient, depending on a type of impurity atoms and their lattice position, C — impurity concentration. The calculations for the oxygen atoms have shown that the strain is approximately equated

10^{-5}. Such strain is starting to decrease the yield stress and cause the subsequent defect formation at the further affecting. If concentration of impurities considerably exceeds 6 atomic percents there are stresses and strains leading to generation not of one dislocation but their accumulations (fig. 5). Thus, impurity atoms are proportioned between dislocations, and process of dislocation generation stop, when stresses relax to level of elastic values.

ENERGY
3.1
TOTAL AREA = 91996
Peak at 8.086 keV
FIT INDEX = 19.62

ELMT	ERROR (WT %)	ELMT	% ELMT	ATOM%
Pt	.433 not used for ZAF	K	.000	.000
Si	.328	Cl	.000	.000
Cl	.120 < 2 sigma	Na	.079	.094
Na	.082 < 2 sigma	Si	93.202	92.812
K	.104 < 2 sigma	O	6.304	6.656
Al	.095 < 2 sigma	Al	.531	.538
20.00 kV		TOTAL	100.016	100.000

Last elmt analysed, NORMALISED

Fig.4. The X-Ray analysis of dislocation core.
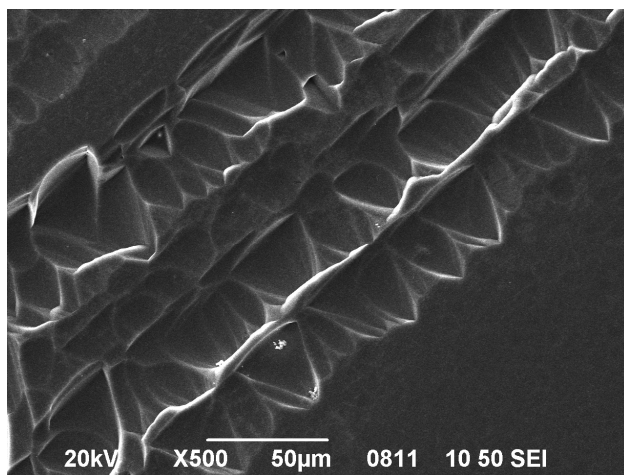
Fig.5. The SEM image of dislocation accumulation.

In very rare cases, when concentration of impurity atoms in silicon is more than solid solubility limit, it can organize macroimperfections known as dendrites (fig. 6). Dendrites consist of a mixture of solid solutions of iron or chromium (fig.7).
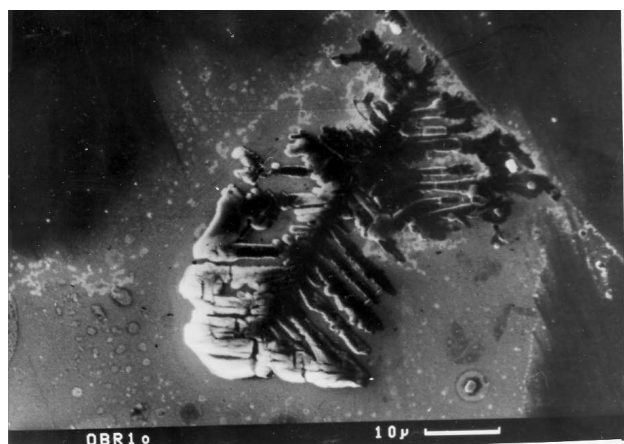

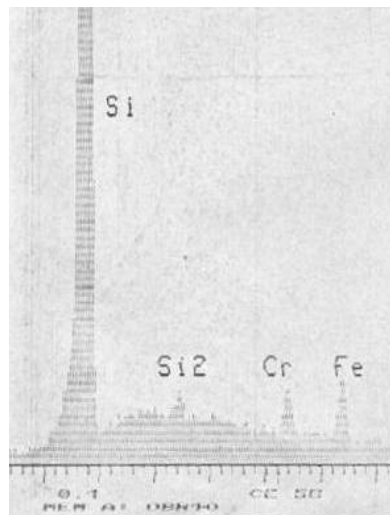Fig. 6. The SEM image of dendrite on a silicon surface.

Fig. 7. The X-Ray analysis of dendrites in silicon.

When silicon atoms are clustering it can form twinning lamellas (fig.8). On the interface line dendrite — silicon are stresses often exceeding the yield stress of silicon. Thus, it is disordered silicon under a dendrite area and the area containing dislocation networks, consisting of 60^0 dislocations (fig. 9).
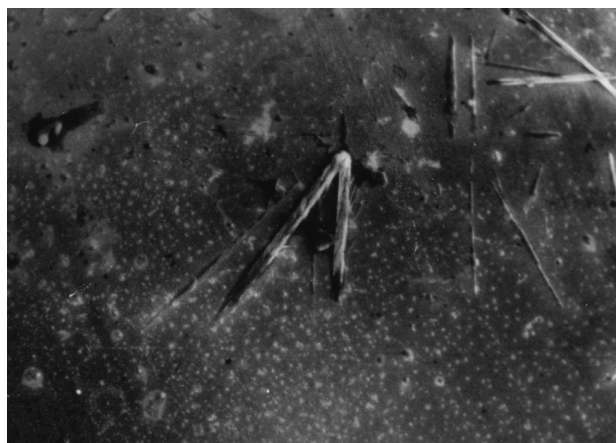

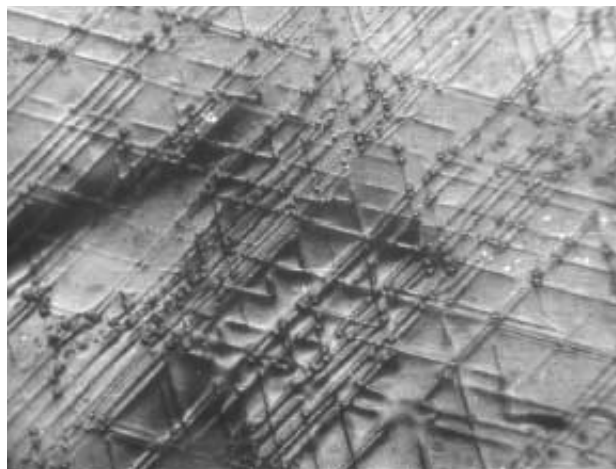Fig. 8. The pattern of twinning lamellas, 1×5000.

Fig. 9. The SEM image of dislocation networks, 1x2300.

In some cases, silicon wafers have layered structure that was revealed as a result of selective chemical etching (fig. 10) [9]. Boundary lines of layers are dis-

oriented under different angles from each other and the strains are localized around boundary lines. These stresses exceed the yield point and can cause the generation of new defects and decrease a silicon plasticity threshold.
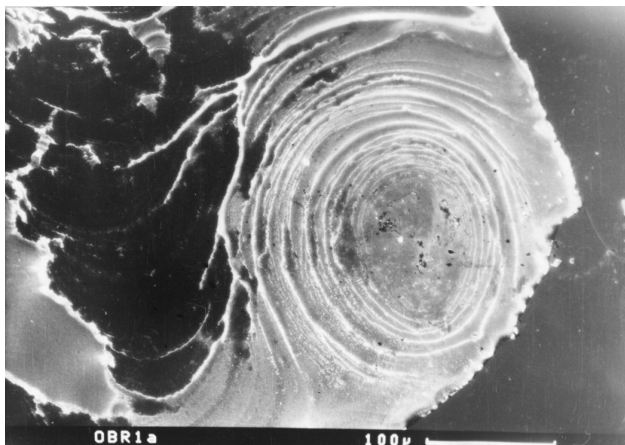

Fig.10. The SEM image of silicon layer structure defects.

4. CONCLUSIONS

On the basis of our researches, the following conclusions can be drawn:

— the yield stress of monocrystallin silicon decrease with increasing of a dislocation density and can vary in the presence of impurities atoms which localized around dislocations;

— in one case, impurity atmospheres participate in processes of "ageing" of dislocations that increases a plasticity threshold of silicon, in another one — presence of oxygen atoms near dislocations creates compensation stresses which can cause to the hardening of the crystal lattice of silicon and increase the magnitude of the yield stress;

— stresses and strains which decrease the yield point and are starting for formation of new defects are a consequence of the background uncontrollable impurity of oxygen atoms in dislocation-free silicon crystals;

— presence of dendrites, lamellas and layered structure of silicon decrease a local magnitude of yield stress due to strains accumulated around a boundary line of defects and monocrystallin silicon.

References

1. H. F. Matare., *Defect Electronics in Semiconductors,* Willey-Interscience, New York, 2000.
2. T Abe, W. M. Bullis, *Defects in silicon,* The Electrochemical Society Inc., New Jersy, 2000.
3. Г. А. Малыгин. Пластичность и прочность микроматериалов // *ФТП.* — 48(6). — 2007. — C.961–982.
4. Б. В. Петухов. Теория зуба текучести в малодислокационных кристаллах // *ЖТФ.* — 36(2). — 2002. — C.129–133.
5. А. М. Орлов, А. А. Соловьев, А. А. Скворцов. Перераспределение дислокаций в кремнии вблизи концентраторов напряжений // *ФТТ.* — 47(11). — 2005. — C.1967–1972.
6. В. Е. Панин, В. Е. Егорушкин, А. В. Панин. Природа локализации пластической деформации твердых тел // *ЖТФ.* — 77(8). — 2007. — C.62–69.
7. В. А. Смынтина, О. А. Кулініч, І. Р. Яцунський. Вплив дефектів на розподіл концентрації легуючої домішки та дефектоутворення при легуванні кремнію // *Фізика і хімія твердого тіла.* — Т.8, №4. — 2007. — С. 698 — 702.
8. V. A. Smyntyna, O. A. Kulinich, M. A. Glauberman, G.G Chtmeresyuk, I.R Yatsunskiy. The structure investigation of near — surface layers in silicon — dioxide silicon structure // *Photoelectronics.* — N. 17. — 2008. — P. 61 — 63.
9. Кулинич О. А. Механизм возникновения и свойства дефектов слоистой неоднородности в кремнии // *Известия вузов. Физика.* — №3. — 2006. — C.3–7.

V. A. Smyntyna, O. A. Kulinich, I. R. Iatsunskyi, I. A. Marchuk

FACTORS INFLUENCING THE YIELD STRESS OF SILICON

Abstract

Factors influencing the yield stress of silicon are investigated with advanced research methods. It is shown that elastic stresses which are concentrated at the structural defects (dislocation, crystalline grain boundary, dendrite and lamella) will influence on the yield stress of silicon.

Key words: silicon, structural defects, the yield stress.

В. А. Смынтына, О. А. Кулинич, И. Р. Яцунский, И. А. Марчук

ФАКТОРЫ, ВЛИЯЮЩИЕ НА ВЕЛИЧИНУ ПОРОГА ПЛАСТИЧНОСТИ В КРЕМНИИ

Резюме

Используя современные методы исследования, определенны факторы, влияющие на величину порога пластичности монокристаллического кремния. Наряду с известными факторами, величина порога пластичности будет зависеть от упругих напряжений, локализованных в области нахождения структурных дефектов.

Ключевые слова: кремний, структурные дефекты, порог пластичности.

УДК 537. 311. 33: 622. 382.33

В. А. Сминтина, О. А. Кулініч, І. Р. Яцунський, І. О. Марчук

ФАКТОРИ, ЩО ВПЛИВАЮТЬ НА ВЕЛИЧИНУ ПОРОГА ПЛАСТИЧНОСТІ В КРЕМНІЇ

Резюме
За допомогою сучасних методів дослідження, визначенні фактори, що впливають на величину порога пластичності в напівпровідниковому кремнію. Поряд з відомими факторами, на величину порога пластичності впливають пружні напруження, що локалізовані в області знаходження структурних дефектів.
Ключові слова: кремній, структурні дефекти, поріг пластичності.

UDC 539.293

M. V. KLYMENKO, S. I. PETROV, O. V. SHULIKA

Kharkov National University of Radio Electronics, Lenin ave. 14, Kharkov 61166, Ukraine

JOINT INFLUENCE OF INTERNAL FIELDS AND INDIUM SURFACE SEGREGATION ON BAND STRUCTURE IN InGaN/GaN SINGLE QUANTUM WELL

In this paper, authors investigate the influence of the indium surface segregation and piezoelectric polarization on the band structure of the InGaN/GaN single quantum well. The obtained results evidence that the indium surface segregation leads to the blue shift of the transition energy (70 meV for the segregation length 1nm at both heterointerfaces) while the piezoelectric polarization itself causes the read shift. Joint action of both effects influence on the potential profile determining the linear dependence of the transition energy on the width of the quantum well. The piezoelectric polarization is prevailed for the high indium amount, and the indium surface segregation is dominated for the low indium amount in the In(x)Ga(1-x)N alloy.

INTRODUCTION

Light-emitting diodes and semiconductor lasers based on InGaN/GaN quantum well structure are of actual interest due to their operation in the spectral range from the visible to the UV radiation [1]. On the other hand, a widespread application and designing of these devices is limited by existed difficulties concerning predictions of their optical spectral characteristics. Indeed, all published theories of the optical response of considered structures contain at least one fitting parameter. The most frequently encountered one is the linewidth of the inhomogeneous broadening [1], [2]. This kind of the broadening is related to 3D random variations of the potential relief caused by the indium composition fluctuations. Effects changing uniform indium distribution are the indium surface segregation [3], [4] and clustering [5]. In this letter, we focus on the indium surface segregation (ISS) and its influence on the band structure in InGaN/GaN single quantum well structure. The aim of this work is the theoretical investigation of traits in the band structure which are caused by the ISS and piezoelectric effects.

As a rule, the ISS is investigated experimentally by using the transition electron microscopy (TEM) [6], [7], reflection high energy electron diffraction (RHEED) [8] and X-rays diffraction (XRD) [9]. All these methods have own disadvantages in case of ultrathin quantum wells. TEM could induce an additional local strain in the crystal lattice after a long duration of the electron beam exposition time [10]. RHEED is realized during the crystal growth and cannot be applied after the fabrication. The XRD technique has low sensitivity for distances up to 2 nm and its experimental data are difficult to interpret. The optical spectroscopy avoids most of these disadvantages. However, the application of the optical spectroscopy requires the theory providing clear connection between the optical spectroscopic data and parameters of the structure imperfections.

Knowing of the band structure is necessary for computations of the optical characteristics using Fermi's Golden Rule, density matrix approach or Green's function method. That is caused the topicality of this paper.

INDIUM DISTRIBUTION PROFILE

There are several approaches to modeling and parametrization of the indium profile in the structure with segregation. One of them is based on the Fick's law [6]. This approach gives the indium distribution profile expressed as a linear combination of the complementary error functions:

$$n_{In}(z) = \frac{n_{nom}}{2}\left[erfc\left(\frac{w_{nom} - 2z}{2L_1} \right) + erfc\left(\frac{w_{nom} + 2z}{2L_2} \right) \right] \quad (1)$$

here: $n_{In}(z)$ is the indium distribution, n_{nom} is the nominal indium molar fraction in QW layer, w_{nom} is the nominal width of QW, L_1 and L_2 are lendth of the surface segregation.

Some authors use the Gaussian function for potential profile approximation for QWs where surface segregation effects take place. In this case, the width of the Gaussian function is a fitting parameter which can be found from experimental data or theory treatment. Gaussian approximation gives symmetrical indium distribution function. However, TEM images of QW structures argue that the surface segregation leads to asymmetrical shape of the indium distribution profile. Therefore, we use more complicated description of the surface segregation based on kinetic equations [7]. The solution of the coupled kinetic equations is fitted by the following expression [3]:

$$n_{In}(z) = \begin{cases} 0, & z \le z_1, \\ n_0 erf\left(\dfrac{z - z_1}{L_1} \right), & z_1 < z \le z_2, \\ n_0 erf\left(\dfrac{z_2 - z_1}{L_1} \right)\left[1 - n_0 erf\left(\dfrac{z - z_1}{L_1} \right) \right], & z_2 \le z. \end{cases} \quad (2)$$

here $z_2 - z_1 = w_{nom}$ This formula approximates with high accuracy the indium distribution obtained by means of the theory of Muraki *et al.* [11], [12]. Expression (2) gives asymmetrical indium distribution. This approximation contains two fitting parameters instead of single one as in case of Gaussian approximation. That gives more freedom to provide accurate fitting. As it follows from the experimental data, fitting parameters L_1 and L_2 are not equal that means inequality of the segregation effect for switch-on and switch-off regimes of the MBE indium source evaporator. Hereafter, we name parameters L_1 and L_2 the segregation lengths.

POSITION-DEPENDENT MATERIAL PARAMETERS AND INTERNAL ELECTRIC FIELDS

In this paper, we consider nitride single quantum well structure with layers made of In(x)Ga(1-x)N and GaN semiconductor alloys. All position-dependent material parameters except the band gap energy have been computed using linear interpolation formulas. We use the second order interpolation formula with the bowing parameter to compute the band gaps. Material parameters for relevant binary semiconductors have been taken from [17]. In the case of In(x)Ga(1-x)N QW heterostructure, the molar fraction of indium x is a position-dependent parameter. All other position-depended quantities are related to the indium distribution in the structure.

Well-known peculiarity of the wurtzite crystal heterostructure is strong internal electric fields caused by spontaneous polarization and piezoelectric effects. In this paper, we neglect the spontaneous polarization and focus our attention on piezoelectric fields. This is good approximation in case of high indium amount in In(x)Ga(1-x)N alloy.

High indium amount leads to significant lattice constant mismatch for In(x)Ga(1-x)N/GaN material pair. Lattice mismatch causes strong strain giving origin to piezoelectric effects. Piezoelectric polarization P_{piezo} is calculated using Vegard's interpolation formula [13]:

$$P_{piezo}(z) = xP_{piezo}^{InN}[\varepsilon(z)] + (1-x)P_{piezo}^{GaN}[\varepsilon(z)] \quad (3)$$

where the strain coefficient $\varepsilon(z)$ is defined as

$$\varepsilon(z) = \frac{a_{subs} - a(z)}{a(z)} \quad (4)$$

here a_{subs} is the lattice constant of the substrate and $a(z)$ is the lattice constant of the unstrained semiconductor alloy at a point z.

As has been shown in Ref. [13], piezoelectric polarization of binary strained semiconductors can be expressed as:

$$P_{piezo}^{InN}(\varepsilon(z)) = -1.373\varepsilon(z) + 7.559\varepsilon^2(z) \quad (5)$$

$$P_{piezo}^{GaN}(\varepsilon(z)) = -0.918\varepsilon(z) + 9.541\varepsilon^2(z) \quad (6)$$

When the piezoelectric is absent, the quantum well is characterized by the square potential profile.

The piezoelectric effect leads to zigzag shape of the quantum well.

BAND STRUCTURE

The electron wave function is obtained as solution of the Ben-Daniel-Duke equation resulted from joint action of the single-band and the envelope function approximations [16]. This approach is based on the following representation of the electron wave function [15]:

$$\langle r | \psi_j^e \rangle = \exp(i\vec{k}_\parallel \vec{r}_\parallel) \varphi_j(z) \langle r | S \rangle, \quad (7)$$

where $\langle r | S \rangle$ is the periodic Bloch function in the position-coordinate representation, $\varphi_j(z)$ is the envelope function for the electron's j-th state, $\vec{k}_\parallel$ is in-plane wave vector and $\vec{r}_\parallel$ is the in-plane radius-vector. Solving of the Ben-Daniel-Duke problem gives unknown envelope functions $\varphi_j(z)$ and band structure of the conduction band. The valence band structure is computed separately in more complicated manner to include into consideration intense band mixing effects. In the frame of the envelope function approximation, we use six-band model including into consideration interaction between heavy hole, light hole and spin-orbit split-off states with all possible directions of the spin. This approximation is widely used for semiconductor nitrides with wurtzite crystal structure [14]. In this case, wave functions for the valence band are represented as [13]:

$$\langle r | \psi_j^h \rangle = \exp(i\vec{k}_\parallel \vec{r}_\parallel) \sum_{\substack{m=X\uparrow,Y\uparrow \\ Z\uparrow,X\downarrow,Y\downarrow,Z\downarrow}} \sum_{j=1}^{N_m} g_j^m(z) \langle r | m \rangle, \quad (8)$$

where m \$m\$ is an index indicating type of the basis function in the bulk Hamiltonian, N_m is number of considered subbands for the m-th band, $\langle r | m \rangle$ is the periodic Bloch function of the m-th type and g_j^m are the hole envelope functions.

Usually, to simplify the problem, the block-diagonal representation of Hamiltonian is applied. In this case, the problem is solved for each block of the Hamiltonian separately. The wave functions in the block-diagonal representation are modified as:

$$\langle r | \psi_j^h \rangle = \exp(i\vec{k}_\parallel \vec{r}_\parallel) \sum_{\sigma=U,L} \sum_{m=1}^{3} \sum_{j=1}^{N_m} g_{j,\sigma}^m(z) \langle r | m \rangle, \quad (9)$$

here index σ refers to upper $\sigma = U$ or lower $\sigma = L$ blocks of the Hamiltonian. The 6×6 Hamiltonian in block-diagonal form [14] is

$$H_{6\times6} = \begin{pmatrix} H^U & 0 \\ 0 & H^L \end{pmatrix}, \quad (10)$$

with H^U and H^L being

$$H^U = \begin{pmatrix} F & K & -iH \\ K & G & \Delta - iH \\ iH & \Delta + iH & \lambda \end{pmatrix}, \quad (11)$$

$$H^L = \begin{pmatrix} F & K & iH \\ K & G & \Delta + iH \\ -iH & \Delta - iH & \lambda \end{pmatrix}, \quad (12)$$

here: $F = \Delta_1 + \Delta_2 + \lambda + \theta$, $G = \Delta_1 - \Delta_2 + \lambda + \theta$,

$$\lambda = \frac{\hbar^2}{2m_0}\left(A_1 k_z^2 + A_2 k_t^2\right) + \lambda_\varepsilon, \quad \lambda_\varepsilon = D_1 \varepsilon_{zz} + D_2\left(\varepsilon_{xx} + \varepsilon_{yy}\right),$$

$$\theta = \frac{\hbar^2}{2m_0}\left(A_3 k_z^2 + A_4 k_t^2\right) + \theta_\varepsilon, \quad \theta_\varepsilon = D_3 \varepsilon_{zz} + D_4\left(\varepsilon_{xx} + \varepsilon_{yy}\right),$$

$$\varepsilon_{xx} = \varepsilon_{yy} = \frac{a_{subs} - a}{a}, \quad \varepsilon_{zz} = -\frac{2C_{13}}{C_{33}}\varepsilon_{xx}, \quad \varepsilon_{xy} = \varepsilon_{yz} = \varepsilon_{zx} = 0,$$

$$K = \frac{\hbar^2}{2m_0} A_5 k_t^2, \quad H = \frac{\hbar^2}{2m_0} A_6 k_t k_z, \quad \Delta = \sqrt{2}\Delta_3,$$

$k_t = \left|\vec{k}_\parallel\right|$, A_j ($j = 1 \div 5$) are valence-band structure parameters, D_j ($j = 1 \div 4$) are deformation potentials, Δ_1, Δ_2, Δ_3 are energy parameters, C_{13} and C_{33} are elastic stiffness constants.

In the frame of the envelope function approximation, Hamiltonian (10) is transformed to the differential operator using the transformation $k_z \rightarrow \partial/\partial z$. The band structure and envelope functions have been computed numerically, applying the finite difference method [14].

BAND STRUCTURE

We restrict our consideration here only by the valence band due to its more complicated structure comparing with conduction band.

Computed band structures presented in Fig. 1 uncover effects of joint action of the piezoelectric polarization and indium surface segregation for semiconductor heterostructures with different indium amount (with different depths of the quantum well). Here, the indium surface segregation lengths equals $L_1 = L_2 = 1$ nm that corresponds to the experimental data [2]. As it follows from Fig.1, indium surface segregation does not lead to changes in the shape of the valence band dispersion curves. It means that the influence of surface segregation on the effective mass of carriers is not significant. Also, one can observe the blue energy shift of all states caused by the indium surface segregation effect. The energy shift is equal 20 meV for the conduction band and 50 meV for the valence band. Total blue shift is 70 meV.

For all considered cases, the piezoelectric polarization leads to significant shift of energy subbands in both conduction and valence bands. The resulted shift of the transition energies is red one for all cases that is opposite to the ISS. This feature of the nitrite quantum well structures is well-known and it is proved by several experimental works. Increasing of the indium amount leads to increasing of such an energy shift. That is caused by direct relation between indium amount and piezoelectric polarization following from Eq. 3.

As follow from presented results, the indium surface segregation leads to constant energy shift of subbands relative to subbands for the case when the piezoelectric polarization is present. In the shallow quantum well, the piezoelectric polarization in weak and the indium surface segregation is dominant causing strong blue shift. In the case when the indium amount is equal, the piezoelectric polarization and indium surface segregation have almost the same effect. Acting in opposite direction, their joint action does not change the energy of subbands significantly relative to their position in the square quantum well. At high indium amounts, the indium surface segregation just compensates the piezoelectric effect a little bit.
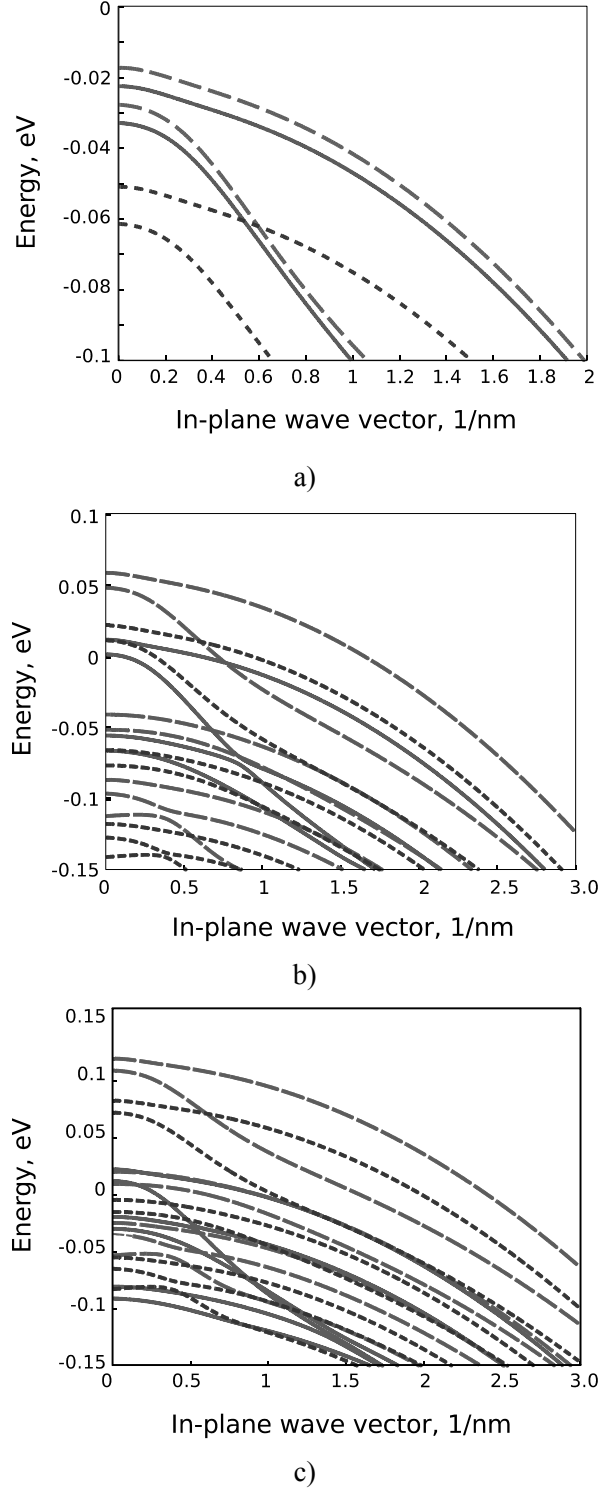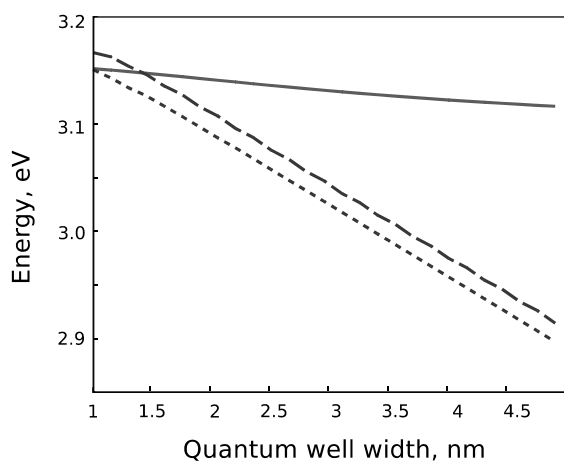
a)

b)

c)

Fig. 1 — Band structures for InGaN/GaN single quantum well with indium amount a) x=0.1, b) x=0.2 and c) x=0.3 for square quantum well (solid curve), quantum well with piezo-electric polarization (dashed curve) and joint action of piezo-electric polarization and indium surface segregation (dotted curve)

WIDTH DEPENDENCE OF THE BAND STRUCTURE

Fig. 2 contains dependences of the valence band edges on the quantum well width. In the case of the square quantum well, dependences of the band edges on the width of the quantum well are nonlinear ones. Especially, this is well-observed for holes which have lager effective mass. The piezoelectric polarization leads to zigzag potential profile of conduction and valence band edges. As s result, the dependence of the band edges on the quantum well width becomes linear. The ISS does not change the charter of this dependence significantly leading to some constant energy shift of subbands. This is the case for both conduction and valence bands.
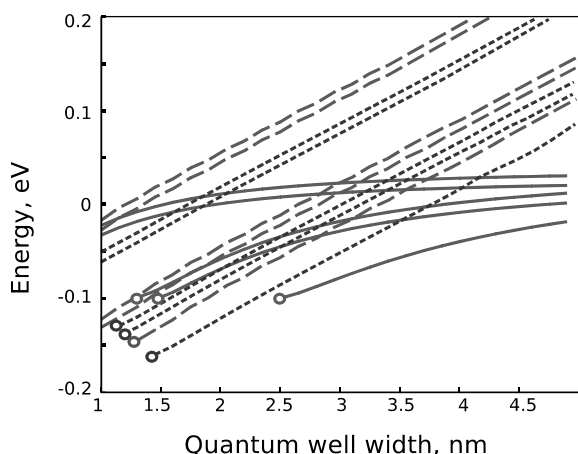
a)

b)

Fig. 2 — Dependences of a) valence and b) conduction band edges on the quantum well width for the square quantum well (solid line), quantum well with piezoelectric fields (dashed line) and quantum well with joint action of piezoelectric polarization and indium surface segregation (dotted line)

Changes in the width of the quantum well can lead to appearing of new confinement states in the quantum well. Such states are denoted by circles in Fig. 2. Conduction band have only one confined state in all cases.

CONCLUSIONS

In this paper, we have investigated the influence of the piezoelectric polarization and indium surface segregation on the band structure in InGaN/GaN single quantum well. Obtained results evidence that the joint action of the piezoelectric polarization and indium surface segregation cause unique position of subbands at the energy axis. The low indium amounts, the indium surface segregation is dominant effect due to piezoelectric polarization is weak in this case. However, the piezoelectric effects are prevailed at the high indium amount. Joint action of the indium surface segregation and piezoelectric polarization causes linear dependence of band edges on the width of the quantum well. This result is confirmed by experimental data based on the photoluminescence measurements [19].

References

1. *Hader J., Moloney J. V., and Koch S. W.,* Influence of internal fields on gain and spontaneous emission in InGaN quantum wells // Appl. Phys. Lett. — 2006. — 89, — P. 171120
2. *Witzigmann B. et al.,* Microscopic analysis of optical gain in InGaN/GaN quantum wells // Appl. Phys. Lett. — 2006. — 88, — P. 021104
3. *Mayrock O., Wunsche H. — J. and Henneberger F.,* Polarization charge screening and indium surface segregation in (In,Ga)N/GaN single and multiple quantum wells // Phys. Rev. B — 2000. — 62. — P. 16870
4. *Potin et al.,* Comparison of the In distribution in InGaN/GaN quantum well structures grown by molecular beam epitaxy and metalorganic vapor phase epitaxy // J. Crystal Growth — 2004. — 262. — P. 145
5. *Ruterana et al.,* Composition fluctuation in InGaN quantum wells made from molecular beam or metalorganic vapor phase epitaxial layers // J. Appl. Phys. — 2002. — 91. — P. 8979
6. *Biswas D., Kumar S. and Das T.,* Band offsets of InXGa1−XN/GaN quantum wells reestimated // Thin Solid Films — 2007. — 515. — P. 4488
7. *Stanlay I., Coleiny G. and Venkat R.,* Theoretical study of In desorption and segregation kinetics in MBE growth of InGaAs and InGaN // J. Crystal Growth — 2003. — 251 — P. 23
8. *Martini S. et al.,* Influence of indium segregation on the RHEED oscillations during the growth of InGaAs layers on a GaAs(0 0 1) surface // J. Crystal Growth — 2003. — 251. — P. 101
9. *Pereira S. et al.,* Strain and composition distributions in wurtzite InGaN/GaN layers extracted from x-ray reciprocal space mapping // Appl. Phys. Lett. — 2002 — 80. — P. 3913
10. *Li T. et al.,* Indium redistribution in an InGaN quantum well induced by electron-beam irradiation in a transmission electron microscope // Appl. Phys. Lett. — 2005. — 86. — P. 241911
11. *Muraki K. et al.,* Surface segregation of In atoms during molecular beam epitaxy and its influence on the energy levels in InGaAs/GaAs quantum wells // Appl. Phys. Lett. — 1992. — 61. — P. 557
12. *Dussainge A. et al.,* In surface segregation in InGaN/GaN quantum wells // J. Crystal Growth — 2003. — 251. — P. 471
13. *Fiorentini V., Bernardini F. and Ambacher O.,* Evidence for nonlinear macroscopic polarization in III—V nitride alloy heterostructures // Appl. Phys. Lett. — 2002. — 80. — P. 1204
14. *Chuang S. L. and Chang C. S.,* Band Structure Model of Strained Quantum-Well Wurtzite Semiconductors // Semicond. Sci. Technol. — 1997. — 12. — P. 252
15. *Chow W. W. and Koch S. W.,* Semiconductor Laser: Fundamentals. Physics of the gain materials — Springer, 1999. — P. 298
16. *Bastard G.,* Wave Mechanics Applied to Semiconductor Heterostructures. — John Wiley & Sons Inc., 1991 — P. 557
17. *Vurgaftman I., Meyer R. and Ram-Mohan L. R.,* Band parameters for nitrogen-containing semiconductors // J. Appl. Phys. — 2003 — 94. — P. 3675

18. *Chuang S. L.*, Optical gain of strained wurtzite GaN quantum-well lasers // IEEE J. Quantum Electron. — 1996. — 32. — P. 1791

19. *Berkowicz E. et al*, Optical spectroscopy in InGaN/GaN quantum wells // Phys. Stat. Sol. (b), — 1999. — 216. — P. 291

UDC 539.293

M. V. KLYMENKO, S. I. PETROV, O. V. SHULIKA

JOINT INFLUENCE OF INTERNAL FIELDS AND INDIUM SURFACE SEGREGATION ON BAND STRUCTURE IN InGaN/GaN SINGLE QUANTUM WELL

Abstract

In this paper, authors investigate the influence of the indium surface segregation and piezoelectric polarization on the band structure of the InGaN/GaN single quantum well. The obtained results evidence that the indium surface segregation leads to the blue shift of the transition energy (70 meV for the segregation length 1nm at both heterointerfaces) while the piezoelectric polarization itself causes the read shift. Joint action of both effects influence on the potential profile determining the linear dependence of the transition energy on the width of the quantum well. The piezoelectric polarization is prevailed for the high indium amount, and the indium surface segregation is dominated for the low indium amount in the In(x)Ga(1-x)N alloy.

Key words: surface segregation, internal fields, structure.

УДК 539.293

М. В. КЛИМЕНКО, С. И. ПЕТРОВ, А. В. ШУЛИКА

СОВМЕСТНОЕ ВЛИЯНИЕ ВНУТРЕННИХ ЕЛЕКТРОСТАТИЧЕСКИХ ПОЛЕЙ И ПОВЕРХНОСТНОЙ СЕГРЕГАЦИИ ИНДИЯ НА ЗОННУЮ СТРУКТУРУ В InGaN/GaN ОДИНОЧНОЙ КВАНТОВОЙ ЯМЕ

Резюме

В этой работе, авторы исследуют влияние поверхностной сегрегации индия и пьезоэлектрической поляризации на зонную структуру InGaN/GaN одиночной квантовой ямы. Полученные результаты свидетельствуют, что поверхностная сегрегация индия приводит к "синему" сдвигу энергии перехода (70 мэВ для длины сегрегации 1 нм на каждом гетероинтерфейсе) в то время как пьезоэлектрическая поляризация обуславливает "красный" сдвиг. Совместное действие обоих эффектов оказывает влияние на потенциальный профиль определяя линейную зависимость энергии перехода от ширины квантовой ямы. Пьезоэлектрическая поляризация является преобладающей при больших содержаниях индия, а поверхностная сегрегация индия преобладает при малом содержании индия в In(x)Ga(1-x)N твердом растворе.

Ключевые слова: поверхностная сегрегация, структура, квантовое поле.

УДК 539.293

М. В. КЛИМЕНКО, С. И. ПЕТРОВ, О. В. ШУЛИКА

СУМІСНИЙ ВПЛИВ ВНУТРІШНІХ ЕЛЕКТРОСТАТИЧНИХ ПОЛІВ ТА ПОВЕРХНЕВОЇ СЕГРЕГАЦІЇ ІНДІЯ НА ЗОННУ СТРУКТУРУ В InGaN/GaN ПООДИНОКІЙ КВАНТОВІЙ ЯМІ

Резюме

У роботі автори досліджують вплив поверхневої сегрегації індія і п'єзоелектричної поляризації на зонну структуру InGaN/GaN поодинокої квантової ями. Отримані результати свідчать, що поверхнева сегрегація індія приводить до "синього" зміщення енергії переходу (70 мэв для довжини сегрегації 1 нм на кожному гетероінтерфейсі) у той час як п'єзоелектрична поляризація обумовлює "червоне" зміщення. Спільна дія обох ефектів впливає на потенційний профіль визначаючи лінійну залежність енергії переходу від ширини квантової ями. П'єзоелектрична поляризація є переважаючою при великому вмісті індія, а поверхнева сегрегація індія переважає при малому вмісті індія в In(x)Ga(1-x)N твердому розчині.

Ключові слова: поверхнева сегрегація, структура, квантове поле.

V. I. IRKHA, V. E. GORBACHEV

Department of Physics of Optical Communication, Odessa National Academy of Telecommunications named after A. S. Popov, Kuznechna str., 1, Odessa, 65029, Ukraine, phys@onat.edu.ua, tel./fax: +380–723–61–18

INFLUENCE OF γ-IRRADIATION ON EMITTING PROPERTIES OF MULTILAYER HETEROSTRUCTURES

The results of investigations of gamma irradiation-induced resistance degradation of optical emitters manufactured using of the multilayer GaAlAs-heterostructures are described. Some associations in changing of electrical and electroluminescent characteristics of emitters with exposure parameters are obtained.

INTRODUCTION

During an exposure by a hard radiation in semiconductor materials irradiation-induced defects appear, which change the basic electrical materials properties, such as a lifetime, mobility and carrier density. Such modifications lead to degradation of biographic parameters of electronic devices and often are the main reason of decrease of their working life. Wide spreading of A_3B_5 type of semiconductor materials in microelectronics [1] provokes interest to investigations of irradiation-induced effects in their compounds and alloys. The interaction of gamma radiation with solid state, ionisation and the displacement effects in atomic subsystem of material, as well the defect formation, processes of their accumulation and reorganization depend on irradiation energy and intensity, on exposing time and temperature and on type of doping elements. The question about the nature of irradiation-induced defects formation, leading to degradation of A_3B_5 semiconductors, remains open.

A LEDs fabricated in a GaAlAs- multilayer heterostructures (MLH-structures) have several advantages. Withing forming of the intermediate GaAlAs-layers between the GaAs-substrate and GaAlAs-active region it is possible to achieve the considerable decrease of a defect level in active region, what results to magnification of a quantum efficiency of emission. Additional reemission of photons by the intermediate GaAlAs-layer significantly increases the total emission intensity of LED [2]. Spatial separation of the intermediate GaAlAs-layer and active region promotes a resistance magnification to irradiation-induced degradation of MLH-structures which are emitting light [3]. Use of MLH-structures allows us to separate degradation processes related to redistribution of an electric charge from degradation what causes increasing of charge carriers recombination.

Layer-to-layer difference of electronic and emitting properties of MLH-structures also affects characteristic properties of their degradation. Thus, by means of selection of gamma quanta exposure irradiation parameters it is possible to control a process of nonradiative recombination centres formation both in an active region and in other layers which participate in the generating processes or in outputting of photons [4].

RESULTS AND DISCUSSION

The experimental investigation of irradiation-induced degradation of GaAlAs MLH-structures at various irradiation parameters of gamma quanta Co^{60} exposure have been carried out. The structure of samples and experimental technique are described in papers [2,3].

As it was considered in previous papers [2–4], the electroluminescence spectra of the test MLH-structures have two emission bands. The long-wave component of a spectrum appears as a result of reemission of a short-wave component. For all samples, the maximums of emission bands match to energies 1,61 and 1,48 *eV*.

Electroluminescent characteristics of the LEDs before and after exposure by integral gamma-quantum's flux with intensity from $10^{16} quanta/cm^2$ to $10^{18} quanta/cm^2$ have been measured. After the radiation exposure of samples the quenching of luminescence at a long wavelength component of a spectrum and some decreasing of intensity of a short-wave component was observed. However, even for various parameters of exposure no shifting of maximums of a emitting intensity and no modification of a halfwidth of spectrum bands have been detected.

As it was expected, that after the gamma-radiation treatment which speeds up formation of defects in a semiconductor and appearance of additional levels in semiconductor forbidden band, new emission bands in spectrum of the samples should be observed. Absence of additional emission bands is an argument in favour of the fact, that irradiation-induced defects are the nonradiative recombination centres, which decreasea total efficiency of process of light emitting.

Thus, we conclude that gamma-radiation of such intensity doesn't change the main mechanism of generation of photons at the recombination kind of emission.

To figure out the ways of decreasing the role of the irradiation-induced effects on LED's the influence of hard radiation on a current-voltage characteristic of p-n- junction has been studied. The current-voltage curves of the test samples before (1) and after (2) of radiation exposure by integral gamma-quantum's flux with intensity $5 \cdot 10^{16} \, quanta/cm^2$ are shown in a Fig. 1. As the one can see from the figure, the current-voltage diagrams have a several slopes, which indicate that the charge transfer mechanism across a MLH-structure

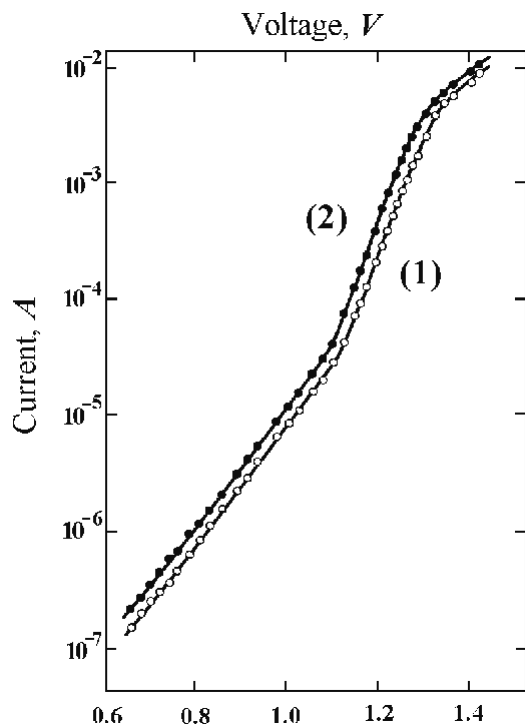changes with growing the level of injection of charge carriers.

Fig. 1. Current-voltage characteristic of the test LED before (1) and after (2) of gamma radiation exposure by integral flux with intensity $5 \cdot 10^{16} quanta/cm^2$

In an absolute majority of the tested samples at small values of direct current (10^{-7}—$10^{-5}A$), the current-voltage characteristic is being well described by the tunnel mechanism of carriers transfer. In this region of a current-voltage characteristic after exposing, there is small magnification of the current. We relate this fact to insignificant magnification of concentration of irradiation-induced deep levels that is the parent of increment of tunnel current.

At the second region of a slope of a characteristic at direct currents 10^{-4}—$10^{-2}A$ the recombination component of a current predominates. Good approximation of this region of the current-voltage characteristic is an exponential function:

$$I = I_0 \cdot \exp\left(\frac{eU}{n \cdot kT}\right). \quad (1)$$

Coefficient n for the test samples varies in the range from 1,68 to 1,73.

After the exposing by gamma-radiation, the current-voltage characteristic with the parallel shift to high-currents region (Curve 2 on a Fig. 1) was obtained. We consider such modifications of this region of the current-voltage characteristic as result of decreasing of a lifetime of charge carriers after the exposure. During an exposure by a hard radiation in a volume of MLH-structure irradiation-induced defects are formed, which act as active recombination centres that shorten lifetime of charge carriers.

The lifetime of minority charge carriers on second current-voltage characteristic slope region that corresponds to a dominance of recombination-current component has been experimentally estimated. The

value of lifetime of $1,86 \cdot 10^{-9}s$ before irradiation and of $1,23 \cdot 10^{-9}s$ after exposure was calculated.

The magnification of the reverse current after of irradiation has been experimentally observed.

For investigation of influence of an irradiation on carrier concentration in MLH-structures, we have measured an avalanche breakdown voltage. An empirical equation of a dependence of value of a breakdown voltage from impurity density has been derived:

$$U_B = 60 \cdot \left(\frac{E_g}{1,1}\right)^{3/2} \left(\frac{10^{16}}{N_{A,D}}\right)^{3/4}, \quad (2)$$

where E_g — energy gap and $N_{A,D}$ — impurity density in high-resistance region of p-n-junction.

Values of an avalanche breakdown voltage for all tested samples were within the interval from $6,5V$ to $12,5V$. We did not observe any variations in these values after an exposure by integral gamma-quantum's flux with intensity up to $10^{18} quanta/cm^2$. This fact indicates that intensity of irradiating, which we used in experiments, is insufficient to produce essential changes in impurity concentration. Similar results were mentioned earlier [1].

The above mentioned statements indicate, after irradiation of MLH-structures the significant increasing of number of a nonradiative recombination centres shorten a lifetime of charge carriers. It can lead to practically full decreasing of emission intensity even at such irradiation integral fluxes when carrier density does not considerably vary yet.
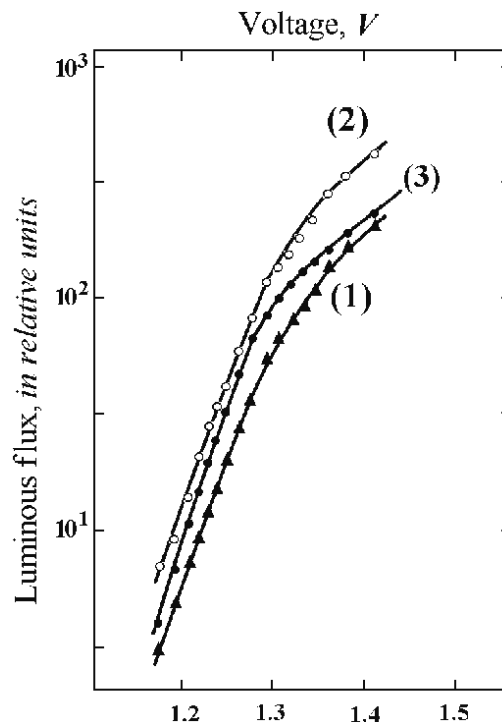

Fig. 2. Luminous-voltage characteristic of the test LED for long-wave band (1) and short-wave band (2) of an emission spectrum before, but (3) — for short-wave band after of gamma radiation exposure by integral flux with intensity $5 \cdot 10^{16} quanta/cm^2$

The luminous-voltage and luminous-current characteristics of the test samples before (1), (2) and after (3) of radiation exposure by integral gamma-quantum's flux with intensity $5 \cdot 10^{16} quanta/cm^2$ are

shown in a Fig. 2 and 3. Curves (2) and (3) relate to short-wave component, but curve (1) relates to long-wave component of an MLH-structure emission spectrum. Absence of long-wave component of a spectrum after radiation exposure indicates above mentioned cancellation. As it follows from figures, irradiation has no effect on slope of curve. It confirms the absence of essential variations of carrier density after the radiation exposure.
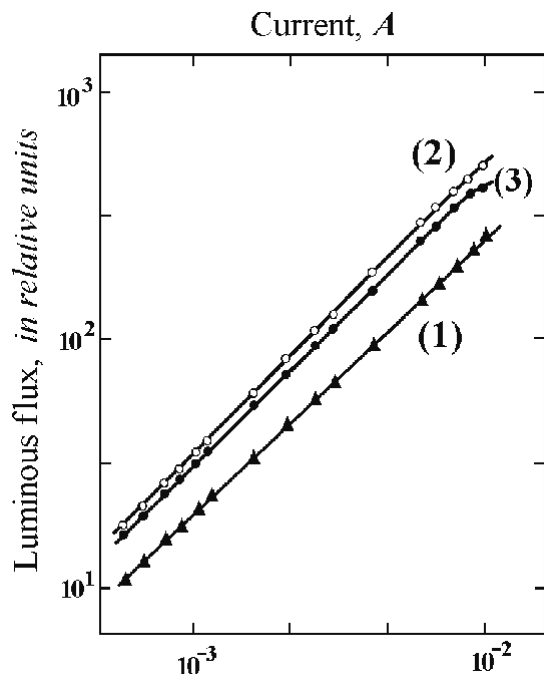

Fig. 3. Luminous-current characteristic of the test LED for long-wave band (1) and short-wave band (2) of an emission spectrum before, but (3) — for short-wave band after of gamma radiation exposure by integral flux with intensity $5 \cdot 10^{16} quanta/cm^2$

In comparison of current-voltage and luminous-voltage characteristics (Figs. 1 and 2) it can be seen, that the most effective emission corresponds to second current-voltage characteristic slope region in which total recombination current dominates.

CONCLUSION

The obtained experimental information allows to making some conclusions about the main mechanism of GaAlAs MLH-structure optical emitters irradiation-induced degradation phenomenon.

After the radiation exposure by integral gamma-quantum's flux with intensity up to $10^{17} quanta/cm^2$ of optical emitters a significant decreasing of emission intensity occurs.

Formation of a nonradiative recombination centres is a dominant result of irradiation-induced degradation of light-emitting MLH-structures.

Opposite to lasers based on MLH-structures, the irradiation-induced optical losses increasing and decreasing of electrons injection in the MLH-LEDs are unnoticeable effects in comparison with predominating of nonradiative recombination.

Using the additional reemission effect of photons by the intermediate layer in multilayer optical emitters leads to considerable decreasing LED's resistance within gamma irradiation-induced degradation.

References

1. А. Берг, П. Дин, *Светоизлучающие диоды* // Мир — Москва — 1999 — 686с.
2. В. Ирха, А. Коваль, Особенности механизма электролюминисценции излучающих диодов для ИК области спектра // *Наукові праці ОНАЗ ім. О. С. Попова* — Одеса — 2002 — №1 — с. 112–115.
3. В. Ирха, А. Коваль, Деградация излучающих диодов на основе GaAlAs для ИК области спектра // *Труды УНИ-ИРТ* — Одесса — 2005 — №2 — с. 17–19.
4. В. Ирха, Влияние радиационных дефектов на характеристики p-n- переходов излучающих диодов // *Моделирование и информационные технологии, Сборник трудов* — в. 54 — Киев — 2009 — с. 113–118.

V. I. Irkha, V. E. Gorbachev

INFLUENCE OF γ-IRRADIATION ON EMITTING PROPERTIES OF MULTILAYER HETEROSTRUCTURES

Abstract
The results of investigations of gamma irradiation-induced resistance degradation of optical emitters manufactured using of the multilayer GaAlAs-heterostructures are described. Some associations in changing of electrical and electroluminescent characteristics of emitters with exposure parameters are obtained.
Key words: Multilayer structures, Optical emitters, Gamma radiation hardness, Degradation.

В. И. Ирха, В. Э. Горбачев

ВЛИЯНИЕ γ-ОБЛУЧЕНИЯ НА ИЗЛУЧАЮЩИЕ СВОЙСТВА МНОГОСЛОЙНЫХ ГЕТЕРОСТРУКТУР

Резюме
Приведены результаты исследований радиационной стойкости оптических излучателей, изготовленных на основе многослойных GaAlAs-гетероструктур. Получены некоторые закономерности в изменении электрических и электролюминесцентных характеристик излучателей в зависимости от дозы гамма-излучения.
Ключевые слова: Многослойные структуры, оптические излучатели, радиационная стойкость, гамма излучение, деградация.

УДК 621.315.592

В. І. Ірха, В. Е. Горбачов

ВПЛИВ γ-ОПРОМІНЕННЯ НА ВИПРОМІНЮЮЧІ ВЛАСТИВОСТІ БАГАТОШАРОВИХ ГЕТЕРОСТРУКТУР

Резюме
Наведено результати досліджень радіаційної стійкості оптичних випромінювачів, виготовлених на основі багатошарових GaAlAs-гетероструктур. Отримано деякі закономірності в зміненні електричних та електролюмінісцентних характеристик випромінювачів в залежності від дози гамма опромінення.
Ключові слова: багатошарові структури, ні випромінювачі, радіаційна стійкість, гамма-опромінення, деградація.

INFORMATION FOR CONTRIBUTORS OF "PHOTOELECTRONICS" ARTICLES

"Photoelectronics" Articles publishes the papers which contain information about scientific research and technical designs in the following areas:
- **Physics of semiconductors;**
- **Physics of microelectronic devices;**
- **Linear and non-linear optics of solids;**
- **Optoelectronics and optoelectronic devices;**
- **Quantum electronics;**
- **Sensorics.**

"Photoelectronics" Articles is defined by the decision of the Highest Certifying Commission as the specialized edition for physical-mathematical and technical sciences and published and printed at the expense of budget items of Odessa I. I. Mechnikov National University.

"Photoelectronics" Articles is published in English. Authors send two copies of papers in English. The texts are accompanied by 3.5" diskette with text file, tables and figures. Electronic copy of a material can be sent by e-mail to the Editorial Board and should meet the following requirements:

1.The following formats are applicable for texts — MS Word (rtf, doc).

2. Figures should be made in formats — EPS, TIFF, BMP, PCX, JPG, GIF, WMF, MS Word I MS Giaf, Micro Calc Origin (opj). Figures made by packets of mathematical and statistic processing should be converted into the foregoing graphic formats.

The papers should be sent to the address:
Kutalova M. I., Physical Faculty of Odessa I. I. Mechnikov National University, 42 Pastera str, 65026 Odessa, Ukraine, e-mail: wadz@mail.ru, tel. +38−0482−7266356. Information is on the site:
http://www.photoelectronics.onu.edu.ua

The title page should contain:
1. Codes of PACS
2. Surnames and initials of authors
3. TITLE OF PAPER
4. Name of institution, full postal address, number of telephone and fax, electronic address

An abstract of paper should be not more than 200 words. Before a text of summary a title of paper, surnames and initials of authors should be placed.

Equations are printed in MS Equation Editor.

References should be printed in double space and should be numbered in square brackets consecutively throughout the text. References for literature published in 2000−2009 years are preferential.

Illustrations will be scanned for digital reproduction. Only high-quality illustrations will be taken for publication. Legends and symbols should be printed inside. Neither negatives, nor slides will be taken for publication. All figures (illustrations) should be numbered in the sequence of their record in text.

For additional information please contact with the Editorial Board.

ИНФОРМАЦИЯ ДЛЯ АВТОРОВ НАУЧНОГО СБОРНИКА "PHOTOELECTRONICS"

В сборнике "Фотоэлектроника" печатаются статьи , которые содержат сведения о научных исследованиях и технических разработках в направлениях
- **физика полупроводников;**
- **гетеро- и низкоразмерные структуры;**
- **физика микроэлектронных приборов;**
- **линейная и нелинейная оптика твердого тела;**
- **оптоэлектроника и оптоэлектронные приборы;**
- **квантовая электроника;**
- **сенсорика.**

Сборник "Photoelectronics" издаётся на английском языке. Рукопись подается автором в двух экземплярах на английском и русском языках. Электронную копию материала необходимо прислать в редакцию по электронной почте.

Электронная копия статьи должна отвечать следующим требованиям:

1. Электронная копия материала присылается одновременно с твердой копией текста и рисунков.

2. Для текста допустимые следующие форматы — MS Word (rtf, doc).

3. Рисунки принимаются в форматах — EPS, TIFF, BMP, PCX, JPG, GIF, CDR, WMF, MS Word И MS Giaf, Micro Calc Origin (opj). Рисунки, выполненные пакетами математической и статистической обработки должны быть конвертируемые в вышеуказанные графические форматы.

Рукописи присылаются по адресу:

Отв. секр. Куталовій М. И., ул. Пастера, 42, физ. фак. ОНУ, г.Одесса, 65026 E-mail: wadz@mail.ru, тел. 0482 — 726 6356 .

Аннотации статей сб."Photoelectronics" находятся на сайте: http://photoelectronics.onu.edu.ua

К рукописи прилагается

1. Коды PAC и УДК. Допускается использование нескольких шифров, которые разделяются запятой. В случае, когда автором (авторами) не будет указан ни один шифр, редакция журнала устанавливает шифр статьи по своему выбору.

2. Фамилия (а) и инициалы автора (ел).

3. Учреждение, полный почтовый адрес, номер телефона, номер факса, адреса электронной почты для каждого из авторов

4. Название статьи

5. Резюме объемом до 200 слов пишется на английском, русском языках, и (для авторов из Украины) — на украинском.,после текста резюме печатаются Ключевые слова.

Текст должен печататься шрифтом 14 пунктов через два интервала на белой бумаге формата А4. Название статьи, а также заголовки подразделов печатаются прописными буквами и отмечаются полужирным шрифтом.

Уравнения необходимо печатать в редакторе формул MS Equation Editor. . Необходимо давать определение величин, которые появляются в тексте впервые.

Таблицы Должны быть выполнены в соответствующих табличных редакторах или представленные в текстовом виде с использованием разделителей (точка, запятая, запятая с точкой, знак табуляции).

Ссылки на литературу должны печататься через два интервала, нумероваться в квадратных дужках (в нормальном положении) последовательно в порядке их появления в тексте статьи. Ссылаться необходимо на литературу, которая издана начиная с 2000 года. Для ссылок используются следующие форматы:

Книги. Автор(и) (инициалы, потом фамилии), название книги курсивом, издательство, город и год издания. (При ссылке на главу книги, указывается название главы, название книги курсивом,

номера страниц). Пример J A Hall, Imaging tubes, Chap 14 ш *The Infrared Handbook,* Eds W W Wolfe, O J' Zissis. 2000,, ERIM, Arm Arbor, MI .pp 132—176,

Журналы (Журналы). Автор(и) (инициалы, потом фамилии), название статьи, название журнала курсивом (используются аббревиатуры только для известных журналов), номер поэтому и выпуска, номер страниц и год издания. Пример N Blutzer and A S Jensen, Current readout of infrared detectors // *Opt Eng 2000,*26(3), pp 241—248

Иллюстрации будут сканироваться цифровым сканером. Принимаются в печать только высококачественные иллюстрации. Подписи и символы должны быть впечатаны. Не принимаются в печать негативы, слайды, транспоранты. Графики и рисунки печатаются в тексте статьи.

Рисунки должны иметь соответствующий к формату журнала размер не больше 160х200 гг. Текст на рисунках должен выполняться шрифтом 12пунктов. На графиках единицы измерения указываются через запятую (а не в скобках). Все рисунки (иллюстрации) нумеруются в порядке их размещения в тексте. Не допускается вносить номер и подпись непосредственно на рисунках.

Резюме объемом до 200 слов пишется на английском, русском языках. и на украинском (для авторов из Украины). Перед текстом резюме соответствующим языком указываются УДК, фамилии и инициалы всех авторов, название статьи, ключевые слова..

ІНФОРМАЦІЯ ДЛЯ АВТОРІВ
НАУКОВОГО ЗБІРНИКА "PHOTOELECTRONICS"

У збірнику "Фотоелектроніка" друкуються статті, які містять відомості про наукові дослідження та технічні розробки у напрямках

* **фізика напівпровідників;**
* **гетеро- та низьковимірні структури;**
* **фізика мікроелектронних приладів;**
* **лінійна та нелінійна оптика твердого тіла;**
* **оптоелектроніка та оптоелектронні прилади;**
* **квантова електроніка;**
* **сенсорика.**

Збірник "Фотоелектроніка" видається англійською мовою. Рукопис подається автором у двох примірниках англійською мовою. До рукопису додається електронна копія матеріалу, яка може бути надіслана до редакції електронною поштою.

Електронна копія статті повинна відповідати наступним вимогам:

1. Електронна копія матеріалу надсилається одночасно з твердою копією тексту та малюнків.

2. Для тексту припустимі наступні формати — MS Word (rtf, doc).

3. Малюнки приймаються у форматах — EPS, TIFF, BMP, PCX, JPG, GIF, CDR, WMF, MS Word I MS Giaf, Micro Calc Origin (opj). Малюнки, виконані пакетами математичної та статистичної обробки повинні бути конвертовані у вищевказані графічні формати.

Рукописи надсилаються на адресу:

Відп. секр. Куталовій М. І., вул. Пастера, 42, фіз. фак. ОНУ, м.Одеса, 65026E-mail: wadz@mail.ru, тел. 0482—23—34—61.

До рукопису додаються:

1. Коди РАС та УДК. Допускається використання декількох шифрів, що розділяються комою. У випадку, коли автором (авторами) не буде вказано жоден шифр, редакція журналу встановлює шифр статті за своїм вибором.

2. Прізвище (а) та ініціали автора (їв), назва статті.

3. Установа, повна поштова адреса, номер телефону, номер факсу, адреса електронної пошти для кожного з авторів.

Резюме об'ємом до 200 слів пишеться англійською, українською та російською мовами Перед текстом резюме відповідною мовою вказуються назва статті, прізвища та ініціали всіх авторів, після закінчення тексту резюме друкуються ключові слова.

Текст повинен друкуватися шрифтом 12 пунктів через два інтервали на білому папері формату А4. Назва статті, а також заголовки підрозділів друкуються прописними літерами і відзначаються напівжирним шрифтом.

Рівняння необхідно друкувати у редакторі формул MS Equation Editor. Статті з вписаними від руки рівняннями до друку не приймаються. Необ-

хідно давати визначення величин, що з'являються в тексті вперше.

*Таблиці п*овинні бути виконані у відповідних табличних редакторах або представлені у текстовому вигляді з використанням роздільників (крапка, кома, кома з крапкою, знак табуляції).

Посилання на літературу повинні друкуватися через два інтервали, нумеруватись в квадратних дужках (у нормальному положенні) послідовно у порядку їх появи в тексті статті. Для посилань використовуються наступні формати:

Книги. Автор(и) (ініціали, потім прізвища), назва книги курсивом, видавництво, місто і рік видання. (При посиланні на главу книги, вказується назва глави, назва книги курсивом, номери сторінок). Приклад J A Hall, Imaging tubes, Chap 14 ш *The Infrared Handbook,* Eds W W Wolfe, O J' Zissis. 2000 ERIM, Arm Arbor, MI, pp132 — 176

Журнали (Часописи). Автор(и) (ініціали, потім прізвища), назва статті, назва журналу курсивом (використовуються абревіатури тільки для відомих журналів), номер тому і випуску, номер сторінок і рік видання. Приклад N Blutzer and A S Jensen, Current readout of infrared detectors // *Opt Eng 2000,* 26(3), p. 241−248

Ілюстрації будуть скануватися цифровим сканером. Приймаються до друку тільки високоякісні ілюстрації. Підписи і символи повинні бути вдруковані. Не приймаються до друку негативи, слайди, транспаранти.

Рисунки повинні мати відповідний до формату журналу розмір не більше 160х200 мм. Текст на рисунках повинен виконуватись шрифтом 10 пунктів. На графіках одиниці виміру вказуються через кому (а не в дужках). Усі рисунки (ілюстрації) розміщуються в тексті і нумеруються в порядку їх розміщення в тексті.